Characterization of *Drosophila* Cyclin J and Mps1

Dissertation
zur
Erlangung der naturwissenschaftlichen Doktorwürde
(Dr. sc. nat.)

vorgelegt der
Mathematisch-naturwissenschaftlichen Fakultät
der
Universität Zürich

von

Friederike Erika Andrea Althoff
aus
Deutschland

Promotionskomitee
Prof. Dr. Christian F. Lehner (Vorsitz)
Prof. Dr. Erich A. Nigg

Zürich, 2011

Contents

Summary

Error-free progression though the cell division cycle requires careful regulation at several distinct control points. The regulation assures that the transition from a given cell cycle phase into the subsequent phase is only permitted when the cellular processes characteristic of the preceding phase have all been completed without mistakes. Cyclins which interact with **C**yclin-**d**ependent **k**inases (Cdks) are central for this regulation. The activities of different Cyclin-Cdk complexes promote distinct transitions. They are inhibited by intricate checkpoint pathways that remain active as long as cell cycle steps remain incomplete or afflicted by mistakes. Thereby checkpoint pathways can pause cell cycle progression and provide time for repair or completion of cellular processes.

The first part of this work describes the characterization of a poorly analyzed Cyclin—Cyclin J. After its original identification in a yeast two-hybrid screen, *Drosophila* Cyclin J was implicated in the control of the specialized early embryonic mitoses. However, Cyclin J was subsequently found to be conserved throughout the metazoan radiation. Paralogs are therefore present in many species that do not progress through syncytial division cycles as characteristically observed during early insect embryogenesis. Cyclin J must therefore have a more general function beyond the control of the specialized cycles of early insect embryos. Based on its expression pattern in *Drosophila* a meiotic function appeared likely. However, careful fertility and non-disjunction assays with flies completely lacking Cyclin J function did not reveal any defects. Moreover, in contrast to earlier claims, loss of Cyclin J did also not affect progression through the early embryonic cycles. Biochemical analyses identified Cyclin J as an interaction partner of Cdk1. Interestingly Cyclin J is not degraded during mitosis in contrast to the other known Cdk1 interaction partners, the mitotic Cyclins A, B and B3.

The second part of this work investigates the function of Mps1, a protein kinase that is known to be involved in the **s**pindle **a**ssembly **c**heckpoint (SAC). The SAC prevents chromosome segregation errors during mitosis by responding to incorrect attachments of kinetochores to the mitotic spindle. The transient accumulation of Mps1 at kinetochores from prophase to metaphase correlates with SAC activity. Therefore, several aspects of Mps1 kinetochore localization in *Drosophila* were addressed. Mps1 recruitment to kinetochores is shown to be dependent on its own kinase activity and in part on the SAC component Mad1, which is present in a complex with Mps1. The disappearance of Mps1 from kinetochores before the metaphase-to-anaphase transition does not correlate with substantial Mps1 degradation or changes in N-terminal phosphorylation. However, the precise control of localization and levels of Mps1 was shown to be crucial for a successful mitosis. Moreover, my analyses suggested that Mps1 might have a previously unrecognized function that inhibits sister chromatid resolution in a SAC-independent manner.

Zusammenfassung

Der fehlerfreie Ablauf des Zellzyklus erfordert eine genaue Regulation an bestimmten Kontrollpunkten. Die Steuerung stellt sicher, dass der Wechsel von der jeweiligen Zellzyklusphase in die nächste nur möglich ist, wenn die zellulären Vorgänge, die für die vorangehende Zellzyklusphase charakteristisch sind, sämtlich ohne Fehler abgeschlossen wurden. Cycline, die mit Cyclin-abhängigen Kinasen (Cdks) interagieren, sind für diese Steuerung wesentlich. Die Aktivitäten der verschiedenen Cyclin-Cdk-Komplexe begünstigen bestimmte Übergänge. Sie werden durch komplexe Kontrollpunkt-Signalwege gesteuert, die aktiv bleiben, solange die jeweilige Zellzyklusphase unvollständig oder fehlerbehaftet ist. So können Kontrollpunkt-Signalwege den Ablauf des Zellzyklus unterbrechen und dadurch Zeit zum Nachbessern oder zum Abschluss der zellulären Vorgänge zur Verfügung stellen.

Der erste Teil dieser Arbeit beschreibt die Charakterisierung eines bisher wenig untersuchten Cyclins – Cyclin J. Nach seiner ursprünglichen Identifizierung in einem Yeast-two-Hybrid-Screen, wurde angenommen, dass *Drosophila* Cyclin J an der Kontrolle der spezialisierten früh-embryonalen Mitosen beteiligt ist. Nachträglich wurde jedoch entdeckt, dass es im gesamten Reich der mehrzelligen Tiere konserviert ist. Paraloge kommen daher in vielen Spezies vor, die nicht durch syncytiale Teilungszyklen, welche charakteristischerweise nur in der frühen Embryogenese bei Insekten vorkommen, gehen. Cyclin J muss daher eine allgemeinere Funktion jenseits der spezialisierten Zyklen von Insektenembryos haben. Sein Expressionsmuster in *Drosophila* zugrundelegend, schien eine meiotische Funktion wahrscheinlich. Allerdings zeigten genaue Fertilitätstests und meiotische Missegregationstests an Fliegen ohne Cyclin J-Funktion keine Defekte. Des weiteren und im Gegensatz zu früheren Behauptungen beeinflusste der Verlust von Cyclin J den Ablauf der frühen embryonalen Zyklen nicht. Biochemische Analysen identifizierten Cyclin J als Interaktionspartner von Cdk1. Interessanterweise wird Cyclin J jedoch nicht während der Mitose degradiert wie die anderen bekannten Cdk1-Interaktionspartner, die mitotischen Cycline A, B und B3.

Der zweite Teil dieser Arbeit untersucht die Funktion von Mps1, einer Proteinkinase, die bekanntermaßen am Spindelkontrollpunkt (SAC) beteiligt ist. Der SAC verhindert Segregationsfehler der Chromosomen während der Mitose, indem er auf fehlerhafte Verknüpfungen zwischen Kinetochoren und mitotischer Spindel anspricht. Die vorübergehende Anreicherung von Mps1 an Kinetochoren von Prophase bis Metaphase korreliert mit SAC-Aktivität. Daher wurden verschiedene Aspekte der Kinetochor-Lokalisierung von Mps1 in *Drosophila* untersucht. Es wurde gezeigt, dass Mps1-Rekrutierung an die Kinetochore von dessen eigener Kinaseaktivität und teilweise von der SAC-Komponente Mad1, welche in einem Komplex mit Mps1 vorliegt, abhängt. Das Verschwinden von Mps1 von den Kinetochoren vor der Metaphasen-zu-Anaphasen-Transition korreliert nicht mit substantieller Mps1-Degradation oder Veränderungen in dessen N-terminaler Phosphorylierung. Allerdings wurde gezeigt, dass die präzise Kontrolle von Lokalisierung und Menge an Mps1 entscheidend für eine erfolgreiche Mitose ist. Weiterhin deuten meine Untersuchungen darauf hin, dass Mps1 eine bisher unerkannte Funktion haben könnte, die die Schwester-Chromatiden-Trennung in einer SAC-unabhängigen Art und Weise inhibiert.

Thesis Introduction

Cell Cycle Regulation by Cyclin-Cdks and Checkpoints

The mitotic cell cycle aims at the generation of two genetically identical daughter cells. It comprises a highly controlled sequence of well-defined steps that need to be coordinated and to be followed strictly. The success of each step is controlled accurately, before the cell cycle is allowed to proceed. Errors during cell cycle progression result in chromosomal instabilities and aneuploidies on the cellular level and severe diseases on the organismal level. Uncontrolled cell proliferation is the cause of cancer.

Certain **C**yclin-**d**ependent **k**inases (Cdks) are essential for the coordination of the cell cycle events. The activities of these Cdks change during the cell cycle and along with them the phosphorylation patterns of their substrates, which are usually involved in cell cycle processes. Cyclins are important regulators of the Cdks, which are, in complex with the Cdks, essential for Cdk activity and substrate specificity. Besides the level of the Cyclins, the post-translational modification of Cyclin-Cdk complexes, in particular their phosphorylation is equally important for regulation of Cyclin-Cdk activity (Malumbres and Barbacid, 2005; Morgan, 1997).

The first Cyclins were discovered and named because of their periodic abundance during the cell cycle (Evans et al., 1983). A regulated balance between Cyclin synthesis and degradation is the basis for this cycling behavior. The different Cyclin-Cdk complexes regulate each other directly and indirectly, which leads to a precise temporal order of cell cycle events. A system of feedback loops leads to switch-like transitions between the individual cell cycle phases (Morgan, 2007).

Cell cycle checkpoints are points, at which the cell can pause progression through the cell cycle in order to have time for error correction before switching to the next cell cycle phase. They play an important role for the faithful progression through the cell cycle and control in particular entry into S phase, entry into mitosis, and exit from mitosis at the **m**etaphase-to-**a**naphase transition (M/A-transition).

For the entry into mitosis, Cdk1 activity is required (Nurse, 1990). Complexes of Cyclin A, B, and B3 with Cdk1 are formed (Draetta et al., 1989; Gallant and Nigg, 1994; Labbe et al., 1989). Activation of these complexes by removal of inhibitory phosphorylations is necessary to promote entry into mitosis (Gautier et al., 1991; Gould et al., 1990) and the early mitotic events such as chromosome condensation, nuclear envelope break-down and the formation of the mitotic spindle (Lohka, 1989).

At M/A-transition, the activity of Cdk1 decreases abruptly, which initiates mitotic exit. The

mitotic Cyclins are degraded (Peters, 2006). This switch from entry into mitosis to exit from mitosis is controlled by the mitotic checkpoint or **s**pindle **a**ssembly **c**heckpoint (SAC), which senses correct attachment of sister chromatids to the mitotic spindle and thus ensures correct chromosome distribution in anaphase (Musacchio and Salmon, 2007).

Cyclins—Central Regulators of the Cell Cycle

Cyclins fulfill important functions as central activators of the Cdks. Based on sequence comparisons animal Cyclins were classified in several families, of which 3—the A-, B-, and E-type Cyclins—were described to oscillate in a cell cycle dependent manner. Cyclin A, B, and B3 are mitotic Cyclins. In complex with Cdk1 they are required for correct entry in and progression through mitosis. The Cyclin E-Cdk2 complex, in contrast, regulates S phase (Malumbres and Barbacid, 2005).

The cyclic abundance of these Cyclins results from a balance between synthesis and degradation. Degradation of Cyclins is done by the proteasome. Ubiquitination by ubiquitin ligases—**S**kp, **C**ullin, **F**-box containing complexes (SCF) (Ang and Wade Harper, 2005) or the **a**naphase-**p**romoting **c**omplex/**c**yclosome (APC/C) (Peters, 2006)—marks the Cyclins for proteasomal degradation. The mitotic Cyclins are substrates of the APC/C. The regulation of APC/C and mitotic Cyclins is mutually dependent; phosphorylations of the APC/C and its activator Cdc20/Fzy by Cyclin-Cdk complexes are required for Cyclin ubiquitination activity. Thereby, the interaction of Cdk and APC/C activity causes a timely regulated sequence of the individual processes.

The activity of the Cyclin-Cdk complexes is not only determined by their abundance. Activating and inhibiting modifications and interacting proteins regulate the activity of Cyclin-Cdk complexes as well. This permits rapid switching from one cell cycle phase to the next by feedback loops (O'Farrell, 2001).

Drosophila Cell Cycle Regulation by Cyclins

The *Drosophila* system is especially well suited for a genetic characterization of Cyclins since each Cyclin family is represented by a single homologue and genetic manipulations are facile. In vertebrate genomes, each Cyclin family is comprised of several homologues with (partially) redundant functions. Thus *Drosophila* can be considered as a minimal system, which provides certain advantages for investigation, but obviously also some peculiarities. *Drosophila* expresses 3 different mitotic Cyclins—Cyclin A, B, and B3 (Follette and O'Farrell,

1997).

One characteristic of the early *Drosophila* embryo is the extreme speed of the initial division cycles, in which cytokinesis and certain cell cycle phases are skipped. The first 13 mitoses are therefore (almost) completely synchronous divisions of nuclei of a syncytium (Foe and Alberts, 1983). The syncytial cycles are a sequence of S and M phases that are completely controlled by maternally contributed cell cycle regulators. After mitosis 13 cell membranes are formed at once around all the nuclei at the egg surface in a process called cellularization. The following 3 cell cycles of the embryonic epidermis contain indeed a G2 phase, but still lack the G1 phase (McKnight and Miller, 1977). The mitoses are now part of real cell divisions and not synchronous anymore, but the pattern of mitosis in the different epidermal domains is still exactly determined (Foe, 1989). Development and cell cycle regulation are interdependent and influence each other here. The entry into these mitoses is dependent on the transcriptional activation of cdc25/string phosphatase, which removes inhibiting phosphorylations from Cyclin-Cdk1 complexes (Lehner, 1991). While Cyclin-Cdk1 complexes are present in excess, cdc25/string is limiting and the regulation of its expression dictates the spatial and temporal progression of the embryonic cell divisions.

The mitotic Cyclins have partially redundant functions in *Drosophila*—Cyclin A is the only Cyclin that is essential for development to the adult stage (Jacobs et al., 1998; Lehner and O'Farrell, 1989).

Surprisingly, the functions of the mitotic Cyclins in the germline are less redundant, and Cyclin B and B3 are essential for female fertility (Jacobs et al., 1998).

Cyclin J

Cyclin J is a poorly characterized member of the Cyclin family that contains the conserved Cyclin Box, but is otherwise less conserved. The role of Cyclin J for the cell cycle has not been investigated in much detail so far. The Cyclin was found in a Yeast-two-hybrid screen for interactors of Cdk2 in *Drosophila* (Finley et al., 1996). A function during the syncytial divisions was suggested (Kolonin and Finley, 2000).

The existence of Cyclin J homologues in vertebrates, which do not undergo syncytial stages during their development, indicated that its function is not restricted to such insect specific cycles (Malumbres and Barbacid, 2005). Its expression pattern during oogenesis suggests a function during female meiosis or during early development (Kolonin and Finley, 2000).

SAC—Mechanism and Effect

At M/A-transition Cyclin-Cdk1 activity drops abruptly by APC/C mediated degradation of the mitotic Cyclins, which initiates exit from mitosis.

The activation of APC/C does not only result in the degradation of the mitotic Cyclins but also in the degradation of securin, the inhibitor of the protease separase (Peters, 2006). Separase cleaves the sister chromatid cohesion, and thus enables the distribution of the sister chromatids to the two daughter cells in anaphase (Hauf et al., 2001; Uhlmann et al., 1999).

Before the cleavage of sister chromatid cohesion, it has to be ensured that all sister chromatids are correctly connected to the mitotic spindle. For this, the SAC is required: It delays M/A-transition until all chromatids are correctly attached. Then only, the APC/C is activated, and anaphase is allowed to start (Musacchio and Salmon, 2007).

The mechanism by which the SAC discriminates between incorrect and correct attachments, sends the wait-anaphase signal and inhibits the APC/C is not yet understood in all details. It does not only sense the attachment as such, but measures correct attachment by reacting on the tension resulting between sister centromeres only in the case of correct attachment. (Figure 1 illustrates the different kinds of incorrect attachments, which are recognized by the SAC and corrected.) Attachments that do not create tension are destabilized (Nicklas, 1997; Nicklas et al., 2001), which serves as mechanism for error correction (Tanaka et al., 2002). Thus the effects of lack of attachment and lack of tension cannot be clearly separated from each other. Only when tension is generated at all sister centromeres the SAC is silenced and anaphase can start.

The key protein components of the SAC were originally identified by screens in budding yeast and shown later to be conserved from yeast to human. They comprise the **m**itotic **a**rrest **d**eficient 1-3 (Mad) (Li and Murray, 1991) and the **b**udding **u**ninhibited by **b**enomyl 1-3 (Bub) proteins (Hoyt et al., 1991). (For a schematic drawing of protein interactions involved in SAC signaling see Figure 2.)

SAC components are observed to accumulate at centromeric regions of unattached chromatids (Taylor et al., 2004). The trigger resulting in the recruitment of SAC components is not fully understood yet. A cascade of recruitment and amplification seems to participate, which eventually results in the recruitment and activation of the SAC component Mad2. Mad2 in its inactive cytosolic **o**pen conformation (O-Mad2) is activated by interaction with kinetochore localized Mad1/Mad2 dimers, which contain Mad2 in its activated **c**losed conformation (C-Mad2). According to the so called template model O-Mad2 is thereby transferred into its active C-form (De Antoni et al., 2005; Howell et al., 2000; Luo et al., 2002; Sironi et al., 2002).

Interaction of the APC/C with a co-activator—Cdc20/Fizzy or Cdh1/Fizzy-related—is required to trigger its activation. C-Mad2 as well as other effector components of the SAC, like

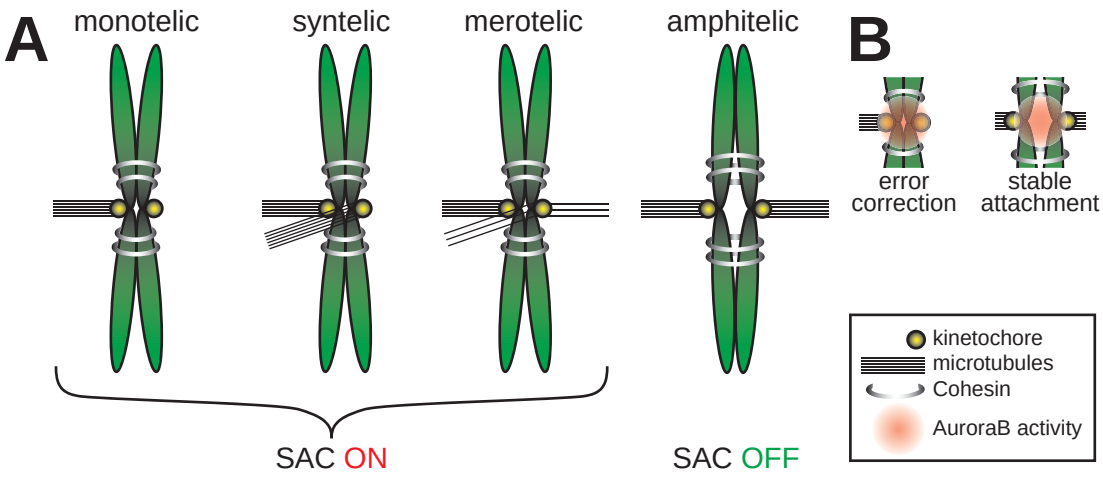

Figure 1. Erroneous and correct attachments between kinetochores and microtubules.
(A) Schematic drawing of single sister chromatid pairs with different types of incorrect attachments that will activate the SAC (SAC ON) and with correct attachments that will silence the SAC (SAC OFF). Monotelic attachment is usually established at first after nuclear envelope break-down. As the search-and-capture process of the mitotic spindle continues, either both sister kinetochores might be captured by microtubules from the same pole (syntelic attachment) or one kinetochore might be captured by microtubules from both poles (merotelic attachment). These attachments do not generate tension between the sister kinetochores and need to be corrected to finally achieve amphitelic attachment or bi-orientation.
(B) The local restriction of AuroraB kinase activity to the inner centromeres allows correction of erroneous attachments. As long as the sister kinetochores are not under tension, AuroraB can phosphorylate distinct kinetochore components, which causes instability of the attachment (*left*). As soon as the sister kinetochores are under tension, these substrates are removed from the activity radius of AuroraB and the attachment is stabilized (*right*).

Bub3 or BubR1, can interact with Cdc20 or APC/C^{Cdc20} respectively, and thereby inhibit APC/C activation (Fang, 2002; Sudakin et al., 2001; Tang et al., 2001). This inhibitory complex is called **m**itotic **c**heckpoint **c**omplex (MCC). It serves as diffusible signal, which transduces and amplifies the wait-anaphase signal. Therefore, a single unattached kinetochore in a cell can stop the whole cell cycle (Rieder et al., 1995).

As soon as the SAC does not sense incorrect attachments anymore, the SAC components disappear from the centromeric regions, probably by Dynein mediated shedding along the spindle microtubules (Howell et al., 2001; Wojcik et al., 2001), Mad2 is not activated any longer, Cdc20 is released, and the APC/C is activated. Then only, Cyclin B and securin are degraded, and anaphase can start (Peters, 2006).

Figure 2. SAC activation and silencing.
Schematic drawing of protein interactions forming the basis of SAC function. This figure is meant to provide an overview over the mechanisms required for SAC activation and SAC silencing with a special focus on suggested Mps1 functions in these processes. Further detailed explanations on the protein interactions are given in the introductions and discussions to part 1 and part 3 of this thesis.

(A) SAC activation at unattached kinetochores: Displayed are SAC component recruitment by interaction with the KMN network, several contributions to SAC induction by MCC formation and stabilization, APC/C inhibition by the MCC, and the effects of APC/C inhibition on Cdk1 and separase activity.

(B) SAC silencing after the establishment of correct attachments: Displayed are interactions of the KNM network and Dynein with the micotubuli, Dynein mediated shedding of SAC components from the kinetochore along the microtubules (the direction of the transport is indicated by the open double arrow), the inhibition of activated Mad2 by p31, APC/C activation by Cdc20, APC/C mediated ubiquitination of securin, Cyclin B and Mps1, activation of separase inducing sister chromatid cohesion cleavage, and inactivation of Cdk1 and Mps1.

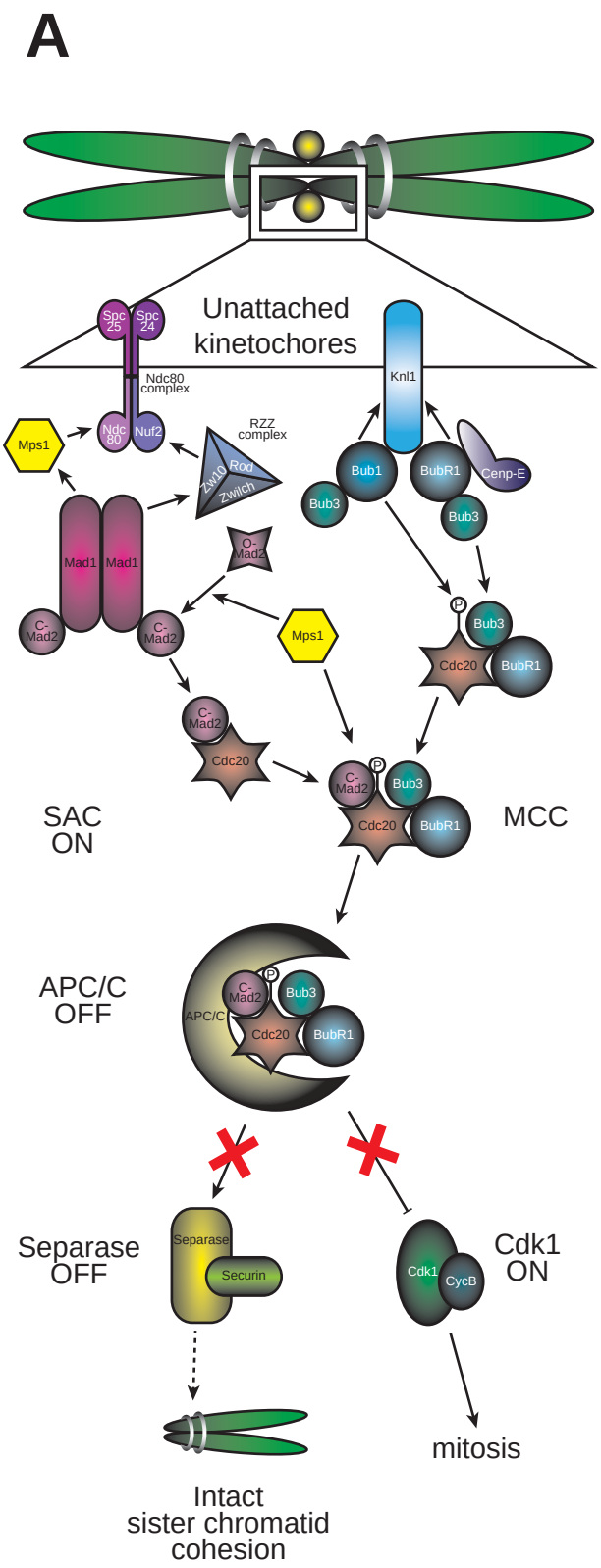

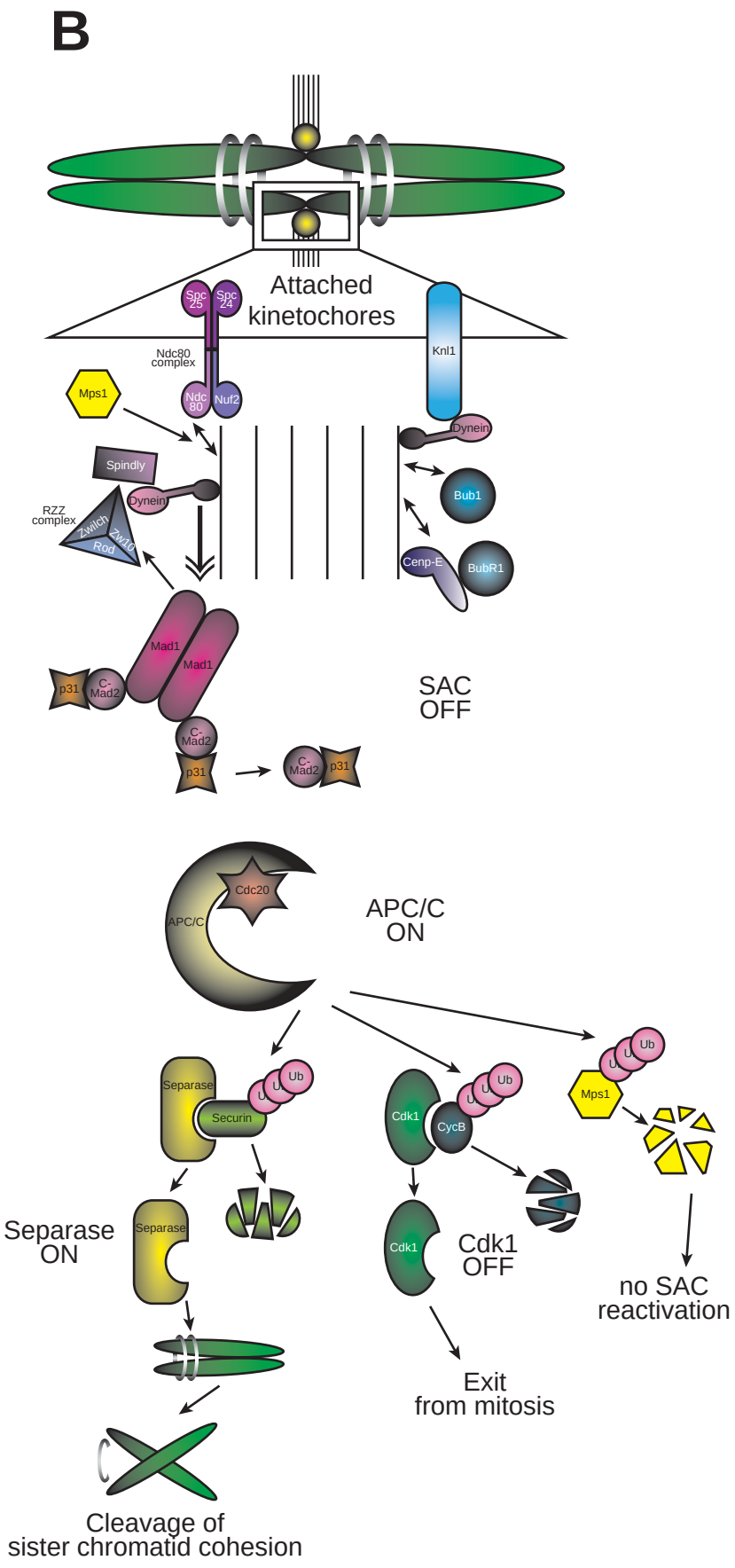
B
Attached kinetochores
Spc 25
Spc 24
Ndc80 complex
Ndc 80
Nuf2
Knl1
Mps1
Spindly
Dynein
RZZ complex
Zwilch
Zw10
Rod
Dynein
Bub1
Cenp-E
BubR1
Mad1
Mad1
p31
C-Mad2
C-Mad2
p31
C-Mad2
p31
SAC OFF
Cdc20
APC/C
APC/C ON
Separase
Ub
Securin
Separase
Separase ON
Cdk1
CycB
Ub
Cdk1
Cdk1 OFF
Mps1
Ub
no SAC reactivation
Exit from mitosis
Cleavage of sister chromatid cohesion

Kinetochore and Mitotic Spindle

As described before, a stable interaction between mitotic spindle and chromatids has to be established before M/A-transition. The mitotic spindle is a highly dynamic structure, comprised of microtubules, which are organized in a bipolar fashion from the spindle poles (yeast) or centrosomes (higher eukaryotes). After nuclear envelope break-down, the spindle microtubules start with a search-and-capture process to quest for attachments of their plus-ends with the kinetochores of the chromatids (Tanaka, 2010).

The kinetochore is a huge protein complex, which assembles at the beginning of mitosis at the centromeric region of each chromatid. It is organized in an inner layer, which resides at the centromere throughout the cell cycle on the basis of a **cen**tromere specific **H**istone **3** variant CenH3 (**Cen**tromere **p**rotein **A**/ **C**entromere **id**entifier: Cenp-A/Cid), which epigenetically marks the centromeres (Dalal and Bui, 2010). At the beginning of mitosis the kinetochore, which consists of several sub-complexes of kinetochore proteins, is assembled. The kinetochore serves as mediator to create stable attachments between sister chromatids and microtubules and thus to arrange for a faithful segregation of the two sister chromatids to the two daughter cells (Cheeseman and Desai, 2008).

Directly associated with this function is the recruitment of SAC components to the centromere/kinetochore, which is most likely required for SAC function and activation. The **K**NL-1/ **M**is12/**N**dc80 (KMN) network, one sub-complex of the kinetochore, is required for for kinetochore recruitment of several SAC components. It consists of 3 parts, **k**inetochore-**n**u**l**-**1**/ ***S**chizosacharomyces **p**ombe* **c**entromere **105** (KNL-1/Spc105), the **h**ighly **e**xpressed in **c**ancer **1**/ **n**uclear **d**ivision **c**ycle **80** (Hec1/Ndc80) complex (with its components Hec1/Ndc80, **nu**clear **f**ilament containing protein **2** (Nuf2), Spc 24 and 25), and the the **m**inichromosome **in**s**t**ability 12 (Mis12) complex (with its components Mis12, **n**ecessary for **n**uclear **f**unction **1** (Nnf1), **N**nf1 **s**ynthetic **l**ethal **1** (Nsl1) and **d**osage **s**uppressor of **N**nf1 1 (Dsn1)) in particular (Cheeseman et al., 2006).

The exact way of how the stable attachment is mediated is not yet clear. In yeast, the Dam1 complex was described, a ring-shaped protein structure on the one hand built around the microtubules, capable of sliding along microtubules, and on the other hand interacting with kinetochore proteins (Miranda et al., 2007; Westermann et al., 2005). In mammalian cells, no similar structure has been identified so far. Nevertheless, the KMN network was suggested to be responsible for this task as well, since Ndc80 and KNL-1/Spc105 interact *in vitro* with microtubules (Cheeseman et al., 2006; Cheeseman et al., 2004; DeLuca et al., 2006; Wei et al., 2007). Furthermore, 2 microtubule motors were shown to reside at the kinetochores, the minus-end directed motor Dynein (Pfarr et al., 1990; Steuer et al., 1990) and the plus-end directed motor Cenp-E (Yen et al., 1992).

A recent model for the establishment of correct attachments says that initially a lateral attachment of kinetochore and microtubules with the help of the kinetochore bound Dynein is formed, which pulls the chromosomes initially towards the poles of the spindle into an area with higher microtubule density (Rieder and Alexander, 1990; Yang et al., 2007). This serves two purposes: first, the probability of contacts of the kinetochores with microtubules is increased, and second, the sister chromatids are arranged in a way that microtubules from the opposite pole can capture the second sister kinetochore more easily because it is facing towards them. Only in a second step the initial lateral attachment is transformed into a stable end-on attachment, which is mediated by Hec1/Ndc80 and KNL-1/Spc105 (Bader and Vaughan, 2010; Cheeseman et al., 2006; Tanaka et al., 2005).

As mentioned before, incorrect attachments can be corrected. The measurement of tension between the two sister kinetochores by AuroraB kinase is supposed to be the key regulator of this process. This kinase is bound to the region between the sister kinetochores by interaction with the other components of the **c**hromosomal **p**assenger **c**omplex (CPC), INCENP, Borealin and Survivin (Adams et al., 2000; Gassmann et al., 2004; Honda et al., 2003; Klein et al., 2006). One of the various substrates of AuroraB is the Ndc80 complex (Cheeseman et al., 2006; DeLuca et al., 2006). Phosphorylation of Ndc80 by AuroraB decreases its interaction with microtubules. As long as the sister kinetochores are not under tension, Ndc80 is close to AuroraB activity and thus phosphorylated. When correct attachment is established, Ndc80 is pulled out of the range of AuroraB activity by the pulling forces of the microtubules, resulting in Ndc80 de-phosphorylation and the stabilization of kinetochore attachment to spindle microtubules (Figure 1). Recently two further members of the KMN network were shown to be AuroraB substrates required for microtubule binding (Welburn et al., 2010).

After correct attachment has been established, SAC components disappear from the kinetochore. This process is thought to be mediated by kinetochore associated Dynein (Howell et al., 2001; Wojcik et al., 2001). SAC components are shed along the spindle microtubules from the kinetochores towards the spindle poles, which is supposed to be relevant for SAC silencing.

The SAC Components Mps1 and Mad1

Mono**p**olar **s**pindles **1** (Mps1) is an essential kinase of the SAC, whose function in the SAC was not recognized initially.

Mps1 was identified as an essential component for spindle pole body duplication in yeast (Winey et al., 1991), hence its name. Only later, its function for the SAC became evident (Weiss and Winey, 1996). The SAC function is better conserved amongst metazoans than its role for centrosome duplication (Abrieu et al., 2001; Fischer et al., 2004; Stucke et al., 2002).

The recent literature attributes several roles to Mps1, like indirect AuroraB regulation for error correction (Jelluma et al., 2008) or interaction with the MCC for its stabilization (Maciejowski et al., 2010). Although several *in vitro* kinase substrates were identified, only few were confirmed *in vivo* (Castillo et al., 2002; Espeut et al., 2008; Hardwick et al., 1996; Holinger et al., 2009; Jelluma et al., 2008; Kemmler et al., 2009; Mattison et al., 2011; Shimogawa et al., 2006; Zhu et al., 2007). The regulation of this non-RD kinase by auto-phosphorylation or additional kinases as well as the relevance of its kinase activity for SAC function are not fully understood (Jelluma et al., 2010; Xu et al., 2009).

A recent model for Mps1 function in the SAC postulates that Mps1 is recruited to kinetochores that are not attached or not under tension in order to assist in error correction and in SAC activation (Jelluma et al., 2008). This function is supposed to require Mps1 dimerization. Mps1 is thought to be activated thereby, and its activation contributes to its own release from the kinetochores in order to stabilize the signal of SAC activation or to silence the SAC (Jelluma et al., 2010).

The kinetochore recruitment of SAC components in general and Mps1 in particular plays a central role in the suggested model of SAC activation. SAC components are activated at the kinetochores, which propagates or stabilizes the signal of the activated SAC. The localization of SAC components to the kinetochore is at least partially interdependent. The concrete dependencies seem to differ partially from system to system and are rather confusing. However, generally Mps1 is considered to be an upstream component, which most other SAC components are dependent on. It was suggested in different systems that Mad1 (Abrieu et al., 2001; Martin-Lluesma et al., 2002), Mad2 (Abrieu et al., 2001; Liu et al., 2003), Bub1 (Sliedrecht et al., 2010; Vigneron et al., 2004), BubR1 (Schmidt et al., 2005; Wong and Fang, 2006), Bub3 (Colombo et al., 2011; Zhao and Chen, 2006), Cenp-E (Hewitt et al., 2010; Vigneron et al., 2004), components of the **Ro**ugh **D**eal-**Z**este-**w**hite **10**-Zwilch (**R**od-**Z**w10-**Z**wilch (RZZ)) complex (Santaguida et al., 2010; Vigneron et al., 2004) and of the APC/C (Vigneron et al., 2004) are dependent on Mps1. However, inconsistent observations were made for almost all of the listed proteins as well (Jelluma et al., 2008; Schmidt et al., 2005; Tighe et al., 2008). In turn only few components were suggested to be required for Mps1 kinetochore recruitment,

such as AuroraB, Bub1 or Cenp-E (Vigneron et al., 2004; Wong and Fang, 2006), and these are controversial as well. Some kinetochore components, like Hec1/Ndc80 or Nuf2, were shown to be required, but for none of them a direct physical interaction with Mps1 was shown (Martin-Lluesma et al., 2002; Stucke et al., 2004).

The dependency of Mad1 kinetochore localization on Mps1 presence was proven in several different systems, although even in this case a contradictive report exist (Schmidt et al., 2005). The scaffold protein Mad1 is another essential component of the SAC (Hardwick and Murray, 1995). In contrast to Mps1, its exclusive function seems to be in the SAC. It was shown that Mad1 is required for the kinetochore recruitment of Mad2 and its activation (Chen et al., 1998; De Antoni et al., 2005; Ikui et al., 2002). Mad1 was shown to be an *in vitro* kinase substrate of Mps1 (Hardwick et al., 1996), the correlation of Mps1 kinase activity and Mad1 phosphorylation indicated an *in vivo* relevance of this interaction.

Spindle Poisons and Their Impact on Research and Clinic

Spindle poisons are chemicals, which interfere with the formation of a functional mitotic spindle and thus activate the SAC. Some spindle poisons induce de-polymerization of the microtubules and thereby disrupt the whole spindle. Colchicine, for example, stimulates the GTPase activity of β-tubulin and thereby causes microtubule disassembly (Ray et al., 1981). Others interfere with the spindle dynamics and stabilize the spindle, such as taxol, which binds to β-tubulin and promotes the formation of highly stable microtubules, which results in an impaired function as well (Lowe et al., 2001).

Spindle poisons are frequently used in research, for example to synchronize cell culture systems in mitosis. The reversible effect of colcemid on spindle polymerization or of the stabilizing effect of taxol are well described and frequently used.

Due to its essential function for genome stability of proliferating cells, the SAC attracts increasing attention in the clinic with regard to cancer treatment as well (Dalton and Yang, 2009; Jackson et al., 2007). Since cancer is caused by a hyper-proliferation of cells, frequent cell division is a common feature of cancer cells. Thus targeting of mitotic cells seems to be a promising approach for cancer therapy.

The spindle poison taxol is used for the treatment of breast cancer since long (Rowinsky and Donehower, 1991). While its mechanism of action on a molecular level is largely understood, its effect on a cellular level has not been studied in detail. Recently, studies in cell culture systems investigated the effects of spindle poisons on living cells in more detail (Brito and Rieder, 2009; Gascoigne and Taylor, 2008). The first effect of a spindle poison is as expected a mitotic arrest. But this arrest is not infinitely stable, and after a certain time

cells are observed that exit from the arrest. Two possibilities of exiting from the arrest have been described: Cells can adapt the SAC even if external circumstances are not favorable for anaphase or they can slip through and exit from mitosis although their SAC had not been silenced (Brito and Rieder, 2006; Rieder and Maiato, 2004).

The exact processes that underlie the two processes are of interest, since they influence directly the survival of the cells after the exit, which is essential when it regards killing hyper-proliferating cells (Brito and Rieder, 2009).

Further research on the consequences of a prolonged SAC activation, and how the mode of action of a spindle poison can influence the exit of the arrest is therefore essential to extend this possibility of cancer treatment.

Meiosis

Meiosis is a special form of cell division in eukaryotes that aims at the formation of haploid gametes. Meiosis is characterized by two successive nuclear divisions—meiosis I and meiosis II—without an intervening S phase. In contrast to mitosis where sister chromatids are separated, during meiosis I both homologous chromosomes associate, exchange parts by homologous recombination (crossover), and are distributed during anaphase I. Meiosis II is more similar to mitosis since in that case sister chromatids are separated.

Like mitosis, meiosis is a strictly regulated process. The influence of the different Cyclin-Cdk complexes on meiosis is not as well understood as in mitosis.

Meiosis specific Cyclins have not been discovered until now. However, for successful meiosis it is required to control the Cdk activity in a way that allows progression from meiosis I to meiosis II without an intervening S phase. To this end, Cdk1 activity must not fall below a certain threshold, which would allow S phase. Nevertheless, APC/C activity has to be induced in a way that activates separase in order to cleave the sister chromatid cohesion in the chromosome arms, which is required to allow exit from meiosis I. Meiosis specific Cyclins would be one possible way of adaptation to the special circumstances during meiosis.

Meiosis and gametogenesis usually go along with each other. The M phases of female meiosis in *Drosophila melanogaster* start at the end of oogenesis and are completed only after fertilization (Spradling, 1993). The mature egg is arrested in metaphase I. *Drosophila* oogenesis takes place in ovarioles. At the tips of the ovarioles in the germarium reside the germline stem cells, which produce with each asymmetric cell division one daughter stem cell, which stays in contact with the stem cell niche, and one differentiating daughter cell, the cystoblast, which starts to proceed through the ovariole while developing. The cystoblast

undergoes four further mitotic divisions, which are accompanied by incomplete cytokineses. Thereby 16 cells are produced, which are connected by ring canals. 15 of these become nurse cells and start endoreduplication cycles by replicating their genome without inserting mitoses, while 1 cell differentiates as oocyte and finally undergoes meiosis. The whole egg chamber is surrounded by a somatic epithelium of follicle cells. The oocyte passes through 14 stages until the maturation is completed; it is stocked with maternal supplies and covered by an egg shell. Towards the end of maturation the oocyte starts the first meiotic division with the germinal vesicle breakdown. Meiosis is arrested at metaphase I and activated at egg deposition. Egg activation resolves the meiotic arrest and leads to the termination of meiosis in the fertilized egg (Page and Orr-Weaver, 1997).

After fusion of the maternal and the paternal pronucleus, the 3 products of female meiosis that are not used for the zygote are arrested in the polar body and finally degraded (Foe et al., 1993).

Thesis Objectives

The Function of Cyclin J during Early Development

The entry into mitotic divisions is regulated by the activity of Cyclin-Cdk1 complexes. In *Drosophila* the three mitotic Cyclins A, B, and B3 are co-expressed during mitotic and meiotic divisions. Their function during mitosis has been well characterized; their expression, localization, and mutant phenotypes have been described (Jacobs et al., 1998; Lehner and O'Farrell, 1989; Lehner and O'Farrell, 1990). They have partially redundant functions during the mitotic cell cycle. Cyclin B and Cyclin B3 are therefore not essential for development to the adult stage. However, all these mitotic Cyclins are required in the female germline for fertility.

It is not understood why all mitotic Cyclins are required in the female germline of *Drosophila*. It is clear, however, that Cyclins have to be controlled in a special way during the meiotic divisions. For example, between the meiotic divisions Cdk1 activity must not decrease below a threshold, at which S phase could be initiated (Iwabuchi et al., 2000; Izawa et al., 2005). In principle, it would not be surprising if the complex meiotic cell cycle control was to include germline specific Cyclins.

Cyclin J, a very poorly characterized Cyclin family member, is a candidate for such a germline specific Cyclin function as it has a restricted expression pattern during oogenesis and in early embryos (Kolonin and Finley, 2000). Based on this expression pattern, it might provide either a meiosis-specific function or work during the special syncytial cycles of early embryogenesis. An initial functional characterization of Cyclin J indeed indicated a requirement during these early syncytial cycles (Kolonin and Finley, 2000).

However, the presence of Cyclin J homologues in vertebrates that do not undergo syncytial divisions during their development suggests that Cyclin J is unlikely to function only during syncytial cell cycles. The function of Cyclin J homologues in mammals has not been characterized so far (Malumbres and Barbacid, 2005).

To study the function of this interesting Cyclin, a genetic approach was therefore started in *Drosophila*. Part 1 of this PhD thesis describes the generation and phenotypic characterization of null mutants. Moreover biochemical approaches were taken to identify the Cdk partner of this Cyclin.

The Influence of Level, Localization, and Activity of Mps1 on the SAC

The function of the SAC is of great interest since it is essential for successful progression through mitosis and error prevention. The interference with correct mitosis by targeting the SAC is an important strategy in cancer treatment (Jackson et al., 2007). When this study was started Mps1 was identified as an essential SAC component not only in *Drosophila* but also in many other species, including humans (Fisk et al., 2004). However, the detailed characterization of its function in the SAC was complicated by its additional involvement in spindle pole body duplication. No SAC relevant *in vivo* kinase substrates and no specific Mps1 kinase inhibitors were known. The regulation of its kinase activity was not clear and interaction partners were unknown.

In vivo imaging of *Drosophila* Mps1 localization and function in the embryo had shown its dynamic localization during the cell cycle (Fischer et al., 2004). The kinetochore recruitment of tagged Mps1 during prometaphase suggested a functional relevance of its localization behavior.

Part 2 of this thesis aimed at the characterization of the relevance of the kinetochore recruitment of Mps1 during prometaphase and shedding before M/A-transition. Conditions that are required for or influence Mps1 kinetochore localization were studied. Moreover, a systematic analysis of the mitotic phenotypes after ectopic SAC induction was initiated to characterize similarities and differences between cultured embryonic *Drosophila* (S2R+) cells (*in vitro*) and embryonic cells in their natural environment of a living organism, the *Drosophila* embryo (*in vivo*).

Thesis Preview

The Function of Cyclin J during Early Development

In order to evaluate the function of *Drosophila* Cyclin J in the female germline, during oogenesis and in the first mitotic divisions, null mutants for *Cyclin J* were generated by creating a small deficiency with defined breakpoints eliminating *Cyclin J* and two neighboring genes. Transgenes that promoted the expression of the neighboring genes under control of their respective cis-regulatory regions were combined with the deficiency in order to study flies that are only missing *Cyclin J* function.

No reduced fertility of *Cyclin J* mutant females and no increase in X-X non-disjunction during female meiosis or impaired progression through early mitoses were observed. These results are in contradiction with the previously observed disturbance of syncytial nuclear divisions by injection of aptamers and antibodies against Cyclin J into *Drosophila* embryos (Kolonin and Finley, 2000). A possible explanation for the obvious discrepancies might be that the injected reagents might cross-react with unrelated proteins instead of just blocking Cyclin J function.

N- and C-terminally EGFP-tagged versions of Cyclin J were expressed under control of its cis-regulatory region in order to study its abundance and localization. An accumulation of tagged Cyclin J in the germinal vesicle of the oocyte was observed from the beginning of oogenesis until stage 12. After germinal vesicle breakdown, no localized, tagged Cyclin J was detected anymore. Moreover, by immunoblotting a decrease in overall protein abundance from stage 12 to stage 14 was observed. These data argue for a non-essential function of Cyclin J during early oogenesis, while late functions during the metaphase I arrest or during completion of meiosis after egg activation and fertilization appear less likely.

Analysis of co-immunoprecipitation by mass spectrometry or western blotting revealed an interaction of Cyclin J with Cdk1 but not with Cdk2. Nevertheless, a mitotic degradation, as observed with all known mitotic Cyclins, which interact with Cdk1, was not observed.

These results are also in conflict with previous work (Finley et al., 1996), where Cyclin J was identified originally as a Cdk2 interactor in a yeast two hybrid screen. However, the number of false positive interactions found in yeast two hybrid assays is up to ~70% (Deane et al., 2002). Tellingly, the interaction between *Drosophila* Cyclin E and Cdk1 that was found in the same screen, is also different from the Cyclin E-Cdk2 preference *in vivo* (Finley and Brent, 1994; Knoblich et al., 1994). The yeast two hybrid results in the case of Cyclin J were also claimed to be confirmed by CoIP experiments (Kolonin and Finley, 2000), which were however misled presumably by an unspecific cross-reaction of the employed antibody with a

protein of similar molecular weight as Cyclin J.

The studies presented in part 2 of this thesis involve the use of tagged Cyclin J variants that could not be proven to be functional due to the lack of a Cyclin J mutant phenotype, which could have been rescued. Nevertheless, since all results were consistently obtained with both the N-terminal as well as the C-terminal tag, and EGFP-tagging of Cyclins was not reported to affect their function, the Cyclin J-Cdk interaction described here is likely to be reliable.

The Influence of Level, Localization, and Activity of Mps1 on the SAC

In part 3 it is shown that the SAC kinase Mps1 in *Drosophila* is phosphorylated during M phase like in many other organisms (Abrieu et al., 2001; Douville et al., 1992; Stucke et al., 2002; Winey et al., 1991). De-phosphorylation with λ-phosphatase removed an electrophoretic mobility shift of Mps1 during mitosis to the interphase level. The modification that is applied at the N-terminal, supposedly regulatory domain is present throughout mitosis as shown by immunoblotting using precisely staged syncytial embryos. Thus the detectable phosphorylation pattern does not correlate with SAC activity. The presented data, however, cannot exclude modifications that do not influence the electrophoretic mobility of Mps1 (Mattison et al., 2007).

By immunoblotting no substantial Mps1 degradation was detected during progression through mitosis, indicating that in *Drosophila* a decrease of Mps1 protein levels is not required for SAC silencing during exit from mitosis.

These results on *Drosophila* Mps1 regulation differ from published data concerning human and yeast Mps1. In these systems, Mps1 degradation was suggested to be required for normal exit from mitosis (Cui et al., 2010; Palframan et al., 2006).

In contrast to protein level and phosphorylation pattern of Mps1, its localization behavior correlates with SAC activity indicating a functional relevance (Fischer et al., 2004). Investigation of EGFP-tagged Mps1 variants in *Mps1* null mutant embryos showed that kinetochore recruitment of Mps1 requires both major domains, the N-terminal regulatory and the C-terminal kinase domain, as well as its kinase activity. Co-immunoprecipitation of tagged Mps1 domains showed that Mps1 self-interacts via its C-terminal domain, even in the absence of Mps1 kinase activity. The detectable phosphorylation at the N-terminal domain was not caused by auto-phosphorylation since it was found to be present even in *Mps1* mutant embryos.

The results on *Drosophila* Mps1 localization are in conflict with some reports from human cells, which indicate that the N-terminal domain is required and sufficient for Mps1 kinetochore recruitment (Stucke et al., 2004). Moreover, it has been suggested that in human cells Mps1 kinase activity is required for Mps1 shedding before onset of anaphase (Hewitt et al., 2010) rather than for kinetochore localization as in *Drosophila*. These discrepancies might re-

flect species-specific or experimental differences. The studies in human cell culture involved chemical inhibitors and RNAi, which can both lead to unexpected side effects in principle and incomplete inhibition.

An approach combining co-immunoprecipitation and mass spectrometry identified the SAC component Mad1 as interaction partner of Mps1. The study of EGFP-tagged Mad1 and Mps1 versions in the respective null mutant embryos showed the kinetochore recruitment of both proteins to be dependent on each other and at least partially on Mad2.

The interaction of Mps1 with Mad1 has been postulated for long, although a physical interaction had not been proven (Hardwick et al., 1996). The finding that Mps1 is required for Mad1 recruitment was therefore not unexpected (Abrieu et al., 2001; Hewitt et al., 2010; Jelluma et al., 2008; Liu et al., 2003; Maciejowski et al., 2010; Martin-Lluesma et al., 2002; Santaguida et al., 2010; Sliedrecht et al., 2010; Tighe et al., 2008; Vigneron et al., 2004; Wong and Fang, 2006; Zhao and Chen, 2006). However, the requirement of Mad2 for Mad1 localization was not reported yet, and seems to be in conflict with the conventional model of linear recruitment of SAC components. Nevertheless, the observation can be brought in line when considering that Mad1 and Mad2 form a tight dimer, which might be recruited preferentially to the kinetochore.

If Mps1's kinetochore presence is required for SAC activation, its disappearance is likely relevant for SAC silencing. To test this assumption, Mps1 versions fused to a constitutive kinetochore targeting domain were created. Expression of these fusion proteins in cellularized *Drosophila* embryos resulted in a kinase activity dependent, aberrant exit from mitosis, reinforcing that correct Mps1 localization is indeed required for successful exit from mitosis, but not supporting the assumption that shedding of Mps1 is required for SAC silencing and the initial onset of anaphase. The observation that an inhibition of Mps1 shedding from the kinetochore does not interfere with the timing of mitotic progression was surprising and differs from very recent data obtained with human cells (Jelluma et al., 2010) presumably because of technical differences. Studies on the *Drosophila* kinetochore were performed in order to find further and more appropriate constitutive kinetochore proteins in *Drosophila* (Schittenhelm et al., 2010; Schittenhelm et al., 2007, see Appendix 1 and 2).

Mps1 over-expression was found to interfere with the correct timing of anaphase onset and exit from mitosis as shown by *in vivo* imaging of cellularized *Drosophila* embryos expressing fluorescent marker proteins labeling chromosomes, microtubules, and kinetochores. Metaphase was prolonged by ~5-fold, velocity of kinetochore movements in anaphase was slowed down, and the survival of embryos was reduced. Not only was the timing of the metaphase delay shown to be dependent on Mad2, also the success of chromosome distribution during anaphase, kinetochore movements in anaphase, and finally survival of embryos was strongly affected by Mps1 over-expression in *mad2* mutants. These results reveal a role of

Mps1 beyond the induction of the SAC.

Mps1 over-expression was shown previously to cause a mitotic arrest in yeast (Hardwick et al., 1996) but not in human cells. Thus the over-expression effect in *Drosophila* was partially surprising. Elimination of Mad2 at the same time leads to a reduced survival of the yeast cells. However, the lethality induced by Mps1 over-expression in *mad2* mutant yeast was suggested previously to be due to interference with the spindle pole body duplication activity of Mps1 (Hardwick et al., 1996). The careful comparison of Mps1 over-expression in the wild type as well as in the *mad2* mutant situation by the *in vivo* imaging presented here suggests a different explanation and raises the possibility of a direct influence of Mps1 on sister chromatid cohesion and its removal at the metaphase-to-anaphase transition. Activated Mps1 might interfere with separase activation or cohesin cleavage, which would explain the slower anaphase movements with the higher effort that is required in order to break apart the residual cohesion after the metaphase arrest. The final (partial) success of anaphase in SAC competent *mad2*$^{+}$ cells over-expressing Mps1 would be explained by cohesion fatigue during the prolonged metaphase. The analysis of the proposed Separase inhibition by Mps1 will require additional work that might establish a more complex interaction between cohesion and Mps1 than presently considered. So far, premature loss of sister chromatid cohesion has been shown to activate the SAC (Mirchenko and Uhlmann, 2010; Oliveira et al., 2010; Pauli et al., 2008; Toyoda and Yanagida, 2006, see also Appendix 3), and conversely, the SAC is known to prevent premature sister separation by preventing securin degradation (Peters, 2006). A SAC independent inhibition of Separase by Mps1 might provide additional protection against chromosomal instability during mitosis.

Finally, the effects of differently induced SAC arrests were compared in cultured embryonic *Drosophila* (S2R+) cells and in living *Drosophila* embryos with special attention to the way and timing of the exit from the arrests. The results show a significant difference between the behavior of cultured cells and cells in the environment of the living organism. This reinforces the cautious interpretation of results from cell culture experiments with regard to mitotic issues. Their transferability to living organisms is not ensured. This finding further emphasizes that the results from SAC studies with cultured cells might have limited validity for the responses *in vivo*.

References

Abrieu, A., Magnaghi-Jaulin, L., Kahana, J. A., Peter, M., Castro, A., Vigneron, S., Lorca, T., Cleveland, D. W., Labbe, J. C., 2001. Mps1 is a kinetochore-associated kinase essential for the vertebrate mitotic checkpoint. Cell. 106**,** 83-93.

Adams, R. R., Wheatley, S. P., Gouldsworthy, A. M., Kandels-Lewis, S. E., Carmena, M., Smythe, C., Gerloff, D. L., Earnshaw, W. C., 2000. INCENP binds the Aurora-related kinase AIRK2 and is required to target it to chromosomes, the central spindle and cleavage furrow. Curr Biol. 10**,** 1075-8.

Ang, X. L., Wade Harper, J., 2005. SCF-mediated protein degradation and cell cycle control. Oncogene. 24**,** 2860-70.

Bader, J. R., Vaughan, K. T., 2010. Dynein at the kinetochore: Timing, Interactions and Functions. Semin Cell Dev Biol. 21**,** 269-75.

Brito, D. A., Rieder, C. L., 2006. Mitotic checkpoint slippage in humans occurs via cyclin B destruction in the presence of an active checkpoint. Curr Biol. 16**,** 1194-200.

Brito, D. A., Rieder, C. L., 2009. The ability to survive mitosis in the presence of microtubule poisons differs significantly between human nontransformed (RPE-1) and cancer (U2OS, HeLa) cells. Cell Motil Cytoskeleton. 66**,** 437-47.

Castillo, A. R., Meehl, J. B., Morgan, G., Schutz-Geschwender, A., Winey, M., 2002. The yeast protein kinase Mps1p is required for assembly of the integral spindle pole body component Spc42p. J Cell Biol. 156**,** 453-65.

Cheeseman, I. M., Chappie, J. S., Wilson-Kubalek, E. M., Desai, A., 2006. The conserved KMN network constitutes the core microtubule-binding site of the kinetochore. Cell. 127**,** 983-97.

Cheeseman, I. M., Desai, A., 2008. Molecular architecture of the kinetochore-microtubule interface. Nat Rev Mol Cell Biol. 9**,** 33-46.

Cheeseman, I. M., Niessen, S., Anderson, S., Hyndman, F., Yates, J. R., 3rd, Oegema, K., Desai, A., 2004. A conserved protein network controls assembly of the outer kinetochore and its ability to sustain tension. Genes Dev. 18**,** 2255-68.

Chen, R. H., Shevchenko, A., Mann, M., Murray, A. W., 1998. Spindle checkpoint protein Xmad1 recruits Xmad2 to unattached kinetochores. J Cell Biol. 143**,** 283-95.

Colombo, R., Caldarelli, M., Mennecozzi, M., Giorgini, M. L., Sola, F., Cappella, P., Perrera, C., Depaolini, S. R., Rusconi, L., Cucchi, U., Avanzi, N., Bertrand, J. A., Bossi, R. T., Pesenti, E., Galvani, A., Isacchi, A., Colotta, F., Donati, D., Moll, J., 2011. Targeting the mitotic checkpoint for cancer therapy with NMS-P715, an inhibitor of MPS1 kinase. Cancer Res. 70**,** 10255-64.

Cui, Y., Cheng, X., Zhang, C., Zhang, Y., Li, S., Wang, C., Guadagno, T. M., 2010. Degradation of the human mitotic checkpoint kinase Mps1 is cell cycle-regulated by APC-cCdc20 and APC-cCdh1 ubiquitin ligases. J Biol Chem. 285**,** 32988-98.

Dalal, Y., Bui, M., 2010. Down the rabbit hole of centromere assembly and dynamics. Curr Opin Cell Biol. 22**,** 392-402.

Dalton, W. B., Yang, V. W., 2009. Role of prolonged mitotic checkpoint activation in the formation and treatment of cancer. Future Oncol. 5**,** 1363-70.

De Antoni, A., Pearson, C. G., Cimini, D., Canman, J. C., Sala, V., Nezi, L., Mapelli, M., Sironi, L., Faretta, M., Salmon, E. D., Musacchio, A., 2005. The Mad1/Mad2 complex as a template for Mad2 activation in the spindle assembly checkpoint. Curr Biol. 15**,** 214-

25.

Deane, C. M., Salwinski, L., Xenarios, I., Eisenberg, D., 2002. Protein interactions: two methods for assessment of the reliability of high throughput observations. Mol Cell Proteomics. 1**,** 349-56.

DeLuca, J. G., Gall, W. E., Ciferri, C., Cimini, D., Musacchio, A., Salmon, E. D., 2006. Kinetochore microtubule dynamics and attachment stability are regulated by Hec1. Cell. 127**,** 969-82.

Douville, E. M., Afar, D. E., Howell, B. W., Letwin, K., Tannock, L., Ben-David, Y., Pawson, T., Bell, J. C., 1992. Multiple cDNAs encoding the esk kinase predict transmembrane and intracellular enzyme isoforms. Mol Cell Biol. 12**,** 2681-9.

Draetta, G., Luca, F., Westendorf, J., Brizuela, L., Ruderman, J., Beach, D., 1989. Cdc2 protein kinase is complexed with both cyclin A and B: evidence for proteolytic inactivation of MPF. Cell. 56**,** 829-38.

Espeut, J., Gaussen, A., Bieling, P., Morin, V., Prieto, S., Fesquet, D., Surrey, T., Abrieu, A., 2008. Phosphorylation relieves autoinhibition of the kinetochore motor Cenp-E. Mol Cell. 29**,** 637-43.

Evans, T., Rosenthal, E. T., Youngblom, J., Distel, D., Hunt, T., 1983. Cyclin: a protein specified by maternal mRNA in sea urchin eggs that is destroyed at each cleavage division. Cell. 33**,** 389-96.

Fang, G., 2002. Checkpoint protein BubR1 acts synergistically with Mad2 to inhibit anaphase-promoting complex. Mol Biol Cell. 13**,** 755-66.

Finley, R. L., Jr., Brent, R., 1994. Interaction mating reveals binary and ternary connections between Drosophila cell cycle regulators. Proc Natl Acad Sci U S A. 91**,** 12980-4.

Finley, R. L., Jr., Thomas, B. J., Zipursky, S. L., Brent, R., 1996. Isolation of Drosophila cyclin D, a protein expressed in the morphogenetic furrow before entry into S phase. Proc Natl Acad Sci U S A. 93**,** 3011-5.

Fischer, M. G., Heeger, S., Hacker, U., Lehner, C. F., 2004. The mitotic arrest in response to hypoxia and of polar bodies during early embryogenesis requires Drosophila Mps1. Curr Biol. 14**,** 2019-24.

Fisk, H. A., Mattison, C. P., Winey, M., 2004. A field guide to the Mps1 family of protein kinases. Cell Cycle. 3**,** 439-42.

Foe, V. E., 1989. Mitotic domains reveal early commitment of cells in Drosophila embryos. Development. 107**,** 1-22.

Foe, V. E., Alberts, B. M., 1983. Studies of nuclear and cytoplasmic behaviour during the five mitotic cycles that precede gastrulation in Drosophila embryogenesis. J Cell Sci. 61**,** 31-70.

Foe, V. E., Odell, G. M., Edgar, B. A., Mitosis and morphogenesis in the Drosophila embryo: point and counterpoint. In: M. Bate, A. M. Arias, Eds.), The development of Drosophila melanogaster. Cold Spring Harbor Laboratory Press, Cold Spring Harbor, NY, 1993, pp. 149-300.

Follette, P. J., O'Farrell, P. H., 1997. Cdks and the Drosophila cell cycle. Curr Opin Genet Dev. 7**,** 17-22.

Gallant, P., Nigg, E. A., 1994. Identification of a novel vertebrate cyclin: cyclin B3 shares properties with both A- and B-type cyclins. Embo J. 13**,** 595-605.

Gascoigne, K. E., Taylor, S. S., 2008. Cancer cells display profound intra- and interline variation following prolonged exposure to antimitotic drugs. Cancer Cell. 14**,** 111-22.

Gassmann, R., Carvalho, A., Henzing, A. J., Ruchaud, S., Hudson, D. F., Honda, R., Nigg, E.

A., Gerloff, D. L., Earnshaw, W. C., 2004. Borealin: a novel chromosomal passenger required for stability of the bipolar mitotic spindle. J Cell Biol. 166**,** 179-91.

Gautier, J., Solomon, M. J., Booher, R. N., Bazan, J. F., Kirschner, M. W., 1991. cdc25 is a specific tyrosine phosphatase that directly activates p34cdc2. Cell. 67**,** 197-211.

Gould, K. L., Moreno, S., Tonks, N. K., Nurse, P., 1990. Complementation of the mitotic activator, p80cdc25, by a human protein-tyrosine phosphatase. Science. 250**,** 1573-6.

Hardwick, K. G., Murray, A. W., 1995. Mad1p, a phosphoprotein component of the spindle assembly checkpoint in budding yeast. J Cell Biol. 131**,** 709-20.

Hardwick, K. G., Weiss, E., Luca, F. C., Winey, M., Murray, A. W., 1996. Activation of the budding yeast spindle assembly checkpoint without mitotic spindle disruption. Science. 273**,** 953-6.

Hauf, S., Waizenegger, I. C., Peters, J. M., 2001. Cohesin cleavage by separase required for anaphase and cytokinesis in human cells. Science. 293**,** 1320-3.

Hewitt, L., Tighe, A., Santaguida, S., White, A. M., Jones, C. D., Musacchio, A., Green, S., Taylor, S. S., 2010. Sustained Mps1 activity is required in mitosis to recruit O-Mad2 to the Mad1-C-Mad2 core complex. J Cell Biol. 190**,** 25-34.

Holinger, E. P., Old, W. M., Giddings, T. H., Jr., Wong, C., Yates, J. R., 3rd, Winey, M., 2009. Budding yeast centrosome duplication requires stabilization of Spc29 via Mps1-mediated phosphorylation. J Biol Chem. 284**,** 12949-55.

Honda, R., Korner, R., Nigg, E. A., 2003. Exploring the functional interactions between Aurora B, INCENP, and survivin in mitosis. Mol Biol Cell. 14**,** 3325-41.

Howell, B. J., Hoffman, D. B., Fang, G., Murray, A. W., Salmon, E. D., 2000. Visualization of Mad2 dynamics at kinetochores, along spindle fibers, and at spindle poles in living cells. J Cell Biol. 150**,** 1233-50.

Howell, B. J., McEwen, B. F., Canman, J. C., Hoffman, D. B., Farrar, E. M., Rieder, C. L., Salmon, E. D., 2001. Cytoplasmic dynein/dynactin drives kinetochore protein transport to the spindle poles and has a role in mitotic spindle checkpoint inactivation. J Cell Biol. 155**,** 1159-72.

Hoyt, M. A., Totis, L., Roberts, B. T., 1991. S. cerevisiae genes required for cell cycle arrest in response to loss of microtubule function. Cell. 66**,** 507-17.

Ikui, A. E., Furuya, K., Yanagida, M., Matsumoto, T., 2002. Control of localization of a spindle checkpoint protein, Mad2, in fission yeast. J Cell Sci. 115**,** 1603-10.

Iwabuchi, M., Ohsumi, K., Yamamoto, T. M., Sawada, W., Kishimoto, T., 2000. Residual Cdc2 activity remaining at meiosis I exit is essential for meiotic M-M transition in Xenopus oocyte extracts. Embo J. 19**,** 4513-23.

Izawa, D., Goto, M., Yamashita, A., Yamano, H., Yamamoto, M., 2005. Fission yeast Mes1p ensures the onset of meiosis II by blocking degradation of cyclin Cdc13p. Nature. 434**,** 529-33.

Jackson, J. R., Patrick, D. R., Dar, M. M., Huang, P. S., 2007. Targeted anti-mitotic therapies: can we improve on tubulin agents? Nat Rev Cancer. 7**,** 107-17.

Jacobs, H. W., Knoblich, J. A., Lehner, C. F., 1998. Drosophila Cyclin B3 is required for female fertility and is dispensable for mitosis like Cyclin B. Genes Dev. 12**,** 3741-51.

Jelluma, N., Brenkman, A. B., van den Broek, N. J., Cruijsen, C. W., van Osch, M. H., Lens, S. M., Medema, R. H., Kops, G. J., 2008. Mps1 phosphorylates Borealin to control Aurora B activity and chromosome alignment. Cell. 132**,** 233-46.

Jelluma, N., Dansen, T. B., Sliedrecht, T., Kwiatkowski, N. P., Kops, G. J., 2010. Release of Mps1 from kinetochores is crucial for timely anaphase onset. J Cell Biol. 191**,** 281-90.

Kemmler, S., Stach, M., Knapp, M., Ortiz, J., Pfannstiel, J., Ruppert, T., Lechner, J., 2009. Mimicking Ndc80 phosphorylation triggers spindle assembly checkpoint signalling. Embo J. 28, 1099-110.

Klein, U. R., Nigg, E. A., Gruneberg, U., 2006. Centromere targeting of the chromosomal passenger complex requires a ternary subcomplex of Borealin, Survivin, and the N-terminal domain of INCENP. Mol Biol Cell. 17, 2547-58.

Knoblich, J. A., Sauer, K., Jones, L., Richardson, H., Saint, R., Lehner, C. F., 1994. Cyclin E controls S phase progression and its down-regulation during Drosophila embryogenesis is required for the arrest of cell proliferation. Cell. 77, 107-20.

Kolonin, M. G., Finley, R. L., Jr., 2000. A role for cyclin J in the rapid nuclear division cycles of early Drosophila embryogenesis. Dev Biol. 227, 661-72.

Labbe, J. C., Capony, J. P., Caput, D., Cavadore, J. C., Derancourt, J., Kaghad, M., Lelias, J. M., Picard, A., Doree, M., 1989. MPF from starfish oocytes at first meiotic metaphase is a heterodimer containing one molecule of cdc2 and one molecule of cyclin B. Embo J. 8, 3053-8.

Lehner, C. F., 1991. Pulling the string: cell cycle regulation during Drosophila development. Semin Cell Biol. 2, 223-31.

Lehner, C. F., O'Farrell, P. H., 1989. Expression and function of Drosophila cyclin A during embryonic cell cycle progression. Cell. 56, 957-68.

Lehner, C. F., O'Farrell, P. H., 1990. The roles of Drosophila cyclins A and B in mitotic control. Cell. 61, 535-47.

Li, R., Murray, A. W., 1991. Feedback control of mitosis in budding yeast. Cell. 66, 519-31.

Liu, S. T., Chan, G. K., Hittle, J. C., Fujii, G., Lees, E., Yen, T. J., 2003. Human MPS1 kinase is required for mitotic arrest induced by the loss of CENP-E from kinetochores. Mol Biol Cell. 14, 1638-51.

Lohka, M. J., 1989. Mitotic control by metaphase-promoting factor and cdc proteins. J Cell Sci. 92 (Pt 2), 131-5.

Lowe, J., Li, H., Downing, K. H., Nogales, E., 2001. Refined structure of alpha beta-tubulin at 3.5 A resolution. J Mol Biol. 313, 1045-57.

Luo, X., Tang, Z., Rizo, J., Yu, H., 2002. The Mad2 spindle checkpoint protein undergoes similar major conformational changes upon binding to either Mad1 or Cdc20. Mol Cell. 9, 59-71.

Maciejowski, J., George, K. A., Terret, M. E., Zhang, C., Shokat, K. M., Jallepalli, P. V., 2010. Mps1 directs the assembly of Cdc20 inhibitory complexes during interphase and mitosis to control M phase timing and spindle checkpoint signaling. J Cell Biol. 190, 89-100.

Malumbres, M., Barbacid, M., 2005. Mammalian cyclin-dependent kinases. Trends Biochem Sci. 30, 630-41.

Martin-Lluesma, S., Stucke, V. M., Nigg, E. A., 2002. Role of Hec1 in spindle checkpoint signaling and kinetochore recruitment of Mad1/Mad2. Science. 297, 2267-70.

Mattison, C. P., Old, W. M., Steiner, E., Huneycutt, B. J., Resing, K. A., Ahn, N. G., Winey, M., 2007. Mps1 activation loop autophosphorylation enhances kinase activity. J Biol Chem. 282, 30553-61.

Mattison, C. P., Stumpff, J., Wordeman, L., Winey, M., 2011. Mip1 associates with both the Mps1 kinase and actin, and is required for cell cortex stability and anaphase spindle positioning. Cell Cycle. 10, 783-93.

McKnight, S. L., Miller, O. L., Jr., 1977. Electron microscopic analysis of chromatin replication

in the cellular blastoderm Drosophila melanogaster embryo. Cell. 12**,** 795-804.

Miranda, J. J., King, D. S., Harrison, S. C., 2007. Protein arms in the kinetochore-microtubule interface of the yeast DASH complex. Mol Biol Cell. 18**,** 2503-10.

Mirchenko, L., Uhlmann, F., 2010. Sli15(INCENP) dephosphorylation prevents mitotic checkpoint reengagement due to loss of tension at anaphase onset. Curr Biol. 20**,** 1396-401.

Morgan, D. O., 1997. Cyclin-dependent kinases: engines, clocks, and microprocessors. Annu Rev Cell Dev Biol. 13**,** 261-91.

Morgan, D. O., 2007. The Cell Cycle: Principles of Control. New Science Press, London.

Musacchio, A., Salmon, E. D., 2007. The spindle-assembly checkpoint in space and time. Nat Rev Mol Cell Biol. 8**,** 379-93.

Nicklas, R. B., 1997. How cells get the right chromosomes. Science. 275**,** 632-7.

Nicklas, R. B., Waters, J. C., Salmon, E. D., Ward, S. C., 2001. Checkpoint signals in grasshopper meiosis are sensitive to microtubule attachment, but tension is still essential. J Cell Sci. 114**,** 4173-83.

Nurse, P., 1990. Universal control mechanism regulating onset of M-phase. Nature. 344**,** 503-8.

O'Farrell, P. H., 2001. Triggering the all-or-nothing switch into mitosis. Trends Cell Biol. 11**,** 512-9.

Oliveira, R. A., Hamilton, R. S., Pauli, A., Davis, I., Nasmyth, K., 2010. Cohesin cleavage and Cdk inhibition trigger formation of daughter nuclei. Nat Cell Biol. 12**,** 185-92.

Page, A. W., Orr-Weaver, T. L., 1997. Activation of the meiotic divisions in Drosophila oocytes. Dev Biol. 183**,** 195-207.

Palframan, W. J., Meehl, J. B., Jaspersen, S. L., Winey, M., Murray, A. W., 2006. Anaphase inactivation of the spindle checkpoint. Science. 313**,** 680-4.

Pauli, A., Althoff, F., Oliveira, R. A., Heidmann, S., Schuldiner, O., Lehner, C. F., Dickson, B. J., Nasmyth, K., 2008. Cell-type-specific TEV protease cleavage reveals cohesin functions in Drosophila neurons. Dev Cell. 14**,** 239-51.

Peters, J. M., 2006. The anaphase promoting complex/cyclosome: a machine designed to destroy. Nat Rev Mol Cell Biol. 7**,** 644-56.

Pfarr, C. M., Coue, M., Grissom, P. M., Hays, T. S., Porter, M. E., McIntosh, J. R., 1990. Cytoplasmic dynein is localized to kinetochores during mitosis. Nature. 345**,** 263-5.

Ray, K., Bhattacharyya, B., Biswas, B. B., 1981. Role of B-ring of colchicine in its binding to tubulin. J Biol Chem. 256**,** 6241-4.

Rieder, C. L., Alexander, S. P., 1990. Kinetochores are transported poleward along a single astral microtubule during chromosome attachment to the spindle in newt lung cells. J Cell Biol. 110**,** 81-95.

Rieder, C. L., Cole, R. W., Khodjakov, A., Sluder, G., 1995. The checkpoint delaying anaphase in response to chromosome monoorientation is mediated by an inhibitory signal produced by unattached kinetochores. J Cell Biol. 130**,** 941-8.

Rieder, C. L., Maiato, H., 2004. Stuck in division or passing through: what happens when cells cannot satisfy the spindle assembly checkpoint. Dev Cell. 7**,** 637-51.

Rowinsky, E. K., Donehower, R. C., 1991. Taxol: twenty years later, the story unfolds. J Natl Cancer Inst. 83**,** 1778-81.

Santaguida, S., Tighe, A., D'Alise, A. M., Taylor, S. S., Musacchio, A., 2010. Dissecting the role of MPS1 in chromosome biorientation and the spindle checkpoint through the

small molecule inhibitor reversine. J Cell Biol. 190**,** 73-87.

Schittenhelm, R. B., Althoff, F., Heidmann, S., Lehner, C. F., 2010. Detrimental incorporation of excess Cenp-A/Cid and Cenp-C into Drosophila centromeres is prevented by limiting amounts of the bridging factor Cal1. J Cell Sci. 123**,** 3768-79.

Schittenhelm, R. B., Heeger, S., Althoff, F., Walter, A., Heidmann, S., Mechtler, K., Lehner, C. F., 2007. Spatial organization of a ubiquitous eukaryotic kinetochore protein network in Drosophila chromosomes. Chromosoma. 116**,** 385-402.

Schmidt, M., Budirahardja, Y., Klompmaker, R., Medema, R. H., 2005. Ablation of the spindle assembly checkpoint by a compound targeting Mps1. EMBO Rep. 6**,** 866-72.

Shimogawa, M. M., Graczyk, B., Gardner, M. K., Francis, S. E., White, E. A., Ess, M., Molk, J. N., Ruse, C., Niessen, S., Yates, J. R., 3rd, Muller, E. G., Bloom, K., Odde, D. J., Davis, T. N., 2006. Mps1 phosphorylation of Dam1 couples kinetochores to microtubule plus ends at metaphase. Curr Biol. 16**,** 1489-501.

Sironi, L., Mapelli, M., Knapp, S., De Antoni, A., Jeang, K. T., Musacchio, A., 2002. Crystal structure of the tetrameric Mad1-Mad2 core complex: implications of a 'safety belt' binding mechanism for the spindle checkpoint. Embo J. 21**,** 2496-506.

Sliedrecht, T., Zhang, C., Shokat, K. M., Kops, G. J., 2010. Chemical genetic inhibition of Mps1 in stable human cell lines reveals novel aspects of Mps1 function in mitosis. PLoS One. 5**,** e10251.

Spradling, A. C., Developmental genetics of oogenesis. In: M. Bate, A. M. Arias, Eds.), The development of Drosophila melanogaster. Cold Spring Harbor Laboratory Press, Cold Spring Harbor, NY, 1993, pp. 1-70.

Steuer, E. R., Wordeman, L., Schroer, T. A., Sheetz, M. P., 1990. Localization of cytoplasmic dynein to mitotic spindles and kinetochores. Nature. 345**,** 266-8.

Stucke, V. M., Baumann, C., Nigg, E. A., 2004. Kinetochore localization and microtubule interaction of the human spindle checkpoint kinase Mps1. Chromosoma. 113**,** 1-15.

Stucke, V. M., Sillje, H. H., Arnaud, L., Nigg, E. A., 2002. Human Mps1 kinase is required for the spindle assembly checkpoint but not for centrosome duplication. Embo J. 21**,** 1723-32.

Sudakin, V., Chan, G. K., Yen, T. J., 2001. Checkpoint inhibition of the APC/C in HeLa cells is mediated by a complex of BUBR1, BUB3, CDC20, and MAD2. J Cell Biol. 154**,** 925-36.

Tanaka, K., Mukae, N., Dewar, H., van Breugel, M., James, E. K., Prescott, A. R., Antony, C., Tanaka, T. U., 2005. Molecular mechanisms of kinetochore capture by spindle microtubules. Nature. 434**,** 987-94.

Tanaka, T. U., 2010. Kinetochore-microtubule interactions: steps towards bi-orientation. Embo J. 29**,** 4070-82.

Tanaka, T. U., Rachidi, N., Janke, C., Pereira, G., Galova, M., Schiebel, E., Stark, M. J., Nasmyth, K., 2002. Evidence that the Ipl1-Sli15 (Aurora kinase-INCENP) complex promotes chromosome bi-orientation by altering kinetochore-spindle pole connections. Cell. 108**,** 317-29.

Tang, Z., Bharadwaj, R., Li, B., Yu, H., 2001. Mad2-Independent inhibition of APCCdc20 by the mitotic checkpoint protein BubR1. Dev Cell. 1**,** 227-37.

Taylor, S. S., Scott, M. I., Holland, A. J., 2004. The spindle checkpoint: a quality control mechanism which ensures accurate chromosome segregation. Chromosome Res. 12**,** 599-616.

Tighe, A., Staples, O., Taylor, S., 2008. Mps1 kinase activity restrains anaphase during an

unperturbed mitosis and targets Mad2 to kinetochores. J Cell Biol. 181, 893-901.

Toyoda, Y., Yanagida, M., 2006. Coordinated requirements of human topo II and cohesin for metaphase centromere alignment under Mad2-dependent spindle checkpoint surveillance. Mol Biol Cell. 17, 2287-302.

Uhlmann, F., Lottspeich, F., Nasmyth, K., 1999. Sister-chromatid separation at anaphase onset is promoted by cleavage of the cohesin subunit Scc1. Nature. 400, 37-42.

Vigneron, S., Prieto, S., Bernis, C., Labbe, J. C., Castro, A., Lorca, T., 2004. Kinetochore localization of spindle checkpoint proteins: who controls whom? Mol Biol Cell. 15, 4584-96.

Wei, R. R., Al-Bassam, J., Harrison, S. C., 2007. The Ndc80/HEC1 complex is a contact point for kinetochore-microtubule attachment. Nat Struct Mol Biol. 14, 54-9.

Weiss, E., Winey, M., 1996. The Saccharomyces cerevisiae spindle pole body duplication gene MPS1 is part of a mitotic checkpoint. J Cell Biol. 132, 111-23.

Welburn, J. P., Vleugel, M., Liu, D., Yates, J. R., 3rd, Lampson, M. A., Fukagawa, T., Cheeseman, I. M., 2010. Aurora B phosphorylates spatially distinct targets to differentially regulate the kinetochore-microtubule interface. Mol Cell. 38, 383-92.

Westermann, S., Avila-Sakar, A., Wang, H. W., Niederstrasser, H., Wong, J., Drubin, D. G., Nogales, E., Barnes, G., 2005. Formation of a dynamic kinetochore- microtubule interface through assembly of the Dam1 ring complex. Mol Cell. 17, 277-90.

Winey, M., Goetsch, L., Baum, P., Byers, B., 1991. MPS1 and MPS2: novel yeast genes defining distinct steps of spindle pole body duplication. J Cell Biol. 114, 745-54.

Wojcik, E., Basto, R., Serr, M., Scaerou, F., Karess, R., Hays, T., 2001. Kinetochore dynein: its dynamics and role in the transport of the Rough deal checkpoint protein. Nat Cell Biol. 3, 1001-7.

Wong, O. K., Fang, G., 2006. Loading of the 3F3/2 antigen onto kinetochores is dependent on the ordered assembly of the spindle checkpoint proteins. Mol Biol Cell. 17, 4390-9.

Xu, Q., Zhu, S., Wang, W., Zhang, X., Old, W., Ahn, N., Liu, X., 2009. Regulation of kinetochore recruitment of two essential mitotic spindle checkpoint proteins by Mps1 phosphorylation. Mol Biol Cell. 20, 10-20.

Yang, Z., Tulu, U. S., Wadsworth, P., Rieder, C. L., 2007. Kinetochore dynein is required for chromosome motion and congression independent of the spindle checkpoint. Curr Biol. 17, 973-80.

Yen, T. J., Li, G., Schaar, B. T., Szilak, I., Cleveland, D. W., 1992. CENP-E is a putative kinetochore motor that accumulates just before mitosis. Nature. 359, 536-9.

Zhao, Y., Chen, R. H., 2006. Mps1 phosphorylation by MAP kinase is required for kinetochore localization of spindle-checkpoint proteins. Curr Biol. 16, 1764-9.

Zhu, S., Wang, W., Clarke, D. C., Liu, X., 2007. Activation of Mps1 promotes transforming growth factor-beta-independent Smad signaling. J Biol Chem. 282, 18327-38.

Part 2:

Drosophila Cyclin J is a mitotically stable Cdk1 partner without essential functions

Althoff, F, Viktorinová, I, Kastl, J, and Lehner, CF
Dev Biol. 2009 Sep 15;333(2):263-72

Contribution to this part:

I performed the co-immunoprecipitations with EGFP-Cyclin J (Figure 4 and S1) and evluated the mass spectrometry data (Figure S1). J.K. and me analyzed viability, fertility and phenotypes of *Cyclin J* mutants (Figure 6 and S2 and Table 1). C.L. and me supervised the experiments on EGFP-Cyclin J localization (Figure 2), EGFP-Cyclin J degradation (Figure 3) and the cloning of constructs for ectopic expression of EGFP-Cyclin J, which were performed by J.K. The manuscript was written by C.L. with contributions from the other authors.

Developmental Biology 333 (2009) 263–272

Contents lists available at ScienceDirect

Developmental Biology

journal homepage: www.elsevier.com/developmentalbiology

Drosophila Cyclin J is a mitotically stable Cdk1 partner without essential functions

Friederike Althoff [a], Ivana Viktorinová [b], Johanna Kastl [c], Christian F. Lehner [a,*]

[a] Institute of Zoology, University of Zurich, Winterthurerstrasse 190, 8057 Zurich, Switzerland
[b] Max-Planck-Institute for Cell Biology and Genetics, Dresden, Germany
[c] Department of Biology, Molecular Genetics, University of Constance, Germany

ARTICLE INFO

Article history:
Received for publication 6 April 2009
Revised 23 June 2009
Accepted 26 June 2009
Available online 8 July 2009

Keywords:
Drosophila
Oogenesis
Meiosis
Syncytial cycles
Cyclin J, Cdk1, Cdk2

ABSTRACT

Cyclin J is a cyclin family member that appears to have evolved before the metazoan radiation. Its evolutionary conservation argues for an important role but functional characterizations of Cyclin J have remained very limited. In *Drosophila*, Cyclin J is expressed only in females. Using transgenic *Drosophila* lines expressing Cyclin J versions with N- or C-terminal GFP extensions, we demonstrate that it is expressed exclusively in the germline. After low level expression in all nuclei within the germarium, it gets highly enriched in the germinal vesicle within the oocyte until stage 12 of oogenesis, followed by disappearance after germinal vesicle breakdown before the first meiotic division. Surprisingly, Cyclin J is not required for female fertility. Chromosome segregation during female meiosis, as well as the rapid early embryonic cell cycles after fertilization, occurs normally in the complete absence of Cyclin J. Cyclin J with EGFP fused at either N- or C-terminus binds to Cdk1 and not to Cdk2. However, in contrast to the other known Cdk1 partners, the A- and B-type cyclins, Cyclin J is not degraded during mitosis.

Introduction

The first cyclin proteins were identified because of their rapid and complete disappearance during the early cleavage divisions in invertebrate embryos (Evans et al., 1983). Additional members of this eukaryotic protein family were subsequently identified and shown to function as regulatory subunits that associate with Cyclin-dependent protein kinases (Cdks) (Morgan, 2007). Various Cyclin–Cdk complexes are involved in the control of progression through the cell cycle or in other fundamental cellular processes like transcription. The originally described, rapid proteolysis during mitosis is only observed for the so-called mitotic cyclins. Based on sequence comparisons these cyclins have also been classified as A- and B-type cyclins. In *Drosophila*, as in other animal species, the mitotic cyclins bind to Cdk1 (Knoblich et al., 1994). The Cdk1 complexes are of special importance for the control of progression through mitosis. Activation of Cdk1 which depends on complex formation with mitotic cyclins results in entry into mitosis and transforms the cellular organization from interphase to metaphase architecture. Progression into anaphase and exit from mitosis requires inactivation of Cdk1 which results from ubiquitin-dependent degradation of the mitotic cyclins after activation of the Anaphase-Promoting Complex/Cyclosome (APC/C) ubiquitin ligase (Peters, 2006).

Cdk2 is involved in the control of progression into S phase (Woo and Poon, 2003). In mammalian cells, Cdk2 associates with A- and E-type cyclins. In *Drosophila*, Cyclin A-Cdk2 complexes have not been observed, while Cyclin E-Cdk2 complexes are clearly present *in vivo* (Knoblich et al., 1994; Meyer et al., 2000). This apparent difference might have evolved in the context of diversification of regulatory mechanisms controlling mitotic and endoreduplication cycles, respectively. While endoreduplication normally occurs only in very few cell types in mammals, this form of genome amplification by periodic S phases without intervening mitoses is extensively exploited during development and adult life of *Drosophila melanogaster* and many other organisms (Edgar and Orr-Weaver, 2001). *Drosophila* Cyclin E and Cyclin A can both trigger entry into S phase (Knoblich et al., 1994; Sprenger et al., 1997) and at the same time contribute to a block to re-replication (Follette et al., 1998; Sauer et al., 1995; Weiss et al., 1998). While this blocking effect is eliminated by mitotic degradation in case of Cyclin A, Cyclin E degradation is not coupled to mitosis and involves different pathways (Hwang and Clurman, 2005; Sauer et al., 1995). In *D. melanogaster*, Cyclin E might therefore have been selected as the unique Cdk2 regulator that works for S phase regulation in both mitotic and endocycles.

In contrast to A-, B- and E-type cyclins, the role of Cyclin J has not yet been characterized in detail. Cyclin J was originally identified in a yeast two hybrid screen for *Drosophila* proteins that interact with *Drosophila* Cdk1/Cdc2 and Cdk2/Cdc2c (Finley et al., 1996). Cyclin J mRNA and protein were detected exclusively during oogenesis and early embryogenesis (Kolonin and Finley, 2000). Microinjection of antibodies against Cyclin J as well as aptamers into early *Drosophila* embryos was reported to cause severe mitotic defects. These findings are consistent with the idea that Cyclin J provides a function

* Corresponding author. Fax: +41 44 63 56820.
E-mail address: christian.lehner@zool.uzh.ch (C.F. Lehner).

0012-1606/$ – see front matter © 2009 Elsevier Inc. All rights reserved.
doi:10.1016/j.ydbio.2009.06.042

specifically required during the special early cycles at the start of *Drosophila* embryogenesis where progression through the cell cycle is extremely rapid, omitting gap phases and cytokinesis.

Based on its expression pattern, Cyclin J might also function during oogenesis. *Drosophila* oogenesis starts with an asymmetric division of germline stem cells at the distal end of an ovariole (for a detailed description of oogenesis see Spradling, 1993). The differentiating daughter cell, progresses through four cell division cycles with incomplete cytokinesis resulting in 16-cell clusters interconnected by ring canals. Fifteen cells of the cluster develop into nurse cells and one into an oocyte. The oocyte enters meiosis and remains arrested in a special diplotene stage with the chromatin compacted into a karyosome for most of oogenesis. The nurse cells progress through several endoreduplication cycles. Egg chambers are completed by the formation of an enveloping epithelial layer of somatic follicle cells at the proximal end of the germarium. During their travel from the distal germarium to the proximal end of the ovariole, egg chambers progress through 14 stages during which the oocyte acquires abundant maternal stores as well as an egg shell. During stage 13, fully grown oocytes enter into the first meiotic division. After germinal vesicle breakdown and spindle formation, they arrest in metaphase of meiosis I in stage 14. Completion of meiosis occurs only after egg activation which is triggered by egg laying.

To evaluate whether *Drosophila* Cyclin J might function already during oogenesis, we have generated *Drosophila* females that completely lack this cyclin. Surprisingly, their fertility was found to be normal. Our genetic characterization demonstrates therefore that Cyclin J is not required for progression through the mitotic cycles of the germline cells at the start of oogenesis. Moreover, it is entirely dispensable for meiosis and the syncytial cycles at the onset of embryogenesis. Like the *Drosophila* A- and B-type cyclins, Cyclin J appears to associate with Cdk1 and not with Cdk2. But in contrast to the other Cdk1 partners this unusual cyclin is not degraded during mitosis.

Materials and methods

Fly strains and genetics

P{wHy}CycJ^{DG29702}, *PBac{5HPw^{+}}CycJ^{A138}* and *Df(3L)Exel6095* which deletes *CycJ* were obtained from the Bloomington *Drosophila* Stock Center at Indiana University. *PBac{RB}e01160* and *PBac{XP}d07385* were obtained from the Exelixis Collection at the Harvard Medical School and used for the generation of *Df(3L)AJ14/TM3, Ser* as described by (Parks et al., 2004; Thibault et al., 2004). *CycE^{01672}* (Lilly and Spradling, 1996) was kindly provided by Mary Lilly (NIH, Bethesda, MD, USA). The lines with *CycA^{C8LR1}* (Sigrist and Lehner, 1997), *CycA^{neo114}* (Lehner and O'Farrell, 1989), *CycB^{2}*, *CycB^{3}*, *CycB3^{3}* (Jacobs et al., 1998), *CycE^{AR95}*, *Cyc^{pz5}* (Knoblich et al., 1994), *P{prd-GAL4}* (Brand and Perrimon, 1993), *P{matα4-GAL-VP16}V2H* (Hacker and Perrimon, 1998), *P{UAS-Cdk1-myc}III.1* or *P{UAS-Cdk2-myc}III.2* (Meyer et al., 2000) or with two *gEGFP-Mps1* transgene insertions (II.1 and II.2) resulting in expression of EGFP-Mps1 under control of the Mps1 cis-regulatory region (Fischer et al., 2004) have been described. Lines with the transgenes *gCycJ*, *gEGFP-CycJ*, *gCycJ-EGFP*, *UAS-EGFP-CycJ*, *UAS-CycJ-EGFP*, *gcal1-EGFP*, *garmi*, or *gCG14971* were obtained after P element-mediated germline transformation with the constructs described below. Selected transgene insertions were combined with *Df(3L)AJ14* by meiotic recombination. *Df(3L)AJ14, garmi III.8, gCG14971 III.10* can be kept as a homozygous stock. The presence or absence of various genes on the original *Df(3L)AJ14* chromosome and its derivatives was confirmed by PCR assays using the following gene-specific primer pairs: IV35 (5′-CGATGGTGGTTC-CAAGACC-3′) and IV36 (5′-GCCTGGTCTATTGATCATCG-3′) for an *eIF5B* fragment, IV37 (5′-CGAGCAGCACTATTCATTCC-3′) and IV38 (5′-GGAATGTTCTCCGCTTCACC-3′) for an *armi* fragment, IV39 (5′-GTCGCGTCGCTTCAGCACG-3′) and IV40 (5′-TTTCGCGCAGTTCA-TAATGCAG-3′) for a *CG14971* fragment, AF22 (5′-CCTGGCTAAGACG-CACTGG-3′) and AF23 (5′-GCTATATGAAGACAAGTGATGG-3′) for a *CycJ* fragment, XP5 (5′-AATGATTCGCAGTGGAAGGCT-3′) and RB3 (5′-TGCATTTGCCTTTCGCCTTAT-3′) for the amplification of the *XP-RB* hybrid transposon.

C(1;Y), y^{1} v^{1} f^{1} B^{1}: y^{+}/C(1)RM, y^{2} su(wa)^{1} w^{a} flies were kindly provided by Terry Orr-Weaver (Whitehead Institute for Biomedical Research, Cambridge, MA, USA). Males from this stock were used for the analysis of X chromosome non-disjunction during meiosis in oocytes as described (Kerrebrock et al., 1992). The different genotypes of the females analyzed were *w^{1}* (for control), or *P{wHy}CycJ^{DG29702}*, or +/+; *Df(3L)AJ14, garmi III.8, gCG14971 III.10*, or *gCycJ II.41/+*; *Df(3L)AJ14, garmi III.8, gCG14971 III.10*. For these genotypes, the corrected total X non-disjunction rate (Kerrebrock et al., 1992) determined from more than 1300 progeny was found to be 0.22%, 1.07%, 0.41% and 0.44%, respectively.

For our analysis of genetic interactions between *CycJ* and *CycE*, we crossed virgin females of the genotype *Df(3L)AJ14, garmi III.8, gCG14971 III.1/Df(3L)AJ14* (*CycJ*-deficient), or *CycE^{01672}* (*CycE* hypomorph), or *CycE^{01672}; Df(3L)AJ14, garmi III.8, gCG14971 III.1/Df(3L)AJ14* (double mutant) with *w^{1}* males and counted the number of progeny which was found to be 440 (+/−40 s.d, $n=3$), 135 (+/−11 s.d, $n=3$) and 127 (+/−34 s.d, $n=2$) with *CycJ*-deficient, *CycE* hypomorph and double mutant females, respectively. Genotypes and results of the experiments addressing genetic interaction between CycJ and CycA, CycB and CycB3 are provided in Supplementary Figure 1.

Plasmid constructions

The DNA fragments used for the *CycJ*, *armi* and *CG14971* transgene constructs were derived from the BACR09B04 clone (Hoskins et al., 2000). A 5 kb BglII fragment including most of *armi* was subcloned into BamH1 and BglII cut pSLfa1180, resulting in cloning intermediate 1. A neighbouring 4 kb BglII fragment with the remainder of *armi*, *CycJ* and a small part of *CG14971* was subcloned into BglII cut pLitmus28, resulting in intermediate 2. The rest of *CG14971* was enzymatically amplified using the primer pair IV5 (5′-CAATGGCCCAAGTTAT-CTCATTCG-3′) and IV6 (5′-CCA GGCGGCCGC ACTCTGACAACTTT-TTGGTGCG-3′) introducing a NotI site. The resulting PCR product was cut with BglII and NotI and inserted into the corresponding sites within the intermediate 1, resulting in intermediate 3. The *CycJ* gene was deleted from intermediate 2 with an inverse PCR with the primer pair IV3 (5′-CCGA GCGGCCGC ACCCATTGAAACACGCC-3′) and IV4 (5′-CGAA GCGGCCGC AGCAGCGTTCCCAGAC-3′) followed by digestion with NotI and re-ligation, resulting in the intermediate 4. The BglII fragment from the intermediate 4 was subsequently inserted into the BglII site within the intermediate 3, resulting in intermediate 6. To arrive at the *garmi* construct, we first transferred a 2.2 kb SalI–XbaI fragment with the 5′ region of *armi* from intermediate 6 into XhoI and XbaI cut pCaSpeR4, resulting in intermediate 7. The construct was completed by transposing a 3.8 kb XbaI–NotI fragment with the 3′ region of *armi* from intermediate 6 into the corresponding sites of intermediate 7. To arrive at the *gCG14971* construct, we transposed a 4.2 kb NotI fragment from intermediate 6 into the NotI site of pCaSpeR4. The *gCycJ* construct was obtained by inserting the 4 kb BglII fragment from intermediate 2 into the BamHI site of pCaSpeR4. For the *gEGFP-CycJ* construct, we first subcloned a 0.5 kb SalI fragment including the translational start site from intermediate 2 into the corresponding site of pBluescript KS+ followed by introduction of an NheI site at the translational start of *CycJ* by inverse PCR using the primer pair IV48 (5′-GGCG GCTAGC ATGGAGCAGAAAGTGGCTGCC -3′) and IV49 (5′-GGAG GCTAGC TGTATCGAAATTGAATGCAATGCC-3′). After inserting the EGFP coding sequence as an XbaI fragment into this newly created site, the modified SalI fragment containing the EGFP sequence was used to replace the original SalI fragment in

intermediate 2, followed by transposition of the BglII fragment into the BamHI site of pCaSpeR4. For the *gCycJ-EGFP* construct, an NheI site was introduced into intermediate 2 immediately upstream of the translational stop of *CycJ* by inverse PCR using the primer pair IV50 (5′-GGCG GCTAGC TAGTAAAAGGGAAAAACGAAACTATTAC -3′) and IV51 (5′-GAGG GCTAGC ATCTTTGGCTACACTCTCCACTTTG-3′). After insertion of the EGFP coding sequence as an XbaI fragment into this newly created site, the BglII fragment was transposed in the BamHI site of pCaSpeR4 These constructs for *CycJ* expression without or with EGFP at either N- or C-terminus under control of the genomic *CycJ* cis-regulatory region contain the complete intergenic regions up- and downstream from *CycJ* as well as the genomic 5′ and 3′ UTRs.

The *pUAST-EGFP-CycJ* construct was obtained by enzymatic amplification of the *CycJ* sequence from the *gEGFP-CycJ* construct with the primer pair JoK10 (5′-AGCTGTAC GCGGCCGC CATGGAGCA-GAAAGTGGC-3′) and JoK11 (5′-TTTTCC GGTACC CTAATCTTTGGCTA-CACTCTC-3′) which introduced flanking NotI and KpnI sites, respectively. After digestions with these enzymes, the PCR fragment was transposed into the corresponding sites within *pUAST-EGFP-MCS* (Schittenhelm et al., 2007). The *pUAST-CycJ-EGFP* construct was obtained by amplification of the *CycJ* sequence from the *gEGFP-CycJ* construct with the primer pair JoK10 and JoK12 (5′-TCCCTT GGTACC ATCTTTGGCTACACTCTCCAC-3′) which also introduced flanking NotI and KpnI sites, respectively. After digestions with these enzymes, the PCR fragment was transposed into the corresponding sites within *pUAST-MCS-EGFP* (Schittenhelm et al., 2007). The *CycJ* region in *pUAST-EGFP-CycJ* and *pUAST-CycJ-EGFP* was completely sequenced and found to be correct.

Sequence comparisons

The cyclin tree (Fig. 1) was constructed using the on-line version of T-REX (Makarenkov, 2001); www.trex.uqam.ca) based on a Clustal W alignment for which only cyclin box regions without N-terminal extensions were used in case of A-, B- and E-type cyclins. The J-type cyclins do not have an N-terminal extension preceding the cyclin box region. Accession numbers of the used Cyclin J sequences are NP_061957.2, AAH35871.3, NP_766427.1, NP_001038995.1, NP_523903.1, XP_001641369.1, XP_001237463.2, EDQ87852.1.

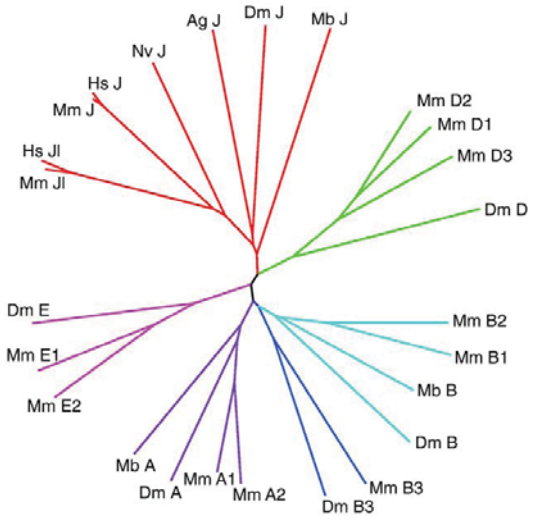

Fig. 1. Cyclin J homologs in metazoans. A tree based on predicted amino acid sequences illustrates that Cyclin J homologs are encoded in unicellular flagellate and metazoan genomes. A duplication resulting in Cyclin J (J) and Cyclin J-like (Jl) has occurred in mammals. Apart from Cyclin J sequences, additional cyclins of the A-, B-, D- and E-type families were included. Ag: *Anopheles gambiae*; Dm: *Drosophila melanogaster*; Hs: *Homo sapiens*; Mb: *Monosiga brevicollis*; Mm: *Mus musculus*; Nv: *Nematostella vectensis.*

Immunoprecipitation, immunoblotting and immunofluorescence

Oocytes for immunoprecipitation experiments were mass isolated (Page and Orr-Weaver, 1997) from *gCycJ-EGFP II.6*, or *gEGFP-CycJ III.16*, or *gcal1-EGFP II.1*, or *gEGFP-Mps1 II.1, II.2* females before extract preparation. Embryos were collected for 3 h on apple agar plates from crosses of *UAS-Cdk1-myc III.1, UAS-Cdk2-myc III.2* males with females, which were either *matα4-GAL-VP16/CyO* or *matα4-GAL-VP16, UAS-EGFP-CycJ II.1/CyO* or *matα4-GAL-VP16, UAS-CycJ-EGFP II.2/CyO*, and aged for 3 h at 25 °C. Immunoprecipitation from native oocyte and embryo extracts as well as protein identification by mass spectroscopy was done essentially as described (Schittenhelm et al., 2007) using affinity-purified rabbit antibodies against GFP (IS28) in combination with Protein-A-Sepharose beads (Affi-Prep, Biorad). The proteins immunoprecipitated from either ovary or embryo extracts which were analyzed by immunoblotting (Fig. 4A or C, respectively) were isolated using an amount of extract which was 16 or 80 times more, respectively, than the amount of extract loaded for parallel analysis.

For immunoblotting, oocytes were mass isolated from *gCycJ-EGFP II.6* females before fixation in a 1:1 mixture of methanol and heptane. Fixed oocytes were transferred to a 1:1 mixture of glycerol and EB buffer (Edgar et al., 1994). After DNA labelling with Hoechst 33258 (1 μg/ml), oocytes were sorted according to their developmental stage with an inverted fluorescence microscope.

Immunoblots were probed with affinity-purified rabbit antibodies against GFP (IS28) at a dilution of 1:3000, affinity-purified rabbit antibodies against Cdk2 at 1:4000, mouse monoclonal antibodies against GFP (Roche) at 1:500, a mouse monoclonal antibody against a PSTAIR peptide (SIGMA, P7962) at 1:50,000 and a mouse monoclonal antibody against a human myc peptide (9E10) at 1:15.

For fluorescence microscopy, ovaries were dissected from *gEGFP-CycJ III.6* females as described (Page and Hawley, 2001). Oocytes were fixed for 20 min in 2% paraformaldehyde in phosphate buffered saline containing 0.5% Nonidet-P40. After DNA labelling with Hoechst 33258 (1 μg/ml), ovaries were analyzed with an Olympus FluoView 1000 laser scanning confocal microscope. For immunofluorescent labeling of embryos, we collected eggs for 1 h on apple agar plates and aged at 25 °C. Eggs were collected from a cross of $CycA^{C8LR1}$, *prd-GAL4/TM3, Sb P{35UZ}2* females with *UAS-CycJ-EGFP II*; $CycA^{C8LR1}$/*TM3, Ser* males and aged for 7 h. Eggs were also collected from a cross of *Df(3L)AJ14, garmiIII.8, gCG14971 III.10/Df(3L)AJ14* females with w^1 males and aged for 1 h. Embryos were fixed essentially as described previously (Karr and Alberts, 1986). For immunofluorescent labeling we used mouse monoclonal antibody DM1A anti-α-tubulin (Sigma) at 1:8000, rabbit serum against *Drosophila* Cyclin A at 1:3000. Secondary antibodies were Cy5-conjugated goat antibodies against mouse IgG (Jackson Immunochemicals) and Alexa 568-conjugated goat antibodies against rabbit IgG (Molecular Probes). For the DNA staining of embryos, we also used Hoechst 33258 at 1 μg/ml. Embryos were analyzed with a Zeiss Cell Observer HS wide field fluorescence microscope.

Results

Cyclin J has evolved before the metazoan radiation

When originally identified in *Drosophila* (Finley et al., 1996), *Cyclin J* did not appear to have homologs in other species. However, subsequent additions to Genbank have revealed that this cyclin type is not restricted to *Drosophila*. While not recognizable in plant genomes (Guo et al., 2007; Wang et al., 2004), *Cyclin J* homologs are present throughout the metazoan radiation (Fig. 1, data not shown). In the mammalian lineage, paralogous cyclin J genes (*Cyclin J* and *Cyclin J-like*) are apparent, as also in case of the better-characterized A-, B-,

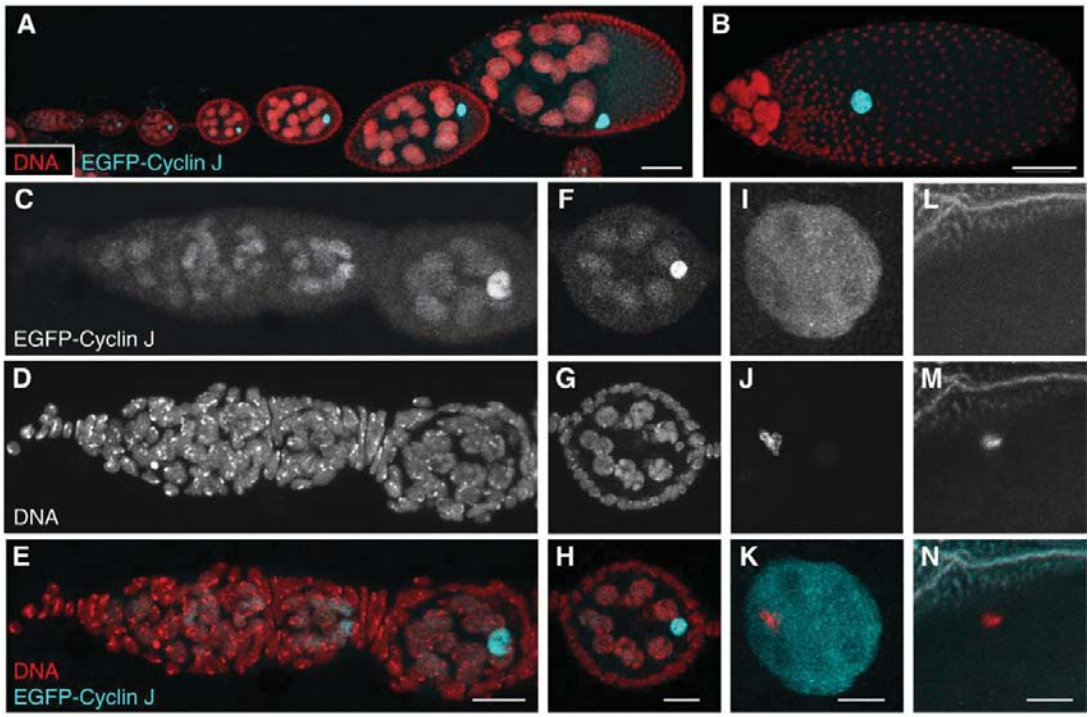

Fig. 2. EGFP-Cyclin J expression during oogenesis. Ovaries from females with *gEGFP-CycJ III.16* resulting in expression EGFP-Cyclin J under control of the *CycJ* regulatory region were fixed and labelled with a DNA stain. (A) ovariole with early stages of oogenesis (germarium until stage 10). (B) stage 12. (C–E) germarium. (F–H) stage 4. (I–K) germinal vesicle region of a stage 12 oocyte. (L–N) region with metaphase I figure of a mature stage 14 oocyte. Bars in A and B correspond to 30 and 100 μm, respectively. All other bars correspond to 10 μm.

D- and E-type cyclins. In contrast, only single orthologs for each of these cyclin types including *Cyclin J* are present in the *Drosophila* genome. Importantly, a cyclin J homolog can also be identified in *Monosiga brevicollis*, a member of the choanoflagellates which are considered to be the closest unicellular relatives of metazoans.

The pattern of Cyclin J expression revealed by EGFP fusion transgenes

Cyclin J has evolved before the specialized syncytial cycles characteristic of early insect embryogenesis. Consistent with the known expression pattern (Finley et al., 1996; Kolonin and Finley, 2000), it might therefore have functions already during oogenesis and not just during the syncytial cycles where it has been characterized functionally so far. For a more detailed analysis of Cyclin J expression during oogenesis, we generated transgenic lines expressing Cyclin J fused to EGFP either at the N- or the C-terminus under the control of the genomic Cyclin J regulatory sequences. The results obtained with multiple *gEGFP-CycJ* and *gCycJ-EGFP* lines were essentially identical (Fig. 2 and data not shown).

EGFP-Cyclin J signals above background were detected in the germarium at the distal end of ovarioles. Based on the EGFP pattern in the germarium, all germline cells appeared to be weakly positive in contrast to somatic cells (Figs. 2C–E). In the newly formed egg chambers at stage 1 of oogenesis, the peripheral somatic follicle cells did definitely not display EGFP fluorescence, while the germ line derivatives in the interior were positive (Figs. 2C–E). Signals in the oocyte were stronger than in the nurse cells. All signals were nuclear. In the oocyte, EGFP-Cyclin J was observed throughout the germinal vesicle, whereas the condensed DNA was restricted to the compact karyosome (Figs. 2I–K). After germinal vesicle break down during stage 13, we were unable to detect signals that were clearly above the uniform substantial background fluorescence (Figs. 2L–N). Similarly, after egg deposition and fertilization, we were unable to detect signals that were clearly above background (data not shown).

For further clarification whether Cyclin J is still present in oocytes after germinal vesicle breakdown, we performed immunoblotting experiments. Egg chambers were sorted microscopically before extract preparation. In extracts prepared from stage 12 egg chambers (i.e. before germinal vesicle breakdown) Cyclin J-EGFP was clearly

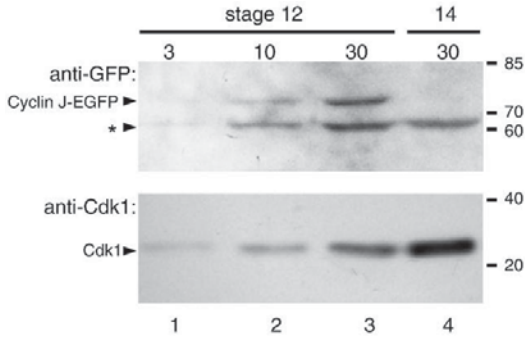

Fig. 3. Cyclin J-EGFP levels during oocyte maturation. Oocytes from *gCycJ-EGFP II.6* females at either stage 12 or stage 14 were analyzed by immunoblotting for the presence of Cyclin J-EGFP using antibodies against GFP (anti-GFP, upper panel). Apart from Cyclin J-EGFP, this antibody detects a second band (see asterisk) which is also observed in control ovaries that do not express GFP (data not shown). An anti-PSTAIR peptide antibody, which reacts predominantly with Cdk1 in *Drosophila* was used as an additional loading control (anti-Cdk1). The number of loaded oocytes is indicated on top of lanes 1–4. The position of molecular weight markers is indicated on the right side.

detectable by immunoblotting with antibodies against GFP (Fig. 3, lane 3), as expected from the observed pattern of EGFP fluorescence in ovaries (Fig. 2). However, in extracts prepared from stage 14 egg chambers, Cyclin J-EGFP was essentially no longer detectable (Fig. 3, lane 4). Similar observations (data not shown) were made with extracts from females expressing EGFP-Cyclin J, although expression levels on average appeared somewhat lower with *gCycJ-EGFP* lines in comparison to *gEGFP-CycJ* lines. In extracts prepared from early embryos collected from females with either a *gEGFP-CycJ* or a *gCycJ-EGFP* transgene, we were also unable to detect the EGFP tagged Cyclin J variants (data not shown). We conclude therefore that the levels of Cyclin J fused to EGFP decrease during the final stages of oogenesis following germinal vesicle breakdown.

Cyclin J binds to Cdk1

To identify proteins that associate with Cyclin J we immunoprecipitated CycJ-EGFP from extracts prepared from ovaries of *gCycJ-EGFP* females. In control experiments, we used the same affinity-purified antibodies against EGFP for immunoprecipitation of Cal1-EGFP from extracts prepared from ovaries of *gcal1-EGFP* females. MS/MS analysis was used to identify co-immunoprecipitated proteins. Among the proteins which were specifically co-immunoprecipitated with Cyclin J-EGFP, we clearly detected Cdk1 but not Cdk2 (Supplementary Table 1). Immunoblot analyses confirmed that Cdk1 but not Cdk2 was co-immunoprecipitated with Cyclin J-EGFP (Fig. 4A). Moreover, in a similar experiment using EGFP-Mps1 as a control, we also observed co-immunoprecipitation of Cdk1 but not Cdk2 with N-terminally EGFP tagged Cyclin J in immunoblot and MS/MS analyses (data not shown).

Cdk1 and Cdk2 expression levels appear to be comparable (Karsten Sauer and C.F.L., unpublished information) and both have been readily detected by shot gun proteomics (Brunner et al., 2007). Therefore, the observation that Cdk1 was co-immunoprecipitated by both EGFP-Cyclin J and Cyclin J-EGFP from ovary extracts strongly suggested that Cyclin J prefers Cdk1 over Cdk2 as partner kinase. To confirm this partner preference and circumvent the limited detection sensitivity

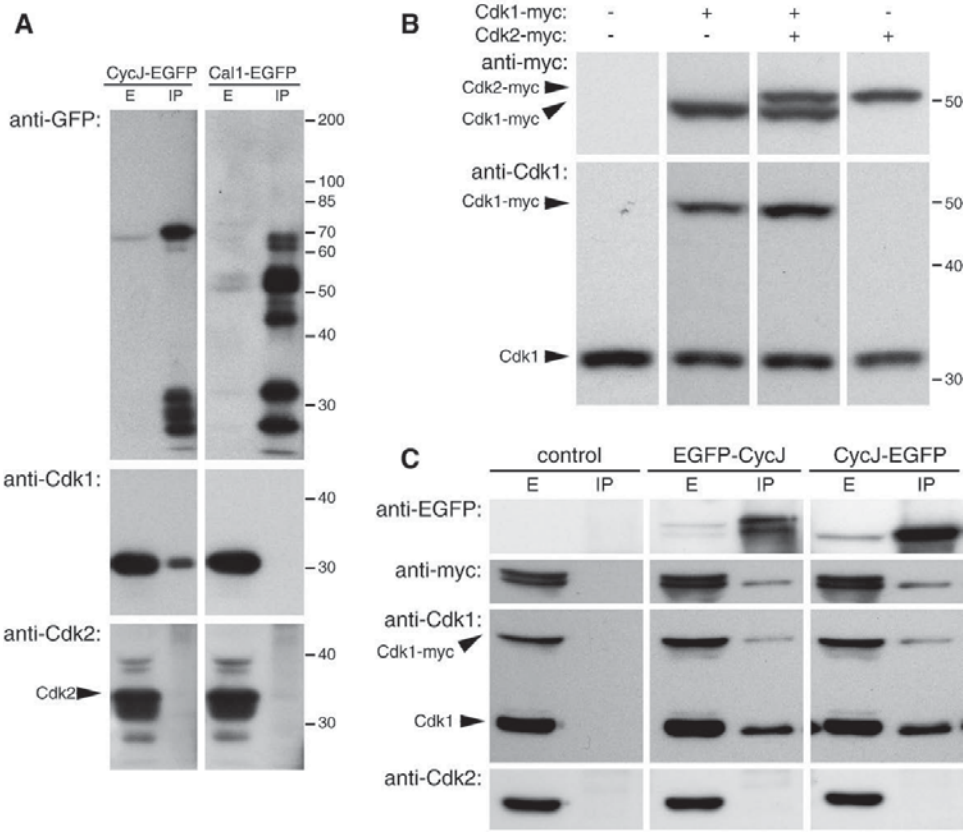

Fig. 4. Cyclin J is a Cdk1 partner. Panel A: Proteins immunoprecipitated with antibodies against GFP from ovary extracts (E) of either *gcal1-EGFP* (Cal1-EGFP) and *gCycJ-EGFP* (CycJ-EGFP) females were analyzed by immunoblotting with anti-GFP, anti-Cdk1 and anti-Cdk2. Cdk1 but not Cdk2 could be detected in the CycJ-EGFP immunoprecipitates (IP). The long exposures shown for maximal anti-Cdk2 sensitivity reveal some non-specific reactions in the extracts apart from the reaction with Cdk2 (arrowhead). The absence of Cdk1 in the control Cal1-EGFP immunoprecipitate (IP) indicates that the interaction of Cdk1 with CycJ-EGFP is specific. The presence of multiple bands after immunoblotting with anti-GFP presumably reflects proteolytic degradation. The position of molecular weight markers is indicated on the right side. Panel B and C: The binding preference of EGFP-Cyclin J and Cyclin J-EGFP for Cdk1-myc or Cdk2-myc was analyzed after coexpression in embryos using the UAS/GAL4 system. Panel B: Extracts of embryos expressing Cdk1-myc and/or Cdk2-myc as indicated above the lanes were analyzed by immunoblotting with anti-myc and anti-PSTAIR (anti-Cdk1) which in *Drosophila* detects almost exclusively Cdk1. Probing with anti-myc demonstrates that Cdk1-myc and Cdk2-myc have a distinct electrophoretic mobility and are expressed at equal levels. Anti-PSTAIR reveals equal loading. Panel C: After coexpression of EGFP-Cyclin J or Cyclin J-EGFP with Cdk1-myc and Cdk2-myc, the former but not the latter was co-immunoprecipitated with antibodies against GFP, as revealed by immunoblotting with anti-myc. Moreover, the endogenous Cdk1 but not the endogenous Cdk2 was co-immunoprecipitated as well, as revealed by immunoblotting with either mouse anti-PSTAIR (anti-Cdk1) or rabbit anti-Cdk2. These antibodies also detected the myc-tagged versions. However, the corresponding region is not shown in case of the anti-Cdk2 immunoblot because the reaction with Cdk2-myc was obscured in the immunoprecipitates by a strong signal caused by commigrating heavy chains from rabbit anti-GFP used for immunoprecipitation.

resulting from the low expression of transgenes driven by the *CycJ* cis-regulatory region we performed experiments after overexpression in embryos. Overexpression of EGFP-Cyclin J during the embryonic cell division cycles was achieved with an appropriate UAS transgene inherited from the father in combination with maternally expressed *matα4-GAL-VP16*. Moreover, in addition to *UAS-EGFP-CycJ*, we simultaneously expressed *UAS-Cdk1-myc* and *UAS-Cdk2-myc*. The simultaneous overexpression of EGFP-Cyclin J, Cdk1-myc and Cdk2-myc did not noticeably affect embryonic development (data not shown). Immunoblotting experiments with embryonic extracts and anti-myc antibodies clearly demonstrated that Cdk1-myc and Cdk2-myc can be identified unambiguously even after coexpression because of their distinct electrophoretic mobility (Fig. 4B). Immunoblotting with anti-myc also demonstrated that Cdk1-myc and Cdk2-myc were expressed at comparable levels (Fig. 4B, data not shown). However, after immunoprecipitation with anti-EGFP, we observed only Cdk1-myc and not Cdk2-myc in the EGFP-Cyclin J immunoprecipitates (Fig. 4C). Moreover, we also detected the endogenous untagged Cdk1 in the

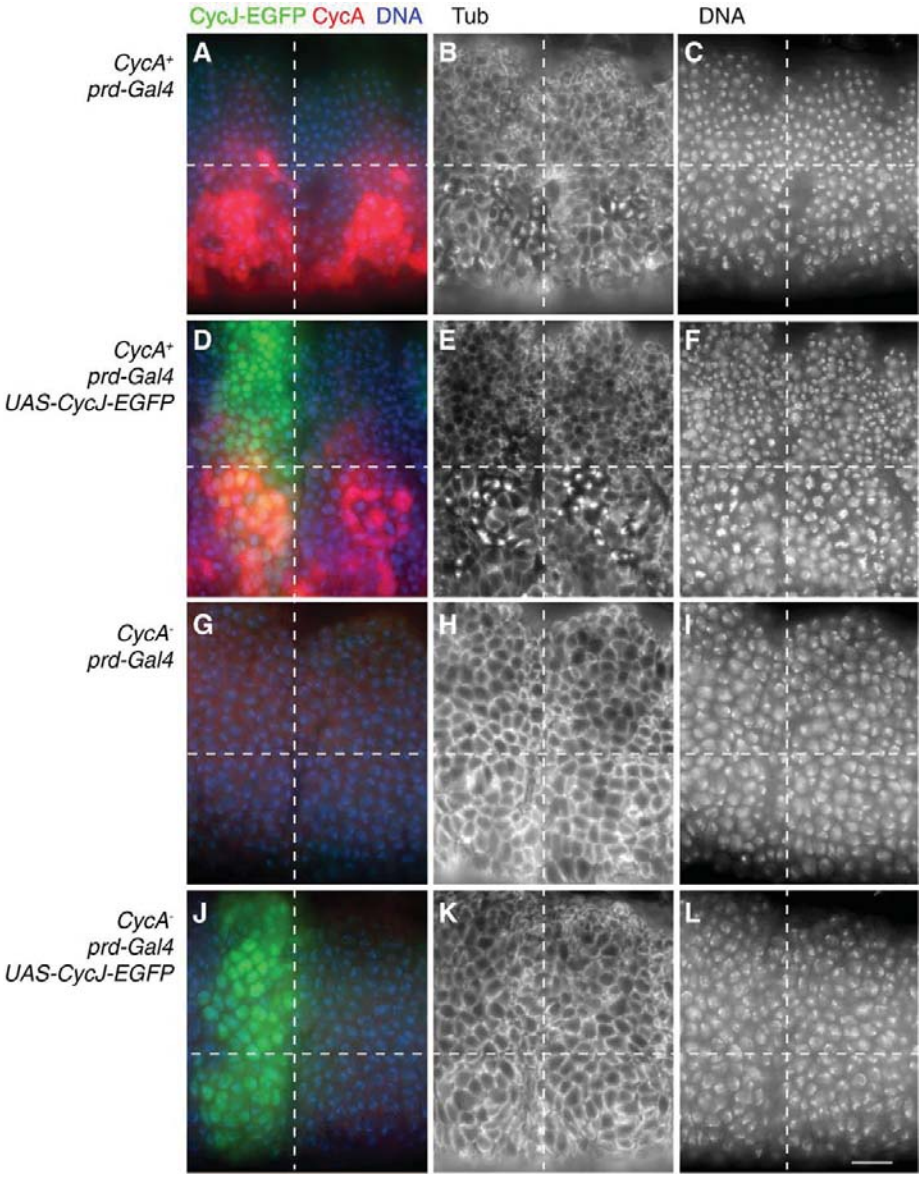

Fig. 5. Cyclin J-EGFP is stable during M and G1 and cannot replace Cyclin A. Sibling embryos with (*CycA*$^{+}$, A–F) or without (*CycA*$^{-}$, G–L) zygotic Cyclin A expression which either did not express Cyclin J-EGFP (A–C, G–I) or expressed it (D–F, J–L) were collected for 1 h and aged to the stage where the cells in the dorsal epidermis (above the hatched horizontal lines) are in G1 of cycle 17 and those in the ventral epidermis (below the hatched horizontal line) in G2 or M of cycle 16 during normal development. Progression through mitosis 16 does not occur in *CycA*$^{-}$ embryos and therefore all epidermal cells remain in G2. *prd-GAL4* drives expression on the left of the hatched vertical line in the epidermal regions shown after labelling with antibodies against Cyclin A (CycA), Tubulin (Tub) and a DNA stain (DNA). In contrast to Cyclin A, Cyclin J-EGFP is not degraded during mitosis 16 and G1 of cycle 17. Moreover, Cyclin J-EGFP cannot prevent the cell cycle arrest in G2 of cycle 16 when expressed in *CycA*$^{-}$ embryos. Bar corresponds to 10 μm.

EGFP-Cyclin J immunoprecipitates while Cdk2 was not detectable (Fig. 4C). These results strongly support the notion that Cyclin J associates specifically with Cdk1.

Cyclin J-EGFP is not degraded during M phase

The known *Drosophila* Cdk1 partner cyclins, the A- and B-type cyclins, become rapidly degraded during mitosis (Lehner and O'Farrell, 1990). In the germarium, therefore, these mitotic cyclins are absent from cells in late mitosis and early G1 (Hatfield et al., 2005; Wang and Lin, 2005). Our observation that EGFP-Cyclin J and Cyclin J-EGFP was present at comparable levels in all germline cells within the germarium suggested that Cyclin J is not degraded during mitosis. To evaluate the behavior of Cyclin J during mitosis, we used the UAS/GAL4 system to drive its expression during embryogenesis. The developmentally controlled, highly reproducible division programme of embryogenesis facilitates careful analyses. We used *prd-GAL4* to drive expression of Cyclin J-EGFP (Fig. 5) or EGFP-Cyclin J (data not shown) in alternating epidermal stripes. Embryos were fixed at the stage of mitosis 16. Progression through mitosis 16 occurs earlier in the dorsal epidermis than in the ventral epidermis. After fixation at the stage of mitosis 16, cells in the dorsal epidermis in many embryos are already in G1 of cycle 17 while the cells in the ventral epidermis are still in G2 before mitosis 16. As each embryonic division partitions the embryo into progressively smaller cells, the nuclear density revealed by DNA staining in such embryos is twice as high in the dorsal epidermis in comparison to the ventral epidermis (Figs. 5C, F). Moreover, as previously described, the A- and B-type cyclins are degraded in mitosis 16 and remain unstable during G1 of cycle 17 (Sigrist and Lehner, 1997). Therefore, anti-Cyclin A labeling is absent from the dorsal epidermal cells and, conversely, present in the cytoplasm of ventral epidermal cells in such embryos (Figs. 5A, D).

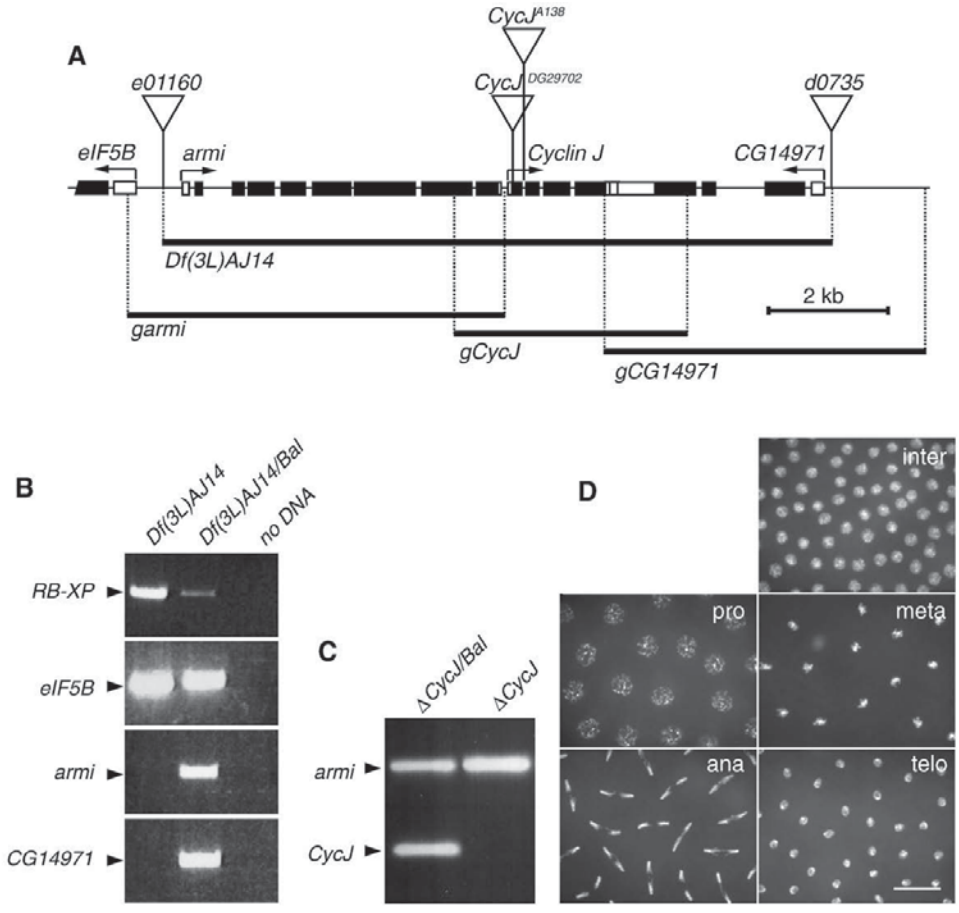

Fig. 6. Genetic elimination of Cyclin J. Panel A: The genomic region with *CycJ* and the neighbouring genes *eIF5B*, *armi* and *CG14971* is illustrated schematically. Start sites and direction of transcription are indicated by arrows. Exons are represented by boxes with black filling indicating coding regions. Flp-mediated recombination between FRT sites present within the transposons *PBAC{RB}e01160* and *P{XP}d0735* (insertion sites indicated by triangles) resulted in the deficiency *Df(3L)AJ14*. Genes deleted by *Df(3L)AJ14* were re-introduced by transgenes (*garmi*, *gCycJ* and *gCG14971*) carrying genomic fragments including the genes *armi*, *CycJ* or *CG14971*, respectively, as indicated by the black horizontal lines. Moreover, the position of additional transposon insertions (*P{wHy}CycJ*^{DG29702} and *PBac{5HPw}CycJ*^{A138}) in *CycJ* is indicated by triangles. Panel B: The presence of the expected Flp/FRT-induced deletion was verified by PCR assays using genomic DNA isolated from flies which were homozygous for *Df(3L)AJ14* (*Df(3L)AJ14*) or carried *Df(3L)AJ14* over a balancer chromosome (*Df(3L)AJ14/Bal*). Primer pairs amplifying the recombined hybrid *RB-XP* transposon (*RB-XP*), or fragments from the genes *eIF5B* (*eIF5B*), *armi* (*armi*) or *CG14971* (*CG14971*) were used in parallel reactions. These primers did not amplify products when used without template DNA (no DNA). Panel C: Genomic DNA was isolated from flies which carried *Df(3L)AJ14, garmi III.8, gCG14971 III.10* either over a balancer chromosome (*ΔCycJ/Bal*) or homozygously (*ΔCycJ*). A duplex PCR with primer pairs amplifying fragments from the *armi* and *CycJ* genes confirmed the absence of *CycJ* in the flies homozygous for *Df(3L)AJ14, garmi III.8, gCG14971 III.10*. Panel D: *Df(3L)AJ14, garmi III.8, gCG14971 III.10* embryos which completely lack maternal and zygotic *CycJ* function were fixed during the syncytial stages and labelled with a DNA stain. Spacing and appearance of nuclei during interphase (inter) and during mitotic pro- (pro), meta- (meta), ana- (ana), and telophase (telo) was observed to be indistinguishable from wild type controls (not shown).

However, Cyclin J-EGFP fluorescence in the expressing epidermal stripes was not decreased in the dorsal G1 region compared to the ventral G2 region (Fig. 5D). These observations indicate that Cyclin J is an unusual Cdk1 partner. In contrast to the other Cdk1 partners, i.e. the A- and B-type cyclins, Cyclin J does not appear to become degraded during mitosis. The absence of D- and KEN boxes from the predicted Cyclin J amino acid sequence further supports this notion. These sequence motifs are known to mediate the APC/C-dependent polyubiquitylation and consequential proteasomal degradation of A- and B-type cyclins during M and G1 phases (Peters, 2006).

prd-GAL4 driven *UAS-CycJ-EGFP* expression in *CycA* mutant embryos allowed us also to address whether Cyclin J might be able to replace Cyclin A functionally. We have previously demonstrated that the failure of epidermal cells to progress beyond G2 of cycle 16 which is caused by a loss of zygotic *CycA* function is readily prevented by *prd-GAL4* driven *UAS-CycA* expression (Reber et al., 2006). However, this premature cell cycle arrest in G2 before mitosis 16 in *CycA* mutants (Figs. 5G–I) was not prevented by analogous Cyclin J-EGFP expression (Figs. 5J–L). In both, *CycA* mutants and sibling embryos, we observed the same results after *prd-GAL4* driven expression of either *UAS-CycJ-EGFP* (Fig. 5) or *UAS-EGFP-CycJ* (data not shown).

Cyclin J is not required for oogenesis and early embryonic development

To address the function of Cyclin J, we generated lines completely lacking the *CycJ* gene. Transposon insertions carrying FRT sites allowed a Flp recombinase-mediated isolation of an 11 kb chromosomal deletion, *Df(3L)AJ14*, removing *CycJ* and the flanking genes *armitage (armi)* and *CG14971* (Fig. 6A). Characterization of the *Df(3L)AJ14* chromosome by PCR confirmed the presence of the expected deletion (Fig. 6B). To restore the function of the flanking genes, we introduced transgenes (*garmi* and *gCG14971*) carrying genomic fragments including *armi* and *CG14971*, respectively, by P element-mediated germline transformation and recombined insertions with *Df(3L)AJ14*.

Initial analyses revealed that homozygous *Df(3L)AJ14* progeny from heterozygous parents eclosed as adults. The frequency of these adults in comparison to heterozygous siblings (Table 1) indicated that the genes *CycJ*, *armi* and *CG14971* are completely dispensable for development to the adult stage. We also obtained normal numbers of adults homozygous for *Df(3L)AJ14* which had in addition either one or the other or both transgene insertions (*garmi III.8* and *gCG14971 III.10*). These transgene insertions therefore do no disrupt gene functions required for development to the adult stage.

Table 1
Viability and fertility of flies without *CycJ*, *armi* or *CG14971*.

Genotype	Viability[a]	Fertility[b]	
		Female	Male
w^1	N.d.[c]	100	100
$CycJ^{DG29702}/CycJ^{DG29702}$	N.d.[d]	102	N.d.
$CycJ^{DG29702}/Df(3L)AJ14$	N.d.[d]	113	N.d.
$CycJ^{DG29702}/Df(3L)Exel6095$	N.d.[d]	110	N.d.
Df(3L)AJ14/Df(3L)AJ14, garmi III.8, gCG14971 III.10	122	111	140
gCycJ II.41/+; Df(3L)AJ14/Df(3L)AJ14, garmi III.8, gCG14971 III.10	124	115	163
Df(3L)AJ14/Df(3L)AJ14, garmi III.8	114	90	120
Df(3L)AJ14/Df(3L)AJ14	97	0	29

[a] Progeny flies with the listed genotypes as well as balanced siblings eclosing from the same cross were counted ($n>300$). The fraction of progeny with the listed genotype was calculated and expressed in percent of the fraction predicted in case of full viability.
[b] Parallel crosses (3–4 for each genotype) with a fixed number of either test females or test males were crossed with the same number w^1 flies. The total number of progeny was counted and expressed in percent of the number of progeny obtained with the w^1 control crosses ($n=1324$).
[c] N.d., not determined.
[d] Although not precisely quantified, the viability appears to be normal.

Subsequent analysis of flies lacking one or several of the genes *CycJ*, *armi* and *CG14971* indicated that *armi* but not the other genes are required for normal fertility (Table 1). *armi* encodes a putative RNA helicase involved in the RNA interference pathway and is known to be required for normal fertility (Cook et al., 2004). Females without the *armi* gene did not produce eggs and males had a reduced fertility (Table 1). The *armi* null phenotype therefore might be more severe than the phenotypes observed previously with partial loss of function alleles which result in abnormally patterned eggs in reduced numbers (Cook et al., 2004). *CG14971* is an uncharacterized gene which appears to encode a ubiquitously expressed member of the solute carrier protein family.

Our conclusion that *CycJ* is not required for viability and fertility was further supported by our characterization of a recently isolated transposon insertion $P\{wHy\}CycJ^{DG29702}$ (Huet et al., 2002). Our sequence analysis of a PCR fragment confirmed that this insertion disrupts the *CycJ* coding sequence after the second codon. Therefore the insertion is likely to cause a complete loss of *CycJ* function. Flies homozygous or hemizygous for this insertion eclosed in normal numbers and were found to be fully fertile (Table 1). The same findings (data not shown) were also observed with flies hemizygous for $PBac\{5HPw^+\}CycJ^{A138}$, a transposon insertion which we also confirmed to reside in the first intron and therefore might not necessarily impair *CycJ* gene function.

To evaluate whether loss of *CycJ* might result in more subtle defects during the syncytial cycles of early embryogenesis, we collected eggs from *CycJ*-deficient females (Fig. 6C) and analyzed the frequency and appearance of mitotic figures after fixation and DNA staining. However, apart from rare abnormalities, which were also observed to the same extent in control collections, defects were not apparent (Fig. 6D). Similarly, we failed to detect an increased rate of X chromosome non-disjunction during meiosis in *CycJ*-deficient females (see Materials and methods). A double mutant analysis confirmed that Cyclin J is unlikely to have substantial functional overlap with Cyclin E. The reduced fertility of females homozygous for the hypomorphic mutation $CycE^{01672}$ (Lilly and Spradling, 1996) was marginally enhanced in double mutants lacking *CycJ* function completely (see Materials and methods). Moreover, additional attempts to detect potential genetic interactions between *CycJ* and *CycA*, *CycB*, *CycB3* or *CycE* equally failed to reveal clear evidence for functional redundancies (Supplementary Figure 1). *CycJ*-deficient females with only one functional gene copy of *CycA*, *CycB*, *CycB3* or *CycE* had a very similar fertility as those with two functional copies. In addition, progression through the syncytial cycles was not compromised by reducing the number of functional copies of these other cyclin genes in *CycJ*-deficient mothers.

Discussion

Sequence comparisons demonstrate that Cyclin J is an evolutionary conserved cyclin family member. *Cyclin J* homologs are present throughout the metazoan radiation, as well as in their unicellular sister group. While this evolutionary conservation points to an important role of Cyclin J, its functional characterization has remained very limited. Moreover, our analyses contradict previous conclusions and reveal a number of unexpected findings. Using transgenic *Drosophila* lines expressing Cyclin J versions with N- or C-terminal EGFP extensions, we demonstrate that it binds to Cdk1 and not to Cdk2. However, in contrast to the other known Cdk1 partners, the A- and B-type cyclins, Cyclin J does not appear to become proteolysed during mitosis. In addition, its expression pattern is far more restricted. While A- and B-type cyclin expression is observed in all mitotically proliferating and meiotic cells, Cyclin J is only expressed in the female germ line. While initially present at low levels in all nuclei within the germarium, it gets highly enriched in the germinal vesicle within the oocyte during egg chamber development until stage 12, and

disappears again later concomitant with germinal vesicle breakdown at the start of the first meiotic division. Surprisingly, we find that Cyclin J is not required for female fertility. Chromosome segregation during female meiosis as well as the rapid early embryonic cell cycles after fertilization occurs normally in the complete absence of Cyclin J. Only a slight increase in the number of embryos that do not develop beyond cycle 1 is noticeable when averaging over many collections from *CycJ*-deficient females.

Most of our results are at variance with those published earlier (Finley and Brent, 1994; Kolonin and Finley, 2000). Based on the described yeast two hybrid and co-immunoprecipitation experiments, *Drosophila* Cyclin J for instance was suggested to prefer Cdk2 over Cdk1 as a partner kinase. Curiously, in these same yeast two hybrid experiments, *Drosophila* Cyclin E was also observed to have the opposite preference from what we have observed *in vivo* (Finley and Brent, 1994; Knoblich et al., 1994). In case of the published co-immunoprecipitation experiments (Kolonin and Finley, 2000), a cross reaction of the affinity-purified rabbit antibodies against Cyclin J with a protein of similar molecular might have compromised the validity of these earlier conclusions. Concerning the validity of our present discordant conclusions, we emphasize that we cannot exclude the possibility that the EGFP fusions, which we have studied, do not behave like the untagged endogenous Cyclin J. We consider this possibility to be unlikely, as we have obtained consistent results with EGFP fused at either the N- or the C-terminus of Cyclin J. Moreover, experiments with other cyclins have clearly demonstrated that EGFP extensions do not affect their function (Buszczak et al., 2007; den Elzen and Pines, 2001; Hagting et al., 1998; Jackman et al., 2002). Finally, our finding that progression through the syncytial cycles of early *Drosophila* embryogenesis is not noticeably affected by the complete absence of Cyclin J is entirely independent of assumptions concerning the functionality of our Cyclin J fusions. The severe mitotic defects reported to occur after injection of antibodies or aptamers against Cyclin J (Kolonin and Finley, 2000) might reflect cross-reactions or indicate that the binding of these reagents to Cyclin J has other consequences than eliminating Cyclin J altogether.

The absence of obvious phenotypic abnormalities after complete elimination of *CycJ* function might indicate functional redundancies. Our preliminary evidence argues against the suggestion that it is the function of Cyclin A, B, B3 or E which masks a Cyclin J requirement. Our failure to prevent the characteristic *CycA* zygotic effect mutant phenotype by expression of Cyclin J fusions with EGFP in embryos argues against major functional overlap between Cyclin A and Cyclin J. In addition, a reduction of the number of functional *CycA*, *CycB*, *CycB3* or *CycE* gene copies in *CycJ*-deficient females using multiple strong or null alleles did not consistently reduce their fertility or affect progression through the syncytial cycles in progeny. Moreover, genetic elimination of *CycJ* in females with reduced *CycE* function did not further reduce their compromised fertility. Future unbiased genetic screens in our *CycJ*-deficient background might lead to an identification of components acting redundantly with Cyclin J.

Redundant functional pathways might also explain that some metazoans like *C. elegans* appear to have lost Cyclin J and that the expression pattern of Cyclin J varies in different metazoan lineages. In contrast to *Drosophila* Cyclin J, which appears to be expressed exclusively in the female germline, the human Cyclin J paralogs are much more widely expressed in various somatic tissues according to the tissue distribution of the expressed sequence tags. The apparent somatic expression in humans, as well as the presence of a Cyclin J homolog in the choanoflagellate *Monosiga brevicollis*, clearly argues against the notion that the primordial Cyclin J function is oogenesis-specific.

Acknowledgments

We thank Anja Katzemich, Brigitte Jaunich and Dirk Beuchle for their help during the initial and final phases of the work, respectively. We are also grateful to the Functional Genomics Center Zurich (FGCZ) for support of the MS analyses. The work was supported by the Deutsche Forschungsgemeinschaft (DFG LE 987/5-1).

Appendix A. Supplementary data

Supplementary data associated with this article can be found, in the online version, at doi:10.1016/j.ydbio.2009.06.042.

References

Brand, A.H., Perrimon, N., 1993. Targeted gene expression as a means of altering cell fates and generating dominant phenotypes. Development 118, 401–415.
Brunner, E., Ahrens, C.H., Mohanty, S., Baetschmann, H., Loevenich, S., Potthast, F., Deutsch, E.W., Panse, C., de Lichtenberg, U., Rinner, O., Lee, H., Pedrioli, P.G., Malmstrom, J., Koehler, K., Schrimpf, S., Krijgsveld, J., Kregenow, F., Heck, A.J., Hafen, E., Schlapbach, R., Aebersold, R., 2007. A high-quality catalog of the *Drosophila melanogaster* proteome. Nat. Biotechnol. 25, 576–583.
Buszczak, M., Paterno, S., Lighthouse, D., Bachman, J., Planck, J., Owen, S., Skora, A.D., Nystul, T.G., Ohlstein, B., Allen, A., Wilhelm, J.E., Murphy, T.D., Levis, R.W., Matunis, E., Srivali, N., Hoskins, R.A., Spradling, A.C., 2007. The carnegie protein trap library: a versatile tool for *Drosophila* developmental studies. Genetics 175, 1505–1531.
Cook, H.A., Koppetsch, B.S., Wu, J., Theurkauf, W.E., 2004. The *Drosophila* SDE3 homolog armitage is required for oskar mRNA silencing and embryonic axis specification. Cell 116, 817–829.
den Elzen, N., Pines, J., 2001. Cyclin A is destroyed in prometaphase and can delay chromosome alignment and anaphase. J. Cell Biol. 153, 121–136.
Edgar, B.A., Orr-Weaver, T.L., 2001. Endoreplication cell cycles: more for less. Cell 105, 297–306.
Edgar, B.A., Sprenger, F., Duronio, R.J., Leopold, P., O'Farrell, P.H., 1994. Distinct molecular mechanisms regulate cell cycle timing at successive stages of *Drosophila* embryogenesis. Genes Dev. 8, 440–452.
Evans, T., Rosenthal, E.T., Youngblom, J., Distel, D., Hunt, T., 1983. Cyclin: a protein specified by maternal mRNA in sea urchin eggs that is destroyed with each cleavage division. Cell 33, 389–397.
Finley, R.L., Brent, R., 1994. Interaction mating reveals binary and ternary connections between *Drosophila* cell cycle regulators. Proc. Natl. Acad. Sci. U. S. A. 91, 12980–12984.
Finley, R.L., Thomas, B.J., Zipursky, S.L., Brent, R., 1996. Isolation of *Drosophila* cyclin D, a protein expressed in the morphogenetic furrow before entry into S phase. Proc. Natl. Acad. Sci. U. S. A. 93, 3011–3015.
Fischer, M.G., Heeger, S., Hacker, U., Lehner, C.F., 2004. The mitotic arrest in response to hypoxia and of polar bodies during early embryogenesis requires *Drosophila* Mps1. Curr. Biol. 14, 2019–2024.
Follette, P.J., Duronio, R.J., O'Farrell, P.H., 1998. Fluctuations in cyclin E levels are required for multiple rounds of endocycle S phase in *Drosophila*. Curr. Biol. 8, 235–238.
Guo, J., Song, J., Wang, F., Zhang, X.S., 2007. Genome-wide identification and expression analysis of rice cell cycle genes. Plant Mol. Biol. 64, 349–360.
Hacker, U., Perrimon, N., 1998. DRhoGEF2 encodes a member of the Dbl family of oncogenes and controls cell shape changes during gastrulation in *Drosophila*. Genes Dev. 12, 274–284.
Hagting, A., Karlsson, C., Clute, P., Jackman, M., Pines, J., 1998. MPF localization is controlled by nuclear export. EMBO J. 17, 4127–4138.
Hatfield, S.D., Shcherbata, H.R., Fischer, K.A., Nakahara, K., Carthew, R.W., Ruohola-Baker, H., 2005. Stem cell division is regulated by the microRNA pathway. Nature 435, 974–978.
Hoskins, R.A., Nelson, C.R., Berman, B.P., Laverty, T.R., George, R.A., Ciesiolka, L., Naeemuddin, M., Arenson, A.D., Durbin, J., David, R.G., Tabor, P.E., Bailey, M.R., DeShazo, D.R., Catanese, J., Mammoser, A., Osoegawa, K., de Jong, P.J., Celniker, S.E., Gibbs, R.A., Rubin, G.M., Scherer, S.E., 2000. A BAC-based physical map of the major autosomes of *Drosophila melanogaster*. Science 287, 2271–2274.
Huet, F., Lu, J.T., Myrick, K.V., Baugh, L.R., Crosby, M.A., Gelbart, W.M., 2002. A deletion-generator compound element allows deletion saturation analysis for genomewide phenotypic annotation. Proc. Natl. Acad. Sci. U. S. A. 99, 9948–9953.
Hwang, H.C., Clurman, B.E., 2005. Cyclin E in normal and neoplastic cell cycles. Oncogene 24, 2776–2786.
Jackman, M., Kubota, Y., den Elzen, N., Hagting, A., Pines, J., 2002. Cyclin A- and cyclin E-Cdk complexes shuttle between the nucleus and the cytoplasm. Mol. Biol. Cell 13, 1030–1045.
Jacobs, H.W., Knoblich, J.A., Lehner, C.F., 1998. *Drosophila* Cyclin B3 is required for female fertility and is dispensable for mitosis like Cyclin B. Genes Dev. 12, 3741–3751.
Karr, T.L., Alberts, B.M., 1986. Organization of the cytoskeleton in early *Drosophila* embryos. J. Cell Biol. 102, 1494–1509.
Kerrebrock, A.W., Miyazaki, W.Y., Birnby, D., Orr-Weaver, T.L., 1992. The *Drosophila* mei-S322 gene promotes sister chromatid cohesion in meiosis following kinetochore differentiation. Genetics 130, 827–841.
Knoblich, J.A., Sauer, K., Jones, L., Richardson, H., Saint, R., Lehner, C.F., 1994. Cyclin E controls S phase progression and its downregulation during *Drosophila* embryogenesis is required for the arrest of cell proliferation. Cell 77, 107–120.
Kolonin, M.G., Finley Jr., R.L., 2000. A role for cyclin J in the rapid nuclear division cycles of early *Drosophila* embryogenesis. Dev. Biol. 227, 661–672.
Lehner, C.F., O'Farrell, P.H., 1989. Expression and function of *Drosophila* cyclin A during embryonic cell cycle progression. Cell 56, 957–968.

Lehner, C.F., O'Farrell, P.H., 1990. The roles of *Drosophila* cyclin A and cyclin B in mitotic control. Cell 61, 535–547.
Lilly, M.A., Spradling, A.C., 1996. The *Drosophila* endocycle is controlled by cyclin E and lacks a checkpoint ensuring S-phase completion. Genes Dev. 10, 2514–2526.
Makarenkov, V., 2001. T-REX: reconstructing and visualizing phylogenetic trees and reticulation networks. Bioinformatics 17, 664–668.
Meyer, C.A., Jacobs, H.W., Datar, S.A., Du, W., Edgar, B.A., Lehner, C.F., 2000. *Drosophila* Cdk4 is required for normal growth and is dispensable for cell cycle progression. EMBO J. 19, 4533–4542.
Morgan, D.O., 2007. The Cell Cycle — Principles of Control. New Sience Press Ltd., London.
Page, A.W., Orr-Weaver, T.L., 1997. Activation of the meiotic divisions in *Drosophila* oocytes. Dev. Biol. 183, 195–207.
Page, S.L., Hawley, R.S., 2001. c(3)G encodes a *Drosophila* synaptonemal complex protein. Genes Dev. 15, 3130–3143.
Parks, A.L., Cook, K.R., Belvin, M., Dompe, N.A., Fawcett, R., Huppert, K., Tan, L.R., Winter, C.G., Bogart, K.P., Deal, J.E., Deal-Herr, M.E., Grant, D., Marcinko, M., Miyazaki, W.Y., Robertson, S., Shaw, K.J., Tabios, M., Vysotskaia, V., Zhao, L., Andrade, R.S., Edgar, K.A., Howie, E., Killpack, K., Milash, B., Norton, A., Thao, D., Whittaker, K., Winner, M.A., Friedman, L., Margolis, J., Singer, M.A., Kopczynski, C., Curtis, D., Kaufman, T.C., Plowman, G.D., Duyk, G., Francis-Lang, H.L., 2004. Systematic generation of high-resolution deletion coverage of the *Drosophila melanogaster* genome. Nat. Genet. 36, 288–292.
Peters, J.M., 2006. The anaphase promoting complex/cyclosome: a machine designed to destroy. Nat. Rev., Mol. Cell Biol. 7, 644–656.
Reber, A., Lehner, C.F., Jacobs, H.W., 2006. Terminal mitoses require negative regulation of Fzr/Cdh1 by Cyclin A, preventing premature degradation of mitotic cyclins and String/Cdc25. Development 133, 3201–3211.
Sauer, K., Knoblich, J.A., Richardson, H., Lehner, C.F., 1995. Distinct modes of cyclin E/cdc2c kinase regulation and S phase control in mitotic and endoreduplication cycles of *Drosophila* embryogenesis. Genes Dev. 9, 1327–1339.
Schittenhelm, R.B., Heeger, S., Althoff, F., Walter, A., Heidmann, S., Mechtler, K., Lehner, C.F., 2007. Spatial organization of a ubiquitous eukaryotic kinetochore protein network in *Drosophila* chromosomes. Chromosoma 116, 385–402.
Sigrist, S.J., Lehner, C.F., 1997. *Drosophila* fizzy-related down-regulates mitotic cyclins and is required for cell proliferation arrest and entry into endocycles. Cell 90, 671–681.
Spradling, A.C., 1993. Developmental genetics of oogenesis. In: Bate, M., Martinez Arias, A. (Eds.), The Development of *Drosophila melanogaster*, 1. Cold Spring Harbor Laboratory Press, Cold Spring Harbor, NY, pp. 1–70.
Sprenger, F., Yakubovich, N., O'Farrell, P.H., 1997. S phase function of *Drosophila* cyclin A and its downregulation in G1 phase. Curr. Biol. 7, 488–499.
Thibault, S.T., Singer, M.A., Miyazaki, W.Y., Milash, B., Dompe, N.A., Singh, C.M., Buchholz, R., Demsky, M., Fawcett, R., Francis-Lang, H.L., Ryner, L., Cheung, L.M., Chong, A., Erickson, C., Fisher, W.W., Greer, K., Hartouni, S.R., Howie, E., Jakkula, L., Joo, D., Killpack, K., Laufer, A., Mazzotta, J., Smith, R.D., Stevens, L.M., Stuber, C., Tan, L.R., Ventura, R., Woo, A., Zakrajsek, I., Zhao, L., Chen, F., Swimmer, C., Kopczynski, C., Duyk, G., Winberg, M.L., Margolis, J., 2004. A complementary transposon tool kit for *Drosophila melanogaster* using P and piggyBac. Nat. Genet. 36, 283–287.
Wang, Z., Lin, H., 2005. The division of *Drosophila* germline stem cells and their precursors requires a specific cyclin. Curr. Biol. 15, 328–333.
Wang, G., Kong, H., Sun, Y., Zhang, X., Zhang, W., Altman, N., DePamphilis, C.W., Ma, H., 2004. Genome-wide analysis of the cyclin family in *Arabidopsis* and comparative phylogenetic analysis of plant cyclin-like proteins. Plant Physiol. 135, 1084–1099.
Weiss, A., Herzig, A., Jacobs, H., Lehner, C.F., 1998. Continuous cyclin E expression inhibits progression through endoreduplication cycles in *Drosophila*. Curr. Biol. 8, 239–242.
Woo, R.A., Poon, R.Y., 2003. Cyclin-dependent kinases and S phase control in mammalian cells. Cell Cycle 2, 316–324.

Drosophila Cyclin J is a mitotically stable Cdk1 partner without essential functions

Friederike Althoff[1], Ivana Viktorinová[2], Johanna Kastl[3] and Christian F. Lehner[1,*]

[1] Institute of Zoology, University of Zurich, Zurich, Switzerland

[2] Max-Planck-Institute for Cell Biology and Genetics, Dresden, Germany

[3] Department of Biology, Molecular Genetics, University of Constance, Germany

[*] Correspondence to: Christian F. Lehner, University of Zurich, Institute of Zoology Winterthurerstrasse 190, 8057 Zurich, Switzerland, Tel.: 41 44 63 54871; FAX: 41 44 63 56820; E mail: christian.lehner@zool.uzh.ch

Supplementary Material

- Supplementary Table1.
Proteins co-immunoprecipitated with CycJ-EGFP

- Supplementary Figure 1.
Progression through the syncytial division cycles in *CycJ*-deficient embryos heterozygous for mutations in other cyclin genes

Supplementary Table 1: Proteins co-immunoprecipitated with CycJ-EGFP

Immunoprecipitates isolated with anti-GFP from ovary extracts of either *gCycJ-EGFP II.6* or *gCal1-EGFP II.1* females were resolved by gel electrophoresis. Thereafter the gel lanes were cut from top to bottom into 15 slices, each of which was digested with trypsin before MS/MS analysis of the resulting peptides using the MASCOT search engine (www.matrixscience.com). The table includes all Drosophila proteins for which at least one peptide with either an ion score of >40 or an expect value of $<10^{-4}$ was detected. For each gel slice, the identified proteins are ordered from top to bottom according to the number of different peptides detected with the protein revealed by the maximal number of detected peptides on top. Proteins which were observed in both immunoprecipitates (CycJ-EGFP and Cal1-GFP control) and thus appear to represent non-specifically associated contaminants are marked in green. Cdk1/Cdc2 which is marked in red was only detected in the CycJ-EGFP immunoprecipitate. The other proteins that were only detected in the CycJ-EGFP immunoprecipitate are in general highly abundant proteins (like ribosomal proteins) and some of these have been detected as contaminants in earlier co-immunoprecipitation experiments (unpublished observations). None of these proteins is a protein kinase family member.

region	MW	CG number	name	comment
1	> 270 kD	-		
2	~ 150-270 kD	-		
3	~ 100-150 kD	CG3999		glycine dehydrogenase
		CG2331	TER94	
		CG34333		APAAPSYS repeat protein
4	~ 80-100 kD	CG3999		glycine dehydrogenase
		CG4264	Hsc70-4	
		CG2175	dec-1	
		CG1242	Hsp83	
		CG34333		APAAPSYS repeat protein
		CG4147	Hsc70-3	
		CG8542	Hsc70-5	
		CG7470		aldehyde dehydrogenase family member
5	~ 65-80 kD	CG2175	dec-1	
		CG4246	Hsc70-4	alternatively CG8937(Hsc70-1)
		CG12101	Hsp60	alternatively CG7235 (Hsp60C)
6	~ 52-65 kD	CG2175	dec-1	
		CG9277	βTub56D	
		CG4799	Pen	
		CG3612	blw	
		CG2512	αTub84D	alternatively CG1913 (αTub84B)
		CG9050	Fcp26Aa	
		CG3999		glycine dehydrogenase
		CG8351	Tcp-1η	
		CG1799	ras	
		CG34333		APAAPSYS repeat protein
		CG2985	Yp1	
7	~ 45-52 kD	CG2985	Yp1	
		CG2979	Yp2	
		CG11129	Yp3	
		CG9277	βTub56D	
		CG4027	Act5C	alternatively product of other Actin paralogs
		CG2175	dec-1	
		CG11154	ATPsyn-β	
		CG8280	Ef1α48D	
		CG1489	Pros45	
		CG2152	Pcmt	
		CG34333		APAAPSYS repeat protein
		CG4863	RpL3	
		CG9677	Int6	
		CG3999		glycine dehydrogenase
		CG9124	eIF-3p40	
		CG5502	RpL4	
		CG2098	ferrochelatase	
8	~ 38-45 kD	CG11129	Yp3	
		CG8882	Trip1	
		CG34333		APAAPSYS repeat protein
		CG14792	sta	
		CG9124	eIF-3p40	
		CG7010	l(1)G0334	
		CG2175	dec-1	
9	~ 34-38 kD	CG5363	cdc2	
10	~ 32-34 kD	CG2152	Pcmt	
		CG5363	cdc2	
		CG3999		glycine dehydrogenase
		CG4183	Hsp26	
		CG9769		eIF3f
11	~ 26-32 kD	CG2152	Pcmt	
		CG1633	Jafrac1	
		CG3481	Adh	
12	~ 18-26 kD	-		
13	~ 12-18 kD	CG17949	His2B	
		CG14542		charged multivesicular body protein 2A (ESCRT-III)
		CG34333		APAAPSYS repeat protein
		CG9916	Cyp1	
		CG4464	RpS19a	
		CG4918	RpLP2	
		CG3922	RpS17	
14	~ 8-12 kD	CG3999		glycine dehydrogenase
15	< 8 kD	-		

Supplementary Figure 1: Progression through the syncytial division cycles in *CycJ*-deficient embryos heterozygous for mutations in other cyclin genes

Embryos were collected from females that either had one copy of the *CycJ* gene (*Df(3L)AJ14*/+) or none (*Df(3L)AJ14/ΔCycJ = Df(3L)AJ14, garmi III.8, gCG14971 III.10*). In addition, these females had either two functional copies of other cyclin genes (+/+) or only one functional copy of a particular cyclin gene in trans over a mutant allele ($CycA^{neo114}$/+, $CycA^{C8LR1}$/+, $CycB^{2}$/+, $CycB^{3}$/+, $CycB3^{3}$/+, $CycE^{AR95}$/+, or $CycE^{pz5}$/+). After one hour of egg collection, one half was fixed immediately (red bars) while the other half was aged for an additional hour at 25°C before fixation (blue bars). The embryos were stained with a DNA stain and staged microscopically (n > 200 for each genotype). The bar diagram displays the fraction of embryos which were found to be at a developmental stage either before mitosis 1 (before M1), during cycles 1-4 (1-4), 5-9 (5-9), 10-13 (10-13), interphase 14 (I14), or after onset of mitosis 14 (>M14). The fraction of embryos with abnormal phenotypes like chromatin bridges during anaphase and telophase or irregular spacing of nuclei or mitotic figures was found to be below 3% for all of the analyzed genotypes. The embryos in the aged collections obtained from *CycJ*-deficient females which were before M1 (blue bars marked by asterisks) represent either unfertilized embryos or fertilized embryos which have failed to develop beyond completion of female meiosis. Since their fraction appeared to vary extensively for the different genotypes, we evaluated two additional independent collections and noted a surprisingly poor reproducibility. The average obtained for the three collections (+/- s.d.) is given on the right side. In particular, the high fractions of embryos before M1 observed with some of the *CycJ*-deficient female genotypes (first, second and sixth row from the top) could not be confirmed in these additional experiments.

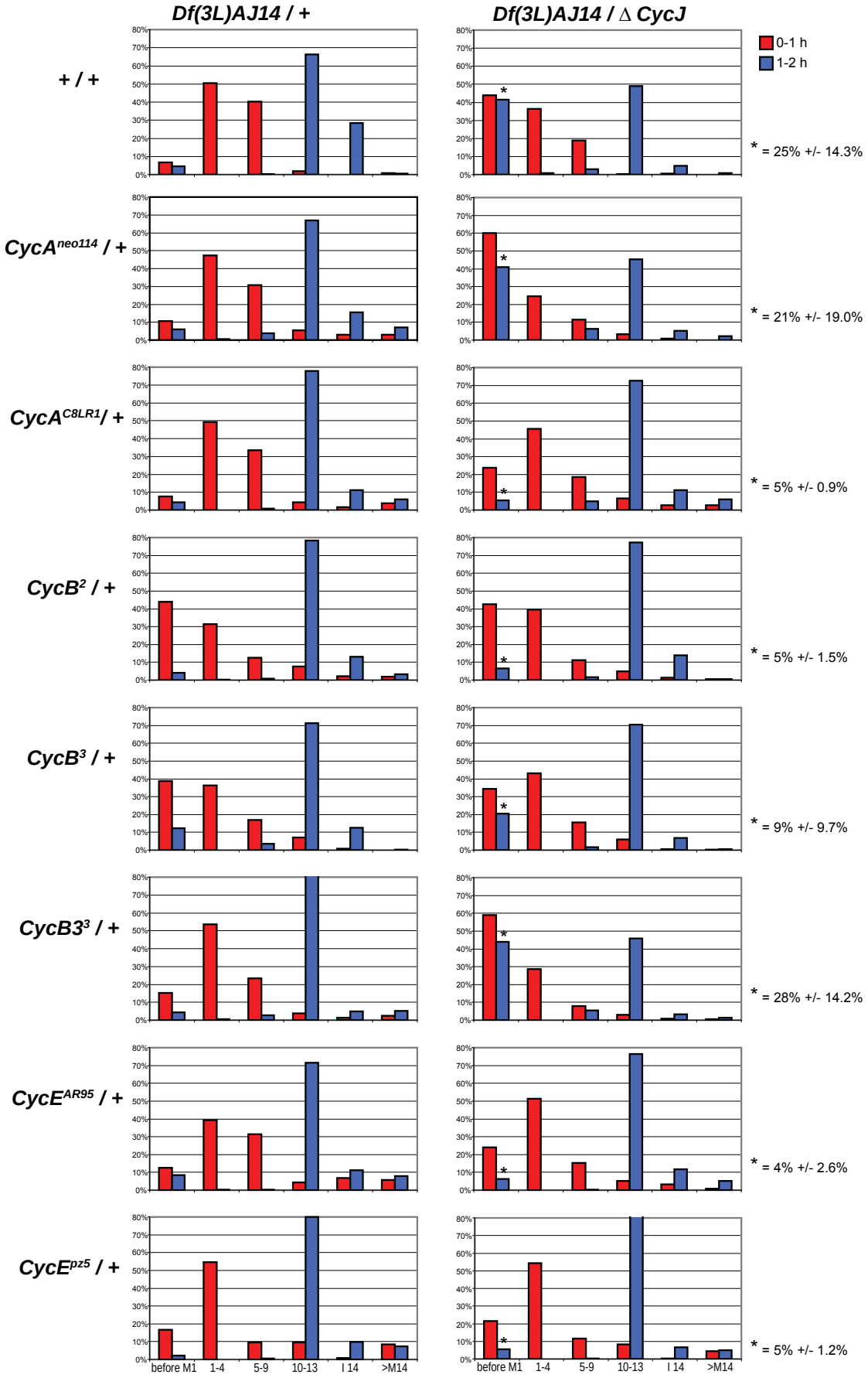
Df(3L)AJ14 / +
Df(3L)AJ14 / Δ CycJ
0-1 h
1-2 h
+ / +
CycA neo114 / +
CycA C8LR1 / +
CycB 2 / +
CycB 3 / +
CycB3 3 / +
CycE AR95 / +
CycE pz5 / +
* = 25% +/- 14.3%
* = 21% +/- 19.0%
* = 5% +/- 0.9%
* = 5% +/- 1.5%
* = 9% +/- 9.7%
* = 28% +/- 14.2%
* = 4% +/- 2.6%
* = 5% +/- 1.2%
before M1
1-4
5-9
10-13
l 14
>M14

Part 3:

Level and localization of *Drosophila* Mps1 are crucial for checkpoint-dependent and independent functions

Contribution to this part:

Christian F. Lehner and me designed the experiments. I performed the experiments with technical help from Brigitte Jaunich, Christian Sollmann, and Sina Moser. I analyzed the data and wrote the manuscript with contributions from Christian F. Lehner.

Abstract

The **s**pindle **a**ssembly **c**heckpoint (SAC) effectively reduces chromosome segregation errors during mitotic divisions. It is activated in early mitosis by kinetochores that are not yet attached to the mitotic spindle. Moreover, it is also activated (although perhaps indirectly) by kinetochores of chromosomes that are incorrectly attached and hence misoriented within the mitotic spindle. SAC activity blocks the onset of anaphase and exit from mitosis. Thereby it provides time for the correction of incomplete and erroneous sister kinetochore attachments to the mitotic spindle. The SAC is silenced when all chromosomes are properly oriented within the spindle. SAC silencing allows anaphase and exit from mitosis to proceed.

Mps1 kinase is essential for SAC function in several organisms including *Drosophila*. Its localization pattern changes dynamically during the cell cycle. It accumulates transiently on kinetochores from early mitosis until metaphase when the SAC is active. I have exploited advantages of the *Drosophila* system (like the availability of null mutants and other genetic methodology) for an analysis of Mps1 function.

Addressing the reasons for Mps1 disappearance from the kinetochores before the metaphase-to-anaphase transition, I find that it is not accompanied by substantial Mps1 degradation. Furthermore, N-terminal phosphorylation of Mps1, which is detectable by an electrophoretic mobility shift, was found to endure into anaphase, indicating that it is also not directly controlling kinetochore localization. Dissecting the role of different Mps1 domains, I find that neither the N-terminal regulatory nor the C-terminal kinase domain is sufficient for kinetochore recruitment of EGFP. Moreover, a predicted kinase-dead Mps1 variant also failed to localize to kinetochores, although it still is capable of self-interaction. Screening for Mps1 interaction partners by co-immunoprecipitation and mass spectrometry identified Mad1. Kinetochore localization of Mad1 was found to depend on Mps1, and vice versa Mps1 at kinetochores is partially dependent on Mad1. Moreover, kinetochore levels of both Mad1 and Mps1 were reduced in the absence of Mad2. Thus kinetochore localization of the three SAC proteins Mps1, Mad1 and Mad2 is at least partially interdependent.

An experiment designed to evaluate the functional significance of Mps1 disappearance from kinetochores for SAC silencing revealed that both correct localization and level of Mps1 are important for a successful mitosis. Constitutive kinetochore localization of Mps1 resulted in severe anaphase defects, while over-expression resulted in SAC activation and SAC-independent mitotic defects. A careful characterization of these latter defects led me to propose that Mps1 might inhibit sister chromatid resolution in a previously unrecognized, SAC-independent manner.

Finally, an initial comparison of SAC function in cultured embryonic S2R+ cells and cells in living embryos revealed striking differences between the systems.

Introduction

For genetic stability, it is important for the cell to distribute the two sister chromatids of every chromosome 1:1 into the two daughter cells during mitosis. To this end, it is extremely important to establish correct attachments between the kinetochores and the spindle microtubules before anaphase starts. The **s**pindle **a**ssembly **c**heckpoint (SAC) is crucial for this process (Musacchio and Salmon, 2007). Correct attachment cannot only be sensed as occupancy of the kinetochore by spindle microtubules but—in order to prevent syntelic and merotelic attachments—also as physical tension between the sister kinetochores. Tension results from pulling forces towards the opposite spindle poles that is counteracted by sister chromatid cohesion, and is only present if the two sister chromatids are properly bioriented (Maresca and Salmon, 2010). The SAC is sending a wait-anaphase signal inhibiting **a**naphase-**p**romoting **c**omplex/**c**yclosome (APC/C) dependent degradation of mitotic regulators until all sister kinetochores are correctly attached to the mitotic spindle. Thereby it is allowing for extra time to detect incorrect or missing attachments and correct errors before anaphase onset. Anaphase is only allowed to start when all kinetochores in the cell are attached correctly.

The SAC consists of a highly regulated interacting network of proteins, comprising several scaffold components mediating protein interactions, like Bub3 or Mad1, and components with enzymatic activity, such as the kinases BubR1 and Mps1. SAC effectors are Mad2 and BubR1, which can bind and inhibit Cdc20 function (Sudakin et al., 2001). SAC components display a very dynamic localization behavior. During prophase they accumulate at the kinetochores from where they disappear before **m**etaphase-to-**a**naphase transition (M/A-transition) (Howell et al., 2004; Shah et al., 2004). This localization pattern, which correlates perfectly with site and time period of the establishment of correct attachments, suggests a functional relevance for the SAC.

If a cell is treated with spindle poisons that interfere with the mitotic spindle, it reacts with a delay of anaphase onset and tries to establish correct attachments anyhow. During this delayed mitosis (D-mitosis), an increased accumulation of SAC components at the kinetochores is observed (Rieder and Maiato, 2004).

Albeit under the influence of spindle poisons and thus being incapable of forming a functional mitotic spindle and correct attachments, cells will exit from mitosis after a while. In this situation the SAC is not satisfied. Thus cells have either adapted their SAC activity (adaptation) or they have slipped though and exited from mitosis in the presence of an activated SAC (slippage). During slippage, only basal APC/C activity and kinetochores with high levels of SAC components are observed. Nevertheless, exit from mitosis takes place, and it has been suggested that this is due to a slow basal degradation of Cyclin B and a concomitant decrease of Cdk1 activity (Brito and Rieder, 2006).

During unchallenged mitosis, the SAC is silenced as soon as correct attachments have been established. The APC/C is activated, causing abrupt Cyclin B degradation, separase activation and an efficient exit from mitosis. Checkpoint silencing is accompanied by shedding of SAC components from the kinetochore (Chen et al., 1996; Li and Benezra, 1996). However, it was not shown explicitly that shedding alone is sufficient to keep the SAC silenced during exit from mitosis.

The Mps1 family of protein kinases is conserved from yeast to human. It is a family of non-RD protein kinases (Nolen et al., 2004) with dual specificity (Ser/Thr and Tyr) being composed of two major domains, an N-terminal domain (Mps1(N)), which is supposed to have a regulatory function, and a C-terminal kinase domain (Mps1(C)) (Fisk et al., 2004). Mps1 was originally discovered in yeast to be required for spindle pole body duplication, hence the name, **m**ono**p**olar **s**pindle **1** (Winey et al., 1991). However, its involvement in duplication of centrosomes (the metazoan equivalents to the yeast spindle pole bodies) is controversial in higher organisms (Fisk et al., 2003; Stucke et al., 2002). In *Drosophila melanogaster*, Mps1 is dispensable for centrosome duplication (Fischer et al., 2004).

The SAC function of this kinase has been confirmed in all species studied so far (*Saccharomyces cerevisiae* (Weiss and Winey, 1996), *Schizosaccharomyces pombe* (He et al., 1998), *Xenopus laevis* (Abrieu et al., 2001), *Danio rerio* (Poss et al., 2002), *Drosophila melanogaster* (Fischer et al., 2004), *Homo sapiens* (Stucke et al., 2002)). Nevertheless, certain aspects of its involvement in the SAC vary in different experimental systems. In yeast, Mps1 over-expression has been described to result in ectopic SAC activation and a mitotic arrest (Hardwick et al., 1996). In human cells, however, Mps1 over-expression does not seem to have an effect (Fisk et al., 2003; Stucke et al., 2002).

A number of studies with regard to the SAC function of Mps1 have been performed in human cells. However, these have to rely on chemical kinase inhibitors or RNAi (Lan and Cleveland, 2010). A real null mutant situation, which would be highly informative, is not available in this system.

Based on current insight three aspects appear to be of particular interest in the case of Mps1 function: First the regulation of Mps1 protein level during the cell cycle, second the regulation of its kinase activity by posttranslational modifications, and third the dynamics of its intracellular localization. These aspects are likely to be tightly interconnected.

The overall abundance of Mps1 is regulated by the balance between expression and degradation. Mps1 degradation has been shown to be relevant for the irreversibility of SAC

silencing in yeast during exit from M phase. When sister chromatid cohesion is cleaved at the M/A-transition, tension between sister kinetochores is decreasing abruptly. In principle, this lack of tension might reactivate the SAC. However, in yeast, SAC silencing, once started, has been shown to be irreversible. Mps1 degradation during anaphase was suggested to be responsible for the refractory SAC state during exit from M phase in yeast (Palframan et al., 2006). Also in human cells, Mps1 degradation was suggested to occur during exit from mitosis (Cui et al., 2010).

Posttranslational modification of kinases for the purpose of their regulation is well established. For example, phosphorylation in the activation loop of RD-kinases changes the conformation of the active site to facilitate substrate interactions (Nolen et al., 2004). This kind of phosphorylation was described to occur in Mps1 as well. Several sites in the kinase domain were mapped and correlated with kinase activity (Kang et al., 2007; Mattison et al., 2007; Tyler et al., 2009). Most of these modifications are created by auto-phosphorylation suggesting a positive-feedback loop for Mps1 kinase activity. In the N-terminal domain, however, no modifications regulating Mps1 kinase activity *in vitro* have been identified so far.

Drosophila Mps1 shows a striking, highly dynamic localization behavior during the cell cycle. While it is present at the centrosomes during interphase, it displays the typical localization behavior of a SAC component during mitosis with relocation to the kinetochores during early mitosis and shedding along the spindle towards the centrosomes before M/A-transition (Fischer et al., 2004).

The kinetochore localization dependencies of several SAC components were studied extensively in many different systems. Although the data are partially inconsistent, the general observation seems to be that most SAC components are dependent on Mps1, whereas Mps1 itself does not seem to be dependent on most of the known SAC components (Jelluma et al., 2008; Maciejowski et al., 2010; Santaguida et al., 2010; Stucke et al., 2004; Wong and Fang, 2006). Therefore, it was suggested that Mps1 is an upstream regulator of the kinetochore recruitment of the SAC network (Lan and Cleveland, 2010; Sliedrecht et al., 2010; Wong and Fang, 2006).

This proposed role raises the question about an upstream kinetochore component interacting physically with Mps1 and recruiting Mps1 to the kinetochore as needed. This issue has not been successfully approached yet. A few kinetochore components were suggested to be essential for kinetochore recruitment of Mps1, like Hec1/Ndc80 (Martin-Lluesma et al., 2002; Stucke et al., 2004). However, a direct interaction with Mps1 has not been demonstrated so far.

The interdependency of kinase activity and localization is complex: Originally it was pos-

tulated that Mps1 self-interaction and auto-activation are required for its kinetochore recruitment (Xu et al., 2009; Zhao and Chen, 2006). However, recent evidence suggests that rather than being required for kinetochore recruitment, kinase activity is involved in Mps1 dissociation from kinetochores (Hewitt et al., 2010).

An interdependence of Mps1 localization, phosphorylation, and degradation has been described as well, although so far only with regard to the spindle pole body function of Mps1 in yeast (Jaspersen et al., 2004). At spindle pole bodies, phosphorylation by Cdks at its N-terminal domain was shown to stabilize the protein. Phosphorylations of Mps1 influencing its localization behavior have been described as well. Several phosphorylation sites have been implicated in kinetochore recruitment of human Mps1 (Xu et al., 2009).

Mps1 needs to interact with other SAC components in order to fulfill its SAC function. The interaction between Mps1 and Mad1 is of increasing interest. Mad1 was shown earlier to be an *in vitro* kinase substrate of Mps1 in yeast (Hardwick et al., 1996), and its kinetochore recruitment was shown to be at least partially dependent on Mps1 in human cells (Lan and Cleveland, 2010). Mad1 is thought to act as scaffold protein, recruiting Mad2 to the kinetochore and aiding in activating it there (De Antoni et al., 2005).

I studied several aspects of Mps1 function and regulation in *Drosophila*. While the overall protein level of Mps1 and its phosphorylation (as detected by electrophoretic mobility shifts) do not correlate with SAC activity in *Drosophila*, my results demonstrate that Mps1 localization and level are crucial for a successful mitosis. Similar to the findings in yeast (Hardwick et al., 1996), increased levels of Mps1 result in a SAC dependent mitotic delay. In addition to the observations in yeast, I found evidence that increased Mps1 levels do not only activate the SAC in *Drosophila*, but interfere—also in a SAC-independent manner—with a normal progression through anaphase. Dissecting the localization behavior of Mps1, I found that both major Mps1 domains (N- and C-terminal domain) as well as kinase activity are required for its initial recruitment to the kinetochore. Since kinase-active Mps1 can interact with kinase dead Mps1, the latter can be recruited to the kinetochore in the presence of the former, which makes my studies in the null mutant background highly significant. Furthermore, I show that kinase activity of Mps1 is not required for self-interaction. Searching for interaction partners of Mps1, I observed co-precipitation of Mps1 and Mad1, and a dependency of Mad1 not only on Mps1 but also on Mad2 for kinetochore recruitment. Finally, I found striking differences between the effect of Mps1 over-expression in living embryos and cell culture, which clearly demonstrate that cell culture results concerning SAC activation and adaptation or slippage, can have limited significance for the situation in the organism.

Results

Stability and Phosphorylation of *Drosophila* Mps1 during Mitosis

Tension resulting from chromosome bi-orientation within the mitotic spindle in combination with sister chromatid cohesion is essential for SAC silencing during metaphase. The fact that premature separation of sister chromatid cohesion before bi-orientation activates the SAC in yeast (Mirchenko and Uhlmann, 2010), human cells (Toyoda and Yanagida, 2006), and *Drosophila* (Oliveira et al., 2010; Pauli et al., 2008, see Appendix 3) supports this notion. In contrast, the normal timely loss of sister chromatid cohesion just before anaphase does not appear to re-activate the SAC.

In budding yeast and human cells, the APC/C-mediated degradation of Mps1 has been suggested to explain why the SAC is no longer activated after the M/A-transition (Cui et al., 2010; Palframan et al., 2006). However, in *Drosophila* the substantial perdurance of maternally provided Mps1 in embryos appeared to argue against extensive Mps1 degradation during each division (Fischer et al., 2004). Thus I examined the Mps1 levels in *Drosophila* embryos during the cell cycle.

I triggered a synchronous progression through mitosis 14 (M14) of embryogenesis and prepared protein extracts from embryos selected microscopically during either pro-/metaphase, ana-/telophase, the preceding or following interphase (Figure 1). Immunoblotting with an antibody against Cyclin B was used as a control for the synchronization and sorting procedure. Extensive Cyclin B degradation during exit from mitosis was clearly detected as expected.

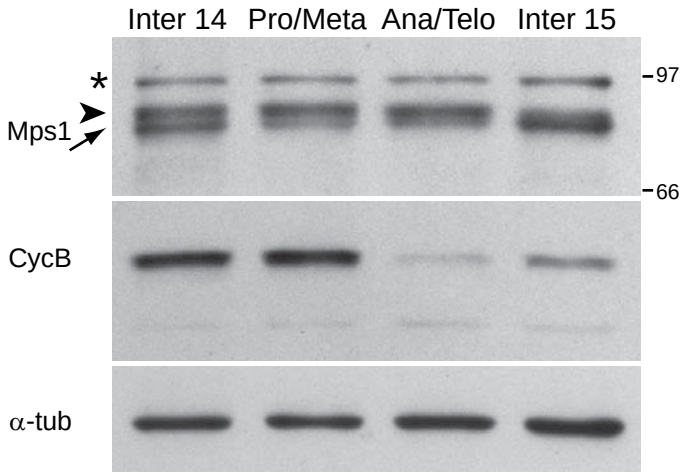

Figure 1. *Drosophila* Mps1 is not degraded during mitosis.
Embryos were synchronized in M14 by ubiquitously expressing a heat-inducible *stg* transgene in a *stg* mutant background. After fixation and DNA labeling embryos in interphase 14, pro/metaphase 14, ana/telophase 14 or interphase 15 were selected manually. Immunoblotting of total embryo extracts with anti-Mps1 shows stable levels during M14. Mps1 appears in two forms of different electrophoretic mobility: a faster migrating form (arrow) more prominent in interphase and a slower migrating form (arrowhead) more abundant during mitosis. The asterisk marks an unspecific band recognized by the anti-Mps1 antibody. Immunoblotting with anti-Cyclin B (CycB) served as control for correct synchonization and sorting, immunoblotting with anti-α-tubulin (α-tub) as loading control.

In contrast, the level of Mps1 did not decrease significantly, indicating that Mps1 degradation cannot explain SAC inactivity after normal loss of tension at the M/A-transition in *Drosophila*.

However, the immunoblotting with antibodies against Mps1 indicated that Mps1 undergoes a shift in electrophoretic mobility during mitosis. Similarly, a fraction of *Drosophila* Mps1 has a reduced electrophoretic mobility in mitotic syncytial embryos (Pandey et al., 2007). λ-Phosphatase treatment of extracts from mitotic syncytial embryos resulted in a shift in electrophoretic mobility towards a faster migrating form (Figure 3A), showing that the reduced electrophoretic mobility of *Drosophila* Mps1 during mitosis is due to phosphorylation. Therefore, the observed electrophoretic mobility shift was used to address a potential Mps1 regulation by phosphorylation.

Previous studies in different systems have shown that Mps1 is phosphorylated during mitosis (Grimison et al., 2006; Liu et al., 2003) and that its kinase activity is regulated by phosphorylation (Kang et al., 2007; Mattison et al., 2007; Tyler et al., 2009).

Various phosphorylation sites in the Mps1 protein have been described in several species and were characterized to have diverse functions (Jaspersen et al., 2004; Kang et al., 2007;

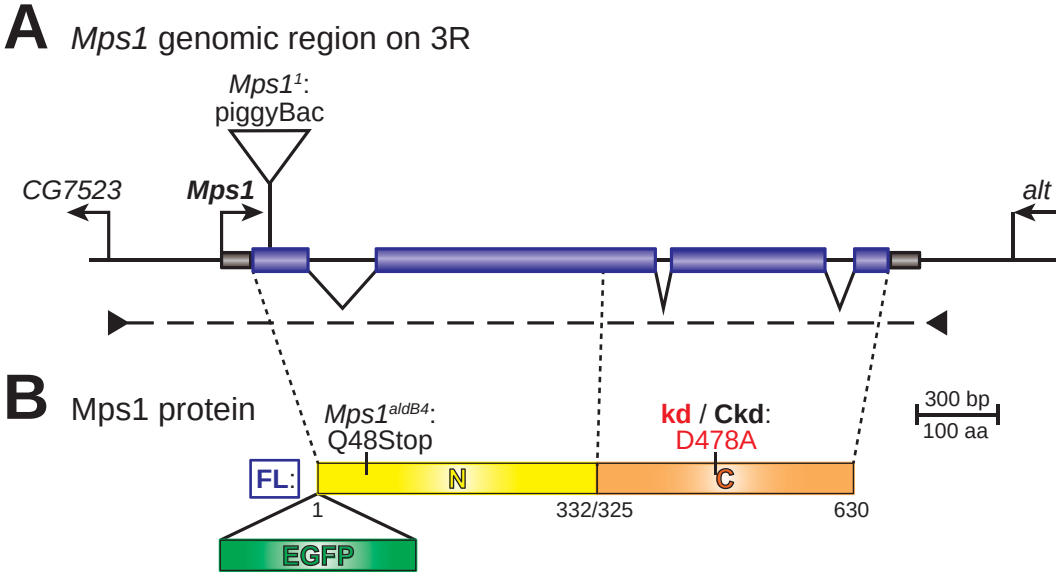

Figure 2. *Drosophila* Mps1—structure of gene, protein, and mutant versions.
(A) Schematic drawing of the *Mps1* genomic region on chromosome arm 3R. The arrows indicate the direction of transcription. Exons are boxed. Blue filling marks the translated region. The *piggyBac* insertion in the $Mps1^{1}$ allele is indicated by the triangle. The chromosome region present in the genomic *EGFP*-fused *Mps1* transgenes is indicated by the dashed inverted double arrow.
(B) Schematic drawing of the Mps1 protein. The premature stop at **a**mino **a**cid (aa) position 48 in the $Mps1^{aldB4}$ allele is marked. Here and in the subsequent figures the full length kinase active protein is depicted in blue, the N-terminal regulatory domain (aa 1 - 332) in yellow, the C-terminal kinase domain (aa 325 - 630) in orange. The single aa exchange at position 478 leading to kinase inactivity (kd, **k**inase **d**ead) of the full length protein is marked in red. The analogous mutation in the C-terminal domain is marked in black. The N-terminal fusion of EGFP to the different Mps1 versions (EGFP-Mps1(FL), EGFP-Mps1(kd), EGFP-Mps1(N), EGFP-Mps1(C)) is indicated with the green box.

Kasbek et al., 2007; Tyler et al., 2009; Wang et al., 2009; Xu et al., 2009; Zhao and Chen, 2006). Only few of the corresponding amino acid residues are conserved in the *Drosophila* homolog. To characterize the spatial distribution of the phosphorylation site(s) in *Drosophila* Mps1, I investigated the mitotic phosphorylation within the two major domains, Mps1(N) and Mps1(C) (N-terminal regulatory domain, aa 1-332, and C-terminal kinase domain, aa 325-630; Figure 2). To identify potential auto-phosphorylation, I also studied Mps1(kd), a version carrying a single amino acid exchange (D478A) predicted to abolish kinase activity (Stucke et al., 2002) (Figure 2). The syncytial stages of *Drosophila* embryogenesis are convenient for this analysis, because nuclei proceed through synchronous mitoses, obviating synchronization by potentially artifact-prone methods. I sorted mitotic and interphase embryos expressing the EGFP-tagged Mps1 versions under control of the endogenous *Mps1* cis-regulatory region.

Immunoblotting of total embryo extracts showed that EGFP-Mps1(kd) (Figure 3B) as well as EGFP-Mps1(N) (Figure 3C) exhibit an electrophoretic mobility shift during mitosis as observed with endogenous Mps1. In contrast, EGFP-Mps1(C) (Figure 3D) did not display any apparent mobility shift during mitosis. These results suggest that the phosphorylation, which causes the mitotic mobility shift, occurs within in the N-terminal regulatory region and not in the C-terminal kinase domain. Moreover, intra-molecular auto-phosphorylation is not involved in N-terminal Mps1 phosphorylation.

Inter-molecular auto-phosphorylation has been suggested to play an important role in the regulation of Mps1 kinase activity (Kang et al., 2007; Mattison et al., 2007; Tyler et al., 2009; Xu et al., 2009). The electrophoretic mobility shift of Mps1(kd) and Mps1(N) described above was observed in the presence of endogenous Mps1 kinase activity. By creating germline clones in *Drosophila* females it is possible to investigate eggs that do not contain any Mps1. I made use of this technique in order to evaluate the effect of endogenous Mps1 kinase activity on the electrophoretic mobility of Mps1. I prepared extracts of sorted embryos derived from females with $Mps1^{aldB4}$ germline clones expressing EGFP-tagged Mps1 versions. By immunoblotting with anti-EGFP (Figure 3E) I found that EGFP-Mps1(N) and EGFP-Mps1(kd) still showed the reduced electrophoretic mobility during mitosis in the absence of endogenous Mps1 kinase activity. I conclude that the mitotic Mps1 phosphorylation, which causes the electrophoretic mobility shift, is not dependent on Mps1 kinase activity.

from page 65:

(E) MeOH fixed syncytial embryos from females with $Mps1^{aldB4}$ germline clones expressing EGFP-Mps1(FL), EGFP-Mps1(kd) or EGFP-Mps1(N) were labeled with a DNA stain and selected manually for embryos in interphase (I) and mitosis (M). Extracts were separated on Phostag containing gels to increase the electrophoretic mobility shifts caused by phosphorylations. Immunoblotting with anti-EGFP shows that EGFP-Mps1(FL), EGFP-Mps1(kd) and EGFP-Mps1(N) appear in a slower migrating form (arrowhead) during mitosis and in a faster migrating form (arrow) during interphase. Immunoblotting with anti-Lamin served as control for equal loading and running behavior.

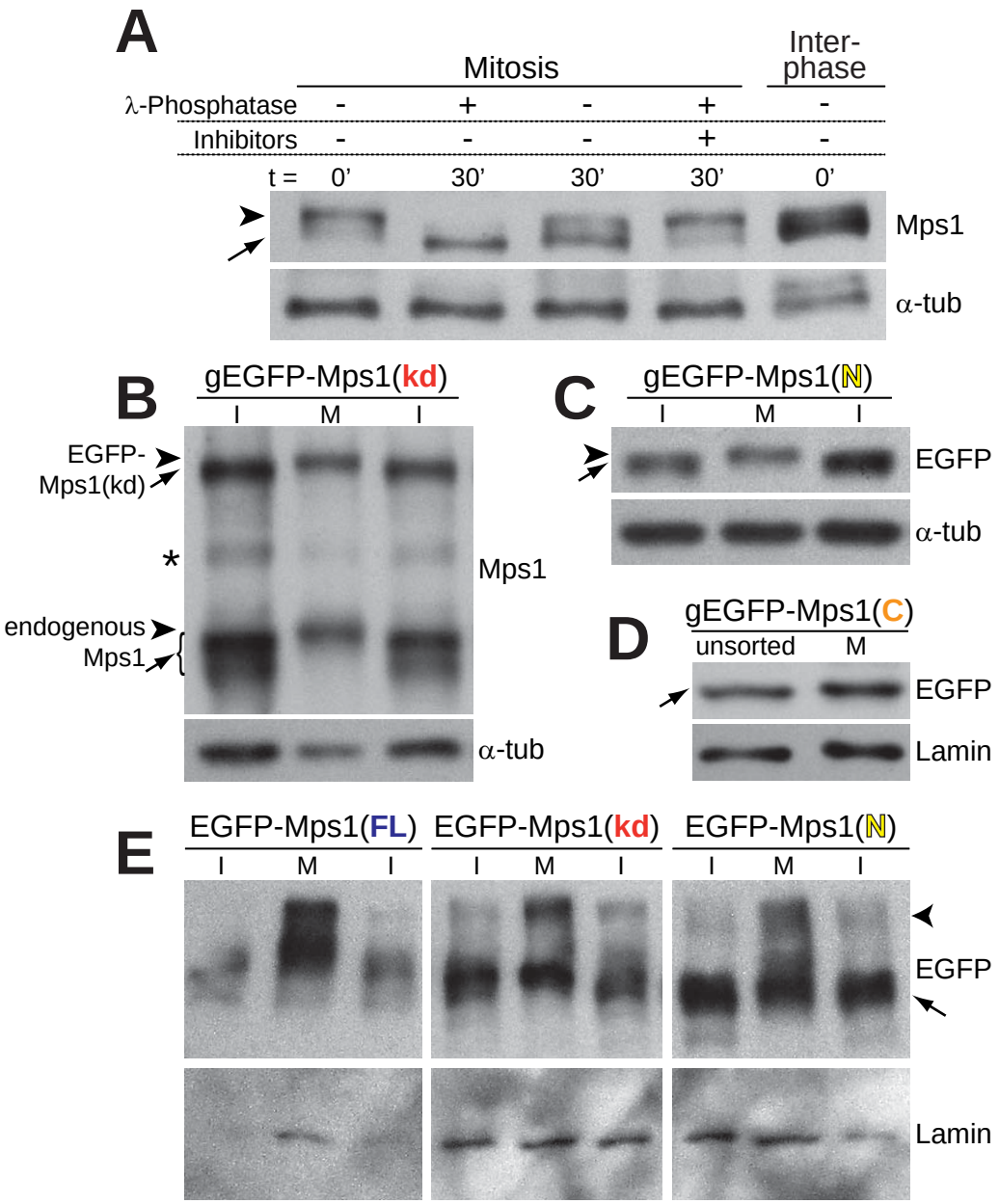

Figure 3. Mitotic phosphorylation of *Drosophila* Mps1 in its N-terminal domain does not require Mps1 kinase activity.

(A) Native protein extracts from syncytial embryos treated with colchicine (mitosis) and cellularizing embryos (interphase) were either loaded without treatment (t = 0') or treated for t = 30' with λ-phosphatase and/or phosphatase-inhibitors (as indicated above the lanes). Immunoblotting with anti-Mps1 shows that the slower migrating form of Mps1 (arrowhead) present in the untreated mitotic extracts is converted into the faster migrating form (arrow) present in the interphase extracts by phosphatase treatment. Increase of the abundance of the faster migrating form of Mps1 in untreated extracts after 30' is probably caused by endogenous phophatase activity present in the native extracts. Immunoblotting with anti-α-tubulin (α-tub) serves as control for equal loading and running behavior.

(B) - (D) MeOH fixed syncytial embryos expressing (B) EGFP-Mps1(kd), (C) EGFP-Mps1(N) or (D) EGFP-Mps1(C) were labeled with a DNA stain and selected manually for embryos in interphase (I) and mitosis (M). Immunoblotting with anti-EGFP or anti-Mps1, respectively, shows that EGFP-Mps1(kd) and EGFP-Mps1(N) appear in a slower migrating form (arrowhead) during mitosis and in a faster migrating form (arrow) during interphase, EGFP-Mps1(C) does not display a change in electrophoretic mobility during mitosis. Immunoblotting with anti-α-tubulin (α-tub) or anti-Lamin served as control for equal loading and running behavior. The asterisk marks an unspecific band recognized by the anti-Mps1 antibody.

continued on page 64.

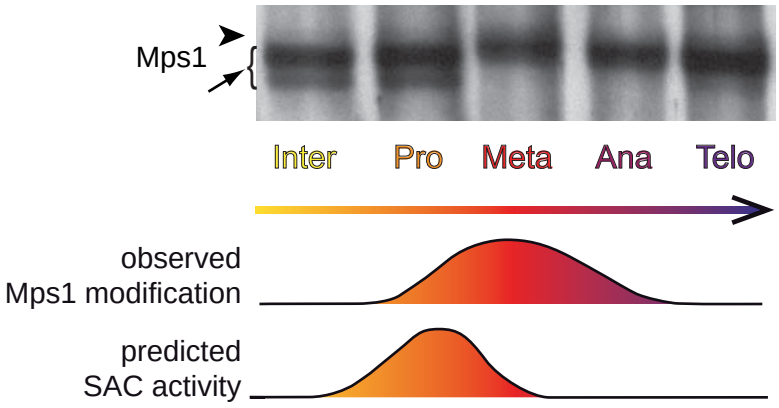

Figure 4. Phosphorylation of Mps1 during mitosis does not correlate with SAC activity.
upper part: MeOH fixed syncytial w^1 embryos were labeled with a DNA stain and selected manually according to cell cycle stage. Interphase, prophase, metaphase, anaphase and telophase embryos were analyzed by immunoblotting with anti-Mps1. Mps1 appears in a faster migrating form (arrow) and in a slower migrating form (arrowhead). Immunoblotting with anti-Lamin (not shown) served as control for equal loading.
lower part: schematic drawing of the observed Mps1 modification compared with predicted SAC activity in the course of the cell cycle.

Phosphorylations in the N-terminal domain of Mps1 were described to be required for kinetochore localization (Xu et al., 2009) and stability of the protein (Jaspersen et al., 2004). However, many additional N- and C-terminal phosphorylation sites have been mapped in human Mps1 without being linked to certain functionalities (Dou et al., 2011; Jelluma et al., 2008; Kang et al., 2007; Tyler et al., 2009; Xu et al., 2009). Most of the observed phosphorylation sites are not unambiguously conserved in the *Drosophila* homolog.

The excellent time resolution of progression through mitosis that can be achieved by the use of syncytial *Drosophila* embryos offered a possibility to evaluate whether the observed phosphorylation correlates with SAC activity.

Syncytial embryos were therefore selected in each of the 4 mitotic phases (pro-, meta-, ana-, and telophase) as well as in interphase. Immunoblotting with anti-Mps1 (Figure 4) revealed phosphorylation throughout mitosis (including anaphase and partially telophase). The observed Mps1 phosphorylation therefore does not occur exclusively during stages of SAC activity (pro-/metaphase).

Localization of *Drosophila* Mps1 Is Dependent on Its Kinase Activity

As neither Mps1 levels nor phosphorylation appeared to be correlated with SAC activity I focused on its intracellular localization. EGFP-Mps1, a functional version fully capable of complementing the recessive lethality caused by *Mps1* null mutations, is largely excluded from the nucleus during interphase (Fischer et al., 2004). After entry into mitosis, EGFP-Mps1 starts to accumulate at kinetochores just before nuclear envelope break-down. Maximal levels are observed at kinetochores during prometaphase. EGFP-Mps1 disappears from kinetochores during metaphase and becomes undetectable during anaphase while a weak but distinct enrichment persists on centrosomes and spindles during exit from mitosis.

Thus Mps1 has a very similar dynamic intracellular localization as other SAC components. Moreover, this characteristic localization behavior is thought to have a functional relevance for SAC activation and silencing. Understanding Mps1 kinetochore localization therefore seems to be important. In order to evaluate the contributions of the individual Mps1 domains to its dynamic kinetochore localization, I analyzed the localization behavior of EGFP-Mps1(N) and EGFP-Mps1(C) in comparison to EGFP-Mps1(FL) and EGFP-Mps1(kd) in syncytial *Drosophila* embryos (Figure 5). EGFP-Mps1(kd) and EGFP-Mps1(C) were found to mimic the localization behavior of EGFP-Mps1(FL) while EGFP-Mps1(N) is neither recruited to the kinetochores in prometaphase nor present at the centrosomes in interphase. The weaker signals of EGFP-Mps1(C) correlate with its reduced expression level compared to EGFP-Mps1(FL), (kd) and (N) (data not shown).

In *Drosophila* embryos, the polar body nuclei are arrested in a mitotic state with condensed chromosomes (Foe et al., 1993). The kinetochores of these chromosomes are known to accumulate high levels of SAC components (Fischer et al., 2004). Therefore, I also analyzed the localization behavior of EGFP-Mps1(FL), EGFP-Mps1(kd), EGFP-Mps1(N) and EGFP-Mps1(C) in this structure confirming that EGFP-Mps1(N) does not localize at the kinetochores of these chromosomes neither. I conclude that the C-terminal kinase domain of Mps1 is required for its kinetochore recruitment.

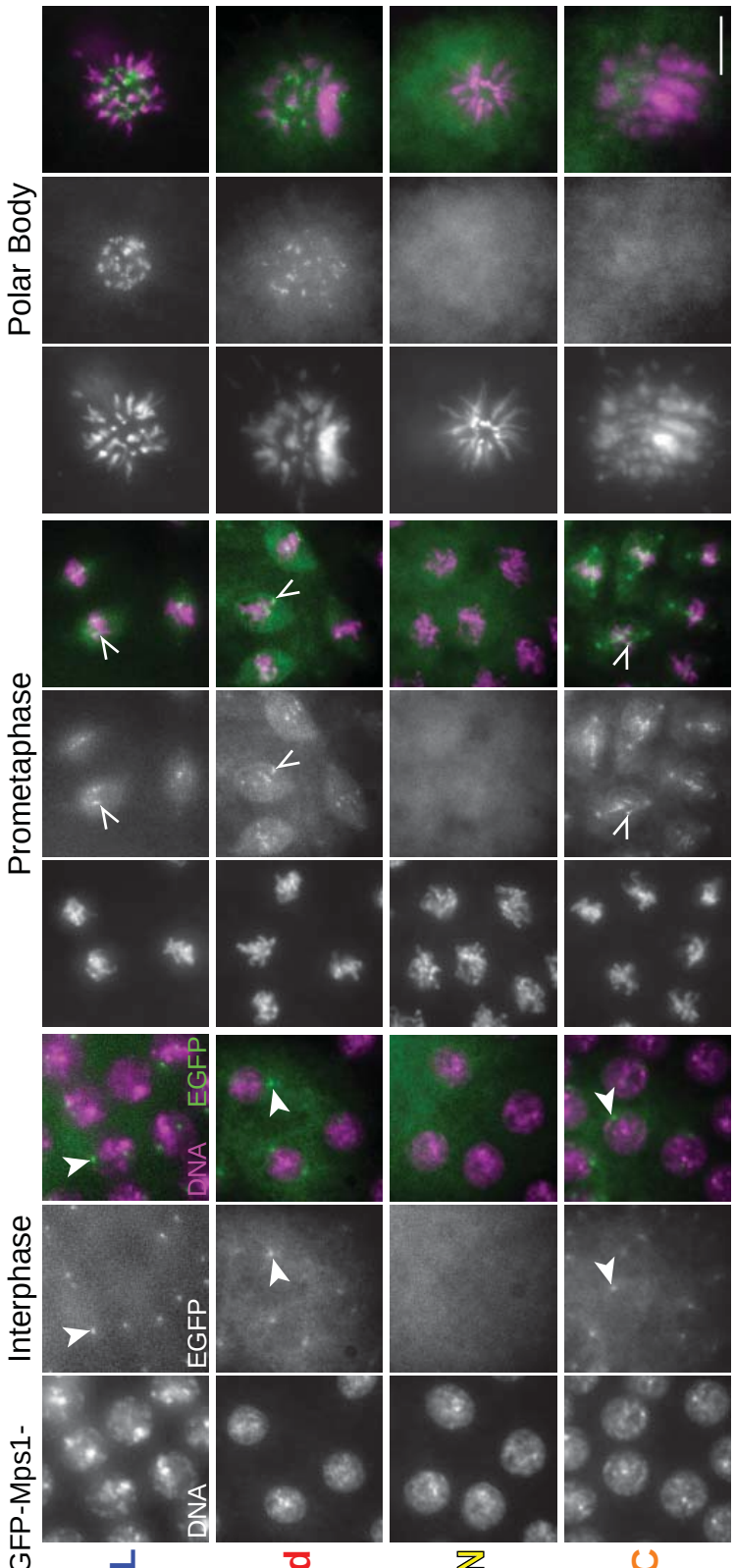

Figure 5. Localization of EGFP-tagged Mps1 versions in the wt background.
Syncytial embryos expressing EGFP-Mps1(FL) (*first row*), EGFP-Mps1(kd) (*second row*), EGFP-Mps1(N) (*third row*) or EGFP-Mps1(C) (*fourth row*) under control of the endogenous cis-regulatory region were fixed with methanol and labeled with a DNA stain.
EGFP-Mps1(FL) shows centrosomal localization during interphase (filled arrowheads) and kinetochore accumulation during prometaphase (open arrowheads) and in the polar bodies. This localization behavior is mimicked by EGFP-Mps1(kd) and EGFP-Mps1(C) while EGFP-Mps1(N) does not show a distinct localization during the cell cycle. Note that expression of EGFP-Mps1(kd) and EGFP-Mps1(C) causes a failure in polar body cell cycle arrest, leading to over-replication and decondensation.
Bar corresponds to 10 µm.

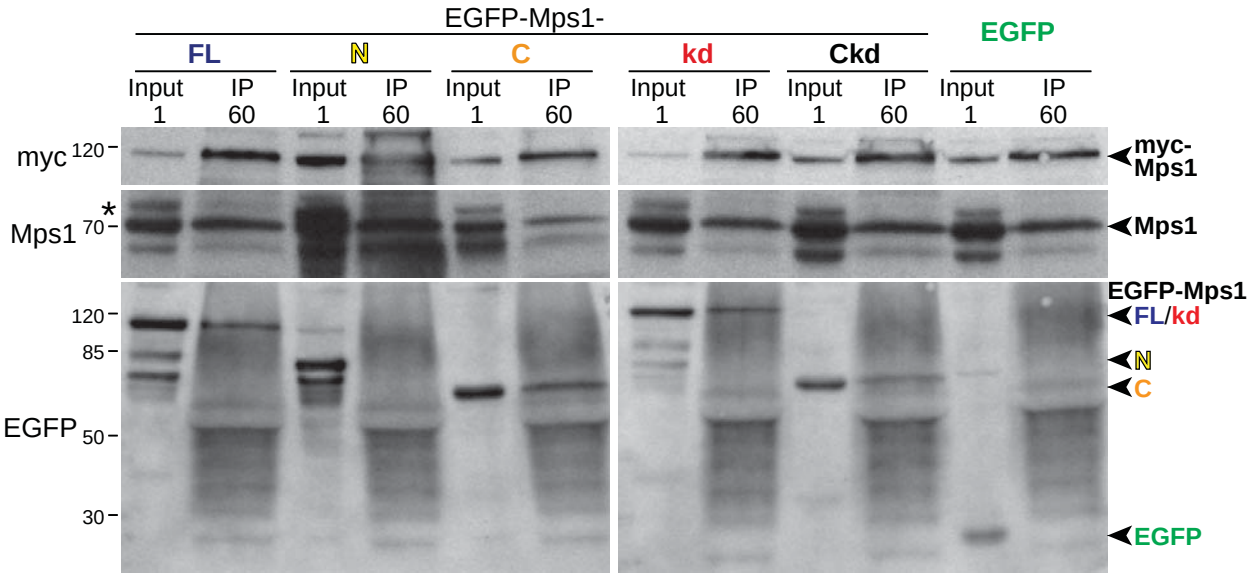

Figure 6. EGFP-tagged Mps1 domains co-immunoprecipitate with myc-Mps1(FL).
IP with anti-myc from S2R+ cell protein extracts after transient transfection with *pCaSpeR4-Actin5c-GAL4*, *pUAST-myc-Mps1(FL)*, and *pUAST-EGFP-Mps1* versions (*FL*, *N*, *C*, *kd*, *Ckd*) or *pUAST-EGFP-STOP*, respectively, as indicated above the lanes (numbers indicate relative loading amounts). Immunoblotting with anti-myc shows comparable precipitation of myc-Mps1(FL), immunoblotting with anti-Mps1 shows co-precipitation of endogenous Mps1. EGFP-tagged Mps1 domains were recognized by the antibody as well, but for clarity only the region of wt Mps1 is shown. Anti-Mps1 recognizes an unspecific band in the input lanes (asterisk), which is not co-precipitated. Immunoblotting with anti-EGFP shows co-precipitation of EGFP-Mps1(FL), EGFP-Mps1(kd), EGFP-Mps1(C) and EGFP-Mps1(Ckd), but not EGFP-Mps1(N) and GFP. The position of molecular weight markers is indicated on the left side.

The C-terminal kinase domain appeared to be sufficient for kinetochore localization. However, the above experiments were done in embryos expressing wild type Mps1. Interaction of Mps1 with itself (dimerization or multimerization) is a well described feature of the kinase (Abrieu et al., 2001; Lauze et al., 1995; Mattison et al., 2007; Stucke et al., 2002) The kinase domain might therefore have been recruited to the kinetochore by wild type Mps1.

To analyze the self-interaction of Mps1, I performed **co**-**i**mmuno**p**recipitation (CoIP) experiments. CoIPs were performed on native protein extracts from S2R+ cells transiently transfected with *pCaSpeR-Actin5c-GAL4* inducing expression of *pUAST-myc-Mps1* and *pUAST-EGFP-Mps1* variants. myc-Mps1 was precipitated with anti-myc; co-precipitation of the EGFP-tagged Mps1 domains was detected by immunoblotting with anti-EGFP (Figure 6). I could co-precipitate the EGFP-tagged C-terminal domain of Mps1 independent of its kinase activity as well as the kinase dead full length protein, but not the N-terminal domain. These results prove that *Drosophila* Mps1 can self-interact via the C-terminal domain.

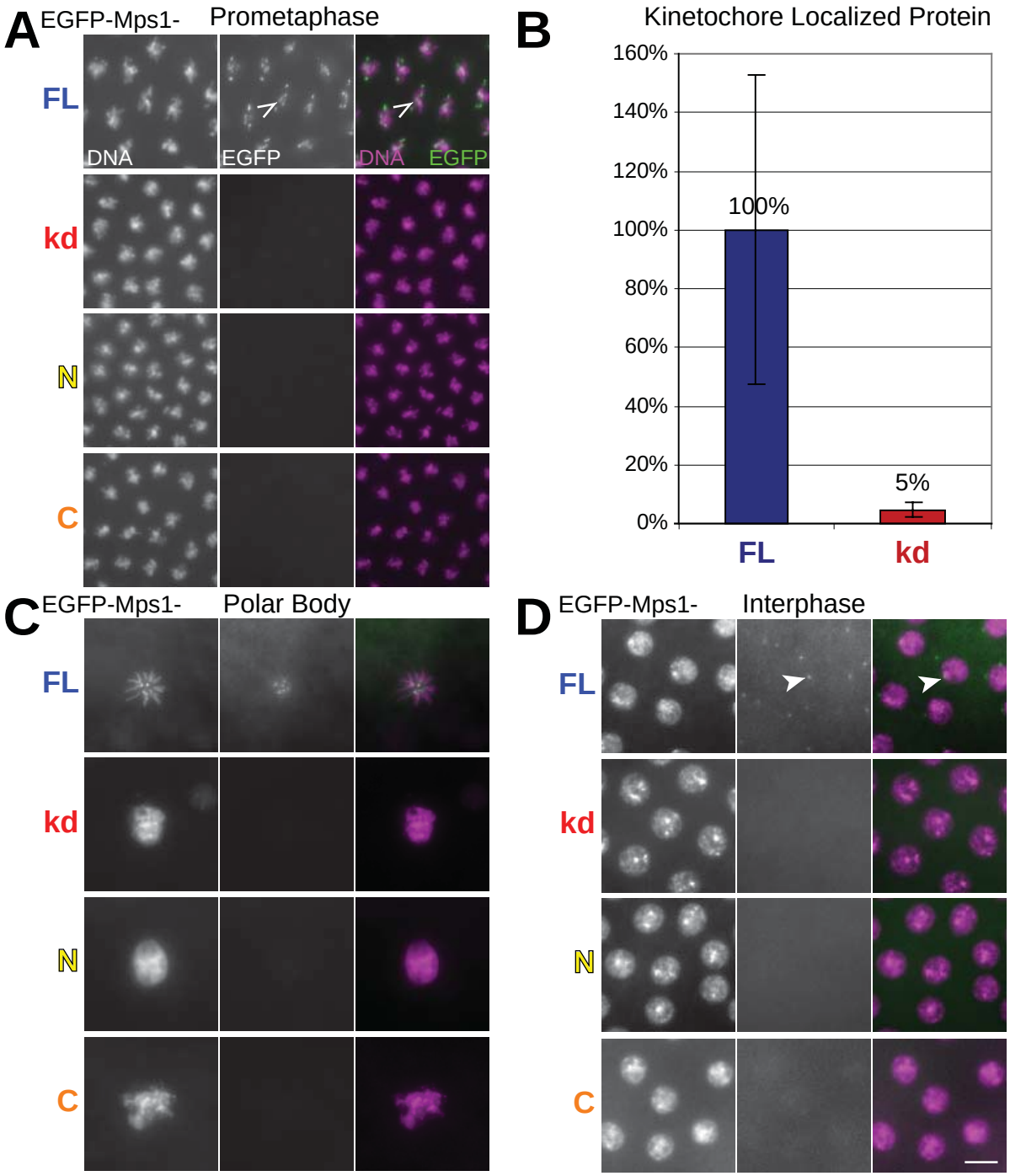

Figure 7. Localization of EGFP-tagged Mps1 versions in the absence of endogenous Mps1 kinase activity.
(A, C, D) Syncytial embryos from females with *Mps1*^{aldB4} germline clones expressing EGFP-Mps1(FL) (*first row*), EGFP-Mps1(kd) (*second row*), EGFP-Mps1(N) (*third row*) or EGFP-Mps1(C) (*fourth row*) under control of the endogenous cis-regulatory region were fixed with methanol and labeled with a DNA stain. In the absence of endogenous wild type Mps1 only EGFP-Mps1(FL) shows kinetochore accumulation during prometaphase (A, open arrowheads) and in the polar bodies (C) and centrosomal localization during interphase (D, filled arrowheads). Neither of the mutant EGFP-tagged Mps1 versions, in particular not EGFP-Mps1(kd) and EGFP-Mps1(C), show a kinetochore or centrosomal localization. Note that only EGFP-Mps1(FL) can restore the polar body cell cycle arrest in *Mps1* mutants. Bar corresponds to 10 µm.
(B) Quantification of kinetochore localized protein was performed by measuring the signal intensities of EGFP-Mps1 and EGFP-Mps1(kd) at the area of condensed DNA and subtracting by the background intensity in neighboring areas. Signal intensities of EGFP-Mps1(kd) were normalized to kinetochore levels of EGFP-Mps1(FL) showing that the kinetochore levels of EGFP-Mps1(kd) decreased to 5%.

Furthermore, my CoIP results were fully consistent with the possibility that the observed localization of EGFP-Mps1(C) and EGFP-Mps1(kd) at the kinetochores might reflect the presence of endogenous Mps1 protein at the kinetochores. To study the localization of the individual domains and kinase dead Mps1 in the absence of endogenous Mps1 kinase activity, I used the germline clone technique. Syncytial embryos, derived from females with *Mps1*^{aldB4} germline clones, expressing EGFP-tagged Mps1 versions under control of the endogenous cis-regulatory regions expressed at most 1% of the wild type levels of Mps1 as shown by immunoblotting (Figure 8A). These embryos were examined for the localization behavior of the EGFP signals (Figure 7). While the kinetochore signals of EGFP-Mps1(FL) were clearly detectable in all inspected prometaphase embryos, neither EGFP-Mps1(kd) nor EGFP-Mps1(C) showed a specific kinetochore or centrosomal localization in the otherwise *Mps1* mutant embryos. The quantification of the kinetochore signal intensity of EGFP-Mps1(kd) showed a > 20-fold reduction compared to EGFP-Mps1(FL) ($p < 0.0001$, $n = 36$) (Figure 7B).

To exclude that the missing kinetochore signals simply reflect low expression levels, I performed immunoblotting experiments with anti-EGFP (Figure 8A) and quantified the signal intensities of the bands. Normalization with the respective signal intensities from the loading control (α-tubulin) allowed comparison of the expression levels (Figure 8B). Compared to EGFP-Mps1(FL), a slight reduction in expression of EGFP-Mps1(kd) and EGFP-Mps1(C) (~2-fold) was observed. However, this reduction was far less than the reduction of kinetochore signal intensities (> 20-fold).

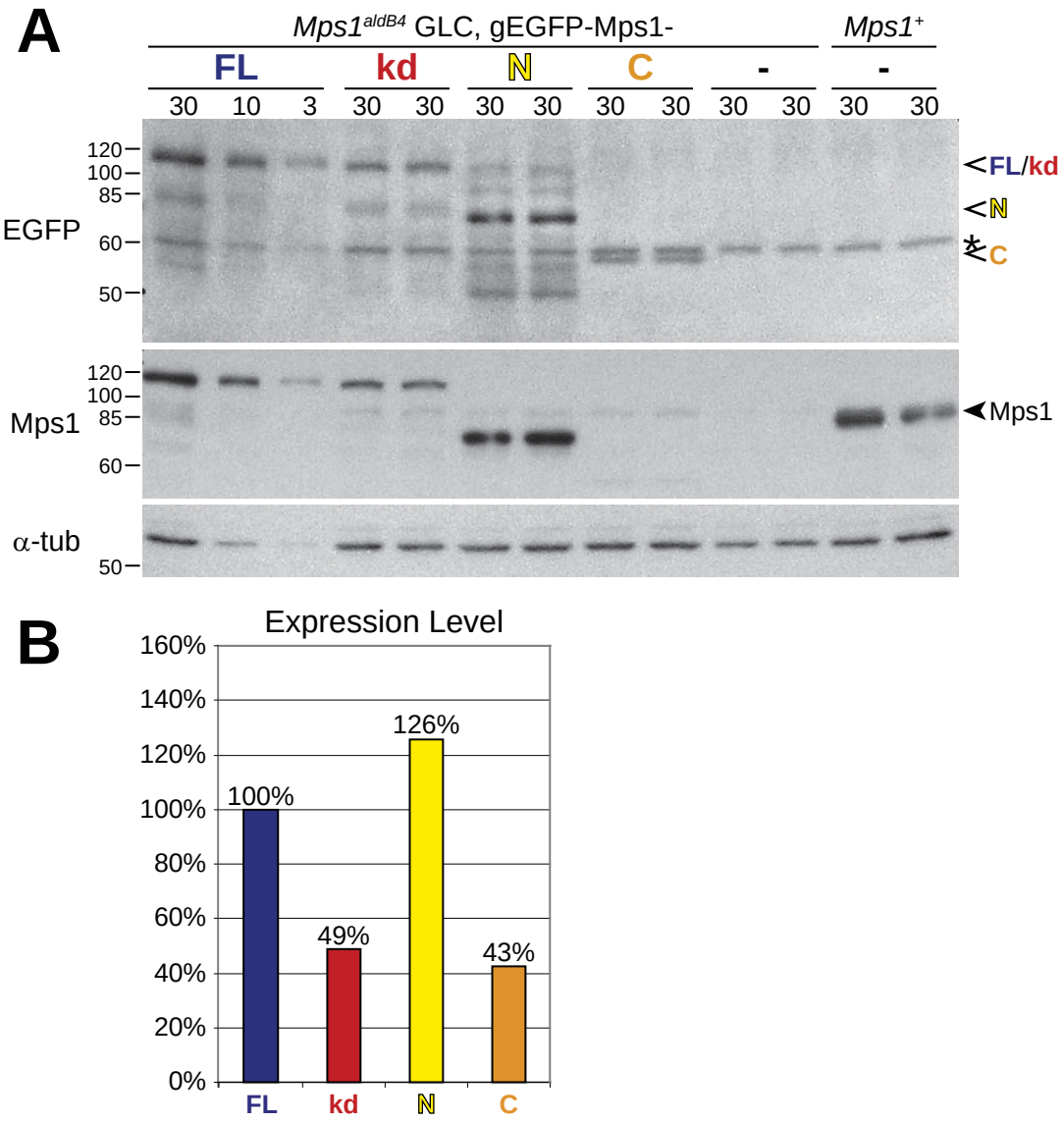

Figure 8. Expression levels of EGFP-tagged Mps1 versions in *Mps1*^{aldB4} mutant embryos.
(A) Protein extracts from syncytial embryos from females with *Mps1*^{aldB4} **g**erm**l**ine **c**lones (*Mps1*^{aldB4}-GLC embryos) expressing EGFP-Mps1(FL), EGFP-Mps1(kd), EGFP-Mps1(N) or EGFP-Mps1(C) under control of the endogenous cis-regulatory region were homogenized, and extracts were immunoblotted. Extracts from w^1 embryos (wt) and from *Mps1*^{aldB4}-GLC embryos (-) without transgene expression were used as controls. Loading is indicated above the lanes (numbers indicate embryo equivalents). Immunoblotting with anti-EGFP shows the expression levels of the different Mps1 domains (open arrowheads), immunoblotting with anti-Mps1 demonstrates the absence of endogenous Mps1 in *Mps1*^{aldB4}-GLC embryos (filled arrowhead), immunoblotting with anti-α-tubulin (α-tub) served as loading control. The asterisk marks an unspecific interaction of the anti-EGFP antibody.
(B) Quantification of expression levels of EGFP-tagged Mps1 domains in *Mps1*^{aldB4}-GLC embryos. Signal intensities of protein bands on the western blot correlating with protein levels in the extracts were quantified. Differences in loading were corrected using the corresponding α-tubulin band intensities. EGFP band intensities were normalized to EGFP-Mps1(FL) expression levels showing that EGFP-Mps1(kd) and EGFP-Mps1(C) are expressed at approximately half the level of EGFP-Mps1(FL) while EGFP-Mps1(N) expression is even higher than EGFP-Mps1(FL).

In principle, kinase activity might be required for Mps1 self-interaction and self-interaction for kinetochore localization. To address this issue, I evaluated whether Mps1(kd) is able to self-interact in the absence of endogenous Mps1 kinase activity.

Endogenous Mps1 is not expressed in the post-mitotic larval tissues (data not shown). To study the self-interaction of Mps1(kd) in the virtual absence of Mps1 kinase activity, I ectopically expressed myc-tagged and EGFP-tagged Mps1(kd) in larvae. This resulted in an over-expression of the tagged Mps1 versions that was far higher than 10-fold compared to endogenous full length Mps1, which was not detectable with the anti-Mps1 antibody in larval extracts (data not shown). myc-Mps1(kd) was found to be co-precipitated by EGFP-Mps1(kd) with comparable efficiency as myc-Mps1(FL) (Figure 9). Thus, independent of Mps1 kinase activity, Mps1(kd) can self-interact. Therefore, the inability of EGFP-Mps1(kd) to localize to the kinetochores reflects a loss of kinase activity, not a self-interaction failure.

Self-interaction of two or more Mps1 molecules is not sufficient to mediate their kinetochore recruitment.

My results show that the C-terminal kinase domain of Mps1 alone is not sufficient for Mps1 localization. Both Mps1 domains together and kinase activity are required to mediate Mps1 kinetochore recruitment during prometaphase.

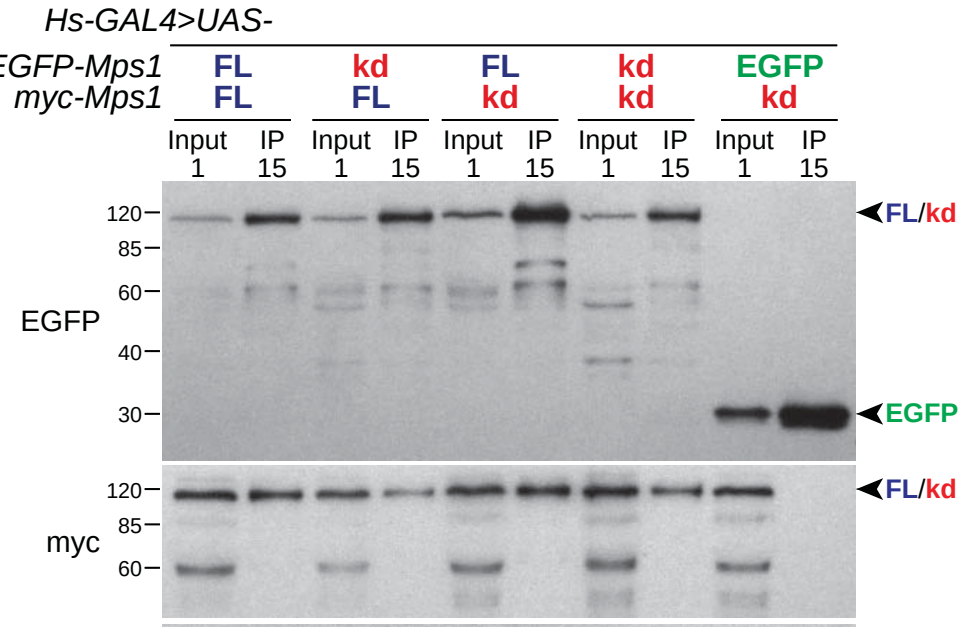

Figure 9. Self-interaction of Mps1(kd) in the absence of Mps1 kinase activity.
IP with GFP-Trap from larval protein extracts ectopically expressing myc- and EGFP-tagged Mps1(FL) or Mps1(kd) versions as indicated. In addition EGFP was expressed for control of non-specific co-precipitation. Numbers indicate relative larval equivalents. Immunoblotting with anti-EGFP shows precipitation of EGFP-Mps1 versions or EGFP alone in all IPs. Immunoblotting with anti-myc shows co-precipitation of myc-Mps1(FL) and myc-Mps1(kd) with EGFP-Mps1(FL) as well as EGFP-Mps1(kd), but not EGFP alone. The position of molecular weight markers is indicated on the left side.

The function of the different Mps1 versions was also evaluated in complementation tests. In absence of zygotic Mps1 function, development does not progress to the adult stage except for some escapers. These escapers display rough eyes and bent wings (Fischer et al., 2004). As already mentioned, expression of *EGFP-Mps1* under control of the endogenous cis-regulatory region is capable of rescuing development of Mps1 mutants to the adult stage. The rescued flies have wild type appearance. I performed rescue experiments in order to detect if one of the EGFP-tagged Mps1 versions could replace endogenous Mps1 and would display full functionality (Figure 10). The proportion of $Mps1^{1}/Mps1^{aldB4}$ "escapers" hatching without influence of any transgene was 41%. This number is higher than reported previously for homozygous *Mps1* mutants (Fischer et al., 2004; Page et al., 2007), indicating second site hits on both the *Mps1* null-mutant chromosomes interfering with viability. However, these flies showed the described Mps1 "escaper" phenotype. Although I found a slightly increased number of "escapers" after expression of EGFP-Mps1(N), EGFP-Mps1(C) and EGFP-Mps1(kd), all these flies displayed the "escaper" phenotype.

Thus I conclude that both domains of Mps1 as well as kinase activity are required for normal development. This requirement correlates with the observation that both domains and Mps1 kinase activity are also essential for kinetochore recruitment of the protein.

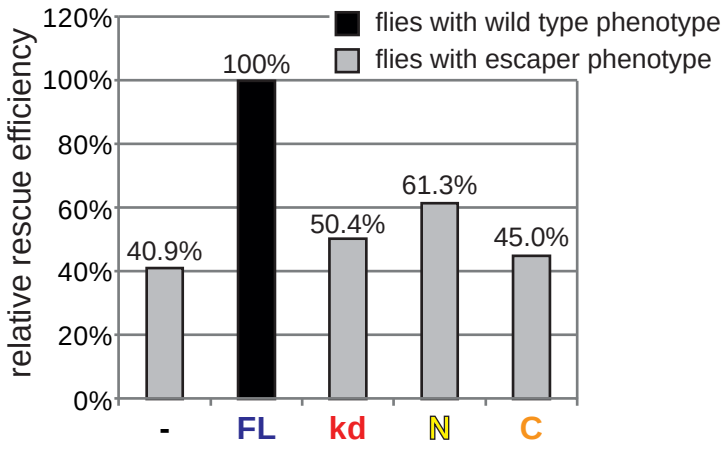

Figure 10. Kinase activity and entire Mps1 protein are required to fully rescue the *Mps1* mutant phenotype.
A rescue assay of $Mps1^{aldB4}/Mps1^{1}$ null mutant viability and adult phenotype by EGFP-Mps1(FL), (kd), (N), (C) was performed by crossing heterozygous $Mps1^{aldB4}$ mutant females carrying homozygously the respective *EGFP*-fused *Mps1* **trans**gene (TG) under control of the endogenous cis-regulatory region (*TG; $Mps1^{aldB4}$/Bal*) with heterozygous $Mps1^{1}$ mutant males ($Mps1^{1}$/*Bal*). From these crosses the number of *Mps1* mutant progeny (*TG/+; $Mps1^{aldB4}$/$Mps1^{1}$*) and the heterozygous *Mps1* progeny (*TG/+; $Mps1^{1}$* or $Mps1^{aldB4}$/*Bal*) were counted. By normalizing the number of hemizygous *Mps1* mutant progeny with the number of heterozygous siblings ($n > 130$), the rescue efficiency of the individual TGs was calculated and compared to the rescue efficiency of *gEGFP-Mps1(FL)*.
The phenotype of the adult $Mps1^{aldB4}$/ $Mps1^{1}$ flies is indicated by grey and black bars, respectively.

Interactions of Mps1 with Mad1 and Mad2

Since Mps1 function and kinetochore localization are correlated, an identification of components required for kinetochore localization should be of interest.

In order to identify such kinetochore components, I chose a CoIP-mass spectrometry approach. I precipitated EGFP-Mps1 as well as an unrelated control protein (Cal1-EGFP) with anti-EGFP antibodies from embryonic protein extracts. The eluates of the IPs were subjected to mass spectrometric analysis. Comparison of the eluate from EGFP-Mps1 with the control eluate identified TXBP181-like as a specific Mps1 interaction partner (Figure 11A). TXBP181-like is the *Drosophila* homolog of Mad1.

To confirm this interaction, I performed CoIP western experiments. Mad1-GFP and GFP as control were precipitated with GFP-Trap from embryonic protein extracts and the eluates were probed for the presence of Mps1 (Figure 11B). I found endogenous Mps1 to be co-precipitated specifically with Mad1-GFP. As expected, Mad2 was also observed to be co-precipitated with Mad1-GFP (Figure 11B).

To characterize the Mps1-Mad1 interaction in more detail, protein extracts from embryos expressing mCherry-Mad1 and the EGFP-tagged Mps1 versions (kd, N, C) were subjected to an IP with GFP-Trap (Figure 11C). My results show that mCherry-Mad1 can interact with EGFP-Mps1(FL) and EGFP-Mps(kd). The EGFP-tagged Mps1 domains (EGFP-Mps1(N) and EGFP-Mps1(C)) were also co-precipitated with mCherry-Mad1, although less efficient than EGFP-Mps1(FL).

Thus I conclude that Mps1 and Mad1 can either interact directly or reside in the same cellular protein complexes. Kinase dead Mps1 can also form such complexes. Similarly, the N-and C-terminal domains seem also to be sufficient to enter these complexes although only with reduced efficiency.

Mad1 is a well-known SAC component required for kinetochore recruitment of Mad2 and its activation at the kinetochore (De Antoni et al., 2005), a process essential for SAC signaling. My CoIP experiments confirm the interaction between Mad1 and Mad2 in *Drosophila*. Studies in human cells showed that Mps1 is required for the kinetochore recruitment of Mad1 (Liu et al., 2003; Martin-Lluesma et al., 2002); a dependency of Mps1 on Mad1 has not been found so far (Martin-Lluesma et al., 2002; Stucke et al., 2004; Wong and Fang, 2006). Most cell culture studies have to rely on the application of RNAi or small molecule inhibitors, in which undesired side-effects cannot be excluded. The *Drosophila* model offers the possibility to study null-mutants. Therefore, I investigated the localization dependencies of the three SAC components Mps1, Mad1 and Mad2 in *Drosophila* null-mutant embryos. Flies homozygous mutant for *mad1* or *mad2* are viable and fertile (Buffin et al., 2007; Emre et al., 2011).

A

CoIP MS/MS—whole eluate from EGFP-Mps1

CG number	name
CG4264-PA	Heat shock prot. cognate 4
CG31618-PA	Histone 2A
CG7643-PA	Mps1
CG2152-PA	Pcmt (prot. modification)
CG4087-PA	Ribosomal protein LP1
CG2072-PA	Mad1 (=TXBP181-like)
CG2985-PA	Yolk protein 1
CG2979-PA	Yolk protein 2
CG11129-PA	Yolk protein 3

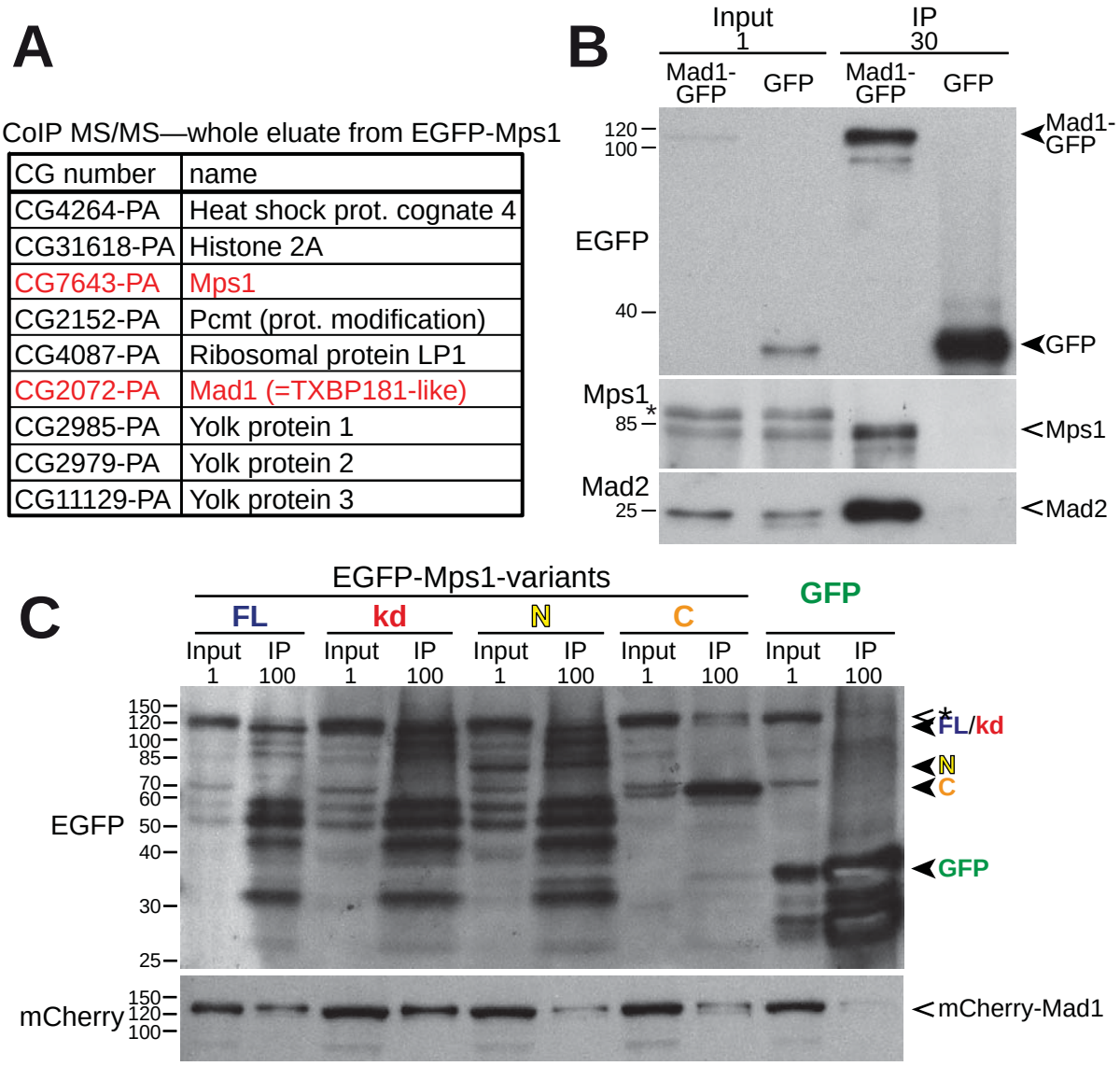

Figure 11. Mps1 interacts with Mad1.

(A) List of proteins identified in anti-EGFP immunoprecipitates from extracts of embryos expressing EGFP-Mps1. All proteins found besides Mps1 and Mad1 (=TXBP181-like) (marked in red) were contaminations of very abundant proteins, which were also found in the control eluates. All proteins where at least one peptide with an ion score >40 or an expect value $<10^{-4}$ was found are listed.

(B) IP with GFP-Trap from embryonic protein extracts (Input) expressing Mad1-GFP or GFP (*Ubi-GFP*) as indicated above the lanes. Immunoblotting with anti-EGFP shows precipitation of both Mad1-GFP and GFP from the respective extracts (arrowheads). Immunoblotting with anti-Mps1 and anti-Mad2 shows co-precipitation of Mps1 and Mad2 (open arrowheads) by Mad1-GFP selectively. The numbers above the lanes indicate the embryo equivalents loaded. The asterisk marks a band that is unspecifically recognized by the anti-Mps1 antibody. The position of molecular weight markers is indicated on the left side.

(C) IP with GFP-Trap from embryonic protein extracts (Input) expressing mCherry-Mad1 and EGFP-Mps1(FL), EGFP-Mps1(kd), EGFP-Mps1(N), EGFP-Mps1(C) or GFP as indicated above the lanes. Immunoblotting with anti-EGFP shows precipitation of all EGFP-Mps1 versions (arrowheads) from the respective extracts. Immunoblotting with anti-mCherry shows co-precipitation of mCherry-Mad1 (open arrowhead) selectively with EGFP-Mps1(FL) and EGFP-Mps1(kd) and somewhat less with EGFP-Mps1(N) and EGFP-Mps1(C), but not with GFP alone. The asterisk marks mCherry-Mad1 signals resulting from residual rabbit anti-mRFP antibodies that were recognized by the secondary goat anti-rabbit antibodies when doing the rabbit anti-EGFP re-probing. The position of molecular weight markers is indicated on the left side.

Therefore, the embryos obtained from such females could be analyzed. *Mps1* mutant eggs were created by the germline clone technique.

To investigate the localization dependencies of Mad1, I analyzed *Mad1-GFP* expressed under control of its endogenous cis-regulatory region in the wild type (Figure 12A) and in *Mps1* (Figure 12B) and *mad2* (Figure 12C) mutant backgrounds.

My analyses revealed that the kinetochore recruitment of Mad1-GFP is dependent on Mps1 and Mad2. I quantified the DNA associated GFP signals in prometaphase nuclei (Figure 12D) and found a decrease to 30% and 50%, respectively, compared to the wild type situation. In both cases the reduction was significant. Similarly, the difference between *Mps1* mutant and *mad2* mutant situation was significant. I point out that this latter difference was not only quantitative, but I recognized the signals to be qualitatively different as well: In *mad2* mutants, I detected residual amounts of Mad1-GFP at the kinetochores as point-shaped signals, indicating that the dependency of Mad1 on Mad2 is only partial. However, in *Mps1* mutants no distinct point-shaped signals were visible.

To investigate the localization dependencies of Mps1, I analyzed *EGFP-Mps1* expressed under control of its endogenous cis-regulatory region in the wild type (Figure 13A) as well as in *mad1* (Figure 13B) and *mad2* (Figure 13C) mutant backgrounds.

My analyses revealed that the kinetochore recruitment of EGFP-Mps1 is dependent on Mad1 and on Mad2. I quantified the DNA associated GFP signals in prometaphase nuclei (Figure 13D) and found a decrease to 42% and 53%, respectively, compared to the wild type situation. In both cases the reduction was significant. The difference between *mad1* mutant and *mad2* mutant situation was not significant neither quantitatively nor qualitatively. In the both mutants, I detected residual amounts of EGFP-Mps1 at the kinetochores as point-shaped signals, indicating that the dependency of Mps1 on Mad1 and Mad2 is only partial.

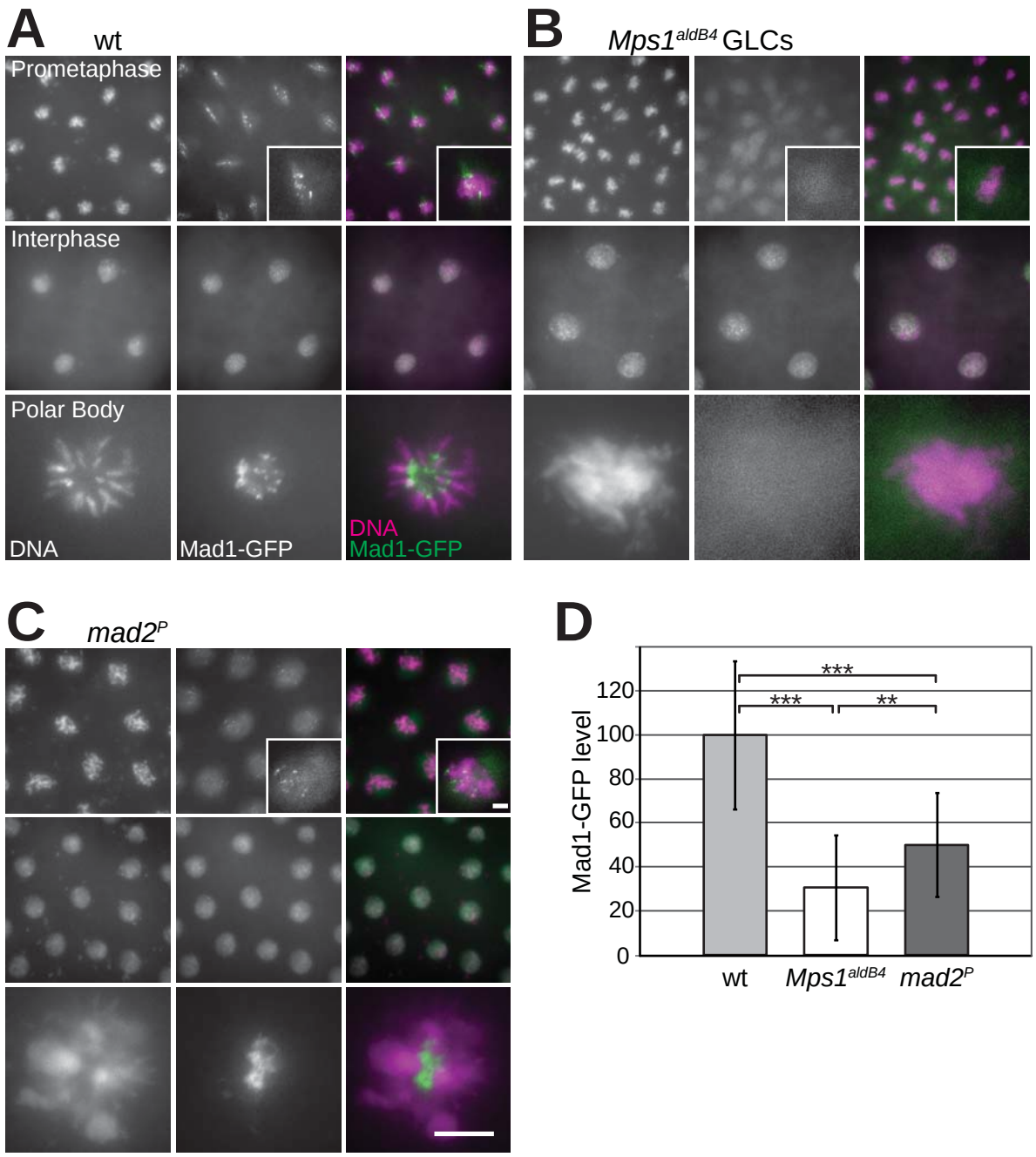

Figure 12. Kinetochore localization of Mad1-GFP is dependent on Mps1 and Mad2.
Syncytial embryos expressing Mad1-GFP were fixed with methanol and labeled with a DNA stain (DNA—magenta). Maximum projections of 7 z-planes are shown.
(A) In the wild type situation (wt) Mad1-GFP accumulates at the kinetochores in prometaphase embryos and in the polar body nuclei. It shows a nuclear localization during interphase.
(B) In embryos from females with *Mps1*^{aldB4} germline clones (*Mps1*^{aldB4} GLCs) Mad1-GFP does not accumulate at the kinetochores neither in prometaphase nor in the polar body nuclei. The nuclear localization during interphase is not disturbed.
(C) In embryos from *mad2* mutant females (*mad2*^{P}) Mad1-GFP shows a reduced localization at the kinetochores in prometaphase and in the polar bodies. The nuclear localization during interphase is not disturbed.
(D) Quantification of the kinetochore levels of Mad1-GFP in *Mps1*^{aldB4} GLCs and *mad2* mutants in comparison to the wild type situation shows a significant reduction in the *Mps1* mutants as well as in the *mad2* mutants. *** = $p < 0.001$, ** = $p < 0.01$, $n > 20$.
Bar corresponds to 10 µm and to 1 µm in the insets.

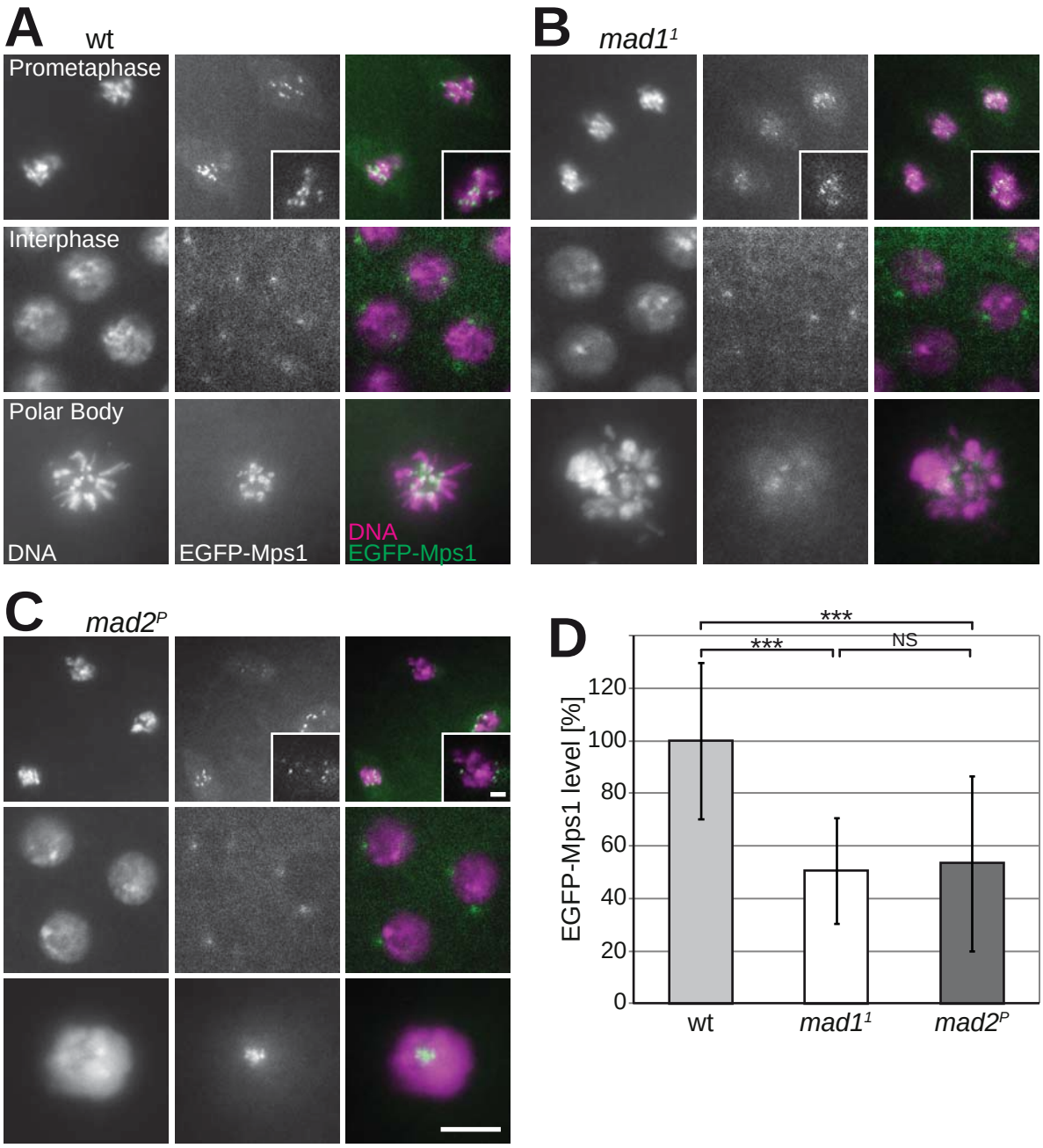

Figure 13. Kinetochore localization of EGFP-Mps1 is partially dependent on Mad1 and Mad2.
Syncytial embryos expressing EGFP-Mps1 were fixed with methanol and labeled with a DNA stain. Single z-planes are shown in prometaphase and interphase panels, maximum projections of 7 z-planes in the polar bodies panels.
(A) In the wild type situation (wt) EGFP-Mps1 accumulates at the kinetochores in prometaphase embryos and in the polar body nuclei. It shows a centrosomal localization during interphase.
(B) In embryos from *mad1* mutant females (*mad1*^{1}) EGFP-Mps1 shows a reduced localization at the kinetochores in prometaphase and in the polar body nuclei. The centrosomal localization during interphase is not disturbed.
(C) In embryos from *mad2* mutant females (*mad2*^{P}) EGFP-Mps1 shows a slightly reduced localization at the kinetochores in prometaphase and in the polar body nuclei. The centrosomal localization during interphase is not disturbed.
(D) Quantification of the kinetochore levels of EGFP-Mps1 in *mad1* and *mad2* mutants in comparison to the wild type situation shows a significant reduction in the *mad1* mutants as well as in the *mad2* mutants. *** = $p < 0.001$, NS = not significant ($p > 0.05$), $n > 15$.
Bar corresponds to 10 µm and to 1 µm in the insets.

Mis-Localization of Mps1 Kinase Activity Interferes with Normal Exit from Mitosis

Mps1 shows a very dynamic localization during the cell cycle. As discussed above, it is recruited to the kinetochores in prometaphase. However, before the M/A transition it is cleared from the kinetochores again.

The clearance from the kinetochores might be a crucial step for SAC silencing. This suggestion seems even more attractive as Mps1 degradation and its mobility shift cannot explain SAC silencing in *Drosophila* embryos and thus was addressed in more detail.

To test whether Mps1 disappearance from the kinetochore is required for SAC silencing before the M/A-transition, I expressed Mps1 variants (Figure 14) fused to protein domains that enforce constitutive kinetochore localization throughout mitosis, and analyzed whether such variants prevent SAC silencing and exit from mitosis despite normal kinetochore attachment.

To identify protein domains that result in constitutive kinetochore localization throughout mitosis, I participated in the functional characterization of various *Drosophila* kinetochore components (Schittenhelm et al., 2010; Schittenhelm et al., 2007, see Appendix 1 and 2).

The Gal4/UAS system was used for the expression of Mps1 variants with constitutive kinetochore localization. The chosen driver line, *mat-GAL4*, results in eggs with a maternal contribution of Gal4. This maternally contributed Gal4 protein activates paternally inherited UAS-transgenes as soon as zygotic transcription is permitted. The protein products encoded by UAS-transgenes start to accumulate during interphase 14 and mitotic effects can be studied in the following **m**itosis **14** (M14).

Expression of EGFP-Cenp-C(C)-Mps1 (Figure 15, second row), which was maintained at the kinetochore throughout the cell cycle (data not shown) by the C-terminal localization domain of Cenp-C (Heeger et al., 2005), did not result in an enrichment of metaphase figures, as expected if it led to a constitutive SAC activation. Instead it caused severe chromosome

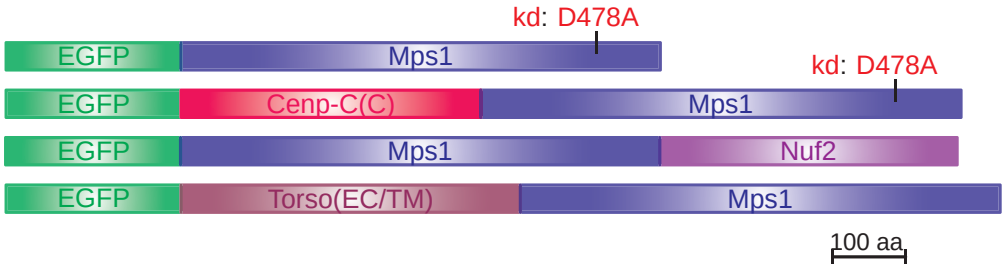

Figure 14. Fusion proteins to induce Mps1 mis-localization.
Schematic drawing of the fusion proteins that were expressed in *Drosophila* embryos using the Gal4/UAS system in order to study the effects of mis-localized Mps1.
Fusions with the C-terminal kinetochore targeting domain of Cenp-C, Cenp-C(C), and full-length Nuf2 were used to study the effects of constitutive kinetochore localization of Mps1.
Fusion with the **e**xtra**c**ellular and **t**rans**m**embrane domain of Torso receptor tyrosine kinase, Torso(EC/TM) was created to tether Mps1 to the cellular membrane.

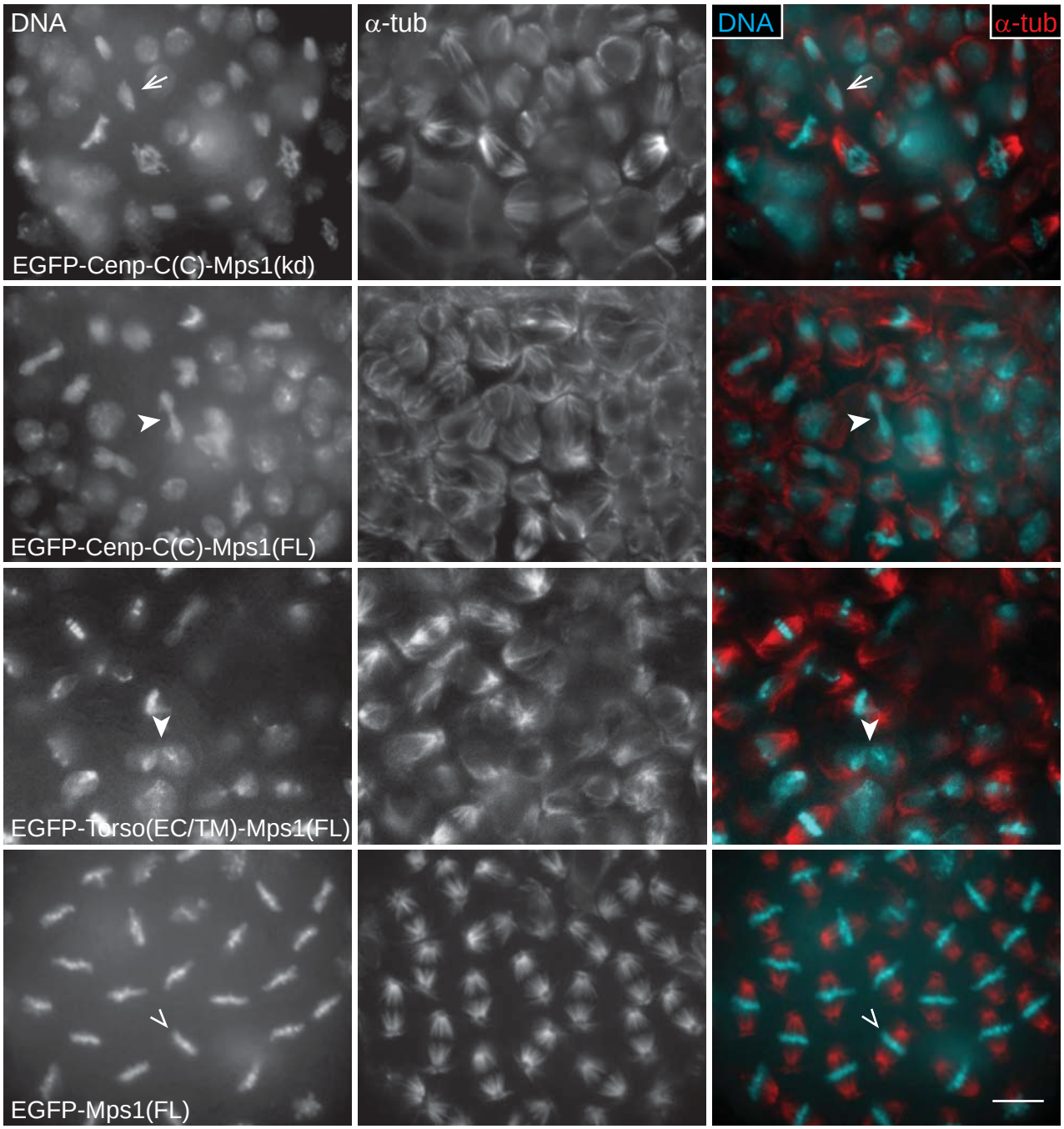

Figure 15. Mis-localization of Mps1 kinase activity interferes with normal exit from mitosis.
Embryos expressing EGFP-tagged mis-localized Mps1 versions during M14 were fixed with PFA following a 2 min taxol treatment to stabilize the spindle, stained with anti-α-tubulin (α-tub—red) and labeled with a DNA stain (DNA—cyan). *first row*: Embryos expressing a mis-localized kinase dead version of Mps1 (EGFP-Cenp-C(C)-Mps1(kd)) do not show abnormalities during exit from mitosis (arrows). *second row*: Embryos expressing a kinetochore bound kinase active Mps1 version (EGFP-Cenp-C(C)-Mps1(FL)) show severe anaphase bridges (arrowheads). *third row*: Embryos expressing a cellular membrane bound kinase active Mps1 version (EGFP-Torso(EC/TM)-Mps1(FL)) show severe anaphase bridges (arrowheads). *fourth row*: Ectopic expression of EGFP-Mps1 without mis-localization signal causes an accumulation of cells in metaphase (open arrowheads). For all genotypes, the same epidermal region (mitotic domain 11, Foe, 1989) at the time of mitosis 14 is shown.
Bar corresponds to 10 µm.

segregation abnormalities during exit from mitosis. Late mitotic figures in fixed embryos were characterized by chromatin bridges pinched by cytokinetic furrows. These bridges harboured kinetochore signals (data not shown). EGFP-Cenp-C(C)-Mps1 therefore interferes with efficient poleward segregation of kinetochores during exit from mitosis. While my experiments failed to provide support for the notion that shedding of Mps1 from kinetochores after spindle attachment is required for SAC silencing, they emphasized the importance of normal Mps1 localization for the success of late mitotic events.

In principle, the chromosome segregation defects caused by EGFP-Cenp-C(C)-Mps1 might reflect a dominant-negative effect of its Cenp-C(C) localization domain. Cenp-C is required for normal chromosome segregation during mitosis, and some of the abnormal mitotic figures observed in Cenp-C mutants (Heeger et al., 2005) are reminiscent of those caused by EGFP-Cenp-C(C)-Mps1. However, EGFP-Cenp-C(C)-Mps1(kd) did not result in mitotic abnormalities when expressed at a comparable level as EGFP-Cenp-C(C)-Mps1 (Figure 15, first row). Therefore, I conclude that the mitotic chromosome segregation defect induced by EGFP-Cenp-C(C)-Mps1 depends on Mps1 kinase activity and does not simply reflect a dominant-negative effect on Cenp-C. I point out that the expected dominant-negative effect of the Cenp-C(C) domain was indeed observed, but only when this domain was expressed at tenfold higher levels (data not shown).

The chromosome segregation defects described above were induced by EGFP-Cenp-C(C)-Mps1 expression in embryos that also expressed endogenous Mps1. The observed defects might therefore reflect increased overall Mps1 levels rather than the enforced persistent kinetochore localization. To analyze the consequences of excess Mps1, I expressed EGFP-Mps1 without the Cenp-C(C) localization domain in embryos with endogenous Mps1 (Figure 15, fourth row). Strikingly, this resulted in a pronounced mitotic delay during metaphase as evidenced by a strong enrichment of metaphase figures in fixed embryos. Quantitative immunoblotting experiments indicated that the level of EGFP-Cenp-C(C)-Mps1, which appears to be a relatively unstable Mps1 variant, was clearly lower than those of EGFP-Mps1 that were sufficient to cause a metaphase delay (data not shown). I conclude that EGFP-Cenp-C(C)-Mps1 expression caused chromosome segregation defects (but not an obvious metaphase delay) at an expression level comparable to endogenous wild-type Mps1, whereas EGFP-Mps1 expression resulted in a metaphase delay, but only after pronounced over-expression. These results demonstrate that normal exit from mitosis depends critically on both a normal localization and a normal level of *Drosophila* Mps1.

This conclusion was further supported by experiments with an EGFP-Mps1 version targeted to the cell membrane by fusion with the **e**xtra**c**ellular and **t**rans-**m**embrane domain (EC/TM) of the Torso receptor tyrosine kinase. Torso(EC/TM)-EGFP-Mps1 expression resulted in a modest metaphase delay and severely abnormal chromosome segregation during exit from

mitosis (Figure 15, third row).

In human cells, Mps1 as well as the other SAC proteins have been shown to localize to the outer corona of prometaphase kinetochores (Dou et al., 2003). In contrast, the C-terminal domain of Cenp-C, which was used for constitutive kinetochore localization of Mps1 in my experiments, is normally found further inwards close to the inner kinetochore plate (Schittenhelm et al., 2007, see Appendix 1). Therefore, I also expressed a variant where Mps1 is fused to Nuf2. The N-terminus of Nuf2, a component of the Ndc80 complex, reaches out into the outer corona of the kinetochore (Schittenhelm et al., 2007, see Appendix 1) (DeLuca et al., 2005; Wan et al., 2009). The expression of EGFP-Mps1-Nuf2 is therefore expected to result in constitutive localization of Mps1 in the region of the kinetochore where it normally resides. However, expression of this variant did not result in EGFP signals that persisted at the kinetochore during exit from M14 at a clearly detectable level and abnormal mitotic phenotypes were not observed (data not shown).

Apart from Mps1, two additional protein kinases Bub1 and BubR1 play a prominent role in the SAC. Mad2 acts as an effector protein of the pathway. Similar to Mps1, these proteins also accumulate on kinetochores during prometaphase and decrease again after chromosome attachment to the spindle before anaphase onset also in *Drosophila* (Logarinho et al., 2004). To address the significance of levels and localization of Bub1, BubR1, and Mad2, I performed mis-localization and over-expression experiments analogous to those with Mps1. Gal4/UAS-mediated expression of wild-type (Bub1, BubR1, Mad2) and variants (BubR1) fused to the constitutive Cenp-C(C) localization domain did not perturb progression through mitosis in *Drosophila* embryos (data not shown).

I conclude that a precise control of Mps1 levels and localization appears to be more crucial than in case of other SAC components.

Over-Expression of Mps1 Kinase in *Drosophila* Embryos Causes a Delay in Metaphase

As described above, **M**ps1 **o**ver-**e**xpression (Mps1 OE) led to an enrichment of metaphase figures in fixed embryos indicating a pronounced delay in metaphase.

On the one hand, this observation was unexpected. No substantial metaphase delays were observed in my earlier experiments involving *Drosophila* strains with two wild-type *Mps1*$^{+}$ alleles and four copies of a transgene (*gEGFP-Mps1*) expressing EGFP-Mps1 under control of the normal *Mps1* cis-regulatory region. The total level of over-expression in these embryos was found to be ~3-fold (Fischer et al., 2004). Moreover, strong Mps1 over-expression in mammalian cells does also not lead to significant delays in metaphase (Kang et al., 2007; Stucke et al., 2002). In budding yeast, on the other hand, *MPS1* over-expression is clearly sufficient for SAC activation and mitotic arrest (Hardwick et al., 1996).

I analyzed whether Mps1 kinase activity is required for the induction of a metaphase delay. However, over-expression of EGFP-Mps1(kd) (Figure 16) did not cause an enrichment of metaphase figures. Quantitative immunoblotting proved that the level of EGFP-Mps1(kd) expression was even slightly higher than that of EGFP-Mps1 resulting in a metaphase enrichment. Therefore, I conclude that kinase activity is required for the induction of the metaphase delay. Experiments with different *UAS-EGFP-Mps1* insertions demonstrated that the over-expression effect is strongly dependent on the level of over-expression. 50% reduction in EGFP-Mps1 over-expression obtained with a weaker *UAS-EGFP-Mps1* transgene insertion did not cause a strong metaphase delay. The observed mitotic effect of Mps1 OE is thus dependent on Mps1 level and kinase activity.

To investigate the effect of Mps1 OE on mitotic progression in further detail, I performed *in vivo* imaging with living embryos in M14. I used different fluorescently labeled marker proteins for this analysis: His2Av-mRFP in combination with Cid-GFP in order to visualize DNA and kinetochores, as well as Jupiter-GFP in combination with 2xtdTom-Cenp-C to visualize spindles and kinetochores. Embryos expressing *UAS-Mps1* were compared to embryos without UAS-transgene as cells proceeded through M14.

To monitor overall progression through M14, I acquired images at 20 s intervals. Comparison of movies from Mps1 OE and wild type embryos confirmed a significant average delay of metaphase of ~12 min in the former (Figure 17). The prolonged metaphase was followed by apparently normal anaphases without chromatin bridges or lagging chromosomes in 53% of the observed mitoses (n = 89). 30% of the mitoses had minor problems like lagging chromosomes but still performed a successful anaphase. The residual 17% of the cells did not exit from mitosis successfully. In wild type embryos, 100% of the observed cells (n = 57) completed mitosis successfully.

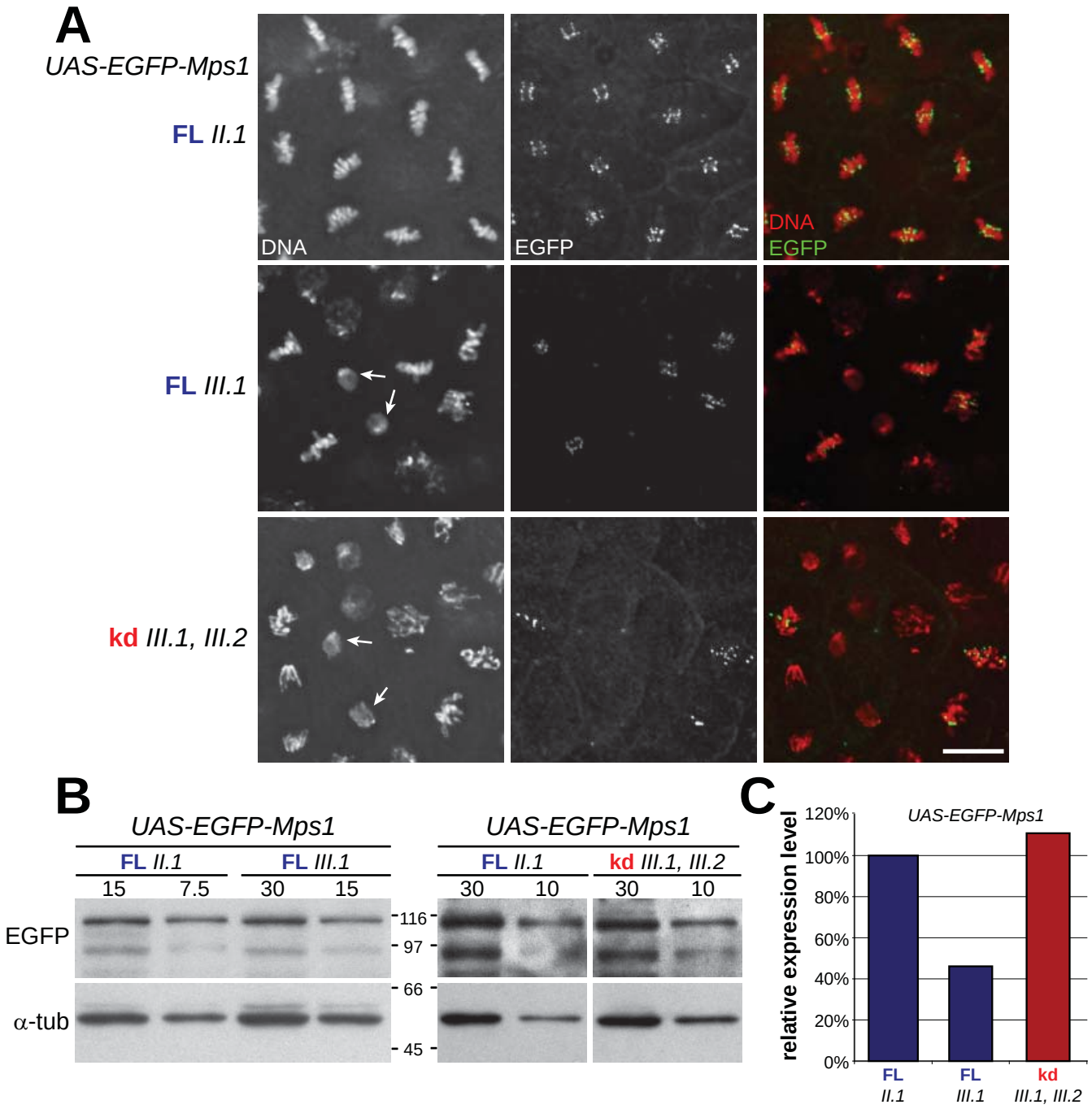

Figure 16. The effect of Mps1 OE depends on its kinase activity and expression level.
(A) Embryos expressing EGFP-Mps1 from two different *UAS*-transgene insertions (*II.1* or *III.1*, respectively) or EGFP-Mps1(kd) (line *III.1, III.2*) (EGFP—green) were fixed in M14 and labeled with DNA stain (DNA—red). Note that the strong metaphase enrichment is only detected after *UAS-EGFP-Mps1 II.1* expression. For all genotypes, the same epidermal region (mitotic domain 11, Foe, 1989) at the time of mitosis 14 is shown. Bar corresponds to 10 μm.
(B) Immunoblotting of total extracts from embryos expressing EGFP-Mps1 from two distinct *UAS*-transgene insertions (*II.1* or *III.1*, respectively) and EGFP-Mps1(kd) with anti-EGFP shows higher expression levels of *EGFP-Mps1 II.1* and *EGFP-Mps1(kd) III.1, III.2* compared to *EGFP-Mps1 III.1*. The number of loaded embryos is indicated above the lanes. Immunoblotting with anti-α-tubulin (α-tub) served as loading control.
The position of molecular weight markers is indicated in the middle.
(C) Quantification of the signal intensities of the EGFP bands shown in (B). Expression levels of *UAS-EGFP-Mps1(FL) III.1* and *UAS-EGFP-Mps1(kd) III.1, III.2* were normalized to the corresponding α-tubulin expression levels, and are depicted relative to the expression level of *UAS-EGFP-Mps1(FL) II.1*.

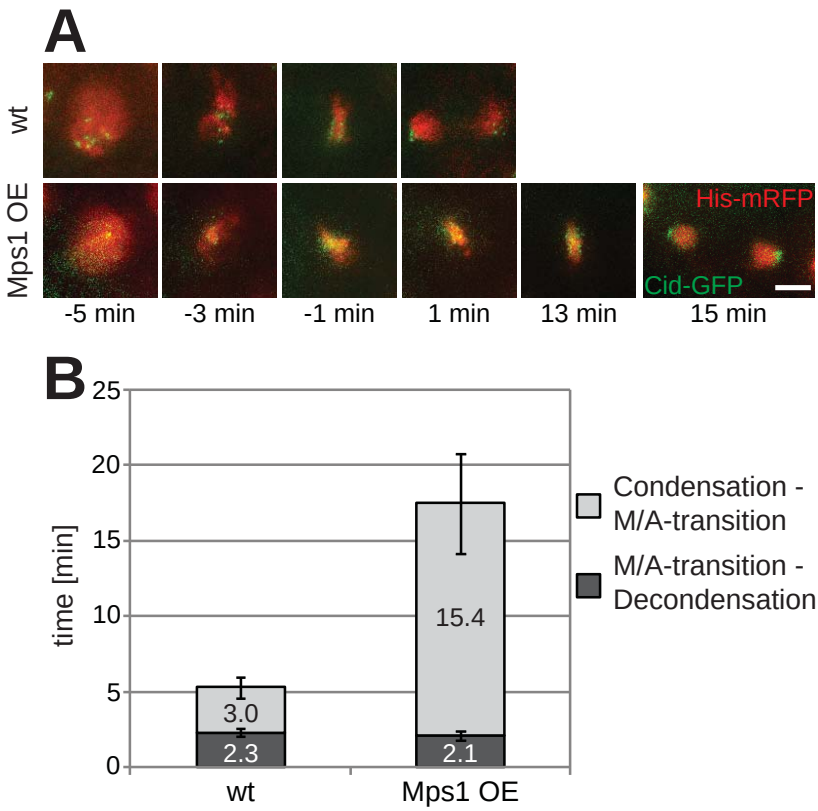

Figure 17. Mps1 OE delays mitosis before M/A-transition.
Movies from embryos expressing His2Av-mRFP and Cid-GFP to label chromatin and kinetochores with wild type (wt) levels of Mps1 or Mps1 OE were evaluated.
(A) Representative stills of single cells proceeding through mitosis 14. Bar corresponds to 5 µm.
(B) The period from the first frame of DNA condensation to the first frame with poleward movement of the kinetochores (condensation - M/A-transition) and the period from M/A-transition to the end of chromatin decondensation (M/A-transition - decondensation) is plotted.
Overall mitotic length was increased from 5.3 min in the wt to 17.3 min after Mps1 OE ($n > 50$). This increase was exclusively caused by a delay before M/A-transition.

To evaluate whether Mps1 OE in M14 is detrimental for development to the adult stage, I counted the number of surviving progeny. The counts indicated that Mps1 OE is highly detrimental for survival to the adult stage (Figure 18), even though *in vivo* imaging had revealed a relatively normal completion of mitosis after the induced anaphase delay.

In principle, differences between fixed samples (as shown in Figure 15 and 16) and the situation during *in vivo* imaging could arise from different genetic backgrounds and/or effects of the fluorescently labeled proteins that are expressed in order to monitor mitotic progression *in vivo*. To address these influences, I analyzed both *in vivo* combinations in my survival assay as well.

I found the survival rate to decrease drastically after Mps1 OE, to 4.8% in case of untagged Mps1 and to 20.6% in case of EGFP-Mps1 (Figure 18). Thus Mps1 OE during the early cellularized embryonic stages interferes with survival to adult stages.

Interestingly, the toxicity of Mps1 OE for development to the adult stage was found to vary in different genetic backgrounds. First, over-expression of untagged Mps1 appeared to be slightly more toxic than over-expression of EGFP-Mps1 (Figure 18). An attempt was made to determine whether this slight difference in toxicity was correlated with a difference in expression levels (Figure 19). However, a conclusive interpretation of the quantification of the immunoblotting data obtained with embryos expressing *UAS-EGFP-Mps1* turned out to be impossible. In the corresponding embryo extracts, a significant amount of anti-Mps1 immunoreactive material was observed within the size range of endogenous Mps1. Presumably

a considerable fraction of this material represents EGFP-Mps1 degradation products which might or might not be functional. Under the assumption that only full length EGFP-Mps1 and endogenous wild type Mps1—which is assumed to be present at the same level as in wild type control embryos—are functional, the levels of functional Mps1 species in the two genotypes are very similar. With *UAS-Mps1* a 5-fold over-expression and with *UAS-EGFP-Mps1* a 5.5-fold over-expression was achieved. Thus if anything, the higher expression of EGFP-Mps1 led to a reduced toxicity compared to the lower expression of untagged Mps1.

Second, Mps1 OE was found to be less toxic in the backgrounds that also expressed the fluorescently labeled marker proteins used for *in vivo* imaging. In particular, the His2Av-mRFP, Cid-GFP background reduced the toxicity to a surprising degree. Possible interpretations of both findings will be discussed below.

If the toxicity of Mps1 OE resulted exclusively from SAC activation, it is expected to be reduced in a SAC-deficient background. Therefore, Mps1 OE was also performed in a *mad2* null mutant background. As mentioned before, *Drosophila mad2*^{P} mutants have been shown to be viable and fertile as well as completely SAC-deficient (Buffin et al., 2007).

However, I found that the toxicity of Mps1 OE was increased rather than decreased in the *mad2* mutant background (Figure 18). Moreover, the protective effect of the backgrounds expressing the fluorescent marker proteins used for *in vivo* imaging was largely abolished in the *mad2*^{P} mutants.

Thus the toxicity of Mps1 OE is unlikely to reflect exclusively SAC hyper-activation. Rather it interferes with development in a way that is less detrimental when the SAC is functional.

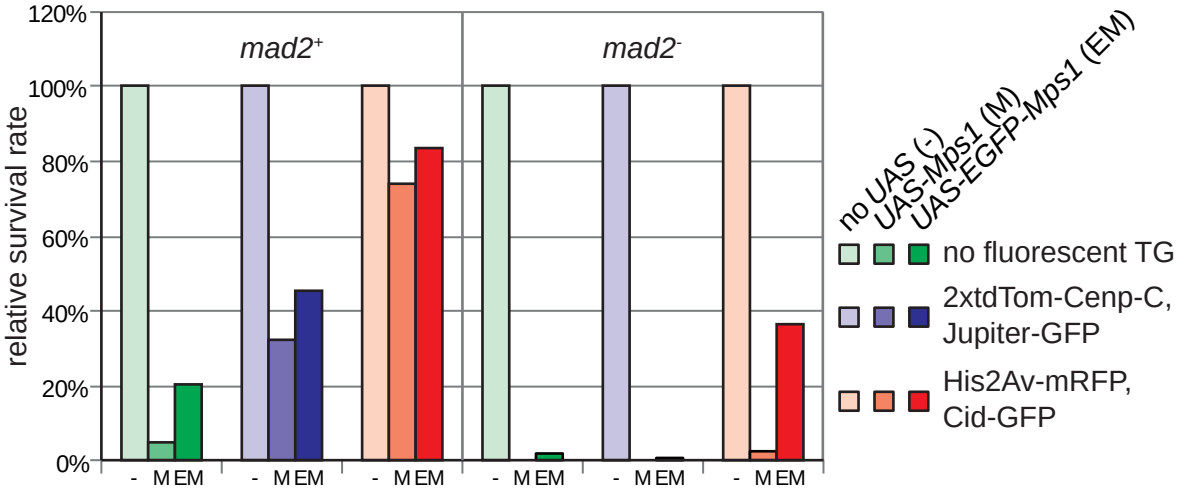

Figure 18. Mps1 OE in M14 reduces survival to adulthood—the effect is enhanced by Mad2 depletion and attenuated by the expression of fluorescently labeled marker proteins.
Females providing Gal4 as well as different fluorescently labeled marker proteins as indicated by different colors into their eggs were crossed with males carrying *UAS*-transgenes over balancer as indicated by color gradation. The adult progeny from these crosses was counted (n > 150) and the ratio between progeny carrying the *UAS*-transgene and their balanced and thus phenotypically marked siblings without expression was normalized to the progeny without *UAS*-transgene (no *UAS*). The number of progeny of *mad2*$^{+}$ flies was compared to the number of progeny of *mad2* mutant flies.

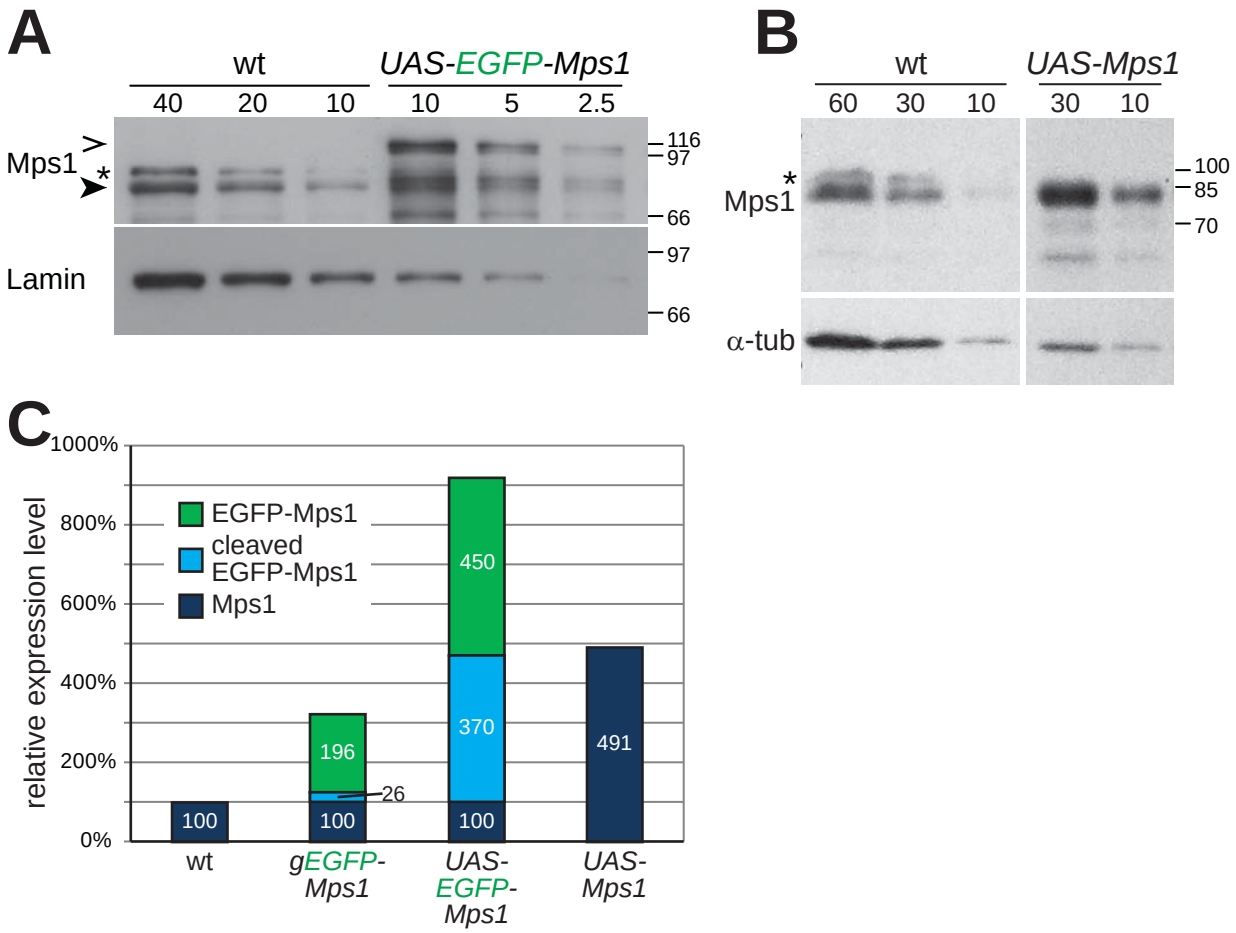

Figure 19. Mps1 levels resulting from expression of *UAS-Mps1* transgenes.
(A) Extracts of wild type (wt) embryos and embryos over-expressing EGFP-Mps1 were compared by immunoblotting with anti-Mps1. showed that wt embryos express endogenous Mps1 (filled arrowhead) only while *UAS-EGFP-Mps1* embryos express EGFP-Mps1 (open arrowhead) in addition. Immunoblotting with anti-Lamin served as loading control. The asterisk marks an unspecific band recognized by the anti-Mps1 antibody. The position of molecular weight markers is indicated on the right side.
(B) Extracts of wild type (wt) embryos and embryos over-expressing Mps1 were immunoblotted with anti-Mps1. Immunoblotting with anti-α-tubulin (α-tub) served as loading control. The asterisk marks an unspecific band recognized by the anti-Mps1 antibody. The position of molecular weight markers is indicated on the right side.
(C) Quantification of the signal intensities of EGFP-Mps1 and Mps1 after the respective over-expression. Signals at the molecular weight of untagged Mps1 at 85 kDa (blue) and signals of EGFP-Mps1 at 115 kDa (green) were quantified. Since the amount of endogenous Mps1 (dark blue) is not expected to be changed by over-expression of EGFP-Mps1, the excess amounts of protein at 85 kDa are probably cleavage products of EGFP-Mps1 (light blue), which should not considered to be functional. Thus expression of *UAS-EGFP-Mps1(FL)* summed up with endogenous Mps1 levels to a ~5.5-fold over-expression, *UAS-Mps1(FL)* induced over-expression was ~5-fold. In comparison expression of *EGFP-Mps1(FL)* under control of the genomic cis-regulatory region of Mps1 (*gEGFP-Mps1(FL)*) lead to a ~3-fold over-expression, but did not induce a metaphase delay (blot not shown).

To monitor and quantify precisely in which way Mps1 OE affects mitosis in the *mad2*$^{+}$ situation (Figure 20) and in *mad2* mutant embryos (Figure 21), I performed high speed *in vivo* imaging in 5 s intervals (10 z-planes, 2 channels) over 10 min and analyzed the behavior of individual chromosomes or kinetochores.

After Mps1 OE in *mad2* mutant embryos, no mitotic delay before the M/A-transition could be observed, in contrast to Mps1 OE in *mad2*$^{+}$ embryos. However, 100% of the anaphases observed after Mps1 OE in *mad2* mutants were abnormal in terms of chromosome segregation (n = 30). Anaphase movements of kinetochores towards the spindle poles were hardly ever perceptible. In contrast, after Mps1 OE in *mad2*$^{+}$ embryos the anaphase following after the metaphase delay appeared far more normal.

I quantified the effect of Mps1 OE on the quality of anaphases in the *mad2*$^{+}$ and in the *mad2* mutant background by measuring the velocity of anaphase movements and the maximum distance of sister kinetochore separation achieved at the end of anaphase (Figure 22A). I found anaphase velocity to be reduced significantly after Mps1 OE in *mad2*$^{+}$ embryos. Importantly, a much more drastic reduction was observed after Mps1 OE in *mad2* mutants. In these embryos, there were no measurable sister kinetochore separation movements at all. Similar findings were made on the extent of sister kinetochore separation achieved by the end of anaphase (Figure 22B), which was reduced to 60% after Mps1 OE in *mad2*$^{+}$ embryos and to < 10% in *mad2* mutants.

These results show clearly that the detrimental effect of Mps1 OE is not simply a result of SAC activation. In fact, the anaphase defects are far stronger after Mps1 OE in SAC-deficient *mad2* mutant embryos.

In yeast and human cells, Mps1 has been shown to have a SAC independent effect on the stability of kinetochore attachment to kinetochore microtubules (Jelluma et al., 2008; Jones et al., 2005; Maure et al., 2007). In principle, therefore, Mps1 OE in *mad2* mutants might destabilize kinetochore attachments and thereby cause the severe anaphase defects. If Mps1 OE interfered with correct attachment, I expect an inefficient chromosome congression into the metaphase plate, an unstable metaphase plate, and a decrease in the inter-sister kinetochore distance. Furthermore, I would predict the unattached kinetochores should recruit higher levels of BubR1.

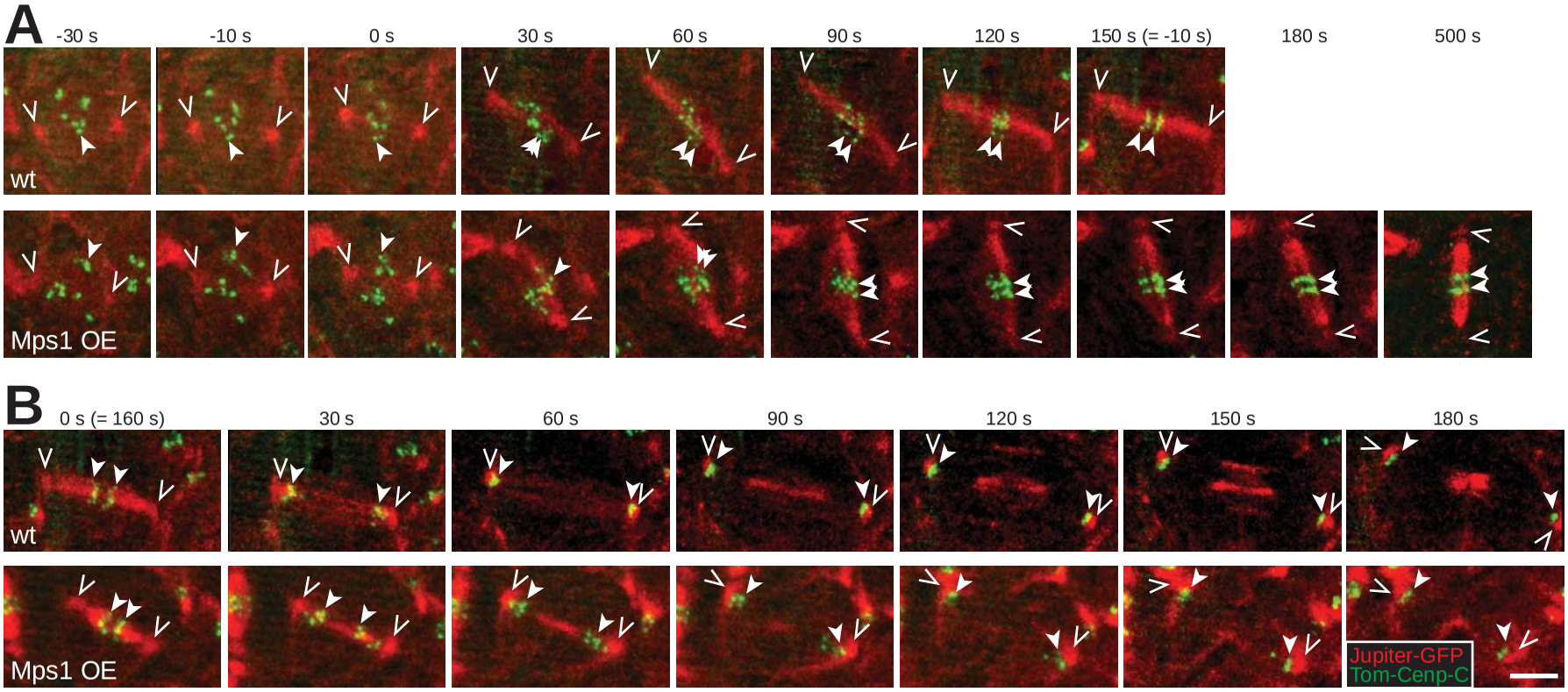

Figure 20. Mps1 OE results in a metaphase delay.
Embryos with a maternal contribution of Gal4, Jupiter-GFP to label the spindle (red) and 2xtdTom-Cenp-C to mark the kinetochores (green) were subjected to high-speed *in vivo* imaging (5 s intervals, 10 z-planes) in order to track individual kinetochores through mitosis. Selected stills from representative movies (deconvolved, max. image projections of 10 z-planes) are shown. Open arrowheads indicate the spindle poles, filled arrowheads indicate two sister kinetochores. *first row*: Embryo without UAS-transgene (**w**ild **t**ype control = wt), *second row*: Embryo expressing an *UAS-Mps1* transgene (Mps1 OE).
(A) Entry into mitosis: Stills were aligned according to the frame of nuclear envelope break-down (0 s) determined on the basis of the first appearance of spindle signals in the nuclear region.
(B) Exit from mitosis: Stills were aligned according to the frame of M/A-transition (0 s) determined on the basis of the first concerted poleward movements of the sister kinetochore signals.
Stills from the wt situation show the same cell in (A) and (B). Time points given in brackets refer to the timescale of the respective other part of the figure.
Bar corresponds to 5 µm.

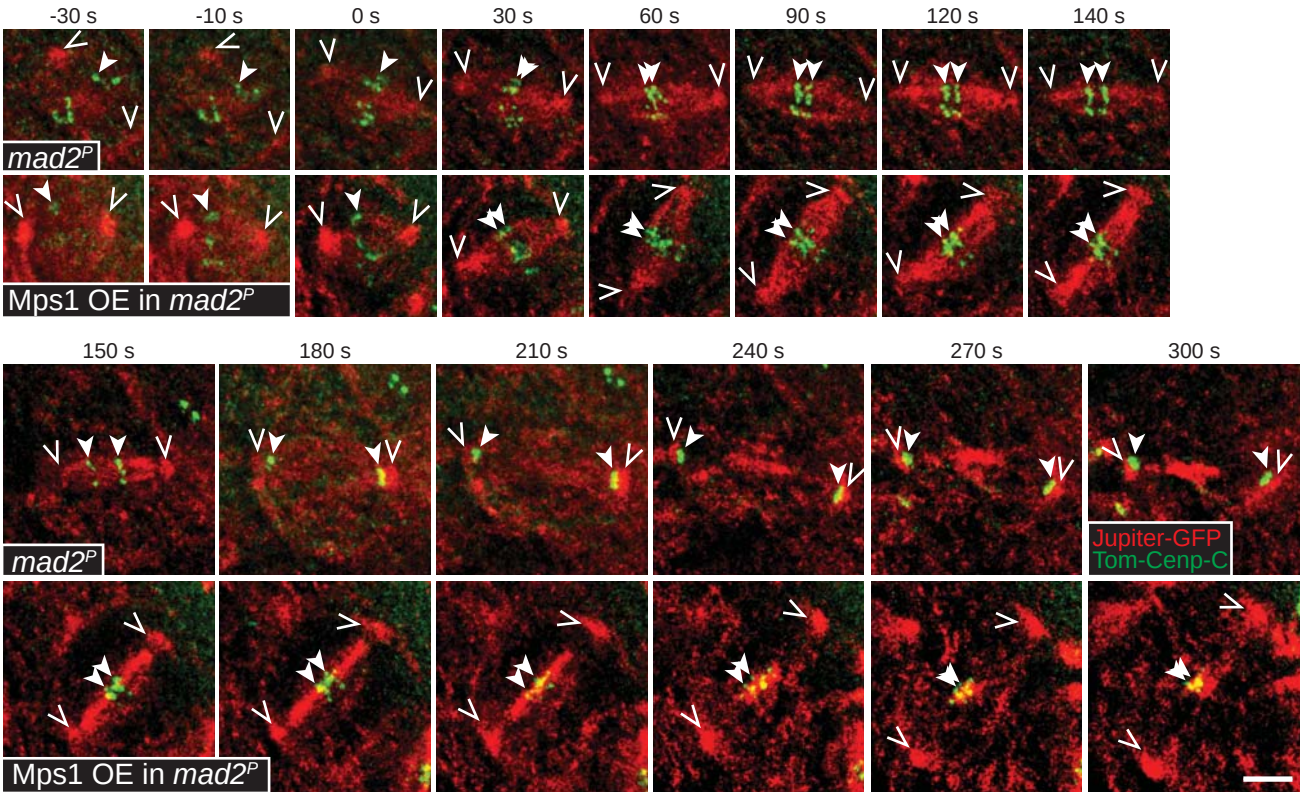

Figure 21. Mps1 OE in *mad2* mutants precludes normal exit from mitosis.
mad2 mutant embryos with a maternal contribution of Gal4, Jupiter-GFP to label the spindle (red) and 2xtdTom-Cenp-C to mark the kinetochores (green) were subjected to high-speed *in vivo* imaging (5 s intervals, 10 z-planes) in order to track individual kinetochores through mitosis. Selected stills from representative movies (deconvolved, max. image projections of 10 z-planes) are shown. Open arrowheads indicate the spindle poles, filled arrowheads indicate two sister kinetochores. *first/third row:* Embryo without UAS-transgene (*mad2*^{P}), *second/fourth row*: Embryo expressing an *UAS-Mps1* transgene (Mps1 OE in *mad2*^{P}).
Stills were aligned according to the frame of nuclear envelope break-down determined on the basis of the first appearance of spindle signals in the nuclear region.
Bar corresponds to 5 µm.

To evaluate the quality of the metaphase plates and the degree of congression, I measured the maximum distance of kinetochore signals along the spindle axis (the overall width of the metaphase plates) at the time, when *mad2* mutants on average undergo a successful anaphase, i.e. 2 min after NEBD (Figure 23). I did not find a significant difference between cells with and without Mps1 OE in both *mad2*$^{+}$ and *mad2* mutant embryos. 2 min after NEBD the chromosomes had aligned into a normally shaped metaphase plate in all of the different genotypes analyzed.

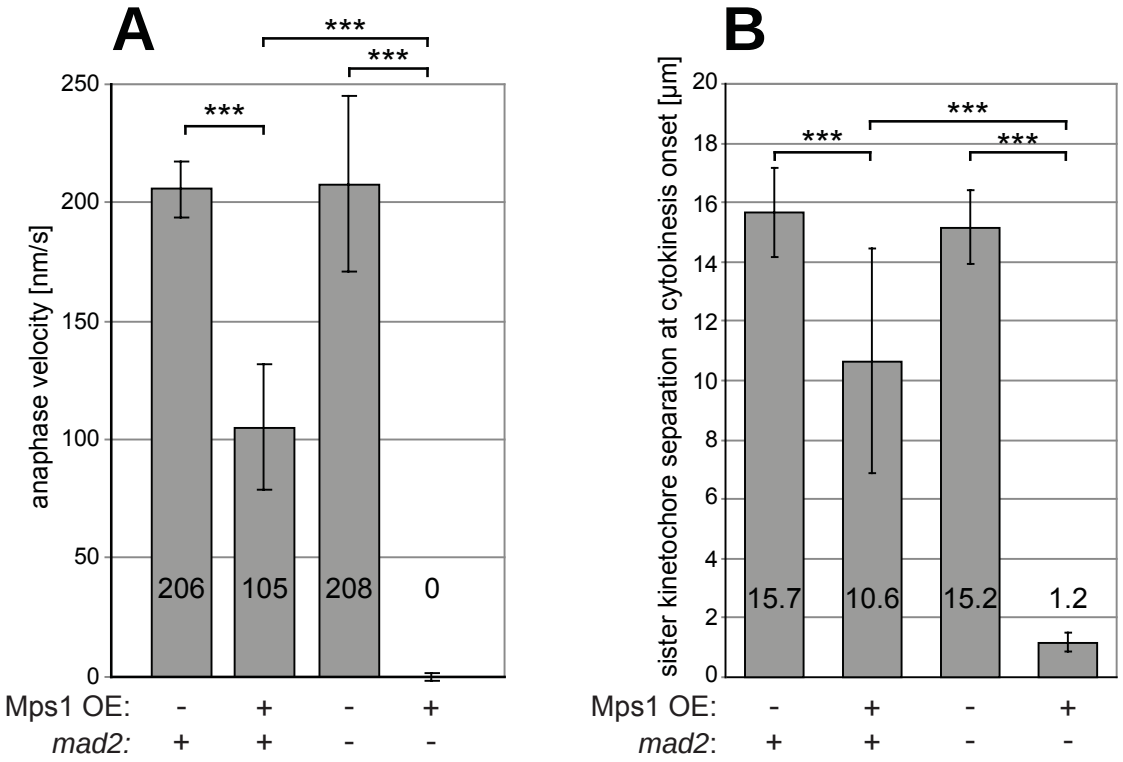

Figure 22. Effect of Mps1 OE on anaphase velocity and the maximum extent of sister kinetochore separation reached during anaphase.
Movies from either *mad2*$^{+}$ (+) or *mad2* mutant (-) embryos expressing 2xtdTom-Cenp-C and Jupiter-GFP to label kinetochores and spindles with (+) and without (-) Mps1 OE as illustrated in Figures 20 and 21 were evaluated.
(A) Distances of Cenp-C signals at M/A-transition and 50 s later were measured, and the difference was divided by 50 s. (M/A-transition was defined as the first frame with concerted poleward movements of the kinetochores. In the case of Mps1 OE in *mad* mutants, where no anaphase movements of the kinetochores were detectable, an increased movement of the spindle followed by detachment of the centrosomes from the spindle was taken as M/A-transition.)
(B) Distances of Cenp-C signals at opposite poles of the spindle at the onset of cytokinesis were measured. (Onset of cytokinesis was defined as the first frame after appearance of the midbody.)
$n = 12$, ***: $p<0.001$.

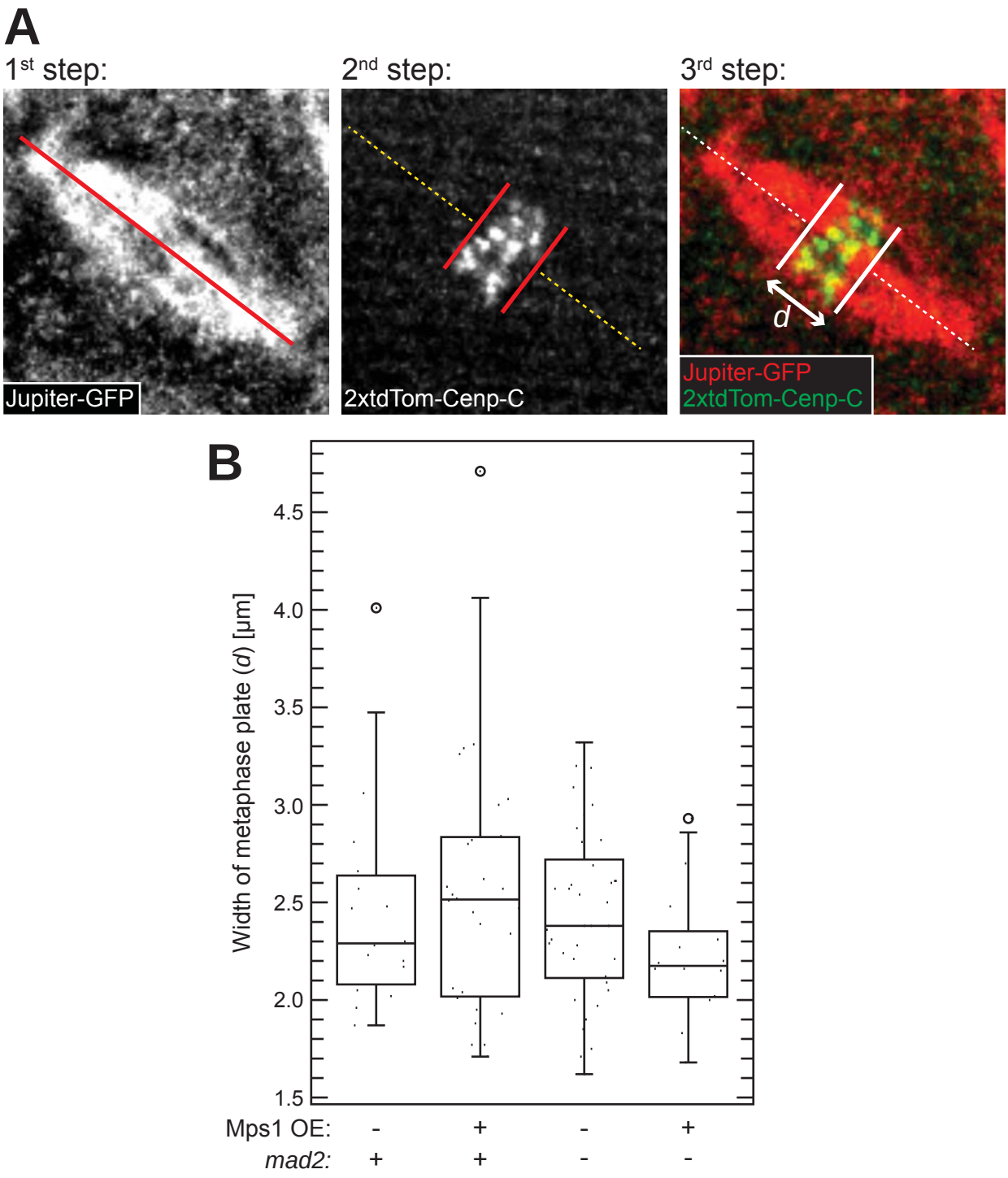

Figure 23. The quality of metaphase plates is not significantly altered by Mps1 OE.
Movies from either *mad2*$^{+}$ (+) or *mad2* mutant (-) embryos expressing 2xtdTom-Cenp-C and Jupiter-GFP to label kinetochores and spindles with (+) and without (-) Mps1 OE as illustrated in Figures 20 and 21 were evaluated.
(A) Method for measuring the width of metaphase plates: 1st step: a line was drawn along the spindle axis, 2nd step: two lines were drawn perpendicularly to the first line, so that all kinetochore signals were located in between them, 3rd step: the distance (*d*) between the two lines was measured.
(B) The width of metaphase plates (*d*) 2 min after nuclear envelope break-down was measured. Results from individual cells are displayed as data swarm in the boxplot. A student's *t*-test did not reveal significant differences between the tested genotypes ($p > 0.05$, $n \geq 15$).

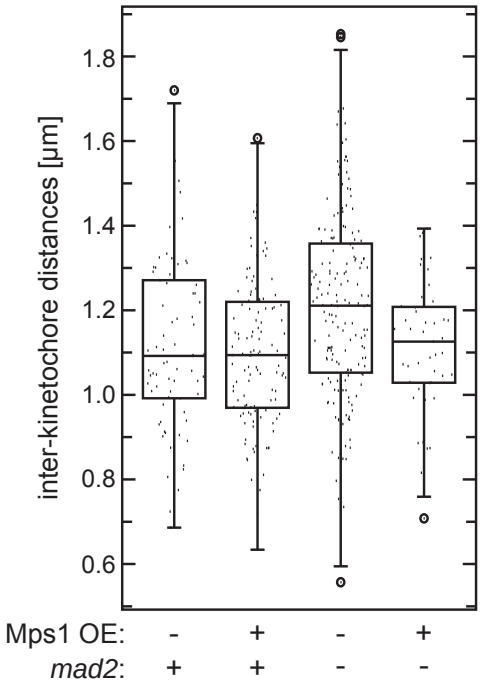

Figure 24. The tension between sister kinetochores in metaphase is not significantly altered by Mps1 OE.
Movies from either *mad2*$^{+}$ (+) or *mad2* mutant (-) embryos expressing 2xtdTom-Cenp-C and Jupiter-GFP to label kinetochores and spindles with (+) and without (-) Mps1 OE as illustrated in Figures 20 and 21 were evaluated.
The inter-sister kinetochore distance 2 min after nuclear envelope break-down was measured. Results from individual sister kinetochores are displayed as data swarm in the boxplot. A student's *t*-test did not reveal significant differences between the tested genotypes ($p > 0.05$, $n \geq 45$) except for the *mad2* mutants, in which some cells had already proceeded to anaphase at the evaluated time point, which increased the inter-sister kinetochore distance significantly ($p < 0.01$).

To evaluate whether sister kinetochores are under tension at the time when anaphase starts in the *mad2* mutants, I measured the distance between sister kinetochore pairs 2 min after NEBD (Figure 24). Again, I did not observe significant differences between the different genotypes analyzed.

Kinetochore recruitment of BubR1 represents an additional sensitive indicator of attachment defects. To observe the behavior of BubR1 localization, I performed *in vivo* imaging of embryos expressing His2Av-mRFP and GFP-BubR1 (Figure 25A). Background corrected kinetochore levels of GFP-BubR1 signals were quantified over time, and normalized to the highest detected intensity value per cell, in order to compare different embryos (Figure 25B). Comparing cells with and without Mps1 OE revealed little differences in BubR1 behavior. BubR1 recruitment at the entry into mitosis appeared to be similar in both situations. Signals increase fast (within 1 min) to the maximum value followed by a linear decrease to 50% of the highest value within the next minute. This initial decrease was found to be even slightly faster after Mps1 OE. In the following minute, kinetochore signals of BubR1 decrease further to reach ~30% at the start of anaphase in embryos without Mps1 OE. In contrast, in Mps1 OE cells BubR1 remains at the kinetochore at an intermediate level for an extended period until shortly before the exit from the arrest. BubR1 signals during the Mps1 OE induced metaphase delay seemed to be high at maximally 1 or 2 kinetochores. Thus my results indicate that individual unattached kinetochores are likely to be present after Mps1 OE. However, these few exceptional unattached kinetochores cannot explain the severe failure of anaphase in the *mad2* mutant situation, which occurs at a time when BubR1 levels at kinetochores are very similar in cells with and without Mps1 OE.

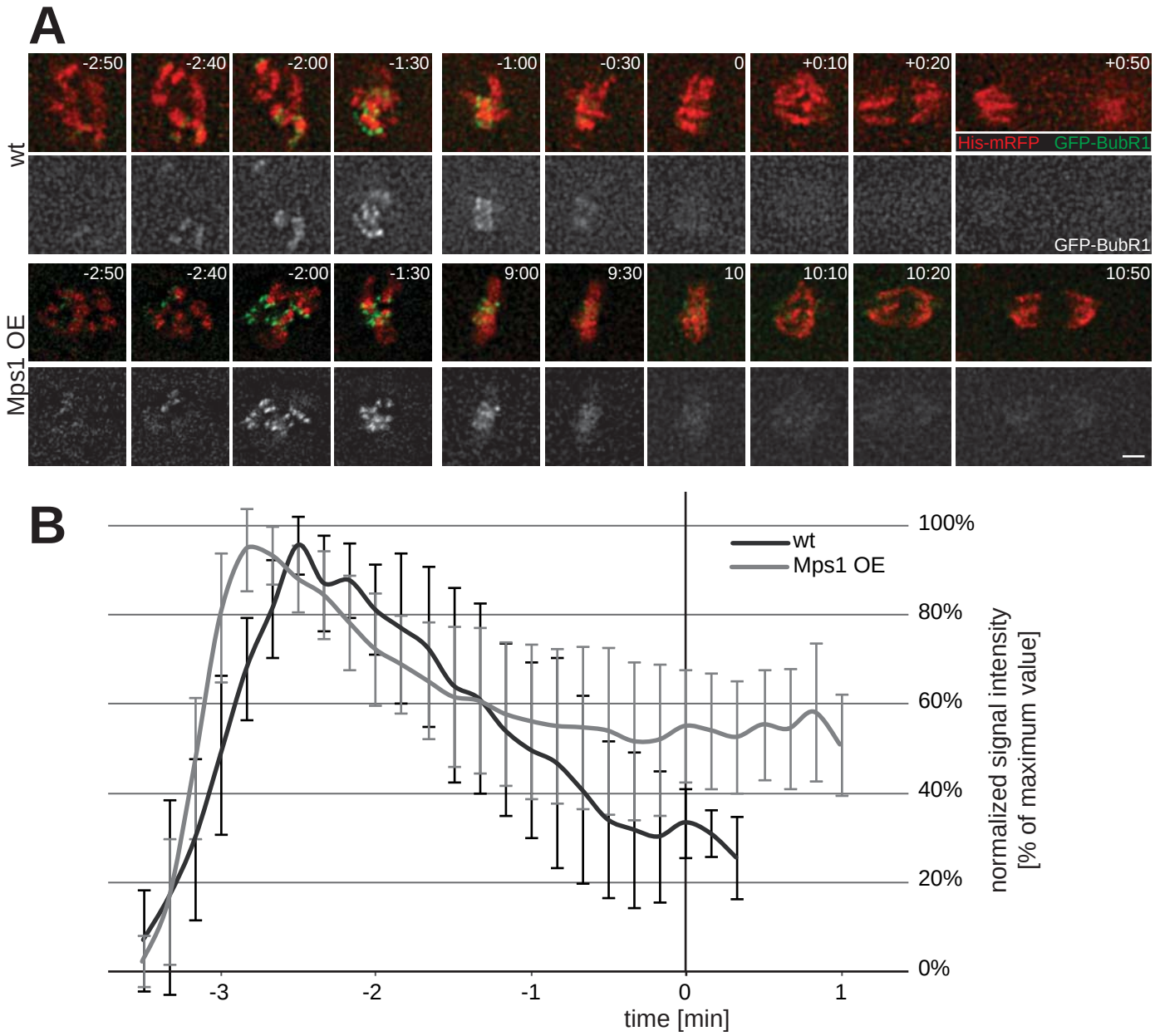

Figure 25. Low levels of GFP-BubR1 are present at the kinetochores during the metaphase delay induced by Mps1 OE.

M14 in embryos expressing His2Av-mRFP (red) and GFP-BubR1 (green) was observed by *in vivo* imaging in 10 s intervals, 10 z-planes at 500 nm spacing.

(A) Selected stills from representative movies (deconvolved, max. image projections of 10 z-planes) are shown. The first 2 rows show the situation with wild type levels of Mps1 (wt), the second 2 rows show the phenotype after Mps1 OE. Bar corresponds to 2 µm.

(B) Quantification of the GFP-BubR1 kinetochore signals during mitosis of cells with wild type Mps1 levels (wt, black, n = 7) and with Mps1 over-expression (Mps1 OE, grey, n = 24). Signal intensities were normalized as percent of the maximum value of the cell. Mitotic timing of individual cells was aligned according to the frame with the first appearance of BubR1-GFP signals at the kinetochores. On average, wild type cells started anaphase 3.5 min later. Therefore, that time point was defined to t = 0.

In the first 2 min of mitosis, kinetochore levels of GFP-BubR1 increase and decrease in the Mps1 OE situation similarly to the wt situation. After having congressed into the metaphase plate and before Mps1 OE cells reach the level of mitotic exit seen in the wt situation (~30%), the decrease slows down, and GFP-BubR1 levels stay at ~50% during the metaphase delay.

Therefore, I conclude that the severe anaphase defect induced by Mps1 OE in *mad2* mutants is not explained by kinetochore attachment defects. Moreover, I propose that the failure of sister chromatid separation after Mps1 OE in *mad2* mutants might reflect an inhibition of sister chromatid separation by Mps1.

Moreover, my results give important hints concerning the mechanism allowing the eventual exit from the metaphase delay after Mps1 OE in *mad2*$^{+}$ embryos. In principle, exit from mitosis after SAC induction can occur in two ways: by eventual SAC silencing or by adaptation (resulting in combination with APC activation and abrupt securin and Cyclin B degradation), or by so called slippage, an exit that is caused by a slow and steady decrease in Cdk1 activity as a result of residual APC activity in the presence of a fully active SAC (Brito and Rieder, 2006). While kinetochore levels of BubR1 are supposed to stay constantly high during slippage, BubR1 shedding is expected in case of SAC silencing by adaptation. My results indicate that the exit from the mitotic delay caused by Mps1 OE occurs by SAC silencing but not slippage.

This conclusion was also supported by the results of Mps1 OE in *roughex (rux)* mutants. The Cdk inhibitor *rux* was suggested to be involved in mitotic exit and slippage (Foley and Sprenger, 2001; Rieder and Maiato, 2004). Thus in its absence I would expect increased difficulties in case of slippage. *rux* mutants did not substantially prolong the mitotic delay in metaphase after Mps1 OE (data not shown), consistent with SAC silencing but not slippage being the reason for the eventual exit from metaphase after Mps1 OE.

For technical reasons (insufficient signal intensities and dominant effects of the transgenes on mitotic progression) a direct measurement of Cyclin B-GFP levels as read-out of APC activity was not successful (data not shown).

Comparison of SAC Activity in *Drosophila* Embryos and S2R+ Cells

The SAC is of considerable importance for etiology and therapy of human cancer. SAC induction by taxol derivatives and vinca alkaloids is currently applied in therapy. Additional ways to interfere with or stimulate the SAC in the context of cancer therapy are being explored. A precise understanding of the behavior of cells upon experimentally induced SAC activation is therefore clearly of interest. Not only the efficiency of the SAC induction was shown to be relevant in the context of cancer therapy, even more important are the length of the induced mitotic arrest and the nature of the eventual exit from the arrest. The manner, in which the mitotic exit occurs, either as SAC silencing by adaptation or slippage, directly affects the fate of the daughter cells and their survival (Gascoigne and Taylor, 2009). Different human cell lines show very different behavior upon chemically induced SAC arrests (Brito and Rieder, 2009).

Thus it must also be expected that cells in living tissues react differently to experimental SAC induction than cultured cells. To characterize such differences I used the *Drosophila* system.

Living *Drosophila* embryos and cultured embryonic (S2R+) cells are both well-suited systems for the study of the effects of SAC induced mitotic arrests. The effects of SAC induction by spindle poisons in *Drosophila* cell culture have not been studied in detail so far. Therefore, I characterized the phenotypic characteristics of differently induced SAC arrests by *in vivo* imaging of S2R+ cell culture and living *Drosophila* embryos expressing His2Av-mRFP. Activation of the SAC was achieved by (i) complete destruction of the mitotic spindle by incubation with colchicine, (ii) interfering with mitotic spindle dynamics and stabilization of the mitotic spindle by incubation with taxol, (iii) decreasing the tension between sister chromatids by premature cohesin cleavage or (iv) Mps1 OE.

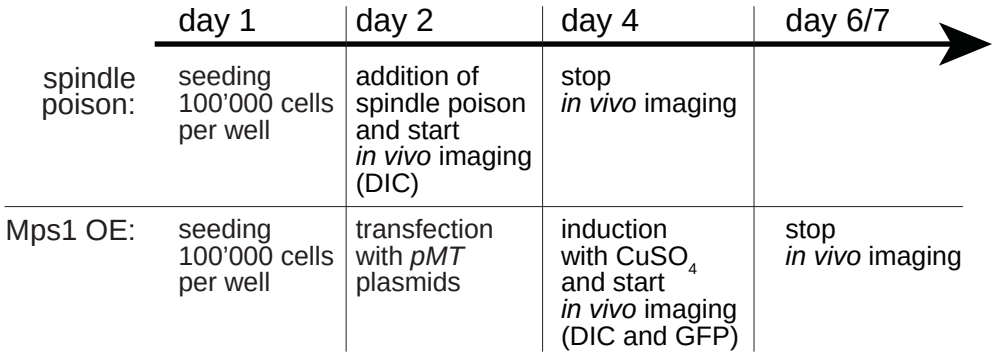

Figure 26. Time line for SAC induction in different ways for *in vivo* imaging experiments in S2R+ cells.
Starting with 100'000 cells each, two ways of SAC induction are described: spindle poison application and Mps1 OE by metallothionein promoter induction. In both situations, *in vivo* imaging was started directly after adding the SAC inducing agent. *In vivo* imaging was done for ~2 d.

First I characterized the effects of ectopic SAC induction in the cell culture system (Figure 26):

Colchicine or taxol were added to the culture medium in order to induce the SAC in S2R+ cells. For technical reasons premature cleavage of sister chromatid cohesion was not feasible in this system. Mps1 OE was induced in cells transiently transfected with a construct allowing Mps1 expression under metallothionein promoter control by $CuSO_4$ addition to the medium. Untreated cells served as controls (Figure 27, row 1 and Figure 28). I performed *in vivo* imaging for ~2 d directly after SAC induction. The timing of the mitotic phases was defined using the criteria explained in Figure 27. Both taxol as well as colchicine induced a significant delay in mitosis (Figure 27, rows 6 - 8). Mps1 OE caused a similar effect (Figure 27 rows 4 and 5). This effect was dependent on the kinase activity of Mps1 since Mps1(kd) did not prolong mitotic progression significantly ($p > 0.05$, $n > 50$) (Figure 27 rows 2 and 3).

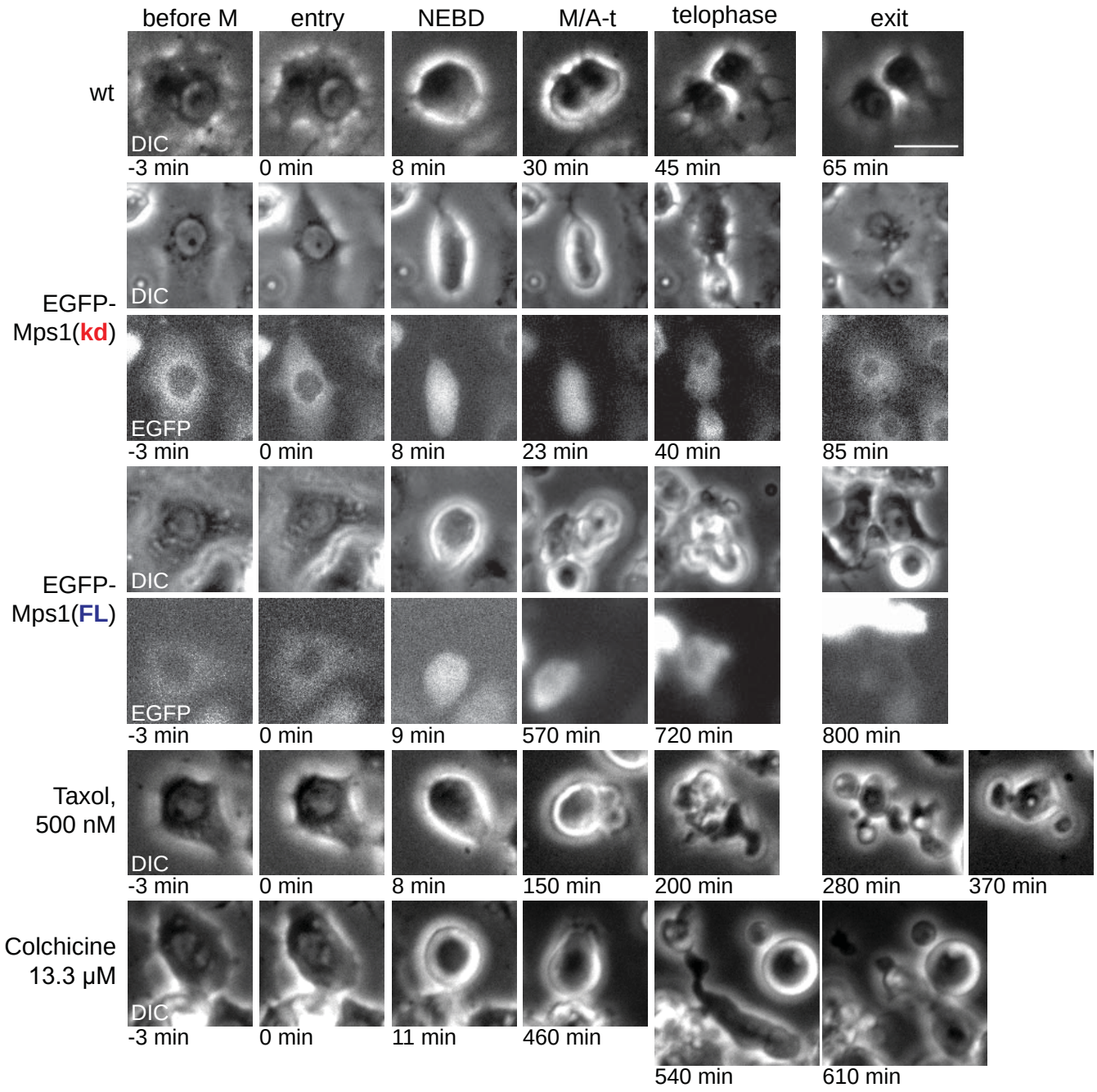

Figure 27. Mitotic delays induced in S2R+ cells by Mps1 OE and spindle poisons.
Selected pictures from *in vivo* imaging of mitotic cells after inducing the SAC by various means. Pictures show a single cell before entry into mitosis (before M—flattened), at entry of mitosis (entry—first cell rounding), nuclear envelope break-down (NEBD—no visible nucleus), at M/A-transition (M/A-t—cell elongation), in telophase (telophase—final cell cortex contractions), and at the exit from mitosis (exit—first picture where nuclei are again clearly visible). The numbers denote the average time a cell takes to proceed from entry into mitosis to the respective mitotic phase under the indicated conditions ($n > 15$).
Row 1: S2R+ cells without transfection or spindle poison incubation.
Row 2-5: S2R+ cells transfected with inducible plasmids for EGFP-Mps1 and EGFP-Mps1(kd) expression. Expression was induced by addition of $CuSO_4$ to the culture medium.
Row 6-8: S2R+ cells incubated with the indicated spindle poisons.
Bar corresponds to 10 µm.

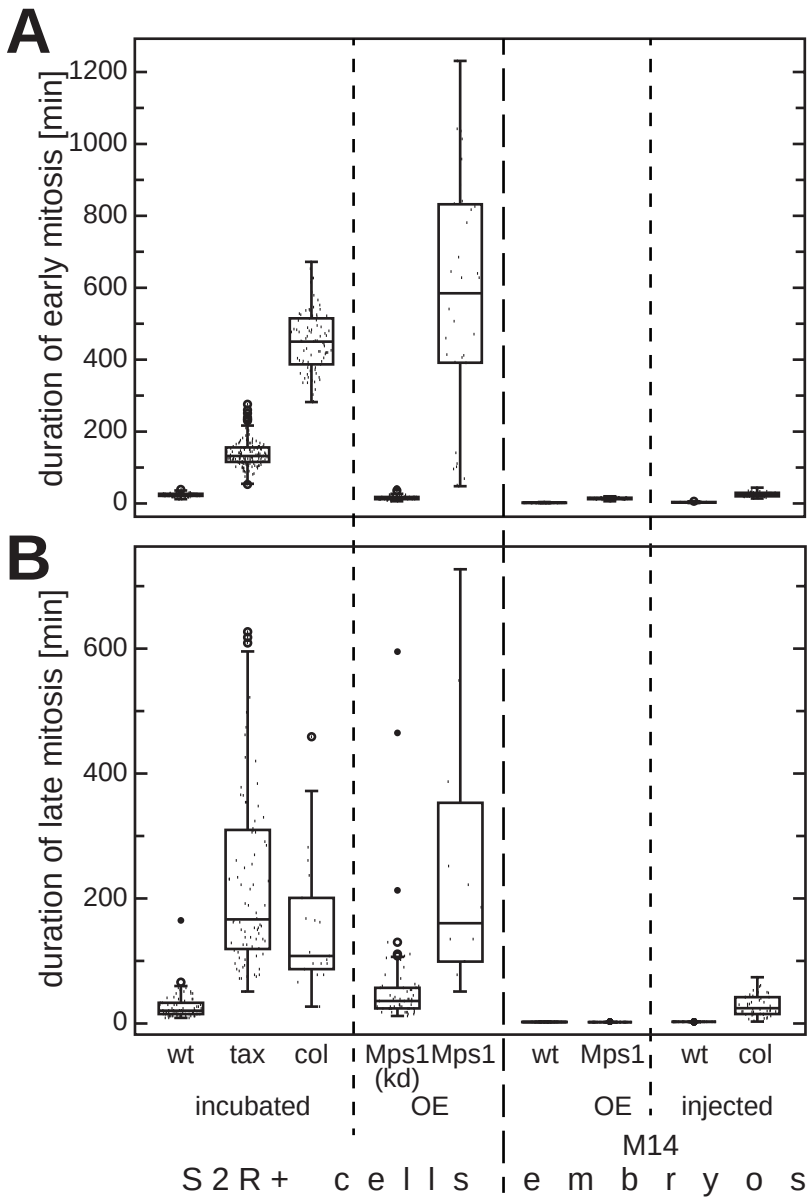

Figure 28. S2R+ cells react on SAC induction with longer mitotic arrests than cells in living embryos.
Comparison of mitotic timing after SAC induction by various means in two different systems. *left side*: Movies from the S2R+ cells described in Figure 27 were evaluated. *right side*: Movies from embryos expressing His2Av-mRFP were evaluated. Wild type M14 (wt) was compared with M14 after Mps1 OE and M14 after injection of Schneider's medium (wt injected) was compared with M14 after injection of colchicine in Schneider's medium (col injected). (A) Duration of early mitosis (period between entry into mitosis and M/A-transition, as defined in Figure 27). (B) Duration of late mitosis (period between M/A-transition and exit from mitosis, as defined in Figure 27). Results from individual cells are represented as data swarm in the boxplot ($n \geq 12$).

As expected, the mitotic delay occurred primarily before M/A-transition (Figure 28A). This early part of mitosis was on average delayed by 560 min after Mps1 OE ($p < 0.001$, $n > 30$) and by 430 min ($p < 0.001$, $n > 80$) after colchicine addition. Taxol treatment prolonged early mitosis only by 120 min ($p < 0.001$, $n > 140$).

Independent of the way of SAC induction, exit from mitosis resulted in very abnormal anaphases. Sudden uncoordinated cell cortex contractions caused an explosive dynamics frequently followed by cell death (Figure 27). These uncoordinated anaphase movements took significantly longer than normal anaphases in untreated cells as well (Figure 28B). On average exit from mitosis was prolonged by 150 min after taxol addition ($p < 0.001$, $n > 80$), by 225 min after colchicine addition ($p < 0.001$, $n > 15$) and by 240 min after Mps1 OE ($p < 0.001$, $n > 25$).

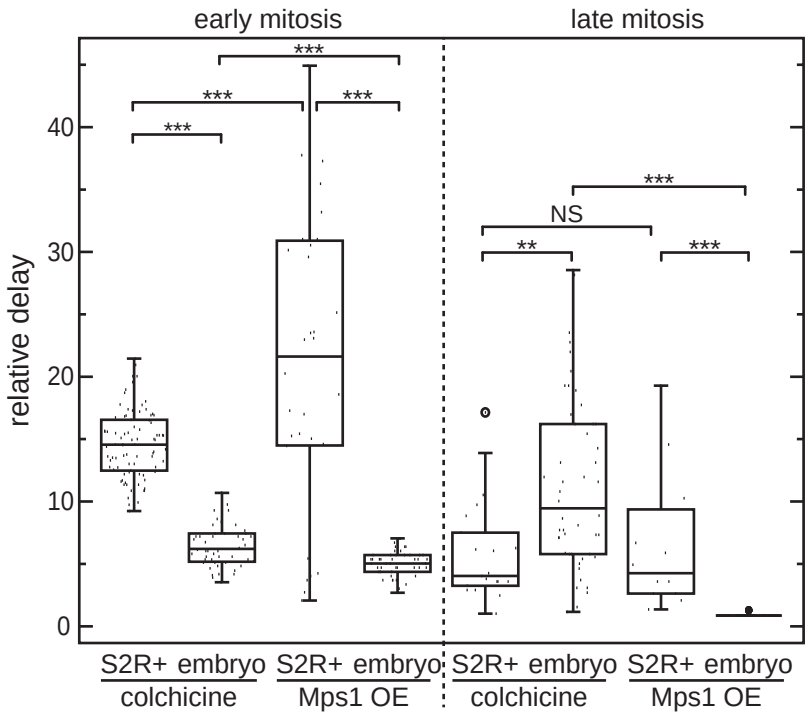

Figure 29. Ectopically induced SAC activation results in different effects dependent on the studied system.
To compare mitotic timing in S2R+ cells and in embryos, the absolute time values were normalized with the respective mitotic timing under undisturbed conditions (as illustrated in Figure 28). *left*: Duration of early mitosis (period between entry into mitosis and M/A-transition, as defined in Figure 27). *right*: Duration of late mitosis (period between M/A-transition and exit from mitosis, as defined in Figure 27). Results from individual cells are represented as data swarm in the boxplot ($n \geq 12$).
The reaction on colchicine treatment and Mps1 OE differs significantly between of S2R+ cells and embryos before M/A-transition as well as after M/A-transition.
***: $p < 0.001$, **: $p < 0.01$, NS: not significant = $p > 0.05$.

Subsequently I characterized the effects of ectopic SAC induction in living *Drosophila* embryos:

The application of spindle poisons in this system was performed by injection in living embryos before M14. Low diffusion of taxol caused a gradient distribution of the effects in the egg that could not be quantified (data not shown). Premature cleavage of cohesin was achieved by targeting a TEV cleavable cohesin subunit ($Rad21^{TEV}$) with TEV protease expression during M14. These experiments were described in detail in Pauli et al., 2008 (see Appendix 3). In brief, although the mitotic phenotype caused by the lack of sister chromatid cohesion differed substantially from the phenotype caused by Mps1 OE, the extent of the induced mitotic delays were very similar. The effects of Mps1 OE during M14 were described above (Figure 17): a ~12 min delay of mitosis before M/A-transition was followed by a timely normal exit from mitosis (Figure 28). Colchicine injection in contrast caused a longer delay of mitotic progression; mitosis was on average delayed by 24 min before and by 27 min after the M/A-transition (both: $p < 0.001$, $n > 45$).

My comparison of S2R+ cells and embryos reveal the following differences. While unperturbed mitosis in S2R+ cells takes > 1 h on average, embryonic M14 takes only ~5 min. Apart from a comparison of the induced mitotic delays in an absolute time scale, a consideration of delays normalized by the respective timing of undisturbed mitosis is therefore also of interest (Figure 29).

The reaction of S2R+ cells to colchicine treatment is clearly different from the reaction of cells in the living embryos. While S2R+ cells delay the early mitosis 15-fold and the late mitosis only 5.5-fold, cells in the living embryos show a converse response and delay the early mitosis only 5-fold; however, the late mitosis is delayed 10-fold.

The reaction to Mps1 OE differs as well. While S2R+ cells react with a 20-fold delay in early mitosis and a 6-fold delay during late mitosis, embryos delay early mitosis only 5-fold and do not delay late mitosis at all.

One caveat concerning these experiments lies in the fact that no careful evaluation of dose dependency was conducted. Control of the amounts of spindle poisons injected into embryos is not trivial. Similarly, higher expression of Mps1 in S2R+ cells might lead to different effects than lower expression in embryos.

Nevertheless, my results support the notion that the effects of ectopic SAC induction in cell culture cannot directly be transferred to living tissue.

Discussion

Part 2 of my thesis describes work addressing SAC functions in *Drosophila melanogaster*, with particular emphasis on the role of Mps1.

SAC Silencing without Mps1 Degradation

I show here that *Drosophila* Mps1 is not degraded substantially at the metaphase to anaphase transition, suggesting that Mps1 degradation is unlikely to be crucial in *Drosophila* for normal exit from mitosis. This suggestion is in conflict with observations in yeast, where Mps1 degradation has been proposed to be essential for correct exit from mitosis (Palframan et al., 2006). The role of Mps1 degradation in human cells appears to be complex. While initial studies indicated that centrosomal Mps1 degradation is required to restrict centrosome duplication, and this degradation was shown to be regulated by Cdk2 phosphorylation of Mps1 (Jaspersen et al., 2004), more recent work identified a D-Box, which was shown to be required for proteasomal degradation of Mps1 during mitosis, and mutational inactivation of this D-Box was claimed to have some effect on exit from mitosis (Cui et al., 2010) although the reported effects appear limited and lack solid statistical support.

While my data suggest that Mps1 degradation is not required for normal exit from mitosis in *Drosophila*, I emphasize that a possible local degradation of a small fraction of Mps1 would not have been detected in my experiments.

In principle, mitotic Mps1 degradation might occur locally restricted, for example on kinetochores or the centrosomes so that the overall decrease of Mps1 levels would be beyond my detection limit by immunoblotting. However, the situation in *Drosophila* is certainly different from yeast, where a > 50% decrease of overall Mps1 levels was observed during anaphase (Hardwick et al., 1996).

In my localization studies I indeed observed a decrease of Mps1 at the kinetochores, but this is more likely caused by a re-localization, since Mps1 levels at the spindle increased during that time. However, *in vivo* imaging has clearly revealed Mps1 particle streaming along kinetochore microtubules after chromosome attachment (Pandey et al., 2007). Of course, Mps1 shedding from the kinetochores leads to a local decrease of Mps1 levels, which might be crucial to keep the SAC silenced after M/A-transition.

It can also be reasonably questioned whether it is really crucial to make SAC reactivation during mitosis impossible. After all, Cyclin B degradation and separase activation have already occurred to a sufficient extent until anaphase onset in *Drosophila* and human cells. The

notion that Mps1 degradation might not be essential for correct exit from mitosis therefore does not seem to be truly heretical.

N-Terminal Phosphorylation of Mps1—Relevant for SAC Function?

Drosophila Mps1, like Mps1 kinases in many other organisms, is subject to phosphorylation. In human as well as in yeast, several phosphorylation sites of Mps1 were mapped (Dou et al., 2011; Jelluma et al., 2008a; Kang et al., 2007; Kasbek et al., 2007; Mattison et al., 2007; Tyler et al., 2009; Xu et al., 2009). Only few of them have been associated with particular functions up to now. Since I find that *Drosophila* Mps1 is phosphorylated in its N-terminal domain, I was interested in characterizing the functions of this phosphorylation. N-terminal phosphorylations in human or yeast Mps1 were described to be important for kinetochore localization (Xu et al., 2009) or protein stability (Jaspersen et al., 2004). The overall conservation between *Drosophila* Mps1 and human Mps1 is ~45% identity, and most of this conservation is observed in the C-terminal kinase domain. In particular within the N-terminal regulatory region, the amino acid residues corresponding to those phosphorylated in human Mps1 cannot be identified in *Drosophila* Mps1. One phosphorylation site within the N-terminal domain of *Drosophila* Mps1 has been predicted *in silico* (Gilliland et al., 2007), but this prediction has not been evaluated experimentally.

I have initiated an analysis of the function of Mps1 phosphorylation in *Drosophila* by characterizing factors that influence it. I show that the observed phosphorylation of the N-terminal domain of Mps1 is not dependent on the presence of a functional C-terminal kinase domain, suggesting that the observed phosphorylation is not due to auto-phosphorylation. These findings are in agreement with reports from human cells and yeast, where the phosphorylation within the N-terminal domain was suggested to be induced by Cdks or **m**itogen-**a**ctivated **p**rotein **k**inase (MAPK) (Jaspersen et al., 2004; Kang et al., 2007). In yeast, this phosphorylation has been implicated in the control of spindle pole body reduplication. *Drosophila* Mps1 is not required for centrosome duplication. Moreover, I find the phosphorylation of *Drosophila* Mps1 to be enriched during mitosis, and thus it might also be involved in SAC function rather than centrosome biology.

SAC related phosphorylations have been described in human Mps1 as well (Kang et al., 2007; Mattison et al., 2007; Tyler et al., 2009; Xu et al., 2009). These were mostly described to be auto-phosphorylations and to occur in the C-terminal kinase domain. The disappearance of these phosphorylations after SAC silencing has not been characterized in detail.

I observe that *Drosophila* Mps1 is phosphorylated before as well as after M/A-transition, which makes it unlikely that this phosphorylation is directly coupled to SAC activity. However,

the observed N-terminal phosphorylation could create a permissive condition for SAC activation or kinetochore recruitment, and could be, for example, induced by Cdk activity. Whether the observed phosphorylation correlates with Mps1 kinase activity, remains to be elucidated. Mps1 kinase activity was shown to influence SAC activity (Hewitt et al., 2010; Kang et al., 2007; Maciejowski et al., 2010; Santaguida et al., 2010; Xu et al., 2009), but the precise dependencies are still poorly understood.

Some phosphorylation sites in the C-terminal domain that have been described to influence Mps1 kinase- and SAC activity are conserved in *Drosophila*. Possibly these sites are phosphorylated in *Drosophila* as well, but do not cause changes in the electrophoretic mobility of the protein. Two examples would be T675 (T489 in *Drosophila*) and T686 (T496 in *Drosophila*) in the activation loop of the kinase (Kang et al., 2007; Mattison et al., 2007; Tyler et al., 2009; Xu et al., 2009). Phosphorylations at these two residues have been described to occur by auto-phosphorylation and are thought to be important for auto-activation in a positive feedback loop. They have also been reported to not influence the electrophoretic mobility of human Mps1 (Mattison et al., 2007).

Mps1 Kinetochore Recruitment Requires Its Kinase Activity

Neither the N-terminal domain nor the C-terminal domain of *Drosophila* Mps1 is sufficient to mediate kinetochore recruitment. These observations are different from findings in human cells, where the N-terminal domain was shown to be sufficient to mediate kinetochore recruitment (Stucke et al., 2004). However, these conclusions are based on experiments performed in the presence of the wild type Mps1 protein. I point out that I find a striking difference between kinetochore recruitment of Mps1 domains in the presence and absence of wild type Mps1 kinase. I show that this might reflect an interaction of the individual domains with wild type Mps1, which could lead to kinetochore recruitment.

Similarly, I provide evidence that Mps1 kinase activity is required for its kinetochore recruitment. Studies performed in human cells have led to conflicting results. Recent studies have suggested that Mps1 kinase activity is required for Mps1 shedding from the kinetochores (Hewitt et al., 2010; Santaguida et al., 2010). In contrast, another study concurs with my results (Xu et al., 2009). The contradicting conclusions from the studies in human cells might reflect technical differences and problems. Both of the employed methods, RNAi and chemical inhibitors, do not always match the selectivity and effectiveness of a clean null mutant situation. An effective elimination seems to be of special importance in the case of Mps1, since it has been demonstrated that Mps1 activity can be reduced to ~10% without resulting in changes that affect the recruitment of other SAC components in human cells (Lan and

Cleveland, 2010). My studies in null mutants can be expected to give definitive insight into localization dependencies of *Drosophila* Mps1. The kinase dead Mps1 version that is used in my experiments has a point mutation in the DFG motive. This mutation does not prevent Mps1 self-interaction, suggesting that Mps1(kd) is not affected by severe structural alterations precluding protein interactions. Moreover, this observation shows that self-interaction is not sufficient for kinetochore recruitment of Mps1.

To reconcile my observations with the findings from other studies, it could be proposed that kinase activity might be required for initial kinetochore recruitment of Mps1, but not for its maintenance at the kinetochore. Mps1 might need to phosphorylate an upstream component at the kinetochore and thereby create the foundation for its own recruitment. If this step was already performed when an Mps1 kinase inhibitor is added, Mps1 might be recruited to the kinetochore later on via self-interaction.

Mps1 Interaction with Mad1

My results demonstrate that Mad1 and Mps1 can be found in complexes. Both major Mps1 domains are required for efficient interaction. Mad1 was shown previously to be an *in vitro* kinase substrate of Mps1, and since Mad1 is hyper-phosphorylated during mitosis and after **Mps1 o**ver-**e**xpression (Mps1 OE) (Hardwick et al., 1996), a physiological relevance of this phosphorylation for SAC activity has been suggested. I showed that kinetochore recruitment of Mad1 is dependent on Mps1 presence, which is in agreement with the proposed model, that Mps1 is required to recruit the Mad1-C-Mad2 dimer to the kinetochore. However, the recent literature on human Mps1 includes conflicting reports on this issue. While all reports agree on the fact that Mps1 is somewhat required for Mad1 recruitment (Abrieu et al., 2001; Hewitt et al., 2010; Jelluma et al., 2008b; Liu et al., 2003; Maciejowski et al., 2010; Martin-Lluesma et al., 2002; Santaguida et al., 2010; Sliedrecht et al., 2010; Tighe et al., 2008; Vigneron et al., 2004; Wong and Fang, 2006; Zhao and Chen, 2006), only some show a full requirement. These discrepancies might be explained primarily by the different inhibitors or cell lines used.

Furthermore, I showed that Mad1 kinetochore localization is impaired in the absence of Mad2, but not fully absent. This observation expands the model of linear SAC component recruitment, in which Mad1 is acting upstream of Mad2, and suggests that a certain portion of Mad1 can only be recruited to the kinetochore in dependency of Mad2, for example as dimer together with C-Mad2.

Finally and surprisingly, I find that EGFP-Mps1 kinetochore recruitment is reduced in the absence of Mad1 or Mad2. Previous reports did not find a requirement of Mad1 or Mad2 for Mps1 kinetochore localization (Stucke et al., 2004; Wong and Fang, 2006). However, these

findings were based on RNAi or antibody depletion, which might not have been sufficient to detect such partial effects. Very recent data on Mps1 kinetochore localization in *mad1* mutant *Drosophila* neuroblasts suggested the kinetochore recruitment of Mps1 to be independent of Mad1 (Emre et al., 2011). However, the kinetochore recruitment of EGFP-Mps1 was only studied qualitatively but not quantitatively there. Thus the data is not irreconcilable with my observations. My data suggests a complex interaction of the three SAC components in order to activate the SAC (Figure 30). However, the fact that Mad1 recruitment seems to be fully dependent on Mps1, while Mps1 is only partially dependent on Mad1 still places Mps1 upstream of Mad1 in *Drosophila* as well.

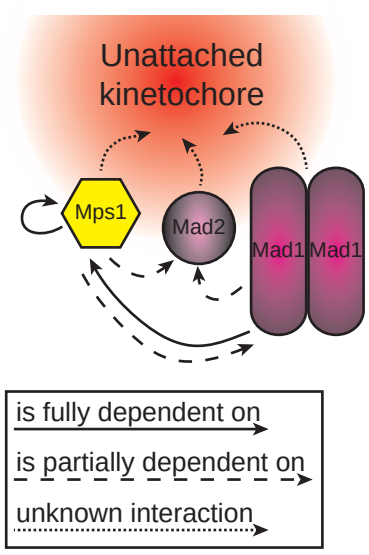

Figure 30. Localization dependencies of Mps1, Mad1, and Mad2. Schematic illustration of the model drawn from the observed localization dependencies of Mps1, Mad1 and Mad2 in *Drosophila*. While Mad1 was shown to be fully dependent on Mps1 and partially on Mad2, Mps1 was shown to be fully dependent on its own kinase activity and partially on both Mad1 and Mad2. Still, the interactions mediating recruitment of these SAC components to the unattached kinetochores are unknown.

Mis-Localization of Mps1 Interferes with Normal Exit from Mitosis

The dynamic localization behavior of Mps1 at kinetochores suggests a functional relevance for the SAC. Accordingly, shedding of Mps1 might be essential for SAC silencing. In this case, cells should be unable to proceed through M/A-transition when Mps1 cannot be shed from the kinetochores.

In fact, this prediction has very recently been verified in human cells (Jelluma et al., 2010).

In contrast, my results do not support this assumption. An Mps1 fusion protein, that includes the constitutive kinetochore localization domain of Cenp-C, remains detectable at the kinetochores throughout mitosis, but is not capable of dominantly arresting the cell in metaphase.

The inability of EGFP-Cenp-C(C)-Mps1 to induce a persistent metaphase arrest clearly does not rule out that Mps1 shedding from the kinetochore is required for SAC silencing. The Cenp-C(C) domain might not localize Mps1 to the correct kinetochore region. While the C-ter-

minal domain of Cenp-C was mapped to the inner kinetochore region at 22 nm distance from the centromeric Histone H3, Cenp-A/Cid, SAC components are thought to reside within the outer corona at > 60 nm from Cid (Schittenhelm et al., 2007, see Appendix 1). This substantial spatial distance might prevent the interaction of Mps1 with (some of) its crucial substrates or interaction partners. My effort to tether Mps1 at an outer and thus more natural place in the kinetochore was not successful and did not lead to evaluable results. The Nuf2 fusion protein did probably not provide a robust enough binding to the kinetochore and thus the localization disposition of Mps1 prevailed over Nuf2. The fusion with Mis12, which was successfully used in human cells (Jelluma et al., 2010), probably combines the two requirements, stable localization at the kinetochore as well as localization at the outer side of the kinetochore, although Mis12 (at 43 nm distance from Cid in *Drosophila* (Schittenhelm et al., 2007, see Appendix 1) probably does not bind Mps1 to the ideal natural place within the kinetochore, neither.

However, my experiments with EGFP-Cenp-C(C)-Mps1 clearly demonstrate the importance of correct Mps1 localization on mitotic progression. I observe an aberrant exit from mitosis without kinetochores being sufficiently pulled towards the poles. A dominant negative effect of the Cenp-C domain could be excluded, as well as interference during interphase (by expressing the fusion protein in *cdc25/string* mutants that are arrested in interphase 14—data not shown).

In fact, expression of a fusion protein of Mad1 with Cenp-B was reported recently to cause mis-alignment and mis-segregation in human cells (Maldonado and Kapoor, 2011). However, the dependency of this phenotype on Mps1 has not been addressed there. It might be interesting to see if this mitotic phenotype is due to effects on one (or several) canonical interaction partner(s) or substrate(s) or is caused by some ectopic influence as a result of the mis-localization.

I show that my observed phenotype does not correspond to an effect of Mps1 OE, since I found a different and earlier mitotic effect to be caused by Mps1 OE.

High Levels of Mps1 Interfere with Normal Exit from Mitosis

Mps1 OE leads to a metaphase delay. Superficially, this phenotype resembles observations in yeast (Hardwick et al., 1996). In yeast as well as in *Drosophila*, Mps1 OE causes a mitotic delay in the presence of a normal looking spindle. Prolonged presence of high Mps1 levels finally leads to adaptation and exit from mitosis via a rather normal anaphase. However, although the mitotic delay was not measured precisely in the case of Mps1 OE in yeast, it seems to be severe, leading an asynchronous culture to be completely arrested in mitosis. *Drosophila* embryonic cells, in contrast, exit from the arrest rather quickly. Anaphase

movements are in fact retarded, but still successful overall. Thus it is not surprising that some embryos survive this challenge and adult flies hatch.

It was suggested based on the experiments in yeast that the arrest is resulting exclusively from direct SAC activation by the over-expressed Mps1. This suggestion was supported by the observation that yeast cells over-expressing Mps1 in the *mad3*, *bub1*, *bub2*, and *bub3* mutant backgrounds do not die, but form viable colonies. The finding that Mps1 OE in *mad2* mutants is far more toxic is more difficult to reconcile with this suggestion. In my experiments with Mps1 OE in *mad2* mutant *Drosophila* embryos toxicity is even considerably stronger. In yeast this result was proposed to be due to effects on centrosome duplication. Moreover, my characterization of the mitotic defects observed during anaphase after Mps1 OE in *mad2* mutant embryos clearly demonstrate that Mps1 OE acts not just by SAC activation. I found an extremely abnormal exit from mitosis in *Drosophila* embryos when I followed the mitotic progression after Mps1 OE *in vivo*.

If the effect of Mps1 OE is not only caused by direct SAC activation—which other mitotic processes are affected in addition?

Based on the functional characterization of Mps1 in other systems, an over-activation of the error correction function of Mps1 appears to be the most attractive explanation. In human cells as well as in yeast, Mps1 has been shown to be involved in the correction of wrong kinetochore attachments (Jelluma et al., 2008b; Maure et al., 2007).

Therefore, Mps1 OE might destabilize not only incorrect but also correct attachments. Such an action should not only interfere with normal anaphase progression, but also with the velocity of kinetochore congression into the metaphase plate. However, I did not find any indications for unstable kinetochore attachments after Mps1 OE. The velocity of congression into the metaphase plate was normal, the tension between the sister kinetochores, as measured by the inter-sister kinetochore distance at the entry into the arrest, was undisturbed. Furthermore, the initial dynamics of BubR1 at kinetochores was similar to the undisturbed situation. Only few occasional kinetochores retained strong BubR1 signals. This cannot explain the complete failure of every chromosome movement during anaphase after Mps1 OE in *mad2* mutants.

Similarly, an effect of Mps1 OE on Dynein or Spindly regulation appears to be unlikely. Spindly was discovered in *Drosophila* as kinetochore Dynein recruitment factor. Its depletion leads to a metaphase delay in the presence of a functional mitotic spindle (Griffis et al., 2007). However, during this delay an accumulation of SAC components at the kinetochores was observed, due to impaired shedding. Furthermore, since Spindly is also involved in the establishment of stable end on attachments, its depletion was shown to cause a congression defect of kinetochores into the metaphase plate (Barisic et al., 2010; Griffis et al., 2007).

Based on my detailed characterization of the mitotic defects observed after Mps1 OE, it is tempting to speculate that Mps1 might in fact also inhibit the resolution of sister chromatid separation in a direct, SAC-independent manner. This could occur by a repressing influence on separase activity (either directly or indirectly for example by stabilizing securin (Figure 31)) interfering with efficient Cohesin cleavage at the onset of anaphase. To explain the nevertheless rather normal anaphases, “cohesion fatigue” is postulated to take place during the extended metaphase, caused by direct SAC activation by Mps1 OE in *mad2*$^{+}$ embryos. The term “cohesion fatigue” denotes the observation that sister chromatid cohesion gets increasingly weaker and sister chromatids can slowly separate without separase activation in the presence of prolonged pulling forces at the kinetochores within a functional mitotic spindle (Daum et al., 2009). This phenomenon has been suggested to be dependent on the prophase pathway (Waizenegger et al., 2000) of cohesin removal and the de-protection of Cohesin after shugoshin relocation at kinetochores that are under tension (Lee et al., 2008). However, a simple topologic mechanism might be considered as well. Assuming that Cohesin rings are opening and closing (‘breathing’) occasionally, applying tension at the centromeric DNA might prevent cohesive re-association of once opened Cohesin rings leading to a gradual loss of centromeric cohesion at stretched centromeres. In fact, reduced levels of centromeric Cohesin were observed after Mps OE compared to SAC induction by nocodazole in yeast (Eckert et al., 2007). However, the temporal dynamics of centromeric Cohesin levels was not studied in detail there.

When anaphase eventually starts in embryos over-expressing Mps1, a slower sister chromatid segregation occurs because residual cohesion might be removed inefficiently. According to the cohesion fatigue model, anaphase is expected to be more normal the longer the metaphase is delayed. Indeed, there is evidence in favor of this prediction:

First, in *mad2* mutants, anaphase is completely abnormal, since there is no time for cohesion fatigue. The force created by the mitotic spindle is not strong enough to overcome the full sister chromatid cohesion. Thus the model explains why anaphases are more successful after Mps1 OE in the presence of Mad2 function.

Secondly, I observed that the expression of fluorescently labeled marker proteins increases the survival rate after Mps1 OE. Intuitively, partially compromised spindle and kinetochore function induced by the fluorescent tags is expected to interfere with rather than to improve the success of mitosis. However, in the context of my suggestion it is conceivable that the slightly deleterious effects of the tags might contribute to SAC activation and thereby improve mitosis.

Third, the increased survival rate after over-expression of EGFP-Mps1 compared to untagged Mps1 might be explained by a longer arrest induced by (slightly) higher levels of Mps1 activity, which might ameliorate mitosis.

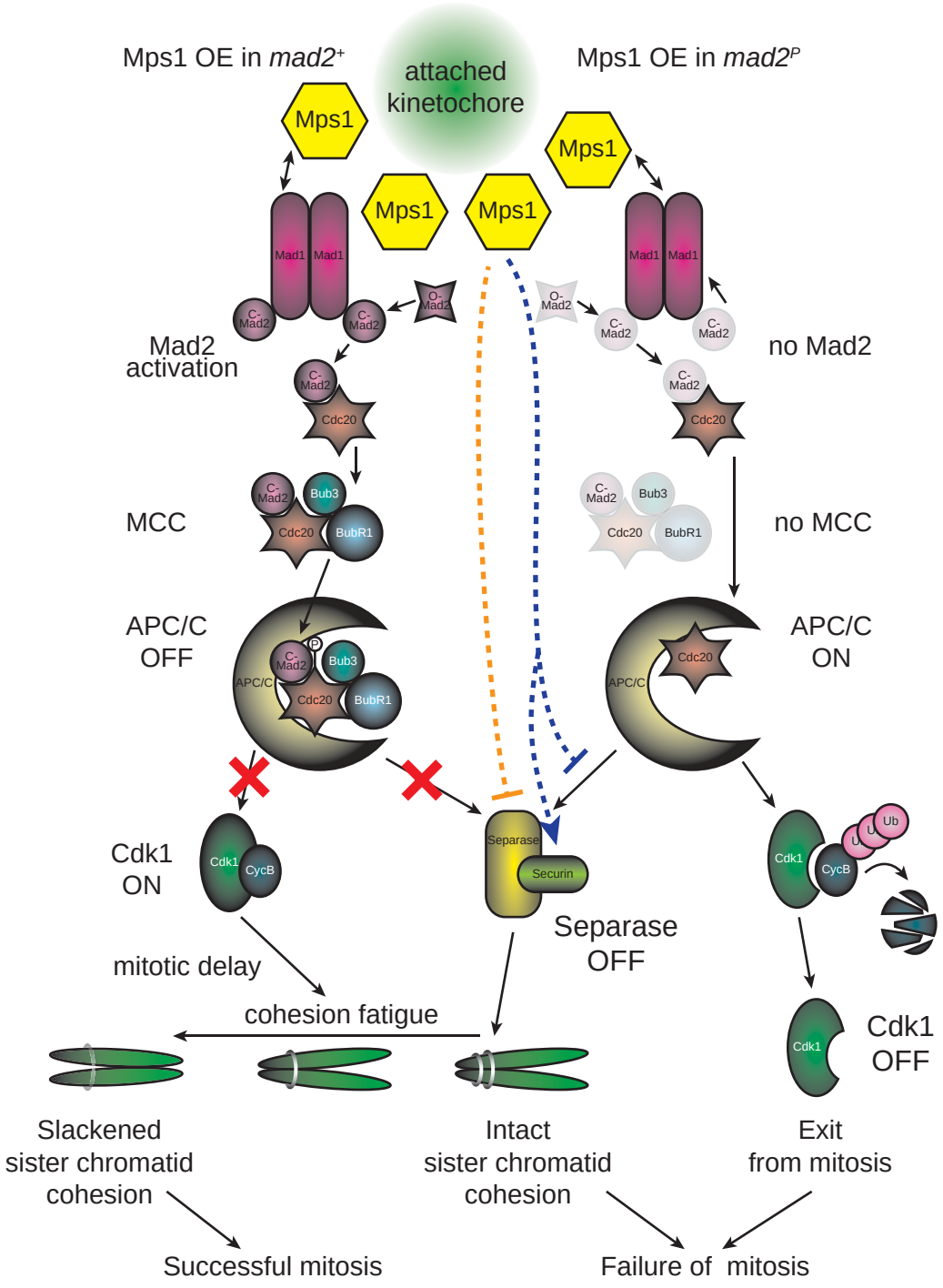

Figure 31. Model for the influence of Mps1 on sister chromatid cohesion.
Schematic illustration of the model drawn from the observed phenotypes at Mps1 OE in *Drosophila* embryos. The dashed arrows indicate that Mps1 is suggested to interfere with either Separase activation via the APC/C (blue arrow)—either by interfering with the APC/C effect on securin or by otherwise stabilizing securin—or it might directly inhibit separase activity on cohesin (orange arrow). The successful mitoses after Mps1 OE (*left*) are explained by cohesion fatigue during the prolonged mitosis. The highly aberrant mitoses at Mps1 OE in *mad2* mutants (*right*) are explained with an early mitotic exit without previous cohesion fatigue.

It will be interesting, although challenging, to test my model in various ways, for example by monitoring levels of chromatin bound cohesin during the arrest *in vivo* or by ectopic cohesin cleavage before mitotic exit. According to my suggestion, I would expect cohesin levels to decrease slowly during the arrest, and ectopic Cohesin cleavage should ameliorate the mitotic phenotype after Mps1 OE in the absence of Mad2.

Differences in SAC Activity in Cultured S2R+ Cells and Living Embryonic Tissue

The observation that Mps1 OE causes a transient metaphase delay raised the question whether it is terminated by adaptation or slippage, i.e. by an exit with silenced or active SAC. My observations by *in vivo* imaging of living embryos indicate that SAC silencing by adaptation takes place but not slippage. Especially the intensity curve of BubR1 levels at the kinetochores shows that before the exit from the arrest the majority of BubR1 has disappeared from the kinetochores just like in the wild type situation. In any case, the observed exit from mitosis is significantly different from the exit following a colchicine induced delay. In the absence of an intact spindle, the exit takes significantly longer than in its presence. After Mps1 OE the exit occurs without delay.

The phenotypes during SAC adaptation or slippage have been described extensively in human cell culture (Gascoigne and Taylor, 2008; Orth et al., 2008; Rieder and Maiato, 2004). Therefore, I considered a cell culture approach to be advantageous for a comparison.

Cultured embryonic *Drosophila* (S2R+) cells were observed to respond to the spindle poisons colchicine and taxol similar as human cells in culture. In response to Mps1 OE S2R+ cells display a much stronger retarded mitosis and a clearly more abnormal exit from mitosis than I described in embryos. This exit resembles the one described after colchicine incubation, which argues for SAC slippage.

My observations caution against an uncritical extrapolation of results concerning SAC function in cell culture to a living organism. The SAC in cultured cells might react in a different way than in cells within the organism.

Mps1 inhibitors, which were proposed as cancer therapeutics will therefore also have to be evaluated carefully. Up to now, one case has been described, in which an Mps1 inhibitor was effective in decreasing tumor size *in vivo* (Colombo et al., 2011). Extensive experimental work in patients will tell whether the optimistic expectations for Mps1 as cancer therapy target are justified.

Materials and methods

Fly Strains and Genetics

Fly Stocks

The following fly stocks have been described before and are available at the Bloomington *Drosophila* Stock Center at Indiana University except when otherwise indicated:
The driver lines *w⁻; P{w⁺, matα4tub-GAL4-VP16}V2H* (= *mat-GAL4*) (Hacker and Perrimon, 1998), and *ry^{506}, P{ry⁺, 2xsev-Hs-GAL4}332.5* (= *Hs-GAL4*) (Ruberte et al., 1995), the stock *w⁻; stg^{7B}, P{w⁺, Hs-stg}* allowing a synchronization of mitosis 14 by heat shock (Figure 1) (Edgar and O'Farrell, 1990), the following mutant alleles: *w⁻; P{FRT(w^{hs})}2A, P{neoFRT}82B, Mps1Bac{3xP3-EYFP, p-Gal4D-K10}715/ TM3, Sb, P{w⁺, Ubx-lacZ}* (= *Mps1^{1}/ TM3*) (Fischer et al., 2004), *w⁻; P{neoFRT}82B, ald^{B4}/ TM6* (= *Mps1^{aldB4}/ TM6*) (Page et al., 2007) (kindly provided by William D. Gilliland, DePaul University, Chicago, USA), *yw⁻; dp, mad1^{1}/ CyO, y⁺, dp* (Emre et al., 2011) and *w⁻; P{EP}mad2^{G6595}* (= *mad2^{P}*) (Buffin et al., 2007) (both kindly provided by Roger E. Karess, Institut Jaques Monod, Université Paris Diderot, Paris, France), *w⁻; Df(2R)w45-30n, cn^{1}/ CyO* (= *Df(mad1)/ CyO*) (Konev et al., 1991), and the following transgene insertions expressing fluorescently labeled proteins under control of their respective genomic cis-regulatory regions: *w⁻; P{w⁺, gEGFP-Mps1} II.1, II.2* (= *gEGFP-Mps1 II.1, II.2*) and *w⁻; P{w⁺, gEGFP-Mps1} III.1* (= *gEGFP-Mps1 III.1*) and *w⁻; P{w⁺, gEGFP-Mps1} III.4* (= *gEGFP-Mps1 III.4*) (Fischer et al., 2004), *w⁻; P{w⁺, GFP-BubR1} X* (= *GFP-BubR1*) (Buffin et al., 2005) and y*w⁻; P{w⁺, mad1-GFP} X* (= *mad1-GFP*) and *w⁻; P{w⁺, mCherry-mad1} II; MKRS/ TM6* (= *mCherry-mad1*) (Emre et al., 2011) (all three kindly provided by Roger E. Karess, Institut Jaques Monod, Université Paris Diderot, Paris, France), *P{Ubi-GFP.nls} 3L1, P{Ubi-GFP.nls} 3L2, P{FRT(w^{hs})}2A* (= *Ubi-GFP*) (Luschnig et al., 2004), *w⁻; P{PTT-GA}Jupiter^{G00147}* (= *Jupiter-GFP*) (Morin et al., 2001), *w⁻; P{w⁺, His2Av-mRFP1} II.2* (= *His2Av-mRFP*) (Schuh et al., 2007), *w⁻; P{w⁺, Cid-GFP} II.1* (= *Cid-GFP*) (Schuh et al., 2007). *w^{1}* flies were used as wild type control stock.

Lines with the transgene insertions
w⁻; P{w⁺, gEGFP-Mps1(kd)} II.3 and *III.1* (= *gEGFP-Mps1(kd) II.3* and *III.1*)
w⁻; P{w⁺, gEGFP-Mps1(N)} II.2 and *III.1* (= *gEGFP-Mps1(N) II.2* and *III.1*)
w⁻; P{w⁺, gEGFP-Mps1(C)} II.3 and *II.4* and *III.1* (= *gEGFP-Mps1(C) II.3* and *II.4* and *III.1*)
w⁻; P{w⁺, UAS-EGFP-STOP} II.1 (= *UAS-EGFP*)
w⁻; P{w⁺, UAS-Mps1} II.4 (= *UAS-Mps1*)
w⁻; P{w⁺, UAS-EGFP-Mps1} II.1 and *III.1* (= *UAS-EGFP-Mps1 II.1* and *III.1*)

w⁻; P{w⁺, UAS-EGFP-Mps1(kd)} II.1 and *III.1* and *III.2* (= *UAS-EGFP-Mps1(kd) II.1* and *III.1* and *III.2*)
w⁻; P{w⁺, UAS-EGFP-bub1} II.1 and *III.1*
w⁻; P{w⁺, UAS-EGFP-bubR1} II.1 and *III.1*
w⁻; P{w⁺, UAS-EGFP-mad2} II.1 and *III.1*
w⁻; P{w⁺, UAS-myc$_{10}$-Mps1} II.6 (= *UAS-myc-Mps1*)
w⁻; P{w⁺, UAS-myc$_{10}$-Mps1(kd)} III.1 (= *UAS-myc-Mps1(kd)*)
w⁻; P{w⁺, UAS-EGFP-Cenp-C(C)-Mps1} II.1
w⁻; P{w⁺, UAS-EGFP-Cenp-C(C)-Mps1(kd)} II.1
w⁻; P{w⁺, UAS-EGFP-Mps1-Nuf2} II.1
w⁻; P{w⁺, UAS-Torso(EC/TM)-EGFP-Mps1} II.1 and *II.2* and *III1* and *III.2* and *III.7*
w⁻; P{w⁺, UAS-EGFP-Cenp-C(C)-bubR1} II.1
w⁻; P{w⁺, gi2xtdTom-Cenp-C} II.3 (= *2xtdTom-Cenp-C*)
were obtained after P element-mediated germline transformation of *w¹* flies with the constructs described below.
For the studies on EGFP-Mps1 variants in the wild type background (mitotic shift, Figure 3B – D and localization, Figure 5, except for gEGFP-Mps1(C), see below) the respective insertions on the second chromosome were used.

To increase expression levels, the following combinations of different insertions of the same transgenes were created by meiotic recombination:

For localization studies of EGFP-Mps1(C) (Figure 5):
gEGFP-Mps1(C) II.3, II.4 (= *gEGFP-Mps1(C) II.3, II.4*)

For evaluation of the dependency of the Mps1 OE on Mps1 kinase activity (Figure 16):
UAS-EGFP-Mps1(kd) III.1, III.2

For further crossing (see below):
w⁻; P{w⁺, UAS-Torso(EC/TM)-EGFP-Mps1} II.1, *II.2/ CyO* and *III1*, *III.2*, *III.7*

The following combinations of different transgenes were created by meiotic recombination:

For self-interaction studies of Mps1(kd) (Figure 9):
UAS-myc-Mps1(kd), UAS-EGFP-Mps1 III.1
UAS-myc-Mps1(kd), UAS-EGFP-Mps1(kd) III.1

For *in vivo* imaging and further crossing (see below):
w⁻; mat-GAL4, His2Av-mRFP, Cid-GFP/ CyO
w⁻; mat-GAL4, 2xtdTom-Cenp-C
w⁻; Jupiter-GFP, mad2^{P}

The following fly stocks were created by standard crossing schemes:

For studies of Mps1 variants in Mps1 germline clones (Figure 3E, 7 and 8) and rescue experiments (Figure 10):

gEGFP-Mps1 II.1, II.2/ CyO; Mps1^{aldB4}

gEGFP-Mps1(kd) II.3; Mps1^{aldB4}/ TM6

gEGFP-Mps1(N) II.2; Mps1^{aldB4}/ TM6

gEGFP-Mps1(C) II.3, II.4; Mps1^{aldB4}/ TM6

For self-interaction studies of Mps1(kd) (Figure 9):

UAS-myc-Mps1; UAS-EGFP-Mps1 III.1

UAS-myc-Mps1; UAS-EGFP-Mps1(kd) III.1

UAS-EGFP; UAS-myc-Mps1(kd)

For interaction studies of Mps1 variants with Mad1 (Figure 11C):

mCherry-mad1; gEGFP-Mps1 III.1

mCherry-mad1; gEGFP-Mps1(kd) III.1

mCherry-mad1; gEGFP-Mps1(N) III.1

mCherry-mad1; gEGFP-Mps1(C) III.1

mCherry-mad1; Ubi-GFP

For localization dependency studies of Mps1, Mad1 and Mad2 (Figure 12 and 13):

mad1-GFP; Mps1^{aldB4}/ TM6

mad1-GFP; mad2^{P}

mad1^{1}/ CyO; gEGFP-Mps1 III.1

mad1^{1}/ CyO; gEGFP-Mps1 III.4

Df(mad1)/ CyO; gEGFP-Mps1 III.1

Df(mad1)/ CyO; gEGFP-Mps1 III.4

gEGFP-Mps1 II.1, II.2; mad2^{P}

For phenotypic characterization of the effects of Mps1 mis-localization (Figure 15):

w^{-}; P{w^{+}, UAS-Torso(EC/TM)-EGFP-Mps1} II.1, II.2/ CyO; III.1, III.2, III.7

For *in vivo* imaging (Figure 17, 18, 20 – 25):

w^{-}; mat-GAL4, His2Av-mRFP, Cid-GFP/ CyO; mad2^{P}

w^{-}; mat-GAL4, 2xtdTom-Cenp-C/ CyO; Jupiter-GFP

w^{-}; mat-GAL4, 2xtdTom-Cenp-C/ CyO; Jupiter-GFP, mad2^{P}

UAS-Mps1; mad2^{P}

UAS-EGFP-Mps1 II.1; mad2^{P} (only for survival assays, Figure 18)

GFP-BubR1; mat-GAL4, His2Av-mRFP/ CyO

Mps1 Germline Clones

Females with *Mps1^{aldB4}* germline clones were created using the stock *P{hsFLP}22, yw;*

P{neoFRT}82B, P{ovoD1-18}3R/ TM3, Sb (Chou and Perrimon, 1996) as described before (Fischer et al., 2004).

Rescue of homozygous *Mps1* mutants with genomic transgenes

Mps1^{aldB4}/ TM6 mutant females carrying the respective *EGFP*-fused *Mps1* transgene under control of the endogenous cis-regulatory region homozygously were crossed with *Mps1^{1}/ TM3* mutant males. The number of adult progeny from these crosses was counted, and *Mps1* mutants and heterozygous *Mps1* flies were identified based on the phenotypes of the balancer chromosomes. By normalizing the number of homozygous *Mps1* mutant progeny with the number of heterozygous siblings, the rescue efficiency of the individual transgenes was calculated. This number was compared to the rescue efficiency of *gEGFP-Mps1(FL) II.1, II.2*.

Survival Assay after Embryonic Over-Expression of Mps1

Females providing their eggs with a maternal contribution of Gal4 protein (*mat-GAL4*) were crossed with males contributing the *UAS*-transgene to half of their progeny (*UAS-Mps1 II.4/ CyO* or *UAS-EGFP-Mps1 II.1/ CyO*, respectively). The number of adult progeny from these crosses was counted and classified as “over-expressing” (with *UAS*-transgene) or “not expressing” (without *UAS*-transgene, *CyO*). By correlating the two numbers and normalizing to the progeny from a cross without presence of any *UAS*-transgene the survival rate was calculated. The survival rate in the *mad2* mutant situation was addressed using *mat-GAL4; mad2^{P}* females and *UAS; mad2^{P}* males analogously.

Plasmid Constructions

pCaSpeR4-EGFP-Mps1(kd):

Construct for expression of a kinase dead Mps1 version N-terminally tagged with EGFP under control of the cis-regulatory region of *Mps1*.

pCaSpeR-EGFP-Mps1 (Fischer et al., 2004) was cut with NotI and Asp718. The resulting EGFP-Mps1 fragment was transposed into the two corresponding sites of pBluescriptIIKS(-). The resulting cloning intermediate 1 was *pBluescript-EGFP-Mps1*. The point mutation A1778C in the *Mps1* coding sequence leading to the amino acid exchange Asp478 to Ala (D478A) and thereby abolishing kinase activity of Mps1 was introduced into cloning intermediate 1 using the QuikChangeII site-directed mutagenesis kit (Stratagene) and the primers AF5 (GTTGATCG***C***TTTTGGCATAGCCAG) and AF6 (GCTATGCCAAAA***G***CGATCAACTTC). This step resulted in cloning intermediate 2: *pBluescript-EGFP-Mps1(kd)*. After digestion of cloning intermediate 2 and *pCaSpeR-EGFP-Mps1* with BglII, the fragment from *pCaSpeR-EGFP-Mps1* was replaced by

the fragment from cloning intermediate 2 resulting in *pCaSpeR-EGFP-Mps1(kd)*.

pCaSpeR4-EGFP-Mps1(N):

Construct for expression of the N-terminal domain of Mps1 (aa 1 - 332) N-terminally tagged with EGFP under control of the cis-regulatory region of *Mps1*.

Inverse PCR was performed with cloning intermediate 1 as template using the primers AF1 (ATT***CTCGAG***TTTTAAAATATTAGATGTCTTGTG) and AF2 (AAC***CTCGAGTAA***GCACGAAAGCTCAGCTA), which introduced an XhoI site instead of the sequence of *Mps1(C)*. Cutting of the product with XhoI and ligating resulted in cloning intermediate 3: *pBluescript-EGFP-Mps1(N)*. Cloning intermediate 3 was digested with NotI and Asp718, and the excised fragment containing the *EGFP-Mps1(N)* sequence was transposed into the two corresponding sites in *pCaSpeR4* resulting in *pCaSpeR4-EGFP-Mps1(N)*.

pCaSpeR4-EGFP-Mps1(C):

Construct for expression of the C-terminal domain of Mps1 (aa 325 - 630) N-terminally tagged with EGFP under control of the cis-regulatory region of *Mps1*.

Inverse PCR was performed with cloning intermediate 1 as template using the primers AF3 (TCCC***CCATGG***CATCTAATATTTTAAAAATCAAGAA) and AF4 (CGGGGCACAGGCGTGG), which introduced an NcoI site instead of the sequence of *Mps1(N)*. Cutting of the product with NcoI and ligating resulted in cloning intermediate 4: *pBluescript-EGFP-Mps1(C)*. Cloning intermediate 4 was digested with NotI and Asp718, and the excised fragment containing the *EGFP-Mps1(C)* sequence was transposed into the two corresponding sites in *pCaSpeR4* resulting in *pCaSpeR4-EGFP-Mps1(C)*.

pUAST-EGFP-Mps1 and *pUAST-EGFP-Mps1(kd)*:

Constructs for ectopic expression of wild type or kinase dead Mps1 N-terminally tagged with EGFP by the Gal4/UAS system.

EGFP was amplified from *pUAST-EGFP-Cenp-C(C)* (Heeger et al., 2005) using the primers AF9 (GGGAATTGGGAATTCGTTAAC) and AF10 (GGATTTCTG***GCGGCCGC***CTTGTACAGCTCGTCCATG), which introduced a flanking NotI site. After digestion with BglII and NotI, the PCR fragment was transposed into the two corresponding sites in *pUAST* resulting in cloning intermediate 5: *pUAST-EGFPΔTAA*.

The *Mps1* and *Mps1(kd)* sequences were amplified from *pCaSpeR4-EGFP-Mps1* using the primers AF12 (GAATAAATCG***GCGGCCGC***GATGACCACGCCTGTGCC) and AF13 (TT***GGTACC***TTAATTGCTGTTGGCGGTTC), which introduced flanking NotI or Asp718 sites respectively. After digestion with NotI and Asp718, the PCR fragment was transposed into the two corresponding sites in cloning intermediate 5 resulting in *pUAST-EGFP-Mps1* and *pUAST-EGFP-Mps1(kd)*.

pUAST-EGFP-Mps1(N):

Construct for ectopic expression of the N-terminal domain of Mps1 (aa 1 - 332) N-terminally tagged with EGFP by the Gal4/UAS system.

The *Mps1(N)* sequence was amplified from the EST plasmid *LD04521* (Rubin et al., 2000) using the primers AF12 (GAATAAATCG***GCGGCCGC***GATGACCACGCCTGTGCC) and AF39 (GTATA***GGTACC***T-TACTTGATTTTTAAAATATTAGATGTC), which introduced a flanking NotI or Asp718 site, respectively. After digestion with NotI and Asp718, the PCR fragment was transposed into the two corresponding sites in *pUAST-EGFP-MCS* (Schittenhelm et al., 2007, see Appendix 1) resulting in *pUAST-EGFP-Mps1(N)*.

pUAST-EGFP-Mps1(C):

Construct for ectopic expression of the C-terminal domain of Mps1 (aa 325 - 630) N-terminally tagged with EGFP by the Gal4/UAS system.

The *Mps1(C)* sequence was amplified from the EST plasmid *LD04521* (Rubin et al., 2000) using the primers AF13 (TT***GGTACC***TTAATTGCTGTTGGCGGTTC) and AF40 (CTCCAGAGCAG***GCGGCCGC-***CAAGACATCTAATATTTTAAAAATC), which introduced a flanking NotI or Asp718 site, respectively. After digestion with NotI and Asp718, the PCR fragment was transposed into the two corresponding sites in *pUAST-EGFP-MCS* (Schittenhelm et al., 2007, see Appendix 1) resulting in *pUAST-EGFP-Mps1(C)*.

pUAST-EGFP-Mps1(Ckd):

Construct for ectopic expression of the kinase dead C-terminal domain of Mps1 (aa 325 - 630) N-terminally tagged with EGFP by the Gal4/UAS system.

The point mutation A1778C was introduced into the EST plasmid *LD04521* (Rubin et al., 2000) using the QuikChangeII site-directed mutagenesis kit (Stratagene) and the primers AF5 (GTTGATCG***C***TTTTGGCATAGCCAG) and AF6 (GCTATGCCAAAA***G***CGATCAACTTC). This step resulted in cloning intermediate 6: *LD04521-Mps1(kd)*.

The *Mps1(Ckd)* sequence was amplified from cloning intermediate 6 using the primers AF13 (TT***GGTACC***TTAATTGCTGTTGGCGGTTC) and AF40 (CTCCAGAGCAG***GCGGCCGC***CAAGACATCTAATATTTTAAAAATC), which introduced a flanking NotI or Asp718 site, respectively. After digestion with NotI and Asp718, the PCR fragment was transposed into the two corresponding sites in *pUAST-EGFP-MCS* (Schittenhelm et al., 2007, see Appendix 1) resulting in *pUAST-EGFP-Mps1(Ckd)*.

pUAST-EGFP-bub1:

Construct for ectopic expression of Bub1 N-terminally tagged with EGFP by the Gal4/UAS system.

The *bub1* sequence was amplified from the EST plasmid *LD22858* (Rubin et al., 2000) using

the primers CS6 (CGCGTC***GGTACC***AGATGGCCATGCACTCGTA) and CS7 (GAATA***TCTAGA***TTATCGTCGATGCAGGATGT), which introduced a flanking Asp718 or XbaI site, respectively. After digestion with Asp718 and XbaI, the PCR fragment was transposed into the two corresponding sites in *pUAST-EGFP-MCS* (Schittenhelm et al., 2007, see Appendix 1) resulting in *pUAST-EGFP-bub1*.

pUAST-EGFP-mad2:

Construct for ectopic expression of Mad2 N-terminally tagged with EGFP by the Gal4/UAS system.

The *mad2* sequence was amplified from genomic *Drosophila melanogaster* DNA using the primers RaS232 (CGACT***GCGGCCGC***AATGTCAACTGCCCAGGCG) and RaS233 (GGTAC***GGTACC***TTAAGTGCTCATCTTGTAGTTG), which introduced a flanking NotI or Acc65I site, respectively. After digestion with NotI and Acc65I, the PCR fragment was transposed into the two corresponding sites in *pUAST-EGFP-MCS* (Schittenhelm et al., 2007, see Appendix 1) resulting in *pUAST-EGFP-mad2*.

pUAST-EGFP-STOP:

Construct for ectopic expression of EGFP by the Gal4/UAS system. This plasmid was designed to serve as control plasmid for the expression effects of EGFP-BubR1.

The *bubR1* sequence was amplified from the EST plasmid *LD23835* (Stapleton et al., 2002) using the primers CS8 (TTGAG***GCGGCCGC***T**ATG**GACTTT**TGA**CAATGCGAA) and CS9 (CAAGA***CTCGAG***CTATTTCTGCAATATCGTGTTAA), which introduced a TGA stop-codon by a frameshift directly after the start codon of the *BubR1* sequence and a flanking NotI or XhoI site, respectively. After digestion with NotI and XhoI, the PCR fragment was inserted into the two corresponding sites in *pUAST-EGFP-MCS* (Schittenhelm et al., 2007, see Appendix 1) resulting in *pUAST-EGFP-STOP*.

pUAST-EGFP-bubR1:

Construct for ectopic expression of BubR1 N-terminally tagged with EGFP by the Gal4/UAS system.

pUAST-EGFP-STOP was digested with NotI, and a primer hybrid of CS22 (GGCCCGCCCTCGAGCAATCG) and CS23 (GGCCCGATTGCTCGAGGGCG) was ligated in order to reverse the frameshift causing the premature stop in *pUAST-EGFP-STOP*. This resulted in *pUAST-EGFP-bubR1*.

pUAST-Mps1 and *pUAST-Mps1(kd)*:

Constructs for ectopic expression of wild type or kinase dead Mps1 by the Gal4/UAS system. *pUAST-EGFP-Mps1* and *pUAST-EGFP-Mps1(kd)* were digested with Acc65I and NotI, and

the resulting fragments containing the *Mps1* and *Mps1(kd)* sequences were transposed into the respective sites in *pUAST*, resulting in *pUAST-Mps1* and *pUAST-Mps1(kd)*.

pUAST-myc$_{10}$-Mps1 and *pUAST-myc$_{10}$-Mps1(kd)*:

Constructs for ectopic expression of wild type or kinase dead Mps1, N-terminally tagged with 10xmyc, by the Gal4/UAS system.

myc$_{10}$ was amplified from *pCaSpeR4-myc$_{10}$-Nuf2* (Schittenhelm et al., 2007, see Appendix 1) using the primers AF56 (TCTGGATT***GCGGCCGC***ATGGGCGGCGCCCATG) and AF57 (ATATCGCC***GCGGCCGC***-GCCTGGGTTTTCGAATGCC), which introduced flanking NotI sites. After digestion with NotI, the PCR fragment was transposed into the NotI site in *pUAST-Mps1* or *pUAST-Mps1(kd)*, respectively, resulting in *pUAST-myc$_{10}$-Mps1* and *pUAST-myc$_{10}$-Mps1(kd)*.

pUAST-EGFP-Cenp-C(C)-Mps1 and *pUAST-EGFP-Cenp-C(C)-Mps1(kd)*:

Constructs for ectopic expression of fusion proteins of wild type or kinase dead Mps1 with the C-terminal domain of Cenp-C, N-terminally tagged with EGFP, by the Gal4/UAS system.

EGFP-Cenp-C(C) was amplified without stop codon of Cenp-C from *pUAST-EGFP-Cenp-C(C)* (Heeger et al., 2005) using the primers AF9 (GGGAATTGGGAATTCGTTAAC) and AF11 (CAAA-GATCCT***GCGGCCGC***ACTGCGTATACACATCAGCA), which introduced a flanking NotI site. After digestion with BglII and NotI, the PCR fragment was transposed into the two corresponding sites in *pUAST* resulting in cloning intermediate 7: *pUAST-EGFP-CenpC(C)*Δ*TAG*.

The *Mps1* sequence was amplified from *pCaSpeR4-EGFP-gMps1* (Fischer et al., 2004) and the *Mps1(kd)* sequence was amplified from *pCaSpeR4-EGFP-gMps1(kd)* with AF12 (GAATA-AATCG***GCGGCCGC***GATGACCACGCCTGTGCC) and AF13 (TT***GGTACC***TTAATTGCTGTTGGCGGTTC), which introduced a flanking NotI or KpnI site, respectively. After digestion with NotI and KpnI, the PCR fragments were transposed into the two corresponding sites in cloning intermediate 7 resulting in *pUAST-EGFP-Cenp-C(C)-Mps1* and *pUAST-EGFP-Cenp-C(C)-Mps1(kd)*.

pUAST-Mps1-Nuf2:

Construct for ectopic expression of a fusion protein of Mps1 with Nuf2, N-terminally tagged with EGFP, by the Gal4/UAS system.

The *Mps1* sequence was amplified using the primers RaS27 (TCGTGACCGCCGCCGGG) and CS13 (GCTTT***GCGGCCGC***ATTGCTGTTGGCGGTTCTGC), which introduced a flanking NotI site. After digestion with NotI, the PCR fragment was transposed into the corresponding site in *pUAST-Nuf2* (Schittenhelm et al., 2007, see Appendix 1) resulting in *pUAST-Mps1-Nuf2*.

pUAST-Torso(EC/TM)-EGFP-Mps1:

Construct for ectopic expression of a fusion protein of Mps1 with the **e**xtra**c**ellular and **t**rans-**m**embrane domain (EC/TM) of Torso receptor tyrosine kinase, internally tagged with EGFP, by the Gal4/UAS system.

The *EGFP-Mps1* sequence was amplified from *pUAST-EGFP-Mps1* using the primers AF42 (CCTCCTGGGTCA***CCATGG***TGAGCAAGGGCGAGG) and AF43 (AGCTG***GCTAGC***TATCTTATAAGTAAACGCAAATTA), which introduced a flanking NheI or Eco91I site, respectively. After digestion with NheI and Eco91I, the PCR fragment was transposed into the corresponding sites in *pUAST-Torso-HA-CycA* (Dienemann and Sprenger, 2004) to replace the *HA-CycA* sequence resulting in *pUAST-Torso-EGFP-Mps1*.

pUAST-Cenp-C(C)-bubR1:

Construct for ectopic expression of a fusion protein of BubR1 with the C-terminal domain of Cenp-C, N-terminally tagged with EGFP, by the Gal4/UAS system.

pUAST-EGFP-Cenp-C(C)-Mps1 was digested with EcoRI and NotI and the resulting EGFP-Cenp-C(C) fragment was transposed into the corresponding sites in *pUAST* resulting in cloning intermediate 8: *pUAST-EGFP-Cenp-C(C)-MCS*.

The *bubR1* sequence was amplified as described for *pUAST-EGFP-STOP*. After digestion with NotI and XhoI, the PCR fragment was inserted into the two corresponding sites in cloning intermediate 8 resulting in cloning intermediate 9: *pUAST-EGFP-Cenp-C(C)-STOP*.

Cloning intermediate 9 was digested with NotI, and a primer hybrid of CS22 (GGCCCGCCCTC-GAGCAATCG) and CS23 (GGCCCGATTGCTCGAGGGCG) was ligated in order to reverse the frameshift causing the premature stop in *pUAST-EGFP-Cenp-C(C)-STOP*. This resulted in *pUAST-EGFP-Cenp-C(C)-bubR1*.

pMT-EGFP:

Construct for ectopic expression of EGFP under control of the metallothionein promoter, which can be induced by copper ions, in S2R+ cells.

The *EGFP* sequence was cloned between the NcoI and the PstI site of *pRmHa-1* (Bunch et al., 1988).

pMT-EGFP-Mps1 and *pMT-EGFP-Mps1(kd)*:

Constructs for ectopic expression of wild type or kinase dead Mps1, N-terminally tagged with EGFP, under control of the metallothionein promoter, which can be induced by copper ions, in S2R+ cells.

pUAST-EGFP-Mps1 and *pUAST-EGFP-Mps1(kd)* were cut with XhoI and Acc65I, and the excised fragments containing the *EGFP-Mps1* and *EGFP-Mps1(kd)* sequences were trans-

posed into the two corresponding sites in *pRmHA-RW2* (a *pRmHA-3* (Bunch et al., 1988) derivative, in which the polyadenylation signal from the *ADH* gene was replaced by a more convenient multiple cloning site and the SV40 polyadenylation signal) resulting in *pMT-EGFP-Mps1* and *pMT-EGFP-Mps1(kd)*.

pCaSpeR4-i2xtdTom-Cenp-C:

Construct for the expression of Cenp-C internally tagged with 2xtdTom under control of its cis-regulatory region.

The *tdTom* (*tandemTomato*) sequence was amplified twice from *pRSET-B-tdTom* (Shaner et al., 2004) first using the primers SN1 (GGG***GGTACC***TGGTGAGCAAGGGCGAGG) and SN3 (AGCCGC-***GCTAGC***CTTGTACAGCTCGTCCATGC), which introduced a flanking Acc65I or NheI site, respectively, and second using the primers SN4 (ATTGGG***GCTAGC***GTGAGCAAGGGCGAGGAG) and SN5 (CGC***GGATC-C***GGTACCACTTGTACAGCTCGTCCATG), which introduced a flanking NheI or BamHI site, respectively. After digestion of the first PCR product with Acc65I and NheI, the fragment was transposed into the corresponding sites in *pSLfa1180fa* (Horn and Wimmer, 2000) resulting in cloning intermediate 10: *pSL-tdTom*. After digestion of the second PCR product with NheI and BamHI the fragment was transposed into the corresponding sites in cloning intermediate 10 resulting in cloning intermediate 11: *pSL-2xtdTom*.

The *2xtdTom* sequence was excised from cloning intermediate 11 with Acc65I, and the fragment was transposed into the BsiWI site in *pCaSpeR4-Cenp-C* (Heeger et al., 2005) resulting in *pCaSpeR4-i2xtdTom-Cenp-C*.

In vivo Imaging and Immuno-Fluorescence Microscopy

Embryo Collection

Embryos were collected on apple juice agar plates as described previously (Pandey et al., 2005). Collection time and aging at 25°C was dependent on the experimental question: To retrieve embryos in the syncytial blastoderm stage, 1 h collection was followed by 1 h of aging; for embryos in mitosis 14, 1 h collection was followed by 3 h of aging. To retrieve more embryos for biochemical studies the collection time was increased to up to 3 h.

In vivo Imaging of Embryos

Embryos were aligned and immobilized on glass slides as described before (Pandey et al., 2005). When indicated, spindle poison injections were done using a FemtoJet microinjection setup (Eppendorf). Assuming that 2% v/v of the embryo will be replaced by the spindle poison solution (Basto et al., 2004), I injected 5 µM to 75 µM taxol or 1 mM colchicine in Schneider's

medium, respectively. Imaging was performed on a Zeiss CellObserver HS equipped with a COLIBRI light source with a 470 nm (GFP) and a 555 nm (Tom/mRFP) light emitting diode using a 63x/1.4 oil immersion objective or a 20x/0.5 objective. Depending on the experimental question, time intervals and number and distance of z-planes were adjusted. For high speed *in vivo* imaging at a time interval of 5 s 10 z-planes with 500 nm spacing were acquired.

In vivo Imaging of S2R+ Cells

100'000 S2R+ cells were seeded in 24-well lumox black gas permeable plates (Greiner Bio-one), cultured for one day before starting the imaging or transfection procedure, respectively. Spindle poisons were added, if required, in Schneider's medium (Gibco) at a concentration of 13.3 µM for colchicine (Sigma) and 500 nM for taxol (Sigma). If required, cells were transfected with pMT derived plasmids using FuGENE HD transfection reagent (Roche) according to manufactorer's instructions. Induction of the metallothionein promoter activity was done by adding 1 mM $CuSO_4$ to the medium two days later. Imaging was performed on a Zeiss CellObserver HS using a 20x/0.5 objective with DIC. 3 z-planes were acquired at a distance of 2.5 µm and at a time interval of 3 min.

Evaluation of *in vivo* Imaging Movies

Movies acquired from *in vivo* imaging were handled, processed and evaluated using AxioVision (Zeiss) (for acquisition, ROI definition, systematic storage), Huygens Remote Manager, v.1.2.3 (Ponti et al., 2007) (for deconvolution), Imaris (Bitplane Scientific Software) (for movie processing and evaluation of aspects concerning time and space), VirtualDub (at http://www.virtualdub.org/) (for movie compression), ImageJ (at http://rsbweb.nih.gov/ij/index.html) (for evaluation and measurement of aspects concerning time and space and automatized image processing), Photoshop (Adobe) (for stills processing), Excel (Microsoft) (for statistic evaluation and plotting), and the statistics to use website (Kirkman, 1996) (at www.physics.csbsju.edu/stats/) (for T-tests and boxplots).

Fixation, Staining and Mounting of *Drosophila* Embryos

Embryos were dechorionized for 2 min in 7% NaOCl. If required, spindle poisons (10 µM colchicine (Sigma), 730 nM taxol (Sigma)) were applied in a 1:1 mixture of heptane and Schneider's medium (Gibco) for 20 min before fixation. For MeOH fixation embryos were fixed for 1 min with a 1:1 mixture of heptane and methanol. For **p**ara**f**orm**a**ldehyde (PFA) fixation embryos were fixed for 20 min with a 1:1 mixture of heptane and 4% PFA in **p**hosphate **b**uffered **s**aline (PBS: 140 mM NaCl, 2.6 mM KCl, 1.47 mM KH_2PO_4, 6.3 mM Na_2HPO_4, pH7.4). Afterwards the vitelline membrane was removed by shaking 1 min. with a 1:1 mixture of heptane and 90% methanol/50 mM EGTA.

DNA was stained with Hoechst 33258 at 1 µg/ml in PBS.
Embryos were mounted in 70% glycerol, 50 mM Tris-HCl, pH8.5, 5 mM p-phenlenediamine, 50 mM n-propylgallate.

Quantification of Fluorescence Intensities

Fluorescence intensities of kinetochore signals were measured by subtracting the intensity in a background rectangle from the signal intensity in a rectangle placed at the DNA as described before (Schittenhelm et al., 2010, see Appendix 2).

Immunoblotting

Sorting of Fixed *Drosophila* Embryos for Immunoblotting

Cellularized embryos were synchronized in mitosis 14 basically as described before (Sauer et al., 1995). Embryos were collected for 1 h and aged for 3 h. The heat shock was given for 15 min in a 37°C water bath. Afterwards embryos were either recovered for 10 min or 20 min at 25°C, respectively, or immediately MeOH fixed. Syncytial embryos were directly MeOH fixed. DNA was stained with Hoechst 33258 (1 µg/ml in PBS) and embryos were transferred to a 1:1 mixture of glycerol and EB buffer (Edgar et al., 1994) and sorted according to their cell cycle phase with an inverted fluorescence microscope.

Protein Extracts

Denatured protein extracts were prepared by solubilising the embryos in SDS-PAGE sample buffer.
Native protein extracts from *Drosophila* embryos were prepared as described before (Jager et al., 2001). Native protein extracts from *Drosophila* larvae were prepared analogously using 1 larva instead of 50 embryos. For *Hs-GAL4* induction in larvae, a heat shock was given for 2 h in a 37°C water bath, followed by a recovery time of 1 h at 25°C. Native protein extracts from S2R+ cells were prepared as described before (Furrer et al., 2010). 300’000 cells were seeded in T25 flasks one day before transfection with the driver plasmid *pCaSpeR4-Actin5c-GAL4* (Heeger et al., 2005) and the respective *pUAST*-plasmids. Transfection was performed using FuGENE HD transfection reagent (Roche) according to manufactorer’s instructions two days before extract preparation. All buffers used for native extract preparation were supplemented with protease inhibitor cocktail (P8340, Sigma).

λ-Phosphatase Treatment

λ-Phosphatase (NEB) was used according to manufacturer's instructions. 50 µl of native protein extracts were incubated with 1600 U λ-phosphatase for 30 min at 30°C. 50 mM NaF and 10 mM Na_3VO_4 (activated as described, Gordon, 1991) were used as phosphatase inhibitors.

Co-Immunoprecipitation

Co-immunoprecipitation from native protein extracts for western blotting was performed using GFP-Trap coupled to agarose beads (Chromotek) according to manufacturer's instructions. Co-immunoprecipitation for mass spectrometry was performed as described before (Schittenhelm et al., 2007, see Appendix 1).

Western Blotting

Discontinuous polyacrylamide gel electrophoresis was performed according to standard protocols. To increase electrophoretic mobility shifts caused by phosphorylations, Phostag (Wako) was added according to manufactorer's instructions.

Immunoblots were probed with affinity purified rabbit antibodies against GFP (IS28) (Schittenhelm et al., 2007, see Appendix 1) at a dilution of 1:3000, affinity purified rabbit antibodies against GFP (Torrey Pines) at a dilution of 1:5000, affinity purified rabbit antibodies against mRFP (IS743) (H. Pauli, S. Herzog, S. Heidmann, Univ. Bayreuth, Germany, unpublished) at a dilution of 1:3000 (this antibody also reacts with mCherry and is therefore designated as anti-mCherry in the results section), affinity purified rabbit antibodies against Mps1 (Rb1) (Pandey et al., 2007) at a dilution of 1:5000, rabbit antibodies against Mad2 (IS793) (a kind gift from D. Sharp, Albert Einstein College of Medicine, New York, USA) at a dilution of 1:1500, mouse monoclonal antibody DM1A against α-tubulin (Sigma) at a dilution of 1:50'000, mouse monoclonal antibody F2 against Cyclin B (Knoblich and Lehner, 1993) at a dilution of 1:3, mouse monoclonal antibody 9E10 against c-myc (Evan et al., 1985) at a dilution of 1:15, and mouse monoclonal antibody (ADL67.10) against Lamin (developmental studies hybridoma bank (Stuurman et al., 1996)) at a dilution of 1:200.

Quantification of Protein Expression Levels by Quantitative Immunoblotting

Protein extracts were loaded on PAA gels with a reference extract loaded in a dilution series in order to obtain the actually loaded amounts from linear regression. The protein to be quantified as well as an independent protein (loading control) was probed on the western blot; exposure times were adjusted in order to get unsaturated exposures, in which the signals of a dilution series behaved linear.

Size (A_{band}) as well as signal intensities (I_{band}) of the respective bands were measured using ImageJ software. The average signal intensity of each band was background corrected by

subtracting the average intensity from a background square next to the band of interest ($I_{corr}/A_{band} = I_{band}/A_{band} – I_{back}/A_{back}$). The product of band sizes and corrected average signal intensities in the loading control of the dilution series (I_{corr}) were used to correlate the signal intensities with the amount of loaded embryos—linearity of the signal intensities in the measurement range was a prerequisite for the evaluation of the respective exposures. Linear regression revealed the amount of actually loaded embryos as a function of the signal intensity of the loading control ($E_{real} = m * I_{corr} + b$).

The amount of actually loaded embryos (E_{real}) in the respective lanes was derived from the signal intensity of the respective signal intensity in the loading control. The ratio of corrected signal intensities of the bands of interest and the number of really loaded embryos (I_{corr}/E_{real}) was formed in order to obtain comparable numbers.

References

Abrieu, A., Magnaghi-Jaulin, L., Kahana, J. A., Peter, M., Castro, A., Vigneron, S., Lorca, T., Cleveland, D. W., Labbe, J. C., 2001. Mps1 is a kinetochore-associated kinase essential for the vertebrate mitotic checkpoint. Cell. 106**,** 83-93.

Barisic, M., Sohm, B., Mikolcevic, P., Wandke, C., Rauch, V., Ringer, T., Hess, M., Bonn, G., Geley, S., 2010. Spindly/CCDC99 is required for efficient chromosome congression and mitotic checkpoint regulation. Mol Biol Cell. 21**,** 1968-81.

Basto, R., Scaerou, F., Mische, S., Wojcik, E., Lefebvre, C., Gomes, R., Hays, T., Karess, R., 2004. In vivo dynamics of the rough deal checkpoint protein during Drosophila mitosis. Curr Biol. 14**,** 56-61.

Brito, D. A., Rieder, C. L., 2006. Mitotic checkpoint slippage in humans occurs via cyclin B destruction in the presence of an active checkpoint. Curr Biol. 16**,** 1194-200.

Brito, D. A., Rieder, C. L., 2009. The ability to survive mitosis in the presence of microtubule poisons differs significantly between human nontransformed (RPE-1) and cancer (U2OS, HeLa) cells. Cell Motil Cytoskeleton. 66**,** 437-47.

Buffin, E., Emre, D., Karess, R. E., 2007. Flies without a spindle checkpoint. Nat Cell Biol. 9**,** 565-72.

Buffin, E., Lefebvre, C., Huang, J., Gagou, M. E., Karess, R. E., 2005. Recruitment of Mad2 to the kinetochore requires the Rod/Zw10 complex. Curr Biol. 15**,** 856-61.

Bunch, T. A., Grinblat, Y., Goldstein, L. S., 1988. Characterization and use of the Drosophila metallothionein promoter in cultured Drosophila melanogaster cells. Nucleic Acids Res. 16**,** 1043-61.

Chen, R. H., Waters, J. C., Salmon, E. D., Murray, A. W., 1996. Association of spindle assembly checkpoint component XMAD2 with unattached kinetochores. Science. 274**,** 242-6.

Chou, T. B., Perrimon, N., 1996. The autosomal FLP-DFS technique for generating germline mosaics in Drosophila melanogaster. Genetics. 144**,** 1673-9.

Colombo, R., Caldarelli, M., Mennecozzi, M., Giorgini, M. L., Sola, F., Cappella, P., Perrera, C., Depaolini, S. R., Rusconi, L., Cucchi, U., Avanzi, N., Bertrand, J. A., Bossi, R. T., Pesenti, E., Galvani, A., Isacchi, A., Colotta, F., Donati, D., Moll, J., 2011. Targeting the mitotic checkpoint for cancer therapy with NMS-P715, an inhibitor of MPS1 kinase. Cancer Res. 70**,** 10255-64.

Cui, Y., Cheng, X., Zhang, C., Zhang, Y., Li, S., Wang, C., Guadagno, T. M., 2010. Degradation of the human mitotic checkpoint kinase Mps1 is cell cycle-regulated by APC-cCdc20 and APC-cCdh1 ubiquitin ligases. J Biol Chem. 285**,** 32988-98.

Daum, J. R., Wren, J. D., Daniel, J. J., Sivakumar, S., McAvoy, J. N., Potapova, T. A., Gorbsky, G. J., 2009. Ska3 is required for spindle checkpoint silencing and the maintenance of chromosome cohesion in mitosis. Curr Biol. 19**,** 1467-72.

De Antoni, A., Pearson, C. G., Cimini, D., Canman, J. C., Sala, V., Nezi, L., Mapelli, M., Sironi, L., Faretta, M., Salmon, E. D., Musacchio, A., 2005. The Mad1/Mad2 complex as a template for Mad2 activation in the spindle assembly checkpoint. Curr Biol. 15**,** 214-25.

DeLuca, J. G., Dong, Y., Hergert, P., Strauss, J., Hickey, J. M., Salmon, E. D., McEwen, B. F., 2005. Hec1 and nuf2 are core components of the kinetochore outer plate essential for organizing microtubule attachment sites. Mol Biol Cell. 16**,** 519-31.

Dienemann, A., Sprenger, F., 2004. Requirements of cyclin a for mitosis are independent of its subcellular localization. Curr Biol. 14**,** 1117-23.

Dou, Z., Sawagechi, A., Zhang, J., Luo, H., Brako, L., Yao, X. B., 2003. Dynamic distribution of TTK in HeLa cells: insights from an ultrastructural study. Cell Res. 13**,** 443-9.

Dou, Z., von Schubert, C., Korner, R., Santamaria, A., Elowe, S., Nigg, E. A., 2011. Quantitative mass spectrometry analysis reveals similar substrate consensus motif for human mps1 kinase and plk1. PLoS One. 6**,** e18793.

Eckert, C. A., Gravdahl, D. J., Megee, P. C., 2007. The enhancement of pericentromeric cohesin association by conserved kinetochore components promotes high-fidelity chromosome segregation and is sensitive to microtubule-based tension. Genes Dev. 21**,** 278-91.

Edgar, B. A., O'Farrell, P. H., 1990. The three postblastoderm cell cycles of Drosophila embryogenesis are regulated in G2 by string. Cell. 62**,** 469-80.

Edgar, B. A., Sprenger, F., Duronio, R. J., Leopold, P., O'Farrell, P. H., 1994. Distinct molecular mechanism regulate cell cycle timing at successive stages of Drosophila embryogenesis. Genes Dev. 8**,** 440-52.

Emre, D., Terracol, R., Poncet, A., Rahmani, Z., Karess, R. E., 2011. A mitotic role for Mad1 beyond the spindle checkpoint. J Cell Sci.

Evan, G. I., Lewis, G. K., Ramsay, G., Bishop, J. M., 1985. Isolation of monoclonal antibodies specific for human c-myc proto-oncogene product. Mol Cell Biol. 5**,** 3610-6.

Fischer, M. G., Heeger, S., Hacker, U., Lehner, C. F., 2004. The mitotic arrest in response to hypoxia and of polar bodies during early embryogenesis requires Drosophila Mps1. Curr Biol. 14**,** 2019-24.

Fisk, H. A., Mattison, C. P., Winey, M., 2003. Human Mps1 protein kinase is required for centrosome duplication and normal mitotic progression. Proc Natl Acad Sci U S A. 100**,** 14875-80.

Fisk, H. A., Mattison, C. P., Winey, M., 2004. A field guide to the Mps1 family of protein kinases. Cell Cycle. 3**,** 439-42.

Foe, V. E., 1989. Mitotic domains reveal early commitment of cells in Drosophila embryos. Development. 107**,** 1-22.

Foe, V. E., Odell, G. M., Edgar, B. A., Mitosis and morphogenesis in the Drosophila embryo: point and counterpoint. In: M. Bate, A. M. Arias, Eds., The development of Drosophila melanogaster. Cold Spring Harbor Laboratory Press, Cold Spring Harbor, NY, 1993, pp. 149-300.

Foley, E., Sprenger, F., 2001. The cyclin-dependent kinase inhibitor Roughex is involved in mitotic exit in Drosophila. Curr Biol. 11**,** 151-60.

Furrer, M., Balbi, M., Albarca-Aguilera, M., Gallant, M., Herr, W., Gallant, P., 2010. Drosophila Myc interacts with host cell factor (dHCF) to activate transcription and control growth. J Biol Chem. 285**,** 39623-36.

Gascoigne, K. E., Taylor, S. S., 2008. Cancer cells display profound intra- and interline variation following prolonged exposure to antimitotic drugs. Cancer Cell. 14**,** 111-22.

Gascoigne, K. E., Taylor, S. S., 2009. How do anti-mitotic drugs kill cancer cells? J Cell Sci. 122**,** 2579-85.

Gilliland, W. D., Hughes, S. E., Cotitta, J. L., Takeo, S., Xiang, Y., Hawley, R. S., 2007. The multiple roles of mps1 in Drosophila female meiosis. PLoS Genet. 3**,** e113.

Gordon, J. A., 1991. Use of vanadate as protein-phosphotyrosine phosphatase inhibitor. Methods Enzymol. 201**,** 477-82.

Griffis, E. R., Stuurman, N., Vale, R. D., 2007. Spindly, a novel protein essential for silencing the spindle assembly checkpoint, recruits dynein to the kinetochore. J Cell Biol. 177**,** 1005-15.

Grimison, B., Liu, J., Lewellyn, A. L., Maller, J. L., 2006. Metaphase arrest by cyclin E-Cdk2

requires the spindle-checkpoint kinase Mps1. Curr Biol. 16**,** 1968-73.

Hacker, U., Perrimon, N., 1998. DRhoGEF2 encodes a member of the Dbl family of oncogenes and controls cell shape changes during gastrulation in Drosophila. Genes Dev. 12**,** 274-84.

Hardwick, K. G., Weiss, E., Luca, F. C., Winey, M., Murray, A. W., 1996. Activation of the budding yeast spindle assembly checkpoint without mitotic spindle disruption. Science. 273**,** 953-6.

He, X., Jones, M. H., Winey, M., Sazer, S., 1998. Mph1, a member of the Mps1-like family of dual specificity protein kinases, is required for the spindle checkpoint in S. pombe. J Cell Sci. 111 (Pt 12)**,** 1635-47.

Heeger, S., Leismann, O., Schittenhelm, R., Schraidt, O., Heidmann, S., Lehner, C. F., 2005. Genetic interactions of separase regulatory subunits reveal the diverged Drosophila Cenp-C homolog. Genes Dev. 19**,** 2041-53.

Hewitt, L., Tighe, A., Santaguida, S., White, A. M., Jones, C. D., Musacchio, A., Green, S., Taylor, S. S., 2010. Sustained Mps1 activity is required in mitosis to recruit O-Mad2 to the Mad1-C-Mad2 core complex. J Cell Biol. 190**,** 25-34.

Horn, C., Wimmer, E. A., 2000. A versatile vector set for animal transgenesis. Dev Genes Evol. 210**,** 630-7.

Howell, B. J., Moree, B., Farrar, E. M., Stewart, S., Fang, G., Salmon, E. D., 2004. Spindle checkpoint protein dynamics at kinetochores in living cells. Curr Biol. 14**,** 953-64.

Jager, H., Herzig, A., Lehner, C. F., Heidmann, S., 2001. Drosophila separase is required for sister chromatid separation and binds to PIM and THR. Genes Dev. 15**,** 2572-84.

Jaspersen, S. L., Huneycutt, B. J., Giddings, T. H., Jr., Resing, K. A., Ahn, N. G., Winey, M., 2004. Cdc28/Cdk1 regulates spindle pole body duplication through phosphorylation of Spc42 and Mps1. Dev Cell. 7**,** 263-74.

Jelluma, N., Brenkman, A. B., McLeod, I., Yates, J. R., 3rd, Cleveland, D. W., Medema, R. H., Kops, G. J., 2008a. Chromosomal instability by inefficient Mps1 auto-activation due to a weakened mitotic checkpoint and lagging chromosomes. PLoS One. 3**,** e2415.

Jelluma, N., Brenkman, A. B., van den Broek, N. J., Cruijsen, C. W., van Osch, M. H., Lens, S. M., Medema, R. H., Kops, G. J., 2008b. Mps1 phosphorylates Borealin to control Aurora B activity and chromosome alignment. Cell. 132**,** 233-46.

Jelluma, N., Dansen, T. B., Sliedrecht, T., Kwiatkowski, N. P., Kops, G. J., 2010. Release of Mps1 from kinetochores is crucial for timely anaphase onset. J Cell Biol. 191**,** 281-90.

Jones, M. H., Huneycutt, B. J., Pearson, C. G., Zhang, C., Morgan, G., Shokat, K., Bloom, K., Winey, M., 2005. Chemical genetics reveals a role for Mps1 kinase in kinetochore attachment during mitosis. Curr Biol. 15**,** 160-5.

Kang, J., Chen, Y., Zhao, Y., Yu, H., 2007. Autophosphorylation-dependent activation of human Mps1 is required for the spindle checkpoint. Proc Natl Acad Sci U S A. 104**,** 20232-7.

Kasbek, C., Yang, C. H., Yusof, A. M., Chapman, H. M., Winey, M., Fisk, H. A., 2007. Preventing the degradation of mps1 at centrosomes is sufficient to cause centrosome reduplication in human cells. Mol Biol Cell. 18**,** 4457-69.

Kirkman, T. W., Statistics to use. 1996.

Knoblich, J. A., Lehner, C. F., 1993. Synergistic action of Drosophila cyclins A and B during the G2-M transition. Embo J. 12**,** 65-74.

Konev, A., Varentsova, E. R., Sarantseva, S. V., Khromykh Iu, M., 1991. [Cytogenetic analysis of chromosome segments containing radiosensitivity genes in Drosophila. Radiation mutagenesis in the 44-45 region of chromosome 2 of Drosophila melanogaster]. Genetika. 27**,** 77-87.

Lan, W., Cleveland, D. W., 2010. A chemical tool box defines mitotic and interphase roles for Mps1 kinase. J Cell Biol. 190**,** 21-4.

Lauze, E., Stoelcker, B., Luca, F. C., Weiss, E., Schutz, A. R., Winey, M., 1995. Yeast spindle pole body duplication gene MPS1 encodes an essential dual specificity protein kinase. Embo J. 14**,** 1655-63.

Lee, J., Kitajima, T. S., Tanno, Y., Yoshida, K., Morita, T., Miyano, T., Miyake, M., Watanabe, Y., 2008. Unified mode of centromeric protection by shugoshin in mammalian oocytes and somatic cells. Nat Cell Biol. 10**,** 42-52.

Li, Y., Benezra, R., 1996. Identification of a human mitotic checkpoint gene: hsMAD2. Science. 274**,** 246-8.

Liu, S. T., Chan, G. K., Hittle, J. C., Fujii, G., Lees, E., Yen, T. J., 2003. Human MPS1 kinase is required for mitotic arrest induced by the loss of CENP-E from kinetochores. Mol Biol Cell. 14**,** 1638-51.

Logarinho, E., Bousbaa, H., Dias, J. M., Lopes, C., Amorim, I., Antunes-Martins, A., Sunkel, C. E., 2004. Different spindle checkpoint proteins monitor microtubule attachment and tension at kinetochores in Drosophila cells. J Cell Sci. 117**,** 1757-71.

Luschnig, S., Moussian, B., Krauss, J., Desjeux, I., Perkovic, J., Nusslein-Volhard, C., 2004. An F1 genetic screen for maternal-effect mutations affecting embryonic pattern formation in Drosophila melanogaster. Genetics. 167**,** 325-42.

Maciejowski, J., George, K. A., Terret, M. E., Zhang, C., Shokat, K. M., Jallepalli, P. V., 2010. Mps1 directs the assembly of Cdc20 inhibitory complexes during interphase and mitosis to control M phase timing and spindle checkpoint signaling. J Cell Biol. 190**,** 89-100.

Maldonado, M., Kapoor, T. M., 2011. Constitutive Mad1 targeting to kinetochores uncouples checkpoint signalling from chromosome biorientation. Nat Cell Biol.

Maresca, T. J., Salmon, E. D., 2010. Welcome to a new kind of tension: translating kinetochore mechanics into a wait-anaphase signal. J Cell Sci. 123**,** 825-35.

Martin-Lluesma, S., Stucke, V. M., Nigg, E. A., 2002. Role of Hec1 in spindle checkpoint signaling and kinetochore recruitment of Mad1/Mad2. Science. 297**,** 2267-70.

Mattison, C. P., Old, W. M., Steiner, E., Huneycutt, B. J., Resing, K. A., Ahn, N. G., Winey, M., 2007. Mps1 activation loop autophosphorylation enhances kinase activity. J Biol Chem. 282**,** 30553-61.

Maure, J. F., Kitamura, E., Tanaka, T. U., 2007. Mps1 kinase promotes sister-kinetochore biorientation by a tension-dependent mechanism. Curr Biol. 17**,** 2175-82.

Mirchenko, L., Uhlmann, F., 2010. Sli15(INCENP) dephosphorylation prevents mitotic checkpoint reengagement due to loss of tension at anaphase onset. Curr Biol. 20**,** 1396-401.

Morin, X., Daneman, R., Zavortink, M., Chia, W., 2001. A protein trap strategy to detect GFP-tagged proteins expressed from their endogenous loci in Drosophila. Proc Natl Acad Sci U S A. 98**,** 15050-5.

Musacchio, A., Salmon, E. D., 2007. The spindle-assembly checkpoint in space and time. Nat Rev Mol Cell Biol. 8**,** 379-93.

Nolen, B., Taylor, S., Ghosh, G., 2004. Regulation of protein kinases; controlling activity through activation segment conformation. Mol Cell. 15**,** 661-75.

Oliveira, R. A., Hamilton, R. S., Pauli, A., Davis, I., Nasmyth, K., 2010. Cohesin cleavage and Cdk inhibition trigger formation of daughter nuclei. Nat Cell Biol. 12**,** 185-92.

Orth, J. D., Tang, Y., Shi, J., Loy, C. T., Amendt, C., Wilm, C., Zenke, F. T., Mitchison, T. J., 2008. Quantitative live imaging of cancer and normal cells treated with Kinesin-5 inhibitors indicates significant differences in phenotypic responses and cell fate. Mol

Cancer Ther. 7, 3480-9.

Page, S. L., Nielsen, R. J., Teeter, K., Lake, C. M., Ong, S., Wright, K. R., Dean, K. L., Agne, D., Gilliland, W. D., Hawley, R. S., 2007. A germline clone screen for meiotic mutants in Drosophila melanogaster. Fly (Austin). 1, 172-81.

Palframan, W. J., Meehl, J. B., Jaspersen, S. L., Winey, M., Murray, A. W., 2006. Anaphase inactivation of the spindle checkpoint. Science. 313, 680-4.

Pandey, R., Heeger, S., Lehner, C. F., 2007. Rapid effects of acute anoxia on spindle kinetochore interactions activate the mitotic spindle checkpoint. J Cell Sci. 120, 2807-18.

Pandey, R., Heidmann, S., Lehner, C. F., 2005. Epithelial re-organization and dynamics of progression through mitosis in Drosophila separase complex mutants. J Cell Sci. 118, 733-42.

Pauli, A., Althoff, F., Oliveira, R. A., Heidmann, S., Schuldiner, O., Lehner, C. F., Dickson, B. J., Nasmyth, K., 2008. Cell-type-specific TEV protease cleavage reveals cohesin functions in Drosophila neurons. Dev Cell. 14, 239-51.

Ponti, A., Gulati, A., Bäcker, V., Schwarb, P., 2007. Huygens remote manager: a web interface tool for high-volume batch deconvolution. Imaging & Microscopy. 9, 57-58.

Poss, K. D., Nechiporuk, A., Hillam, A. M., Johnson, S. L., Keating, M. T., 2002. Mps1 defines a proximal blastemal proliferative compartment essential for zebrafish fin regeneration. Development. 129, 5141-9.

Rieder, C. L., Maiato, H., 2004. Stuck in division or passing through: what happens when cells cannot satisfy the spindle assembly checkpoint. Dev Cell. 7, 637-51.

Ruberte, E., Marty, T., Nellen, D., Affolter, M., Basler, K., 1995. An absolute requirement for both the type II and type I receptors, punt and thick veins, for dpp signaling in vivo. Cell. 80, 889-97.

Rubin, G. M., Hong, L., Brokstein, P., Evans-Holm, M., Frise, E., Stapleton, M., Harvey, D. A., 2000. A Drosophila complementary DNA resource. Science. 287, 2222-4.

Santaguida, S., Tighe, A., D'Alise, A. M., Taylor, S. S., Musacchio, A., 2010. Dissecting the role of MPS1 in chromosome biorientation and the spindle checkpoint through the small molecule inhibitor reversine. J Cell Biol. 190, 73-87.

Sauer, K., Knoblich, J. A., Richardson, H., Lehner, C. F., 1995. Distinct modes of cyclin E/cdc2c kinase regulation and S-phase control in mitotic and endoreduplication cycles of Drosophila embryogenesis. Genes Dev. 9, 1327-39.

Schittenhelm, R. B., Althoff, F., Heidmann, S., Lehner, C. F., 2010. Detrimental incorporation of excess Cenp-A/Cid and Cenp-C into Drosophila centromeres is prevented by limiting amounts of the bridging factor Cal1. J Cell Sci. 123, 3768-79.

Schittenhelm, R. B., Heeger, S., Althoff, F., Walter, A., Heidmann, S., Mechtler, K., Lehner, C. F., 2007. Spatial organization of a ubiquitous eukaryotic kinetochore protein network in Drosophila chromosomes. Chromosoma. 116, 385-402.

Schuh, M., Lehner, C. F., Heidmann, S., 2007. Incorporation of Drosophila CID/CENP-A and CENP-C into centromeres during early embryonic anaphase. Curr Biol. 17, 237-43.

Shah, J. V., Botvinick, E., Bonday, Z., Furnari, F., Berns, M., Cleveland, D. W., 2004. Dynamics of centromere and kinetochore proteins; implications for checkpoint signaling and silencing. Curr Biol. 14, 942-52.

Shaner, N. C., Campbell, R. E., Steinbach, P. A., Giepmans, B. N., Palmer, A. E., Tsien, R. Y., 2004. Improved monomeric red, orange and yellow fluorescent proteins derived from Discosoma sp. red fluorescent protein. Nat Biotechnol. 22, 1567-72.

Sliedrecht, T., Zhang, C., Shokat, K. M., Kops, G. J., 2010. Chemical genetic inhibition of Mps1 in stable human cell lines reveals novel aspects of Mps1 function in mitosis. PLoS One. 5, e10251.

Stapleton, M., Carlson, J., Brokstein, P., Yu, C., Champe, M., George, R., Guarin, H., Kronmiller, B., Pacleb, J., Park, S., Wan, K., Rubin, G. M., Celniker, S. E., 2002. A Drosophila full-length cDNA resource. Genome Biol. 3**,** RESEARCH0080.

Stucke, V. M., Baumann, C., Nigg, E. A., 2004. Kinetochore localization and microtubule interaction of the human spindle checkpoint kinase Mps1. Chromosoma. 113**,** 1-15.

Stucke, V. M., Sillje, H. H., Arnaud, L., Nigg, E. A., 2002. Human Mps1 kinase is required for the spindle assembly checkpoint but not for centrosome duplication. Embo J. 21**,** 1723-32.

Stuurman, N., Sasse, B., Fisher, P. A., 1996. Intermediate filament protein polymerization: molecular analysis of Drosophila nuclear lamin head-to-tail binding. J Struct Biol. 117**,** 1-15.

Sudakin, V., Chan, G. K., Yen, T. J., 2001. Checkpoint inhibition of the APC/C in HeLa cells is mediated by a complex of BUBR1, BUB3, CDC20, and MAD2. J Cell Biol. 154**,** 925-36.

Tighe, A., Staples, O., Taylor, S., 2008. Mps1 kinase activity restrains anaphase during an unperturbed mitosis and targets Mad2 to kinetochores. J Cell Biol. 181**,** 893-901.

Toyoda, Y., Yanagida, M., 2006. Coordinated requirements of human topo II and cohesin for metaphase centromere alignment under Mad2-dependent spindle checkpoint surveillance. Mol Biol Cell. 17**,** 2287-302.

Tyler, R. K., Chu, M. L., Johnson, H., McKenzie, E. A., Gaskell, S. J., Eyers, P. A., 2009. Phosphoregulation of human Mps1 kinase. Biochem J. 417**,** 173-81.

Vigneron, S., Prieto, S., Bernis, C., Labbe, J. C., Castro, A., Lorca, T., 2004. Kinetochore localization of spindle checkpoint proteins: who controls whom? Mol Biol Cell. 15**,** 4584-96.

Waizenegger, I. C., Hauf, S., Meinke, A., Peters, J. M., 2000. Two distinct pathways remove mammalian cohesin from chromosome arms in prophase and from centromeres in anaphase. Cell. 103**,** 399-410.

Wan, X., O'Quinn, R. P., Pierce, H. L., Joglekar, A. P., Gall, W. E., DeLuca, J. G., Carroll, C. W., Liu, S. T., Yen, T. J., McEwen, B. F., Stukenberg, P. T., Desai, A., Salmon, E. D., 2009. Protein architecture of the human kinetochore microtubule attachment site. Cell. 137**,** 672-84.

Wang, W., Yang, Y., Gao, Y., Xu, Q., Wang, F., Zhu, S., Old, W., Resing, K., Ahn, N., Lei, M., Liu, X., 2009. Structural and mechanistic insights into Mps1 kinase activation. J Cell Mol Med. 13**,** 1679-94.

Weiss, E., Winey, M., 1996. The Saccharomyces cerevisiae spindle pole body duplication gene MPS1 is part of a mitotic checkpoint. J Cell Biol. 132**,** 111-23.

Winey, M., Goetsch, L., Baum, P., Byers, B., 1991. MPS1 and MPS2: novel yeast genes defining distinct steps of spindle pole body duplication. J Cell Biol. 114**,** 745-54.

Wong, O. K., Fang, G., 2006. Loading of the 3F3/2 antigen onto kinetochores is dependent on the ordered assembly of the spindle checkpoint proteins. Mol Biol Cell. 17**,** 4390-9.

Xu, Q., Zhu, S., Wang, W., Zhang, X., Old, W., Ahn, N., Liu, X., 2009. Regulation of kinetochore recruitment of two essential mitotic spindle checkpoint proteins by Mps1 phosphorylation. Mol Biol Cell. 20**,** 10-20.

Zhao, Y., Chen, R. H., 2006. Mps1 phosphorylation by MAP kinase is required for kinetochore localization of spindle-checkpoint proteins. Curr Biol. 16**,** 1764-9.

Appendix 1:

Spatial Organization of a Ubiquitous Eukaryotic Kinetochore Protein Network in *Drosophila* Chromosomes

Schittenhelm, RB, Heeger, S, Althoff, F, Walter, A, Heidmann, S, Mechtler, K, and Lehner, CF

Chromosoma. 2007 Aug;116(4):385-402

Contribution to this part:

I characterized the mutant alleles of the kinetochore protein genes *Nuf2*, *Spc25*, and *Mis12* molecularly, analyzed the resulting phenotypes, and performed rescue experiments with the EGFP-tagged kinetochore proteins (Figure 5). The manuscript was written by C.L. with contributions from S.H., R.B., and the other authors.

Chromosoma (2007) 116:385–402
DOI 10.1007/s00412-007-0103-y

RESEARCH ARTICLE

Spatial organization of a ubiquitous eukaryotic kinetochore protein network in *Drosophila* chromosomes

Ralf B. Schittenhelm · Sebastian Heeger · Friederike Althoff · Anne Walter · Stefan Heidmann · Karl Mechtler · Christian F. Lehner

Received: 31 January 2007 / Revised: 4 February 2007 / Accepted: 5 February 2007 / Published online: 1 March 2007

Abstract Chromosome segregation during meiosis and mitosis depends on the assembly of functional kinetochores within centromeric regions. Centromeric DNA and kinetochore proteins show surprisingly little sequence conservation despite their fundamental biological role. However, our identification in *Drosophila melanogaster* of the most diverged orthologs identified so far, which encode components of a kinetochore protein network including the Ndc80 and Mis complexes, further emphasizes the notion of a shared eukaryotic kinetochore design. To determine its spatial organization, we have analyzed by quantitative light microscopy hundreds of native chromosomes from transgenic *Drosophila* strains coexpressing combinations of red and green fluorescent fusion proteins, fully capable of providing the essential wild-type functions. Thereby, Cenp-A/Cid, Cenp-C, Mis12 and the Ndc80 complex were mapped along the inter sister kinetochore axis with a resolution below 10 nm. The C terminus of Cenp-C was found to be near but well separated from the innermost component Cenp-A/Cid. The N terminus of Cenp-C is further out, clustered with Mis12 and the Spc25 end of the rod-like Ndc80 complex, which is known to bind to microtubules at its other more distal Ndc80/Nuf2 end.

Communicated by E.A. Nigg

Ralf B. Schittenhelm and Sebastian Heeger have equal contributions.

R. B. Schittenhelm · S. Heeger · F. Althoff · A. Walter · S. Heidmann · C. F. Lehner (✉)
Department of Genetics, University of Bayreuth,
Universitaetsstr. 30,
95447 Bayreuth, Germany
e-mail: chle@uni-bayreuth.de

K. Mechtler
Institute of Molecular Biotechnology GmbH, IMBA,
Dr. Bohr-Gasse 3,
1030 Vienna, Austria

Introduction

The kinetochore which is formed within the centromeric region of eukaryotic chromosomes is crucial for faithful segregation of genetic information during mitotic and meiotic divisions. Its composition changes during the division cycle. In prometaphase, it allows attachment of chromosomes to spindle fibers (Rieder 2005). Moreover, it is associated with a number of checkpoint proteins that monitor chromosome integration into the spindle and prevent progression into anaphase as long as chromosomes without or with a syntelic attachment to the spindle are present.

Despite their fundamental biological role, centromeric DNA and primary sequences of associated proteins have evolved very rapidly (for recent reviews, see Schueler and Sullivan 2006; Vos et al. 2006). Initially, therefore, it has been difficult to integrate findings from different model organisms into a general model for kinetochore organization in eukaryotes. However, recent progress has dramatically improved the recognition of shared elements of centromere kinetochore complexes (CKC). The basis of CKC assembly appears to be formed by specialized chromatin containing nucleosomes with a centromere-specific histone H3 variant (Vos et al. 2006; Fujita et al. 2007). Cenp-A/Cid, the *Drosophila* centromere-specific histone H3 variant, is found at the centromere throughout the division cycles (Henikoff et al. 2000), as also true in other organisms (Vos et al. 2006). Cenp-C homologs represent another ubiquitous CKC component with a constitutive centromere localization (apart from the mito-

sis-specific association observed in the holocentric chromosomes of *Caenorhabditis elegans*; Moore and Roth 2001; Oegema et al. 2001; Heeger et al. 2005; Vos et al. 2006). Four multiprotein complexes (Sim4/COMA/NAC/Cenp-H/I, Mis12/MIND, Spc105/KNL-1, Ndc80) that were originally identified in yeast have also been characterized, at least partially, in a wide range of eukaryotes (McAinsh et al. 2003; Kline-Smith et al. 2005; Liu et al. 2005; Cheeseman et al. 2006; Foltz et al. 2006; Meraldi et al. 2006; Okada et al. 2006; Vos et al. 2006). Their centromere association in human cells appears to vary from constitutive (Sim4/COMA/NAC/Cenp-H/I; Foltz et al. 2006; McAinsh et al. 2006; Okada et al. 2006), constitutive except for telophase (Mis12; Kline et al. 2006; McAinsh et al. 2006), to mitosis-specific (Ndc80; Chen et al. 1997; Martin-Lluesma et al. 2002; Kline-Smith et al. 2005). Moreover, a number of mitotic spindle checkpoint proteins are conserved and present at high concentrations at those kinetochores, which are either not attached to the spindle or not exposed to the physical tension resulting from bipolar attachment (Vos et al. 2006). Apart from these proteins, about 50 additional CKC components have been described in various experimental systems, and the identification of diverged orthologs in other eukaryotes is progressing in many cases (Meraldi et al. 2006; Vos et al. 2006).

Initial insights into the details of the structural CKC organization were obtained by electron microscopy (EM; Rieder 1982; Vos et al. 2006). In *Drosophila*, kinetochore ultrastructure is similar to the appearance of vertebrate kinetochores (Maiato et al. 2006), in particular, during prometaphase when the hemispherical organization is transformed into a disk with a distinct outer plate of about 40 nm thickness. This outer plate is separated by a gap of about 30 nm from another electron-dense inner plate. In *Drosophila*, this inner plate is poorly resolved from the underlying amorphous inner chromatin mass. On the other side, i.e., distal to the outer plate, prometaphase kinetochores have a fibrous corona of variable depth (up to 200 nm), which has been clearly described in mammalian cells. We point out that kinetochore ultrastructure is known to change significantly from prophase to metaphase (Rieder 1982; Maiato et al. 2006), and that certain aspects like the distinction of the inner plate might reflect artifactual chromatin shrinking during fixation (McEwen et al. 1998).

Only a few CKC components have been localized by immuno-EM at an ultrastructural level. Thereby, vertebrate Cenp-C has been assigned to the inner plate (Saitoh et al. 1992) and the Ndc80 complex components Ndc80/Hec1 and Nuf2 to the outer plate (DeLuca et al. 2005). Moreover, Cenp-E has been located within the outer corona (Cooke et al. 1997). Based on double immunofluorescence comparisons with these well-studied proteins, almost all other CKC components have been tentatively classified as present either in the inner chromatin, the inner or outer plate, or the fibrous corona. Moreover, several studies have characterized kinetochore ultrastructure after RNA interference-mediated depletion of CKC components (Vigneron et al. 2004; DeLuca et al. 2005; Liu et al. 2006). RNA interference mostly in combination with fluorescence microscopy or immunodepletion in *Xenopus* egg extracts has also been used extensively to analyze dependencies in the CKC assembly process (see for instance Emanuele et al. 2005; Liu et al. 2006, and references in Vos et al. 2006). In general, inner components were found to be required for the later assembly of outer components, although certain inconsistencies point to a higher complexity (Liu et al. 2006). Finally, light microscopic analyses have been performed with stretched chromatin fibers, which have argued for a lateral association of repeating units into a kinetochore disk (Blower et al. 2002; Sullivan and Karpen 2004).

In this paper, we describe a light-microscopic approach for kinetochore analysis with unprecedented spatial resolution. This approach exploits some unique advantages of the model organism *Drosophila melanogaster*. Genetic complementation tests were used to demonstrate the functionality of CKC proteins fused to fluorescent proteins. These fluorescent proteins, the enhanced green fluorescent protein (EGFP) and monomeric red fluorescent protein (mRFP), provide localization tags, which are considerably smaller than antibodies. The cylindrical β-barrels formed by EGFP and mRFP have a diameter of 2.4 nm and a height of 4.2 nm (Ormo et al. 1996; Yang et al. 1996; Yarbrough et al. 2001). In contrast, indirect immunolocalization involves detection by two antibodies, each being more than fivefold larger than EGFP/mRFP, in combination with colloidal gold in the case of EM. In addition, fluorescent proteins eliminate potential problems with antibody specificity and antigen accessibility. Moreover, potential fixation artifacts can be avoided by imaging unfixed specimens. In *Drosophila*, the rapid syncytial division cycles of early embryogenesis result in a very high physiological mitotic index approaching 50%, which allows a very efficient preparation of native mitotic chromosomes. After our identification of components of the *Drosophila* Ndc80 and Mis12 complexes, we analyzed their localization in comparison to the previously described Cenp-A/Cid (Henikoff et al. 2000) and Cenp-C proteins (Heeger et al. 2005). By averaging the data obtained with hundreds of native chromosomes released from embryos coexpressing a red and a green fluorescent CKC component, we were able to map these proteins with a spatial resolution well beyond the light diffraction limit. Thereby, we localized Cenp-C to a region between the innermost Cenp-A/Cid and the outer Mis12 and Ndc80 complexes. Moreover, both Cenp-C and

the rod-like Ndc80 complex were found to have a defined, polar orientation along the spindle axis.

Materials and methods

Fly strains

Drosophila stocks with the mutations *Nuf2*^{SH2276} (Oh et al. 2003) and *l(3)A34-1* (synonym: *l(3)87Da*^{2}; Hilliker et al. 1980) or the deficiencies *Df(2L)ade3* and *Df(3R)ry75* were obtained from the Bloomington stock center. The piggyBac insertion line *Spc25*^{c00064} (Thibault et al. 2004) was kindly provided by the Harvard Medical School stock collection.

Nuf2^{SH2276} appears to be a hypomorphic allele. Hemizygotes with *Nuf2*^{SH2276} over *Df(2L)ade3*, which deletes *Nuf2*, were found to die during the late pupal stages, i.e., earlier than *Nuf2*^{SH2276} homozygotes.

The EMS-induced recessive lethal mutation *l(3)A34-1* which had genetically been mapped to a chromosomal region including *Spc25* (Hilliker et al. 1980) failed to complement *Spc25*^{c00064}. Moreover, the lethality of *l(3)A34-1* in trans over the deficiency *Df(3R)ry75*, which deletes *Spc25*, was rescued by the *gSpc25-mRFP* transgene. *Spc25*^{c00064} homozygotes and hemizygotes (in trans over the deficiency *Df(3R)ry75*) displayed an indistinguishable phenotype which was more severe than that of *l(3)A34-1* hemizygotes. Therefore, *Spc25*^{c00064} appears to be an amorphic and *l(3)A34-1* a hypomorphic allele.

The gene trap line *P{w[+mC]=PTT-GA}Jupiter*^{G00147} expresses a fusion of EGFP and Jupiter, a microtubule-binding protein (Morin et al. 2001). Transgenic strains expressing kinetochore proteins fused to fluorescent proteins were generated by standard P-element-mediated germ line transformation. Lines expressing functional Cenp-A/Cid with an internal EGFP insertion 11 amino acids before the start of the histone fold domain (*gcid-EGFP-cid*) have been described before (Schuh et al. 2007). Lines with an *mRFP* insertion in *Cenp-A/Cid* in place of the *EGFP* insertion (*gcid-mRFP-cid*) were generated and also confirmed to express a functional Cid fusion protein (S.H., unpublished observations). Lines expressing Cenp-C with an N-terminal EYFP extension (*gEYFP-Cenp-C*) or with a C-terminal EGFP extension (*gCenp-C-EGFP*) have been described before (Heeger et al. 2005). The *gEGFP-Bub3*, *sryα-GAL4*, and *UAS-EGFP-CG11743* lines will be described in detail elsewhere. A line with *sryα-GAL4* and *UAS-EGFP-CG11743* was used for control in the coimmunoprecipitation experiments.

Additional lines were generated with the constructs described below. Lines with combinations of transgenes resulting in the expression of a red and a green fluorescent CKC component were generated by standard crosses. We analyzed lines with *gcid-mRFP-cid* II.1 in combination with either *gcid-EGFP-cid* III.2, *gEYFP-Cenp-C* II.1, *gCenp-C-EGFP* III.2, *gEGFP-Nuf2* II.1, *gMis12-EGFP* II.1, *gEGFP-Bub3*, or *P{w[+mC]=PTT–GA}Jupiter*^{G00147}. In addition, we also analyzed lines with *gSpc25–mRFP* II.1 in combination with either *gSpc25-EGFP* II.1, *gcid-EGFP-cid* III.2, *gEYFP-Cenp-C* II.1, *gCenp-C-EGFP* III.2, *gEGFP-Nuf2* II.1, or *gMis12-EGFP* II.1. All transgenic lines had a *w* mutant background.

Plasmid constructions and transfections

pP{CaSpeR-4} constructs were made for the expression of kinetochore proteins fused to fluorescent proteins under control of the corresponding genomic regulatory region. Genomic fragments were amplified from bacterial artificial chromosome (BAC) clones characterized by the *Drosophila* genome project (BACR30C16 for *Ndc80*, BACR39J17 for *Nuf2*, BACR17F05 for *Spc25*, BACR14L10 for *Mis12*) (Hoskins et al. 2000). The sequences of the primers were: AnW20 (5′-G GAATTC GTA GAA TCG TTT GGA AAT GC-3′) and AnW21 (5′-G GGATCC CTT GGC GTT ATT GAA ACT AC-3′) for the 5′ part of *Ndc80*, AnW22 (5′-C TCTAGA ATG TCG CAC CTG ATG CCC-3′) and AnW23 (5′-CATTGT AGGCCT ACG TTA GCA CTA TCG GGG-3′) for the 3′ part of *Ndc80*; RaS83 (5′-CACCCAGTTC GCGGCCGC ATG TAT CAA ATG TGT CGC C-3′) and RaS84 (5′-GA GGATCC CAT TCA ATC CAG AGT TTT AAT-3′) for the 5′ part of *Nuf2*, RaS87 (5′-TG TCTAGA ATG GCG TTA TCA GTC GAA A-3′) and RaS88 (5′-A AGGCCT TGC CCC AGA TAA GGA AAA GG-3′) for the 3′ part of *Nuf2*; RaS93 (5′-GTTTAGATGG GCGGCCGC GCC GAT GAT CAG GAC CGG-3′) and RaS94 (5′-GG GGATCC GGT GTG GCT CAT CGG CG-3′) for the 5′ part of *Spc25*; RaS95 (5′-AC TCTAGA CTT CCG ATT AAC TGA TTT AC-3′) and RaS96 (5′-G AGGCCT CGA TTA ACA CCG GCC G-3′) for the 3′ part of *Spc25*; RaS125 (5′-AGC GAATTC GCT TCC TTT GTT TGT TCG GG-3′) and RaS126 (5′-GTT GGATCC ATC AGT CTC CTT CTT TAT CTG-3′) for the 5′ part of *Mis12*; RaS127 (5′-ACT TCTAGA ATA AAC TAA CTG GAT CAA GTT TT-3′) and RaS128 (5′-TCTCCCA AGGCCT CAG GCT TAT AGC AAA ATA TAC G-3′) for the 3′ part of *Mis12*. The polymerase chain reaction (PCR) fragments with the 5′ and 3′ parts of a given gene were introduced into polylinker sites of pP{CaSpeR-4}. Moreover, a PCR fragment containing the coding sequences of either *mRFP1* or *EGFP* was introduced into the *Bam*H1 and *Xba*I sites between the 5′ and 3′ parts. The primers for the amplification of the coding sequences of the fluorescent proteins were: RaS85 (5′-GC GGATCC ATG GTG AGC AAG GGC GAG-3′) and RaS86 (5′-TC TCTAGA CTT GTACAG CTC GTC CAT G-3′) for *EGFP* in *gEGFP-Nuf2*, RaS85 and RaS80 (5′-

GG TCTAGA TTA CTT GTA CAG CTC GTC CAT G-3′) for *EGFP* in *gMis12-EGFP* and *gSpc25-EGFP*, RaS91 (5′-AG GGATCC ATG GCC TCC TCC GAG GAC-3′) and RaS92 (AA TCTAGA TTA GGC GCC GGT GGA GTG-3′) for *mRFP1* in *gSpc25-mRFP*.

The pP{CaSpeR-4} constructs for expression of Cenp-C variants with green and red fluorescent proteins fused to N and C termini were based on a genomic 8.7 kb *Pml*I–*Xba*I fragment used previously for the generation of *gEYFP-Cenp-C* lines (Heeger et al. 2005). Inverse PCR with primers CM51 (5′-GTC GTT GCT AGC GGG CTT CGA CCT GAA AAA CAG-3′) and CM52 (5′-AAG CCC GCT AGC AAC GAC ACT CTG GAG CTG-3′) or MF8 (5′-GGC CTA GCT AGC ACT GCG TAT ACA CAT CAG CAC-3′) and MF9 (5′-CGC AGT GCT AGC TAG TAA TTG CTT TGT AAT TTA-3′) was used to introduce *Nhe*I sites after the start or directly before the stop codon, respectively. EGFP coding sequences were amplified with primers MF11 (5′-GGC CGC TAG CGT GAG CAA GGG CGA GGA GCT G-3′) and HS6 (5′-GGA CTA GTC TTG TAC AGC TCG TCC ATG C-3′) for N-terminal and MF11 and MF12 (5′-GGC CGC TAG CTT ACT TGT ACA GCT CGT CCA TG-3′) for C-terminal fusions. mRFP1 coding sequences were amplified with primers HSmRFP2 (5′-AGC GGC TAG CAT GGC CTC CTC CGA GGA C-3′) and HSmRFP3 (5′-CGA AAC TAG TGG CGC CGG TGG AGT GG-3′).

pPUAST constructs containing cDNAs fused to the EGFP coding sequence were used for transfection of *Drosophila* S2R+ cells. For these constructions, we first generated two pPUAST variants for either N- or C-terminal EGFP fusions. For the former variant, the EGFP coding sequence was amplified using the primers RaS42 (5′-C GAATTC ATG GTG AGC AAG GGC GAG-3′) and RaS43 (5′-TGGATTTCTG GCGGCCGC CTT GTA CAG CTC GTC CAT G-3′), which introduce an *Eco*RI and a *Not*I site before the initiation codon or the stop codon, respectively. This PCR fragment was introduced into the corresponding polylinker sites in pPUAST. For the latter variant, the EGFP coding sequence was amplified with the primers RaS79 (5′-GC GGTACC ATG GTG AGC AAG GGC GAG-3′) and RaS80 (5′-GG TCTAGA TTA CTT GTA CAG CTC GTC CAT G-3′), which introduce a *Kpn*I and an *Xba*I site upstream of the initiation codon and after the stop codon, respectively. The resulting fragment was introduced into the corresponding polylinker sites of pPUAST. The restriction sites remaining in the polylinker of the pPUAST variants were used for the insertion of cDNA fragments amplified from expressed sequence tag (EST) plasmids characterized by the *Drosophila* genome project (Stapleton et al. 2002). The following EST plasmids were used: LD33040 (*Ndc80*), SD05495 (*Nuf2*), LD37196 (*Spc25*), RE19545 (*Mis12*), RE03006 (*Kmn1*), RE42502 (*Nnf1a*). *Nnf1b* and *Kmn2* were amplified from genomic DNA. Primers used for amplification were: RaS74 (5′-GG GAATTC AT GCGGCCGC G ATG TCG CAC CTG ATG CC-3′) and RaS75 (5′-GG TCTAGA CTA ATG ATT CTT GAT GGC ATC TAG-3′) for *pPUAST-EGFP-Ndc80*, RaS77 (5′-GATTAAAACT GCGGCCGC A ATG GCG TTA TCA GTC GAA ATT-3′) and RaS78 (5′-TC TCTAGA TTA AGT GGA ATT CAT CTG CC-3′) for *pPUAST-EGFP-Nuf2*, RaS81 (5′-GG GGTACC GGT GTG GCT CAT CGG CG-3′) and RaS82 (5′-AG AGATCT ATG GCA ATT ATT ATG ACT GAA TC-3′) for *pPUAST-Spc25-EGFP*, RaS113 (5′-GTTA GCGGCCGC A ATG GAC TTC AAT AGC CTA GC-3′) and RaS114 (5′-AGTT GGTACC ATC AGT CTC CTT CTT TAT CTG-3′) for *pPUAST-Mis12-EGFP*, AnW28 (5′-ACGA GCGGCCGC T ATG GAG CCA GCC GAA AGT C-3′) and AnW30 (5′-GC GGTACC CCG TTG GTT GGC CAT ATT C-3′) for *pPUAST-Kmn1-EGFP*, AnW25 (5′-CAAA GCGGCCGC T ATG GAG GAT TCG GAA GCC G-3′) and AnW26 (5′-A CTCGAG TCA GAA GTC GTT CAA TGC-3′) for *pPUAST-EGFP-Nnf1a*, AnW36 (5′-TGTG GCGGCCGC A ATG AAT AAT ATT GAA GAG GAC AC-3′) and AnW37 (5′-TT GGTACC TTA CAT TTC TTC CTG CAC ATA C-3′) for *pPUAST-EGFP-Nnf1b*, RaS137 (5′-CAAAAA GCGGCCGC C ATG GAA AGT AAG CGC-3′) and RaS139 (5′-GA GGTACC CAG CAA GGA CAA GCA GTC C-3′) for *pPUAST-Kmn2-EGFP*.

Before transfection, S2R+ cells were re-plated in 24 well plates containing a coverslip. The culture medium (1 ml) was replaced after 12–24 h, and cells were transfected with a standard calcium phosphate precipitate containing 3 μg of plasmid DNA. Cells were fixed about 24–26 h after transfection and stained with antibodies against Cenp-A/Cid or Cenp-C and the DNA stain Hoechst 33258 essentially as described previously (Vass et al. 2003; Heeger et al. 2005).

Immunoprecipitation

For coimmunoprecipitation experiments, we collected 5–8 h embryos from either *w**;P{w*$^+$*, gEGFP-Nuf2} II.1* or *w*^{1}; P{w$^+$, *sryα-Gal4} II.1, P{w*$^+$*, UAS-EGFP-CG11743} II.1* flies at 25°C. After dechorionization in 50% bleach, eggs were shock frozen in liquid nitrogen and stored at −80°C. 1 ml packed embryos were homogenized in 4 ml lysis buffer [50 mM 4-2-hydroxyethyl-1-piperazineethanesulfonic acid (HEPES) at pH 7.5, 60 mM NaCl, 3 mM $MgCl_2$, 1 mM $CaCl_2$, 0.2% Triton X-100, 0.2% Nonidet NP-40, 10% glycerol, 1 mM dithiothreitol (DTT)] containing 0.2 ml protease inhibitor cocktail (P 8340, Sigma). The extracts were cleared by centrifugation (20 min, 14000×*g*). For further clearing, supernatants were incubated with 0.15 ml Protein-A-Sepharose beads (Affi-Prep, Bio-Rad) during 1 h

followed by another centrifugation. 25 µl Protein-A-Sepharose beads to which about 25 µg affinity-purified rabbit antibodies against GFP or mRFP (J. Dürr, S. Herzog and S. H., unpublished) had been crosslinked with dimethyl pimelimidate (Harlow and Lane 1988) were used for immunoprecipitation from the supernatant. Immunoprecipitates were washed four times with lysis buffer. During the third and fourth washes, 0.5% Nonidet NP-40 and 0.5% Triton-X-100 were present in the lysis buffer. Moreover, during the fourth wash, 300 mM NaCl was also present in the lysis buffer. Immunoprecipitated proteins were eluted for 5 min at 37°C with 0.04 ml 2% sodium dodecyl sulfate (SDS), 50 mM Tris–HCl, pH 7.5, followed by another elution at 94°C. Sodium dodecyl sulfate polyacrylamide gel electrophoresis (SDS-PAGE) sample buffer was added, and the immunoprecipitated proteins were resolved on a large 12% Tris–HCl precast gel (Bio-Rad). Silver staining was performed essentially as described (Blum et al. 1987). Fixation was done in 30% ethanol and 10% acetic acid. After a wash in 30% ethanol, water was used for an additional 20 min wash. 0.02 and 0.05% formaldehyde were included in the silver nitrate solution and the developer, respectively. Staining was terminated in 5% acetic acid. Excised bands were rinsed in water and analyzed by mass spectrometry essentially as described previously (Riedel et al. 2006). Briefly, bands were reduced with DTT, carboxymethylated using iodoacetamide, and digested with trypsin. Tryptic peptides were extracted with formic acid and separated by nano high-performance liquid chromatography (LC-Packings, Netherland) on a PepMap C 18 column. The eluate of the column was applied online to an LTQ ion trap mass spectrometer (Thermo-Fisher) equipped with a nanospray source. Mass data on all peptides and their fragmentation pattern were analyzed using the Mascot software (Matrix Science). Note that Fig. 2 displays proteins eluted at 37°C. The majority of EGFP-Nuf2 and Spc25-mRFP was only eluted during the second elution at 94°C.

Sequence comparison

Secondary structure predictions were performed using Quick2D (Biegert et al. 2006). In case of the human proteins, predictions are based on a multiple sequence alignment obtained with the position-specific iterated basic local alignment search tool (PSI-BLAST) search option. In case of the *Drosophila* proteins, predictions are based on a multiple sequence alignment assembled using ClustalW and ortholog sequences identified in Drosophilid genome sequences (Thompson et al. 1994; Richards et al. 2005; prepublication data from Agencourt Bioscience Corporation and Genome Sequencing Center at Washington University). In case of *Drosophila* Nnf1, the alignment contained both Nnf1a and Nnf1b paralog sequences, which result in essentially indistinguishable predictions when tested individually (data not shown). *Nnf1* homologs in Drosophilid genomes were identified by BLAST searches and compared using ClustalW, which was also used for phylogenetic tree construction.

Preparation and analysis of native chromosomes

Eggs were collected on apple juice agar plates and aged to the syncytial blastoderm stages. After chorion removal with 50% bleach and extensive washing in water, eggs were returned to apple juice agar plates. Three eggs were lined up on a glass slide, and 3.5 µl of phosphate buffered saline containing 2 µg/ml Hoechst 33258 was added. The embryos were squashed by capillary forces after adding a coverslip (24×32 mm). Microscopic analyses were started within a few minutes after turbulent mixing within the specimen had settled. Single focal planes were acquired with a Zeiss Axioplan 2 imaging system using a 100× PlanApo NA 1.4 objective, an AxioCam MRm camera, and an AxioVision software. With this setup, a camera pixel represents about a 68 nm square region of the object. The extent of movement within the unfixed sample was controlled by comparing the spatial distribution of the DNA staining acquired before and after acquisition of the red and green signals. Chromosomes that had moved more than 0.2 µm during acquisition were excluded from the analyses. In addition, chromosomes which did not clearly display two distinct sister kinetochore signals were also excluded from the analyses. Thereby, chromosomes from anaphase embryos, as well as chromosomes from prometa- and metaphase embryos with an orientation of the axis between sister kinetochores perpendicular (or nearly perpendicular) to the slide were eliminated. The majority of chromosomes (about 70%, n=436) from prometaphase and metaphase embryos displayed two distinct sister kinetochores. The squashing procedure therefore appears to result in a preferred planar orientation of the two sister kinetochore on the slide. The relatively weak signals in combination with the extent of bleaching observed especially with the mRFP fusion proteins prevented us from acquiring z stacks followed by three-dimensional analyses of centroid signal maxima. For evaluation, signal intensities along a line connecting the two sister kinetochores were determined using ImageJ software and transferred to MS Excel software for further analysis. The d_{RRinter}, d_{GGinter} and d_{RGintra} values for a given pair of CKC components (see Fig. 7d and Table 1), as well as the d_{inter} values obtained for a given CKC component by pooling the corresponding data from the pairwise analyses (Table 2), were not normally distributed, as expected since chromosomes with closely spaced, overlapping sister kinetochore signals were excluded from the analyses for instance. An

Table 1 Pairwise mapping of CKC components

Red protein	Green protein	$d_{RRinter}$[a] (nm)	$d_{GGinter}$[a] (nm)	$d_{RGintra}$[a] (nm)
Cenp-A/Cid	Cenp-A/Cid	445	455	5
	Cenp-C(C)[b]	460	490	15
	Cenp-C(N)[b]	463	547	42
	Mis12	472	574	51
	Nuf2	451	589	69
Spc25	Cenp-A/Cid	573	475	−49
	Cenp-C(C)[b]	556	511	−23
	Cenp-C(N)[b]	539	512	−14
	Mis12	503	516	7
	Nuf2	547	576	15
	Spc25	531	531	0
(N)[c]-Cenp-C-(C)[c]		575	559	−8
(C)[d]-Cenp-C-(N)[d]		461	491	15

[a] Native chromosomes (n=100) from embryos coexpressing a red and a green fluorescent CKC component were analyzed. Average values for the distances separating the red fluorescent signal maxima of sister kinetochores ($d_{RRinter}$) and the distances separating the green fluorescent signal maxima of sister kinetochores ($d_{GGinter}$) were used for the calculation of the distance separating the two components within a sister kinetochore ($d_{RGintra}$; see also Fig. 7d and experimental procedures)

[b] Cenp-C was expressed as a fusion with EGFP either at the N terminus [Cenp-C(N)] or at the C terminus [Cenp-C(C)]

[c] Cenp-C was expressed with mRFP and EGFP at the N and C termini, respectively

[d] Cenp-C was expressed with EGFP and mRFP at the N and C termini, respectively

adequate statistical error analysis was further complicated by unexplored potential biological (kinetochore variation in chromosome 2, 3, 4, X and Y, or precise mitotic stage), experimental (chromosome orientation and extent of stretch/compression), and instrumental variability (pixelation, background noise). The distribution of all the measured data is therefore given in Fig. 7f–i.

Results

Identification of *Drosophila* Ndc80 and Mis12/MIND complexes

Bioinformatic analysis revealed similarities between known Ndc80/Hec1 proteins and the predicted *Drosophila* *CG9938* product (data not shown). Similar findings from a systematic bioinformatic search for eukaryotic kinetochore proteins were described while this work was in progress (Meraldi et al. 2006). However, the observed similarities are only very limited and not correlated with evolutionary descent. Vertebrate Ndc80/Hec1 proteins are clearly more similar to fungal and plant homologs than to *CG9938*. To confirm therefore that the diverged *CG9938* indeed encodes the *Drosophila* Ndc80 homolog, we expressed an EGFP fusion protein in *Drosophila* S2R+ cells. The subcellular localization of the EGFP signals (data not shown) was found to correspond to the known behavior of human Ndc80/Hec1 (Chen et al. 1997; Martin-Lluesma et al. 2002). Moreover, the expected localization was subsequently also observed in transgenic embryos expressing EGFP-CG9938 fusion protein (Fig. 1a). During

Table 2 Axial positions of CKC components from pooled data

Protein	Number	d_{inter}[a] (nm)	Axial position[b] (nm)
Cenp-A/Cid	700	460	0
Cenp-C(C)	400	505	22
Cenp-C(N)	400	531	36
Spc25	700	540	40
Mis12	200	545	43
Nuf2	200	584	62

[a] All $d_{RRinter}$ and $d_{GGinter}$ measurements obtained for a given CKC in the analyses after pairwise expression of red and green fusion proteins (see Table 1) were summed and averaged to estimate the distance separating the signal maxima of sister kinetochores (d_{inter}). The differences between the d_{inter} values obtained for different CKC components were found to be significant according to Mann-Whitney U tests (p<0.05), except for the closely clustered Cenp-C(N), Spc25 and Mis12

[b] The separation of CKC components from Cenp-A/Cid along the inter sister kinetochore axis in a kinetochore was estimated by halving the difference between the d_{inter} values obtained for Cenp-A/Cid and a given CKC component. Axial separation is given relative to Cenp-A/Cid, which was set to zero

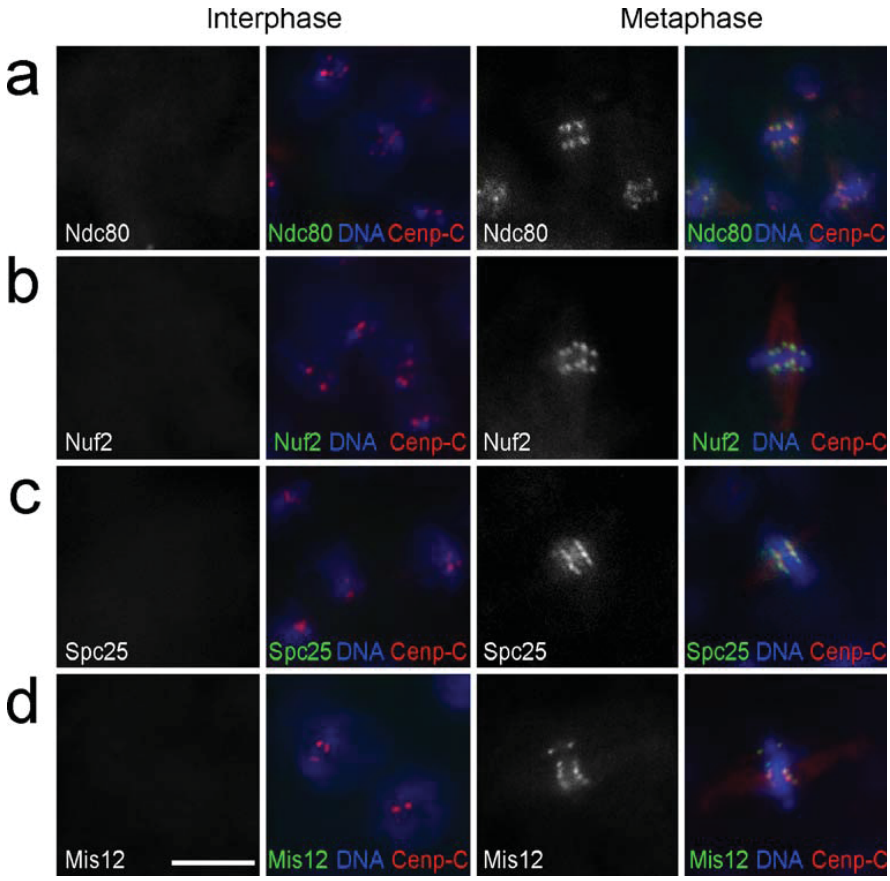

Fig. 1 Localization of *Drosophila* Ndc80 complex components and Mis12. Transgenic embryos expressing EGFP fused to either **a** Ndc80, **b** Nuf2, **c** Spc25, or **d** Mis12 were fixed at the stage when some cells progress through the 14th, asynchronous round of mitosis. Cells in interphase (*left panels*) and metaphase (*right panels*) after double labeling with an antibody against Cenp-C (Cenp-C) and a DNA stain (DNA) illustrate that the EGFP fusion proteins were only associated with centromeres during mitosis. Bar=5 μm

interphase, we did not observe signals above background (Fig. 1a). However, during mitosis, distinct signals were present at the kinetochore from prometaphase until late anaphase. The kinetochore signals were in close proximity to those obtained after double labeling with antibodies against the constitutive centromere protein Cenp-C (Fig. 1a). Based on this and the following evidence, we conclude that *CG9938* represents the *Drosophila Ndc80* gene.

In a genome-wide yeast two hybrid screen, *Drosophila* Ndc80 was reported to support a high confidence interaction with the predicted *CG8902* product (Giot et al. 2003). Moreover, this *CG8902* protein has a very limited similarity to the Ndc80 complex component Nuf2 (Meraldi et al. 2006). To evaluate whether this most distant Nuf2 family member displayed the expected kinetochore localization during mitosis, it was also expressed as an EGFP fusion protein in S2R+ cells. Its subcellular localization (data not shown) was found to be indistinguishable from that of vertebrate Ndc80 components. In addition, the same localization behavior was also observed in transgenic embryos expressing EGFP-CG8902 (Fig. 1b). We conclude that *CG8902* represents the *Drosophila Nuf2* gene.

An additional *Drosophila* Ndc80 interactor (Giot et al. 2003), the *CG7242* product, was observed to have limited similarity to the Ndc80 complex component Spc25. This gene was also identified as the most distant Spc25 family member in the bioinformatic study (Meraldi et al. 2006). An analysis of the intracellular localization of an EGFP fusion protein confirmed the expected kinetochore localization also in this case, both in transfected S2R+ cells (data not shown) and in transgenic embryos (Fig. 1c). We conclude that *CG7242* encodes *Drosophila* Spc25.

Apart from Ndc80 complex members, the bioinformatic search had revealed an additional putative *Drosophila* CKC component. The CG18156 protein was reported to have very limited sequence similarity to fungal and metazoan Mis12 proteins (Meraldi et al. 2006). Mis12 was originally identified in fission yeast and subsequently found to be a component of a conserved CKC complex called Mis12/MIND, which contains three additional proteins (Takahashi et al. 1994; De Wulf et al. 2003; Goshima et al. 2003; Obuse et al. 2004; Kline et al. 2006). Our localization studies after transfection of S2R+ cells with an EGFP-CG18156 expression construct revealed centromere localization. EGFP signals were found to be colocalized with

Cenp-A/Cid at the centromere not only during mitosis but also in interphase cells (Fig. 3a). This localization behavior corresponds to that of human Mis12, which is centromeric throughout the cell cycle except for a brief period in late telophase and early G1 (Kline et al. 2006; McAinsh et al. 2006). In transgenic embryos expressing EGFP-CG18156, we observed the centromeric signals only during mitosis (Fig. 1d). The apparent discrepancy concerning localization during interphase in transfected cells and transgenic embryos might reflect differences in expression levels and background signals. Primary and secondary structure comparisons (Fig. 4a) and kinetochore localization strongly support the proposal that *CG18156* encodes the *Drosophila* Mis12 homolog.

To demonstrate that the identified putative *Drosophila* Ndc80 complex components Ndc80, Nuf2, and Spc25 are indeed present in a complex in vivo, we used mass spectrometry to analyze the proteins coprecipitated with functional EGFP-Nuf2 or Spc25-mRFP from embryo extracts. Antibodies against EGFP and mRFP were used for immunoprecipitation. SDS-PAGE of the immunoprecipitates followed by silver staining revealed the presence of proteins specifically coprecipitated by EGFP-Nuf2 but not by an unrelated control EGFP fusion protein (Fig. 2a,b). Mass spectrometry revealed the identity of these proteins. Among the coimmunoprecipitated proteins were *Drosophila* Ndc80 and Spc25, as expected from the Ndc80 complex characterizations in yeast and vertebrates (Kline-Smith et al. 2005). Moreover, *Drosophila* Mis12 was also coimmunoprecipitated. In addition, we detected the products of the uncharacterized *CG13434* and *CG1558* in the EGFP-Nuf2 immunoprecipitates (Fig. 2a). An expression of corresponding EGFP fusion protein in S2R+ cells revealed a kinetochore localization in both cases (Fig. 3b,d). *CG13434* appears to encode a *Drosophila* homolog of Nnf1, which is a Mis12 complex component in yeast, vertebrates, and *C. elegans* (De Wulf et al. 2003; Nekrasov et al. 2003; Westermann et al. 2003; Cheeseman et al. 2004; Obuse et al. 2004; Kline et al. 2006). While primary structure comparisons revealed only very limited similarity (data not shown), secondary structure comparisons (Fig. 4a) provided additional support for our suggestion that *CG13434* encodes a *Drosophila* Nnf1 homolog. Interestingly, the sequenced genomes of melanogaster subgroup species (*D. melanogaster*, *D. simulans*, *D. sechellia*, *D. erecta*, *D. yakuba*) all encode a *CG13434* paralog, resulting from an apparent duplication of the primordial *CG13434* ortholog at the start of the melanogaster subgroup lineage (Fig. 4b). An EGFP fusion of this paralog, *CG31658*, was also observed to localize to the centromere during interphase and mitosis (Fig. 3c). Therefore, we will designate *CG13434* as *Nnf1a* and *CG31658* as *Nnf1b*. Reverse transcriptase (RT)-PCR experiments suggested coexpression

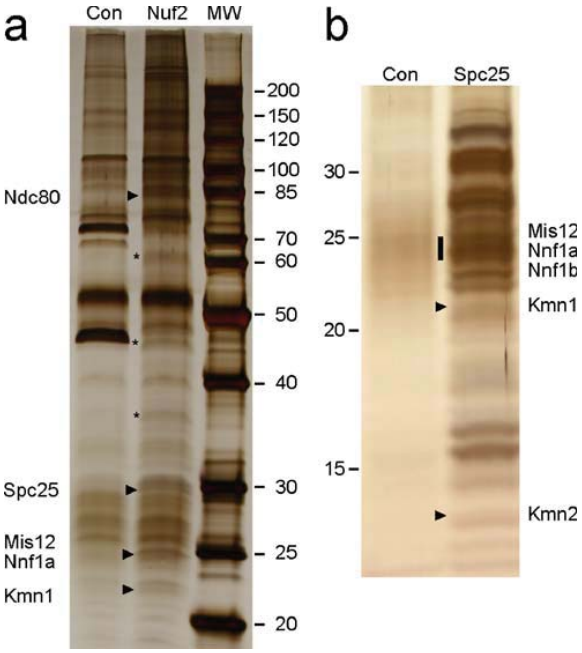

Fig. 2 Coimmunoprecipitation of Ndc80 and MIND complex components. Antibodies against EGFP or mRFP were used for immunoprecipitation from extracts of embryos expressing either EGFP-Nuf2 (Nuf2), Spc25-mRFP (Spc25) or an unrelated EGFP fusion protein (Con) for control. After SDS-PAGE and silver staining, selected bands were characterized by mass spectrometry. Numbers at margins indicate the molecular weight (kDa) of proteins in the marker lane (*MW*). **a** Bands enriched in the EGFP-Nuf2 immunoprecipitates (in comparison to control immunoprecipitates) were found to contain either only highly abundant cellular proteins (mostly ribosomal proteins) presumably reflecting nonspecific contaminations (*stars*) or also some rare proteins (as measured by their representation in EST data bases; *arrowheads*). As indicated by the names on the left margin, these rare proteins were found to be either components of the Ndc80 complex or putative Mis/MIND complex components. **b** In search of a potential *Spc24* homolog, the molecular weight range from 10–35 kDa with proteins in Spc25-mRFP immunoprecipitates was fractioned in slices and analyzed. The position and names of rare proteins (as measured by their representation in EST data bases) which were subsequently confirmed to be kinetochore proteins (see text) are indicated

of the Nnf1 paralogs at least during early *Drosophila* development (Fig. 4c). The coimmunoprecipitation experiments with Spc25-mRFP confirmed an association of the Ndc80 complex components (Ndc80, Nuf2, Spc25) with Mis12, Nnf1a, and Nnf1b (Fig. 2b; data not shown).

The *CG1558* product, which was coimmunoprecipitated with both EGFP-Nuf2 and Spc25-mRFP (Fig. 2), did not display significant similarities to known kinetochore network proteins in its predicted primary and secondary structure. After expression as an EGFP fusion protein, it was detected at the centromeres in both interphase and mitotic S2R+ cells (Fig. 3d). This localization behavior was identical to Mis12 but different from Ndc80, which

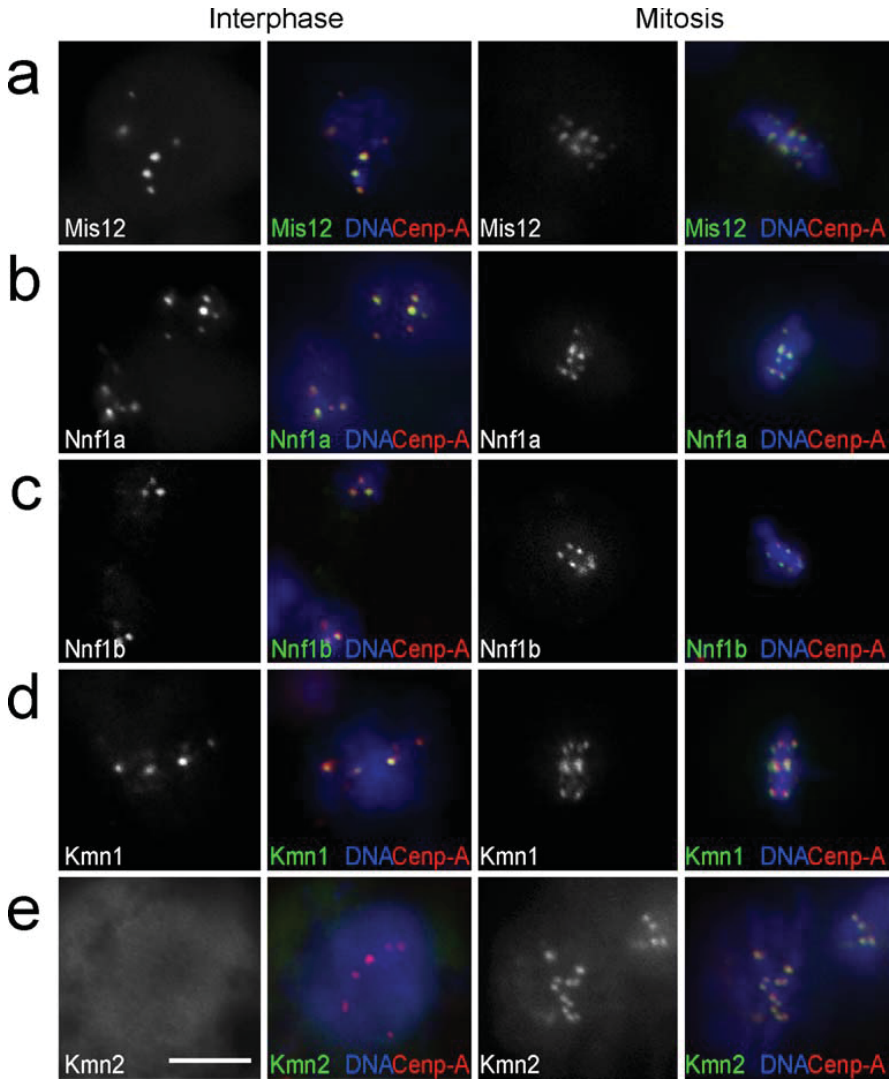

Fig. 3 Localization of additional *Drosophila* kinetochore network components in Schneider cells. S2R+ cells were transfected with constructs allowing expression of EGFP fused to either *Drosophila* **a** Mis12, **b** Nnf1a, **c** Nnf1b, **d** Kmn1, and **e** Kmn2. Fixed cells in interphase (*left panels*) and metaphase (*right panels*) after double labeling with an antibody against Cenp-A/Cid (*Cenp-A*) and a DNA stain (*DNA*) illustrate that association of EGFP fusion proteins with centromeres is either observed during **a**–**d** interphase and mitosis or **e** restricted to mitosis. Bar=5 μm

displayed a mitosis-specific kinetochore localization. Therefore, *CG1558* might encode an additional Mis12 complex subunit. Based on its size, it might correspond to Nsl1. However, both Nsl1 and Dsn1 are very poorly conserved Mis12 complex components according to a comparison of human, *C. elegans*, and yeast sequences. *CG1558* will be designated as *Kmn1* (kinetochore Mis12-Ndc80 network component 1).

Spc24 is present as a fourth 22–24 kDa subunit in both yeast and vertebrate Ndc80 complexes. We did not identify a potential *Drosophila* Spc24 homolog in the EGFP-Nuf2 and Spc25-mRFP immunoprecipitates within the corresponding molecular weight range. However, we detected (Fig. 2b) an 11 kDa product of the predicted gene *HDC12388* (Hild et al. 2003), which is not annotated in FlyBase. Expression of an EGFP fusion protein in S2R+ cells revealed kinetochore localization during mitosis (Fig. 3e). The *C. elegans* Ndc80 complex is thought to contain a rudimentary 11 kDa Spc24 version (Cheeseman et al. 2006, supporting speculations that *HDC12388* might correspond to *Drosophila Spc24*. According to secondary structure predictions, the *HDC12388* product might correspond to the C-terminal globular Spc24 domain (Fig. 4a). At present, *HDC12388* will be designated as *Kmn2*.

More extensive purification of the *Drosophila* Ndc80 and Mis12 complexes will be required for their complete characterization. However, our findings demonstrate that *Drosophila* expresses a network of interacting kinetochore proteins including particularly diverged homologs of the Mis12 and Ndc80 complexes. Although hardly evident

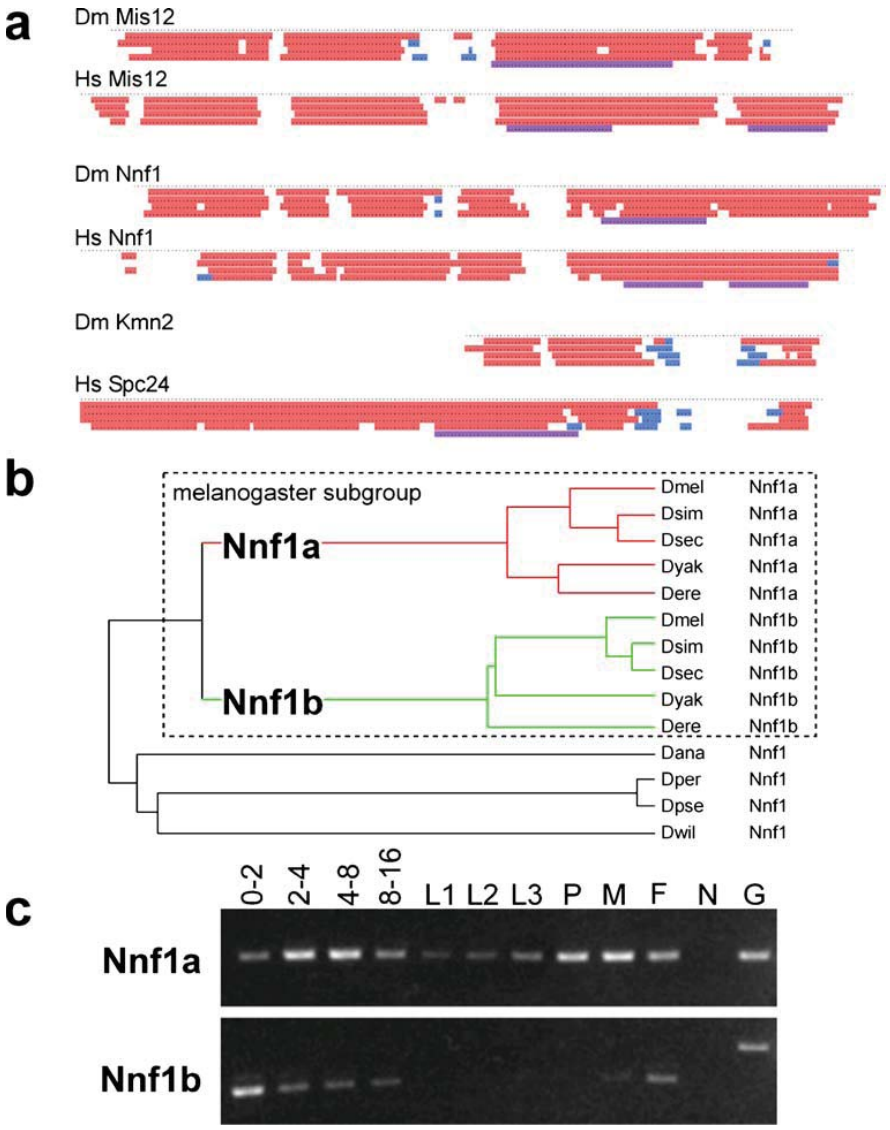

Fig. 4 Secondary structure and genomic comparison of *Drosophila* kinetochore proteins. **a** Secondary structure predictions reveal similarities between *Drosophila* (*Dm*) and human (*Hs*) homologs of Mis12, Nnf1, and between Drosophila Kmn2 and the C-terminal region of human Spc24. Each dot represents an amino acid position. The *lines with colored regions* illustrate predictions obtained with various algorithms (PSIPRED, JNET, PROF Quali and King, PROF Rost, COILS from *top to bottom*). α-helical regions are shown in *red*, regions with β-sheets in *blue* and coiled coils in *magenta*. **b** A phylogenetic tree was constructed after aligning the predicted amino acids sequences encoded by *Nnf1*-like genes in Drosophilid genomes. An *Nnf1* gene duplication resulting in the two paralogs *Nnf1a* and *Nnf1b* early after the divergence of the melanogaster subgroup lineage provides the most parsimonious explanation for the observed branching pattern. *D. melanogaster* (*Dmel*), *D. simulans* (*Dsim*), *D. sechellia* (*Dsec*), *D. yakuba* (*Dyak*), *D. erecta* (*Dere*), *D. ananassae* (*Dana*), *D. persimilis* (*Dper*), *D. pseudoobscura* (*Dpse*), *D. willistoni* (*Dwil*). Synteny considerations (data not shown) indicate that *Nnf1a* represents the primordial homolog. **c** The developmental expression pattern of *D. melanogaster Nnf1a* and *Nnf1b* was analyzed by RT-PCR experiments. The stages analyzed were: embryos 0–2 (*0–2*), 2–4 (*2–4*), 4–8 (*4–8*), and 8–16 (*8–16*) hours after egg deposition; larval stages (*L1*, *L2*, *L3*), pupae (*P*), adult males (*M*) and females (*F*). Control amplifications (*G*) from a cloned *Nnf1a* cDNA and an intron containing genomic *Nnf1b* fragment, as well as amplifications (*N*) with mock reverse transcribed mRNA demonstrated that the RT-PCR products were not derived from contaminating genomic DNA. The results are consistent with *Nnf1a* expression being correlated with mitotic proliferation and *Nnf1b* expression being germline-specific

from simple sequence comparisons, *Drosophila* kinetochore organization obviously shares extensive similarities with yeast, *C. elegans*, and vertebrates, which all have a kinetochore protein network containing the Mis12 and Ndc80 complexes (Wigge and Kilmartin 2001; De Wulf et al. 2003; Goshima et al. 2003; McCleland et al. 2003; Nekrasov et al. 2003; Westermann et al. 2003; Cheeseman et al. 2004; Obuse et al. 2004; Emanuele et al. 2005; Liu et al. 2005; Kline et al. 2006).

Essential functions of *Drosophila* Ndc80 complex components can be provided by fluorescent fusion protein variants

To define the functions of the *Drosophila* Ndc80 complex genetically, we identified and characterized mutations in *Nuf2* and *Spc25* (Fig. 5). A P element insertion in *Nuf2* had been isolated in a transposon mutagenesis screen for recessive lethal mutations (Oh et al. 2003). The insertion SH2276 was confirmed to be located 11 bp upstream of the initiation codon in the 5′ untranslated region (UTR) of *Nuf2*. The insertion leads to a partial loss of function. $Nuf2^{SH2276}$ homozygotes were found to develop to the late pupal stages and to die either as pharate adults or soon after eclosion. The *gEGFP-Nuf2* transgene was found to prevent the lethality of early $Nuf2^{SH2276}$ adults. Our findings demonstrate that *Drosophila Nuf2* is an essential gene. Moreover, they indicate that the EGFP-Nuf2 fusion protein is functional.

The piggyBac transposon insertion c00064 (Thibault et al. 2004) was mapped 38 bp upstream of the initiation codon in the 5′ UTR of *Spc25*. $Spc25^{c00064}$ homozygotes were found to die during the late larval stages. Compared to sibling control larvae, the mutants had only rudimentary imaginal discs and small brains, suggesting that Spc25 is required in mitotically proliferating cells. The late larval lethality of $Spc25^{c00064}$ homozygotes was prevented by a transgene driving expression of a Spc25-mRFP fusion protein under control of the *Spc25* regulatory region (*gSpc25-mRFP*). This transgene also complemented the recessive lethality of $Spc25^{A34-1}$, another independent allele previously isolated as a recessive lethal mutation (Hilliker et al. 1980). Based on these observations, we conclude that *Drosophila Spc25* is an essential gene. In addition, the Spc25-mRFP fusion protein must be functional.

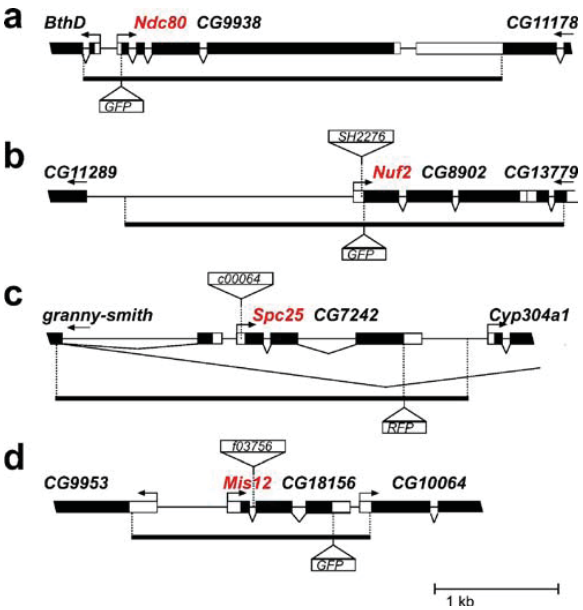

Fig. 5 Genetic characterization of Ndc80 and putative MIND complex components. Gene models are shown for **a** *Ndc80/CG9938*, **b** *Nuf2/CG8902*, **c** *Spc25/CG7242*, and **d** *Mis12/CG18156*. Moreover, transposon insertions present in mutant alleles are indicated by *triangles* above the gene models. In addition, the genomic fragments used for transgene constructions are indicated by the *solid lines* below the gene models. The position where the EGFP or mRFP coding sequence was inserted in these transgenes is illustrated by the *triangles* below the gene models

Mapping of centromere and kinetochore proteins in native chromosomes at high resolution

The accuracy of distance measurements can be increased beyond the diffraction-limited resolution of light microscopy by analyzing the spatial separation between signals from two different fluorophores (Stelzer 1998; Shimogawa et al. 2006). Therefore, we constructed a number of strains that coexpressed both a red and a green fluorescent CKC component. Eggs were collected from these strains and aged to the syncytial blastoderm stage where thousands of nuclei progress synchronously through mitoses. Embryos were gently squashed in a buffer containing a DNA stain. Native chromosomes released from mitotic embryos were analyzed by wide-field fluorescence microscopy. Analyses with embryos expressing red fluorescent Cenp-A/Cid and a green fluorescent microtubule binding protein demonstrated that spindles did not survive the squashing procedure and that sister kinetochores of the released chromosomes were not under tension (Fig. 6a).

Pixel intensities of red and green CKC signals in native chromosomes released from prometa- or metaphase embryos were quantified along the axis connecting the two sister kinetochores (Fig. 7a–c). The distance between the intensity maxima in the two sister kinetochores was determined. The difference between the distances separating the green ($d_{GGinter}$) and red ($d_{RRinter}$) fluorescent maxima, respectively, was calculated and divided by two to obtain an estimate for the distance ($d_{RGintra}$) between the red and the green fluorescent component within a CKC (Fig. 7d). Indepen-

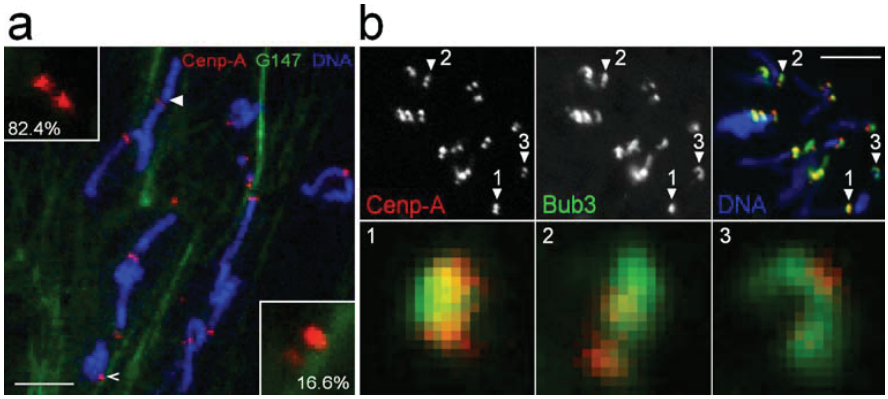

Fig. 6 Association of released native chromosomes with spindles and mitotic checkpoint proteins. **a** To evaluate whether and how kinetochores of released native chromosomes interact with spindle remnants, we performed experiments with embryos expressing a green fluorescent microtubule binding protein (*G147*) and red fluorescent Cenp-A/Cid (Cenp-A). 82.4% of the chromosomes (n=319) had kinetochores which showed no association with microtubules, as illustrated by the inset in the *upper left corner* which displays the kinetochores indicated by the *filled arrowhead* at high magnification. 16.6% had kinetochores with a lateral association with microtubules, as illustrated by the inset in the lower right corner which displays the kinetochores indicated by the *open arrowhead*. 0.3% had kinetochores with a monopolar end-on attachment. 0.6% appeared to have a bipolar attachment with microtubules which however appeared to be so disorganized that the attachment presumably did not result in significant tension across the sister kinetochores. Bar=5 μm. **b** Native chromosomes were released from embryos expressing red fluorescent Cenp-A/Cid and green fluorescent Bub3. In contrast to Cenp-A/Cid, the localization of EGFP-Bub3 in kinetochores from different chromosomes was found to be highly variable, as illustrated by the kinetochores indicated by *numbered arrowheads* in the *top panels* and shown at high magnification in the *lower panels*. Bar=5 μm

dent estimates for d_{RGintra} from at least 100 different chromosomes released from at least five different embryos were averaged to yield an estimate of the distance which separates a given pair of CKC proteins (Table 1). These pair separation values are represented by double arrows in Fig. 7e. Moreover, as an additional estimate for the spatial arrangement of the CKC proteins, we determined the average of all d_{GGinter} and d_{RRinter} values obtained for a given CKC protein in all our analyses. For instance, in the case of Cenp-A/Cid, the 500 d_{RRinter} measurements and 200 d_{GGinter} measurements resulted in an average value for the separation of the two sister kinetochore Cenp-A/Cid signal maxima of 460 nm. From the separation differences apparent when different CKC components were compared (Table 2), the CKC components were positioned along the centromere-spindle axis as indicated by the vertical colored lines in Fig. 7e.

To determine the position of a spindle checkpoint protein in native chromosomes, we used a strain coexpressing red fluorescent Cenp-A/Cid and green fluorescent Bub3. Various mitotic spindle checkpoint components have been reported to localize to the outermost, fibrous corona region of the kinetochore in intact cells (Vos et al. 2006). In our native chromosome preparations, the localization of EGFP-Bub3 was found to be highly variable on different kinetochores (Fig. 6b), precluding a precise mapping.

The following control experiments support the accuracy of our CKC map. We generated a strain in which one of the two transgenes generated green and the other red fluorescent Cenp-A/Cid. In native chromosomes prepared from this strain (Fig. 7a,b), the red or green fluorescent proteins are expected to be perfectly colocalized. Our distance measurement resulted in d_{RGintra}=5 nm (Table 1). In an analogous analysis with a strain coexpressing red and green fluorescent Spc25, we obtained the expected d_{RGintra}= 0 nm (Table 1). These distances were far smaller than the d_{RGintra} values obtained for pairs of different proteins (Table 1). Moreover, the separation between signals from fluorescent protein tags at the N and the C termini of Cenp-C was determined twice using embryos expressing either EGFP-Cenp-C-mRFP or the reverse tag configuration mRFP-Cenp-C-EGFP, yielding 15 and 8 nm, respectively (Table 1). Finally, the additive behavior of different d_{RGintra} values was found to correspond closely to the expectations. For instance, the sum of the measured distances between Cenp-A/Cid and Spc25 signals (d_{RGinter}=49 nm) on one hand and Spc25 and Nuf2 signals (d_{RGinter}=15 nm) on the other hand is only 5 nm different from the measured separation between Cenp-A/Cid and Nuf2 signals (d_{RGinter}= 69 nm). Based on all these findings, we expect the correct signal maxima to be within ±5 nm of the positions indicated in Fig. 7e. We emphasize that our CKC map (Fig. 7e) was obtained by averaging values with distributions illustrated in Fig. 7f–i. As discussed below, averaging has important consequences for the interpretation of our CKC map.

Discussion

Our identification of *Drosophila* kinetochore proteins further exposes hidden similarities of kinetochore design in eukaryotes. In addition to the previously known, highly diverged Cenp-A/Cid and Cenp-C homologs (Henikoff et al. 2000; Heeger et al. 2005), *Drosophila* expresses similarly diverged homologs of the Mis12 and Ndc80 complex network, which is also present in yeast, *C. elegans*, vertebrates, and presumably in plants as well (Sato et al. 2005; Meraldi et al. 2006; Vos et al. 2006). We have been able to position several of these ubiquitous CKC components along the intersister kinetochore axis with unprecedented spatial resolution. Early *Drosophila* embryos allow an efficient isolation of native mitotic chromosomes and thereby imaging with reduced background. Moreover, transgenic strains allow the expression of fluorescent fusion proteins, which were demonstrated to be fully functional by genetic complementation tests.

We have determined the position of fluorescent signal maxima within the kinetochore of native chromosomes released from embryos expressing fluorescent CKC fusion proteins. Our CKC map (Fig. 7e) is based on averaged data from hundreds of analyzed chromosomes. Therefore, its interpretation depends critically on the variability of kinetochore organization in individual chromosomes. For instance, in principle, a given component might be localized on the inner kinetochore side in 50% of the chromatids and on the outer side in the other half of the chromatids, resulting in a misleading central positioning in our CKC map. Theoretically, such variability should widen the distribution of the distances measured in individual chromosomes (Fig. 7f–i). However, kinetochore width is smaller than the spreading of the image of a point light source in the microscope, and several additional factors (like background, noise, pixelation) further limit the precision of our measurements. The effect of positional variability on distribution width of the measured values would therefore be very subtle. Moreover, none of the known CKC proteins has been firmly demonstrated to be a spatially invariable kinetochore component, precluding comparisons to an established standard distribution. However, the reproducible trilaminar structure of the kinetochore during prometaphase which has been documented by EM, argues strongly against extensive organizational variability. We emphasize that the difficulties to detect subtle alterations in the distribution width of the measurements obtained for a given CKC component has important consequences even under the assumption that the spatial distribution of CKC components is essentially invariable in individual kinetochores. These difficulties prevent conclusions concerning the width occupied by a given CKC component within a kinetochore. For instance, Mis12 could either be confined to a single layer in the middle of the kinetochore or spread throughout the kinetochore, and both localization patterns would result in a central signal maximum. However, biochemical analyses of kinetochore proteins, which will be discussed in part below, have so far revealed highly specific interactions, arguing strongly for a precise and restricted localization of CKC components. The following discussion is therefore based on the unproven but likely assumption that the kinetochore represents a precisely defined layered structure.

Based on previous analyses, Cenp-A, Cenp-C, and Mis12 are thought to be components of the inner plate of the characteristic trilaminar kinetochore structure apparent in the EM (Kline et al. 2006; Vos et al. 2006). Our analyses indicate a significant separation between the inner most CKC component Cenp-A and all other CKC components analyzed here. Recently, Cenp-A nucleosomes purified from human cells were found to be intimately associated with the five proteins Cenp-M, Cenp-N, Cenp-T, Cenp-U, and Cenp-H in addition to Cenp-C (Foltz et al. 2006; Izuta et al. 2006; Okada et al. 2006). The apparent space between Cenp-A and Cenp-C might therefore be occupied by some of those proteins.

Many immunolocalization studies, including a recent study with *Drosophila* cells (Maiato et al. 2006), have failed to detect a comparable extensive spatial separation between Cenp-A/Cid and Cenp-C. However, immunolocalization with human chromosomes also revealed little overlap between Cenp-A and Cenp-C, with the latter extending over the top and bottom of a Cenp-A cylinder (Blower et al. 2002). Antigen accessibility problems, which were not excluded by Blower et al. (2002), cannot affect our concurrent findings.

In this paper, Cenp-C is shown to be spread in a polar orientation across a central CKC region. The C-terminal domain of Cenp-C, which contains the most conserved region including the CENP-C motif (Talbert et al. 2004; Heeger et al. 2005), points toward the centromeric DNA. These C-terminal sequences are connected via minimally conserved spacer sequences to the N-terminal domain which is oriented toward the kinetochore spindle fibers. The N-terminal region of *D. melanogaster* Cenp-C contains some blocks which are highly conserved among Drosophilids (Heeger et al. 2005). These blocks might be involved in recruiting the next layer of kinetochore proteins which we suggest to include the Ndc80 and Mis12 complexes. We find Mis12 to be close to the N-terminal Cenp-C region. Moreover, the Ndc80 complex component Spc25 appears to be even a bit closer but well separated by about 20 nm from the other Ndc80 component Nuf2. Apart from a polar Cenp-C orientation, our analyses therefore also indicate a polar orientation for the Ndc80 complex.

The tetrameric Ndc80 complex has a highly elongated, rod-like structure in vitro (Ciferri et al. 2005; Wei et al.

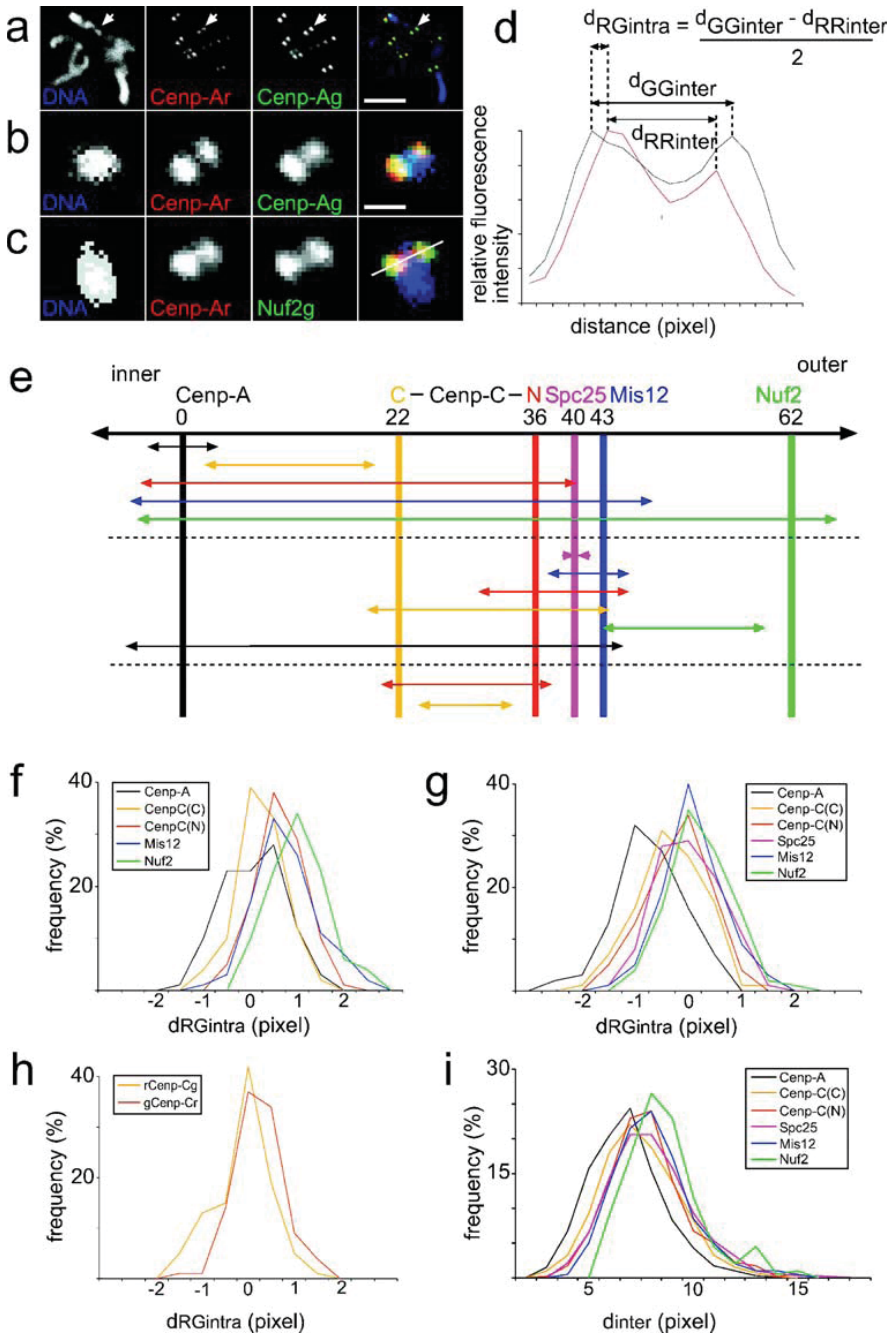

2005). The globular N-terminal domains of Ndc80 and Nuf2 are present on one end of the rod. The remainder of these two subunits forms an extended coiled coil which is further prolonged at its C-terminal end by binding to the N-terminal coiled coil region of the Spc24/Spc25 dimer. Closely associated C-terminal globular domains of Spc24 and Spc25 (Wei et al. 2006) form the other end of the rod. Scanning force microscopy and EM analyses have indicated that the coiled coil region separating the globular domains at the end of the Ndc80 complex has an extension of about 40 nm (Ciferri et al. 2005; Wei et al. 2005). This is twofold longer than the distance that we have observed

◀ **Fig. 7** Axial positions of different kinetochore proteins along the inter sister kinetochore axis. **a** Native chromosomes released from syncytial embryos coexpressing a red and a green fluorescent CKC component were labeled with a DNA stain (*DNA*). The appearance of the native chromosomes with red (*Cenp-Ar*) and green (*Cenp-Ag*) fluorescent Cenp-A/Cid is illustrated at low magnification. Bar=5 μm. **b** The fourth chromosome indicated by the *white arrows* in a is shown at high magnification. Bar=0.5 μm. **c** A fourth chromosome from an embryo expressing red fluorescent Cenp-A/Cid (*Cenp-Ar*) and green fluorescent Nuf2 (*Nuf2g*) is shown at the same magnification as in **b**. These high magnification views, **b** and **c**, display the pixel resolution as acquired. **d** For an estimation of the spatial separation between a red and a green fluorescent CKC component, signal intensities were quantified along the axis running through the two sister kinetochores, as illustrated by the white line in **c**. The displayed intensity profiles are from the chromosome shown in **c**. The spatial separation (d_{RGintra}) was calculated by halving the difference between the distances separating the red (d_{RRinter}) and green (d_{GGinter}) signal maxima of the sister kinetochores, as indicated by the equation. **e** Scheme summarizing the positions of the analyzed CKC components along the spindle axis. *Double arrows* represent the spatial separation as revealed by the pairwise analyses outlined in **a**–**d** with hundreds of native chromosomes (see also Table 1). *Arrows* above the *upper dashed line* represent data from experiments comparing the distance between red fluorescent Cenp-A/Cid and various green fluorescent CKC components. Analogous analyses of the distance between various green fluorescent CKC components and red fluorescent Spc25 are represented by the *arrows between the dashed lines*. The *arrows below the lower dashed lines* represent experiments after expression of Cenp-C versions labeled with both a green and a red fluorescent protein at the N and C termini. Color coding specifies the green fluorescent component in all these pairwise analyses. The *vertical lines* indicate the position of CKC components as revealed by pooling all d_{RRinter} and d_{GGinter} values obtained for a given CKC component during the pairwise analyses (see Table 2). The numbers indicate the spatial separation (*nm*) from the innermost centromere component Cenp-A/Cid, which was set to zero. In case of Cenp-C, the N terminus (*N*) and the C terminus (*C*) were mapped. **f**–**i** Histogram curves illustrate the distribution of the d_{RGintra} values obtained in the pairwise analyses with chromosomes from embryos expressing red fluorescent Cenp-A/Cid and green CKC components, in **f**, as well as in the analogous analyses with red fluorescent Spc25 in combination with green CKC components, in **g**, or with Cenp-C versions carrying red and green fluorescent proteins at N and C termini, in **h**. Moreover, **i** the distribution of the d_{inter} values, i.e., all the d_{RRinter} and d_{GGinter} measurements obtained for a given CKC components (see Table 2) are displayed as well

between fluorescent proteins at the N and C termini of Nuf2 and Spc25 in kinetochores of native *Drosophila* chromosomes. Many of the elongated Ndc80 complexes might not be perfectly oriented along the spindle axis, especially as the kinetochores in our preparations are not under tension. Such a nonuniform orientation could result in spatial distributions of the N and C termini of Nuf2 and Spc25, respectively, with signal maxima that are more closely spaced than their separation within an isolated complex. An analysis of the positions of CKC components in chromosomes that are bi-oriented within the spindle and under tension would clearly be of interest. However, the increased background levels present in living embryos have so far precluded such analyses.

Our observed polar orientation of the Ndc80 complex within the kinetochore confirms the findings of a recent independent study (Deluca et al. 2006). Moreover, the observation that Ndc80 and Nuf2 kinetochore localization is no longer observed in the absence of Spc24 or Spc25 (Bharadwaj et al. 2004) is consistent but does not prove an orientation of the complex with inner Spc24/Spc25 and outer Ndc80/Nuf2 globular domains, because absence of Spc24 or Spc25 for instance might simply result in an instability of other complex components, as often observed in the case of stable complexes.

In budding yeast, the Ndc80 complex has been proposed to function as a connection between the inner components (CBF3 complex, Cenp-A/Cse4 nucleosome, Cenp-C/Mif2, Mis12/MIND complex) and the Dam/DASH complex which is required for bi-orientation and appears to form a ring around the single microtubule attaching to a yeast kinetochore (Cheeseman et al. 2001; Shang et al. 2003; Tanaka et al. 2005; Westermann et al. 2006). More recently, bacterial expression of the *C. elegans* KMN network composed of the Spc105/KNL-1, Mis12 and Ndc80 complexes has led to a convincing identification of two independent sites in this protein network which can bind directly to microtubules in vitro (Cheeseman et al. 2006). One of these microtubule binding sites is present within Spc105/KNL-1. The other is found within the globular N-terminal Ndc80 domain (Cheeseman et al. 2006) which is known to be within the outer kinetochore plates where kinetochore microtubules terminate (DeLuca et al. 2005). In vitro, the Ndc80 complex binds to microtubules at an angle (Cheeseman et al. 2006). A corresponding orientation of the Ndc80 complex within the kinetochore is fully consistent with our finding that the separation of the terminal globular domains of Spc25 and Nuf2 along the intersister kinetochore axis appears to be less than their separation along the axis of isolated complexes (Ciferri et al. 2005; Wei et al. 2005). Accordingly, the "barbed end" of microtubules decorated with the Ndc80 complex would be predicted to correspond to the plus end.

In conclusion, in addition to the identification of *Drosophila* Ndc80 and Mis12 complex components, our work provides a highly resolved structural framework integrating the most widely studied ubiquitous CKC components and a precise method for a future incorporation of additional proteins.

Acknowledgement We thank Brigitte Jaunich for technical help, as well as Julia Dürr and Sabine Herzog for the help with antibody production. Research in the laboratory of Karl Mechtler was supported by the 6th Framework Programme of the European Union via the Integrated Project MitoCheck and the Austrian Proteomics Platform (APP) within the Austrian Genome Program (GENAU), Vienna, Austria. In addition, this work was also supported by the Fonds der Deutschen Chemie and by a grant from the Deutsche Forschungsgemeinschaft (DFG Le 987/3–3 and 3–4).

References

Bharadwaj R, Qi W, Yu H (2004) Identification of two novel components of the human NDC80 kinetochore complex. J Biol Chem 279:13076–13085

Biegert A, Mayer C, Remmert M, Soding J, Lupas AN (2006) The MPI bioinformatics toolkit for protein sequence analysis. Nucleic Acids Res 34:W335–W339

Blower MD, Sullivan BA, Karpen GH (2002) Conserved organization of centromeric chromatin in flies and humans. Dev Cell 2:319–330

Blum H, Beier H, Gross HJ (1987) Improved silver staining of plant proteins, RNA and DNA in polyacrylamide gels. Electrophoresis 8:93–99

Cheeseman IM, Brew C, Wolyniak M, Desai A, Anderson S, Muster N, Yates JR, Huffaker TC, Drubin DG, Barnes G (2001) Implication of a novel multiprotein Dam1p complex in outer kinetochore function. J Cell Biol 155:1137–1145

Cheeseman IM, Niessen S, Anderson S, Hyndman F, Yates JR 3rd, Oegema K, Desai A (2004) A conserved protein network controls assembly of the outer kinetochore and its ability to sustain tension. Genes Dev 18:2255–2268

Cheeseman IM, Chappie JS, Wilson-Kubalek EM, Desai A (2006) The conserved KMN network constitutes the core microtubule-binding site of the kinetochore. Cell 127:983–997

Chen Y, Riley DJ, Chen PL, Lee WH (1997) HEC, a novel nuclear protein rich in leucine heptad repeats specifically involved in mitosis. Mol Cell Biol 17:6049–6056

Ciferri C, De Luca J, Monzani S, Ferrari KJ, Ristic D, Wyman C, Stark H, Kilmartin J, Salmon ED, Musacchio A (2005) Architecture of the human ndc80–hec1 complex, a critical constituent of the outer kinetochore. J Biol Chem 280:29088–29095

Cooke CA, Schaar B, Yen TJ, Earnshaw WC (1997) Localization of CENP-E in the fibrous corona and outer plate of mammalian kinetochores from prometaphase through anaphase. Chromosoma 106:446–455

DeLuca JG, Dong Y, Hergert P, Strauss J, Hickey JM, Salmon ED, McEwen BF (2005) Hec1 and nuf2 are core components of the kinetochore outer plate essential for organizing microtubule attachment sites. Mol Biol Cell 16:519–531

Deluca JG, Gall WE, Ciferri C, Cimini D, Musacchio A, Salmon ED (2006) Kinetochore microtubule dynamics and attachment stability are regulated by hec1. Cell 127:969–982

De Wulf P, McAinsh AD, Sorger PK (2003) Hierarchical assembly of the budding yeast kinetochore from multiple subcomplexes. Genes Dev 17:2902–2921

Emanuele MJ, McCleland ML, Satinover DL, Stukenberg PT (2005) Measuring the stoichiometry and physical interactions between components elucidates the architecture of the vertebrate kinetochore. Mol Biol Cell 16:4882–4892

Foltz DR, Jansen LE, Black BE, Bailey AO, Yates JR 3rd, Cleveland DW (2006) The human CENP-A centromeric nucleosome-associated complex. Nat Cell Biol 8:458–469

Fujita Y, Hayashi T, Kiyomitsu T, Toyoda Y, Kokubu A, Obuse C, Yanagida M (2007) Priming of centromere for CENP-A recruitment by human hMis18alpha, hMis18beta, and M18BP1. Dev Cell 12:17–30

Giot L, Bader JS, Brouwer C, Chaudhuri A, Kuang B, Li Y, Hao YL, Ooi CE, Godwin B, Vitols E, Vijayadamodar G, Pochart P, Machineni H, Welsh M, Kong Y, Zerhusen B, Malcolm R, Varrone Z, Collis A, Minto M, Burgess S, McDaniel L, Stimpson E, Spriggs F, Williams J, Neurath K, Ioime N, Agee M, Voss E, Furtak K, Renzulli R, Aanensen N, Carrolla S, Bickelhaupt E, Lazovatsky Y, DaSilva A, Zhong J, Stanyon CA, Finley RL Jr, White KP, Braverman M, Jarvie T, Gold S, Leach M, Knight J, Shimkets RA, McKenna MP, Chant J, Rothberg JM (2003) A protein interaction map of *Drosophila melanogaster*. Science 302:1727–1736

Goshima G, Kiyomitsu T, Yoda K, Yanagida M (2003) Human centromere chromatin protein hMis12, essential for equal segregation, is independent of CENP-A loading pathway. J Cell Biol 160:25–39

Harlow E, Lane D (1988) Antibodies. A laboratory manual. Cold Spring Harbor Laboratory, New York

Heeger S, Leismann O, Schittenhelm R, Schraidt O, Heidmann S, Lehner CF (2005) Genetic interactions of Separase regulatory subunits reveal the diverged Drosophila Cenp-C homolog. Genes Dev 19:2041–2053

Henikoff S, Ahmad K, Platero JS, van Steensel B (2000) Heterochromatic deposition of centromeric histone H3-like proteins. Proc Natl Acad Sci USA 97:716–721

Hild M, Beckmann B, Haas SA, Koch B, Solovyev V, Busold C, Fellenberg K, Boutros M, Vingron M, Sauer F, Hoheisel JD, Paro R (2003) An integrated gene annotation and transcriptional profiling approach towards the full gene content of the Drosophila genome. Genome Biol 5:R3

Hilliker AJ, Clark SH, Chovnick A, Gelbart WM (1980) Cytogenetic analysis of the chromosomal region immediately adjacent to the rosy locus in *Drosophila melanogaster*. Genetics 95:95–110

Hoskins RA, Nelson CR, Berman BP, Laverty TR, George RA, Ciesiolka L, Naeemuddin M, Arenson AD, Durbin J, David RG, Tabor PE, Bailey MR, DeShazo DR, Catanese J, Mammoser A, Osoegawa K, de Jong PJ, Celniker SE, Gibbs RA, Rubin GM, Scherer SE (2000) A BAC-based physical map of the major autosomes of *Drosophila melanogaster*. Science 287:2271–2274

Izuta H, Ikeno M, Suzuki N, Tomonaga T, Nozaki N, Obuse C, Kisu Y, Goshima N, Nomura F, Nomura N, Yoda K (2006) Comprehensive analysis of the ICEN (interphase centromere complex) components enriched in the CENP-A chromatin of human cells. Genes Cells 11:673–684

Kline-Smith SL, Sandall S, Desai A (2005) Kinetochore-spindle microtubule interactions during mitosis. Curr Opin Cell Biol 17:35–46

Kline SL, Cheeseman IM, Hori T, Fukagawa T, Desai A (2006) The human Mis12 complex is required for kinetochore assembly and proper chromosome segregation. J Cell Biol 173:9–17

Liu X, McLeod I, Anderson S, Yates JR 3rd, He X (2005) Molecular analysis of kinetochore architecture in fission yeast. EMBO J 24:2919–2930

Liu ST, Rattner JB, Jablonski SA, Yen TJ (2006) Mapping the assembly pathways that specify formation of the trilaminar kinetochore plates in human cells. J Cell Biol 175:41–53

Maiato H, Hergert PJ, Moutinho-Pereira S, Dong Y, Vandenbeldt KJ, Rieder CL, McEwen BF (2006) The ultrastructure of the kinetochore and kinetochore fiber in Drosophila somatic cells. Chromosoma 115:469–480

Martin-Lluesma S, Stucke VM, Nigg EA (2002) Role of Hec1 in spindle checkpoint signaling and kinetochore recruitment of Mad1/Mad2. Science 297:2267–2270

McAinsh AD, Tytell JD, Sorger PK (2003) Structure, function, and regulation of budding yeast kinetochores. Annu Rev Cell Dev Biol 19:519–539

McAinsh AD, Meraldi P, Draviam VM, Toso A, Sorger PK (2006) The human kinetochore proteins Nnf1R and Mcm21R are required for accurate chromosome segregation. EMBO J 25:4033–4049

McCleland ML, Gardner RD, Kallio MJ, Daum JR, Gorbsky GJ, Burke DJ, Stukenberg PT (2003) The highly conserved Ndc80 complex is required for kinetochore assembly, chromosome congression, and spindle checkpoint activity. Genes Dev 17:101–114

McEwen BF, Hsieh CE, Mattheyses AL, Rieder CL (1998) A new look at kinetochore structure in vertebrate somatic cells using

high-pressure freezing and freeze substitution. Chromosoma 107:366–375
Meraldi P, McAinsh AD, Rheinbay E, Sorger PK (2006) Phylogenetic and structural analysis of centromeric DNA and kinetochore proteins. Genome Biol 7:R23
Moore LL, Roth MB (2001) HCP-4, a CENP-C-like protein in *Caenorhabditis elegans*, is required for resolution of sister centromeres. J Cell Biol 153:1199–1208
Morin X, Daneman R, Zavortink M, Chia W (2001) A protein trap strategy to detect GFP-tagged proteins expressed from their endogenous loci in Drosophila. Proc Natl Acad Sci USA 98:15050–15055
Nekrasov VS, Smith MA, Peak-Chew S, Kilmartin JV (2003) Interactions between centromere complexes in *Saccharomyces cerevisiae*. Mol Biol Cell 14:4931–4946
Obuse C, Iwasaki O, Kiyomitsu T, Goshima G, Toyoda Y, Yanagida M (2004) A conserved Mis12 centromere complex is linked to heterochromatic HP1 and outer kinetochore protein Zwint-1. Nat Cell Biol 6:1135–1141
Oegema K, Desai A, Rybina S, Kirkham M, Hyman AA (2001) Functional analysis of kinetochore assembly in *Caenorhabditis elegans*. J Cell Biol 153:1209–1226
Oh SW, Kingsley T, Shin HH, Zheng Z, Chen HW, Chen X, Wang H, Ruan P, Moody M, Hou SX (2003) A P-element insertion screen identified mutations in 455 novel essential genes in Drosophila. Genetics 163:195–201
Okada M, Cheeseman IM, Hori T, Okawa K, McLeod IX, Yates JR 3rd, Desai A, Fukagawa T (2006) The CENP-H–I complex is required for the efficient incorporation of newly synthesized CENP-A into centromeres. Nat Cell Biol 8:446–457
Ormo M, Cubitt AB, Kallio K, Gross LA, Tsien RY, Remington SJ (1996) Crystal structure of the Aequorea victoria green fluorescent protein. Science 273:1392–1395
Richards S, Liu Y, Bettencourt BR, Hradecky P, Letovsky S, Nielsen R, Thornton K, Hubisz MJ, Chen R, Meisel RP, Couronne O, Hua S, Smith MA, Zhang P, Liu J, Bussemaker HJ, van Batenburg MF, Howells SL, Scherer SE, Sodergren E, Matthews BB, Crosby MA, Schroeder AJ, Ortiz-Barrientos D, Rives CM, Metzker ML, Muzny DM, Scott G, Steffen D, Wheeler DA, Worley KC, Havlak P, Durbin KJ, Egan A, Gill R, Hume J, Morgan MB, Miner G, Hamilton C, Huang Y, Waldron L, Verduzco D, Clerc-Blankenburg KP, Dubchak I, Noor MA, Anderson W, White KP, Clark AG, Schaeffer SW, Gelbart W, Weinstock GM, Gibbs RA (2005) Comparative genome sequencing of Drosophila pseudoobscura: chromosomal, gene, and cis-element evolution. Genome Res 15:1–18
Riedel CG, Katis VL, Katou Y, Mori S, Itoh T, Helmhart W, Galova M, Petronczki M, Gregan J, Cetin B, Mudrak I, Ogris E, Mechtler K, Pelletier L, Buchholz F, Shirahige K, Nasmyth K (2006) Protein phosphatase 2A protects centromeric sister chromatid cohesion during meiosis I. Nature 441:53–61
Rieder CL (1982) The formation, structure, and composition of the mammalian kinetochore and kinetochore fiber. Int Rev Cytol 79:1–58
Rieder CL (2005) Kinetochore fiber formation in animal somatic cells: dueling mechanisms come to a draw. Chromosoma 114:310–318
Saitoh H, Tomkiel J, Cooke CA, Ratrie H 3rd, Maurer M, Rothfield NF, Earnshaw WC (1992) CENP-C, an autoantigen in scleroderma, is a component of the human inner kinetochore plate. Cell 70:115–125
Sato H, Shibata F, Murata M (2005) Characterization of a Mis12 homologue in Arabidopsis thaliana. Chromosome Res 13:827–834
Schueler MG, Sullivan BA (2006) Structural and functional dynamics of human centromeric chromatin. Annu Rev Genomics Hum Genet 7:301–313
Schuh M, Lehner CF, Heidmann S (2007) Incorporation of Drosophila Cid/Cenp-A and Cenp-C into centromeres during early embryonic anaphase. Curr Biol 17:237–243
Shang C, Hazbun TR, Cheeseman IM, Aranda J, Fields S, Drubin DG, Barnes G (2003) Kinetochore protein interactions and their regulation by the Aurora kinase Ipl1p. Mol Biol Cell 14:3342–3355
Shimogawa MM, Graczyk B, Gardner MK, Francis SE, White EA, Ess M, Molk JN, Ruse C, Niessen S, Yates JR 3rd, Muller EG, Bloom K, Odde DJ, Davis TN (2006) Mps1 phosphorylation of Dam1 couples kinetochores to microtubule plus ends at metaphase. Curr Biol 16:1489–1501
Stapleton M, Carlson J, Brokstein P, Yu C, Champe M, George R, Guarin H, Kronmiller B, Pacleb J, Park S, Wan K, Rubin GM, Celniker SE (2002) A Drosophila full-length cDNA resource. Genome Biol 3:RESEARCH0080.0081-0080.0088
Stelzer EH (1998) Contrast, resolution, pixelation, dynamic range and signal-to-noise ratio: fundamental limits to resolution in fluorescence light microscopy. J Microsc 189:15–24
Sullivan BA, Karpen GH (2004) Centromeric chromatin exhibits a histone modification pattern that is distinct from both euchromatin and heterochromatin. Nat Struct Mol Biol 11:1076–1083
Takahashi K, Yamada H, Yanagida M (1994) Fission yeast minichromosome loss mutants mis cause lethal aneuploidy and replication abnormality. Mol Biol Cell 5:1145–1158
Talbert PB, Bryson TD, Henikoff S (2004) Adaptive evolution of centromere proteins in plants and animals. J Biol 3:18
Tanaka K, Mukae N, Dewar H, van Breugel M, James EK, Prescott AR, Antony C, Tanaka TU (2005) Molecular mechanisms of kinetochore capture by spindle microtubules. Nature 434:987–994
Thibault ST, Singer MA, Miyazaki WY, Milash B, Dompe NA, Singh CM, Buchholz R, Demsky M, Fawcett R, Francis-Lang HL, Ryner L, Cheung LM, Chong A, Erickson C, Fisher WW, Greer K, Hartouni SR, Howie E, Jakkula L, Joo D, Killpack K, Laufer A, Mazzotta J, Smith RD, Stevens LM, Stuber C, Tan LR, Ventura R, Woo A, Zakrajsek I, Zhao L, Chen F, Swimmer C, Kopczynski C, Duyk G, Winberg ML, Margolis J (2004) A complementary transposon tool kit for *Drosophila melanogaster* using P and piggyBac. Nat Genet 36:283–287
Thompson JD, Higgins DG, Gibson TJ (1994) ClustalW: improving the sensitivity of progressive multiple sequence alignment through sequence weighting, position-specific gap penalties and weight matrix choice. Nucleic Acids Res 22:4673–4680
Vass S, Cotterill S, Valdeolmillos AM, Barbero JL, Lin E, Warren WD, Heck MM (2003) Depletion of Drad21/Scc1 in Drosophila cells leads to instability of the cohesin complex and disruption of mitotic progression. Curr Biol 13:208–218
Vigneron S, Prieto S, Bernis C, Labbe JC, Castro A, Lorca T (2004) Kinetochore localization of spindle checkpoint proteins: who controls whom? Mol Biol Cell 15:4584–4596
Vos LJ, Famulski JK, Chan GK (2006) How to build a centromere: from centromeric and pericentromeric chromatin to kinetochore assembly. Biochem Cell Biol 84:619–639
Wei RR, Sorger PK, Harrison SC (2005) Molecular organization of the Ndc80 complex, an essential kinetochore component. Proc Natl Acad Sci USA 102:5363–5367
Wei RR, Schnell JR, Larsen NA, Sorger PK, Chou JJ, Harrison SC (2006) Structure of a central component of the yeast kinetochore: the Spc24p/Spc25p globular domain. Structure 14:1003–1009
Westermann S, Cheeseman IM, Anderson S, Yates JR 3rd, Drubin DG, Barnes G (2003) Architecture of the budding yeast kinetochore reveals a conserved molecular core. J Cell Biol 163:215–222
Westermann S, Wang HW, Avila-Sakar A, Drubin DG, Nogales E, Barnes G (2006) The Dam1 kinetochore ring complex moves

processively on depolymerizing microtubule ends. Nature 440:565–569

Wigge PA, Kilmartin JV (2001) The Ndc80p complex from *Saccharomyces cerevisiae* contains conserved centromere components and has a function in chromosome segregation. J Cell Biol 152:349–360

Yang F, Moss LG, Phillips GN Jr (1996) The molecular structure of green fluorescent protein. Nat Biotechnol 14:1246–1251

Yarbrough D, Wachter RM, Kallio K, Matz MV, Remington SJ (2001) Refined crystal structure of DsRed, a red fluorescent protein from coral, at 2.0-A resolution. Proc Natl Acad Sci USA 98:462–467

Appendix 2:

Detrimental Incorporation of Excess Cenp-A/Cid and Cenp-C into *Drosophila* Centromeres Is Prevented by Limiting Amounts of the Bridging Factor Cal1

Schittenhelm, RB, Althoff, F, Heidmann, S, and Lehner, CF

J Cell Sci. 2010 Nov 1;123(Pt 21):3768-79

Contribution to this part:

I created and analyzed the *Nuf2*^{ex50} imprecise excision allele (Figure 4 and S4) and contributed to the characterization of the effect of excess Cal1, Cid, and Cenp-C (Figure 6). Furthermore, I quantified the expression levels of the tagged Cid, Cenp-C and Cal1 variants and their distribution between different cellular fractions by quantitative immunoblotting (Figure S5). R.S. and C.L. wrote the manuscript with contributions from the other authors.

3768 Research Article

Detrimental incorporation of excess Cenp-A/Cid and Cenp-C into *Drosophila* centromeres is prevented by limiting amounts of the bridging factor Cal1

Ralf B. Schittenhelm[1,*], Friederike Althoff[1], Stefan Heidmann[2] and Christian F. Lehner[1,‡]

[1]Institute of Molecular Life Sciences, University of Zurich, CH-8057 Zurich, Switzerland
[2]Institute of Genetics, University of Bayreuth, D-95447 Bayreuth, Germany
*Present address: Institute of Molecular Systems Biology, ETH Zurich, CH-8093 Zurich, Switzerland
‡Author for correspondence (christian.lehner@imls.uzh.ch)

Accepted 4 July 2010
Journal of Cell Science 123, 3768-3779

doi:10.1242/jcs.067934

Summary

Propagation of centromere identity during cell cycle progression in higher eukaryotes depends critically on the faithful incorporation of a centromere-specific histone H3 variant encoded by *CENPA* in humans and *cid* in *Drosophila*. Cenp-A/Cid is required for the recruitment of Cenp-C, another conserved centromere protein. With yeast three-hybrid experiments, we demonstrate that the essential *Drosophila* centromere protein Cal1 can link Cenp-A/Cid and Cenp-C. Cenp-A/Cid and Cenp-C interact with the N- and C-terminal domains of Cal1, respectively. These Cal1 domains are sufficient for centromere localization and function, but only when linked together. Using quantitative in vivo imaging to determine protein copy numbers at centromeres and kinetochores, we demonstrate that centromeric Cal1 levels are far lower than those of Cenp-A/Cid, Cenp-C and other conserved kinetochore components, which scale well with the number of kinetochore microtubules when comparing *Drosophila* with budding yeast. Rather than providing a stoichiometric link within the mitotic kinetochore, Cal1 limits centromeric deposition of Cenp-A/Cid and Cenp-C during exit from mitosis. We demonstrate that the low amount of endogenous Cal1 prevents centromere expansion and mitotic kinetochore failure when Cenp-A/Cid and Cenp-C are present in excess.

Key words: Centromere, Kinetochore, Mitosis, Chromosome instability, Cal1

Introduction

The centromeric regions of chromosomes direct formation of kinetochores, which allow chromosome attachment to spindle microtubules. Centromeres and kinetochores are therefore of paramount importance for faithful propagation of genetic information (Santaguida and Musacchio, 2009). However, centromeric DNA sequences are not conserved (Vagnarelli et al., 2008). Most eukaryotes (including *Drosophila melanogaster* and humans) have regional centromeres with up to several megabases of repetitive DNA. Importantly, these repetitive sequences are neither necessary nor sufficient for centromere function, indicating that there is an epigenetic centromere specification (Vagnarelli et al., 2008).

A centromere-specific histone H3 variant (CenH3) is thought to be crucial for epigenetic centromere marking (Allshire and Karpen, 2008). CenH3 proteins are present in all eukaryotes (e.g. CENP-A in humans and Cid in *Drosophila*). They replace histone H3 in canonical nucleosomes or possibly variant complexes (Dalal et al., 2007; Mizuguchi et al., 2007; Camahort et al., 2009; Furuyama and Henikoff, 2009). Depletion of CenH3 results in a failure to localize most or all other centromere and mitosis-specific kinetochore proteins. Strong overexpression of *Drosophila* Cenp-A/Cid results in incorporation at ectopic chromosomal sites, which in part also assemble ectopic kinetochores during mitosis (Ahmad and Henikoff, 2002; Heun et al., 2006).

Ectopic kinetochores result in chromosome segregation errors and genetic instability. Ectopic CenH3 incorporation therefore must be prevented. Although still fragmentary, our understanding of the molecular mechanisms that regulate CenH3 incorporation is progressing rapidly (Allshire and Karpen, 2008; Torras-Llort et al., 2009). In proliferating cells, an additional complement of CenH3 needs to be incorporated during each cell cycle. In syncytial *Drosophila* embryos, this occurs during exit from mitosis (Schuh et al., 2007). Similar findings were made in human cells, where Cenp-A deposition occurs during late telophase and early G1 phase (Jansen et al., 2007). The number of factors shown to be required for normal CenH3 deposition is increasing rapidly, which suggests that there is an intricate control mechanism. Various and often dedicated chaperones (Hayashi et al., 2004; Furuyama et al., 2006; Dunleavy et al., 2009; Foltz et al., 2009), chromatin modifying and remodelling factors (Fujita et al., 2007; Maddox et al., 2007; Perpelescu et al., 2009), as well as other centromere components (Takahashi et al., 2000; Okada et al., 2006; Pidoux et al., 2009; Williams et al., 2009) are involved.

In *Drosophila*, Cenp-C is incorporated into centromeres concomitantly with Cenp-A/Cid (Schuh et al., 2007). High-resolution mapping with native *Drosophila* chromosomes has indicated that these two proteins do not have an identical localization within the kinetochore (Blower et al., 2002; Schittenhelm et al., 2007). Although these localization studies cannot exclude an association between subfractions of Cenp-A and Cenp-C, direct molecular interactions between these centromere proteins have not yet been reported. Recently, however, Cal1 has been identified in *Drosophila* and shown to be required for normal centromeric localization of Cenp-A/Cid and Cenp-C (Goshima et al., 2007; Erhardt et al., 2008). Moreover,

these three *Drosophila* centromere proteins can be co-immunoprecipitated from soluble chromatin preparations (Erhardt et al., 2008). Cal1 might therefore provide a physical link between Cenp-A/Cid and Cenp-C.

Here, we report that Cal1 has distinct binding sites for Cenp-A/Cid and Cenp-C. It can link these proteins together according to yeast three-hybrid experiments. However, the level of centromeric Cal1 is far lower than that of Cenp-A/Cid and Cenp-C. Cal1 therefore cannot function as a stoichiometric linker connecting each monomer or dimer of Cenp-C to Cenp-A within the centromere. But the low levels of Cal1 effectively protect cells against mitotic defects resulting from increased centromeric incorporation of excess Cenp-A/Cid and Cenp-C.

Results

cal1 is an essential gene required for centromere and kinetochore protein localization

RNAi-mediated knockdown of *cal1* has been shown to result in substantially diminished Cenp-A and Cenp-C levels at centromeres in *Drosophila* tissue culture cells (Goshima et al., 2007; Erhardt et al., 2008). For a genetic analysis of *cal1* function, we first characterized *cal1* alleles (Fig. 1A). The allele $cal1^{c03646}$ was confirmed to carry a *pBAC{PB}* insertion 69 bp upstream of the start codon within the predicted 5′ untranslated region. The *Mi{ET1}* insertion in $cal1^{MB04866}$ is within the second exon and disrupts the coding sequence after 361 of a total of 979 amino acids. Both insertions are associated with recessive lethality. They failed to complement each other, as well as the deficiency *Df(3R)Exel6176*, which deletes the *cal1* gene. The *gcal1-EGFP II.2* transgene, a genomic *cal1* fragment with the *EGFP* coding sequence inserted immediately before the stop codon (Fig. 1A), completely prevented the lethality of homo-, hemi- and transheterozygous $cal1^{MB04866}$ flies. Moreover, the rescued flies were found to be fertile. These findings demonstrate that *cal1* is an essential gene and that the Cal1-EGFP fusion provides all essential Cal1 functions.

To characterize the expression pattern of *cal1*, we used *gcal1-EGFP II.2* embryos. Microscopic analyses as well as immunoblotting experiments (supplementary material Fig. S1) indicated the presence of a maternal *cal1* contribution at the onset of embryogenesis, as well as a correlation of *cal1* expression with mitotic proliferation.

The maternal *cal1* contribution is expected to delay the onset of phenotypic abnormalities in *cal1* mutants. First abnormalities became apparent during stage 12. At this and later stages, abnormalities were largely restricted to the developing CNS (Fig. 1B). DNA staining revealed a lower number and a more irregular distribution of nuclei in the CNS of *cal1* mutants compared with sibling embryos. In addition, pyknotic nuclei as well as enlarged over-replicated nuclei were more frequently observed in the mutant CNS. Phospho-histone-H3-positive mitotic cells were also more frequent and often enlarged in the mutant CNS. The great majority of mutant progeny did not reach the larval stages (97%, n=100). Comparable observations were made with homo-, hemi- and transheterozygous embryos, suggesting that both alleles ($cal1^{MB04866}$ and $cal1^{c03646}$) result in a complete loss of gene function. The observed abnormalities in *cal1* mutants are consistent with the proposal that after exhaustion of the maternal *cal1* contribution, proliferating cells progress through aberrant mitoses with chromosome segregation errors resulting in aneuploidy and apoptosis.

Even before the onset of mitotic abnormalities, *cal1* homozygous mutant embryos displayed weaker anti-Cenp-A/Cid signals than sibling embryos (Fig. 1B). Later, when the abnormalities in the CNS became evident, Cenp-A/Cid could no longer be detected in *cal1* mutants. Moreover, the same results were also obtained with anti-Cenp-C, as well as with transgenes expressing EGFP fusions of Cenp-C, Spc105, Mis12, Nsl1, Spc25, Ndc80 and Nuf2 (supplementary material Fig. S2). The localization of all these centromere and kinetochore proteins requires Cal1. However, centromere localization of Cal1 was found to depend on

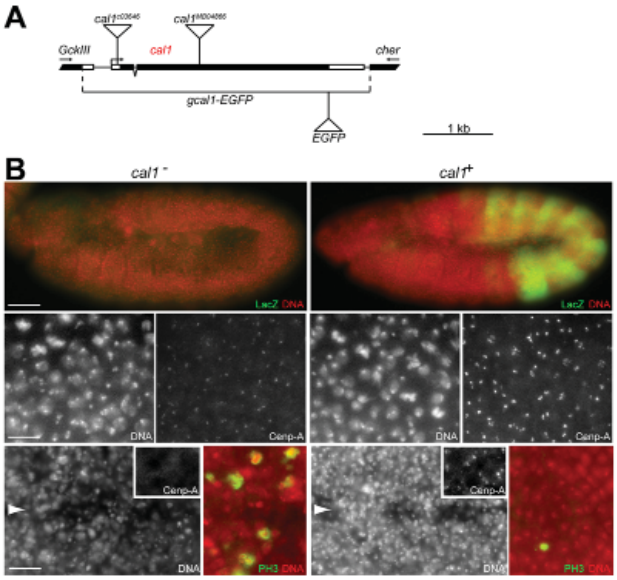

Fig. 1. Expression pattern and mutant phenotype of *cal1*. (**A**) Structure of wild-type and mutant *cal1* alleles. Boxes indicate exons; black fill, coding regions; and triangles, the *pBAC{PB}* and *Mi{ET1}* transposon insertions in $cal1^{c03646}$ and $cal1^{MB04866}$, respectively, as well as the EGFP insertion in the *gcal1-EGFP* transgene. Arrows indicate transcriptional start site and/or direction of transcription. (**B**) *cal1* mutant ($cal1^{-}$) and sibling control embryos ($cal1^{+}$) are shown on the left and right, respectively. Stage 11 is shown in the top and middle row, stage 14 in the bottom row. Embryos were collected from $cal1^{c03646}$/*TM3, Ubx-lacZ* parents, followed by labeling with a DNA stain (DNA) and antibodies against β-galactosidase for genotype determination (lacZ), against Cenp-A/Cid (Cenp-A) or phospho-histone H3 (PH3). The insets in the bottom row display anti-Cenp-A/Cid labeling in CNS cells at higher magnification. Arrowheads in the bottom row indicate the midline of the CNS. Scale bars: 50 μm (top), 6 μm (middle) and 11 μm (bottom).

Cenp-A/Cid and Cenp-C, but not on Spc105, Mis12 and Ndc80 complex components (supplementary material Fig. S2). Moreover, in contrast to initial descriptions (Heeger et al., 2005; Przewloka et al., 2007), quantification of anti-Cenp-A/Cid signals in Cenp-C mutant embryos confirmed (data not shown) that normal levels of centromeric Cenp-A/Cid depend on Cenp-C (Erhardt et al., 2008). All our findings in mutant embryos confirm and extend previous observations made after RNAi in *Drosophila* tissue cultures (Goshima et al., 2007; Erhardt et al., 2008). Cal1 clearly functions together with Cenp-A/Cid and Cenp-C in kinetochore assembly.

Cal1 promotes an interaction between Cenp-A/Cid and Cenp-C

Cal1, Cenp-A/Cid and Cenp-C can be co-immunoprecipitated (Erhardt et al., 2008). We analyzed whether Cal1 can interact simultaneously with Cenp-A/Cid and Cenp-C. Yeast two-hybrid (Y2H) assays clearly revealed an interaction of Cal1 with Cenp-A/Cid (Fig. 2A), but not with the kinetochore proteins Spc105, Mis12, Nsl1, Nnf1a, Bub1 or BubR1 (data not shown). The N-terminal region of Cal1 (residues 1–407) but not its middle (residues 392–722) and C-terminal (residues 699–979) regions were observed to interact with full-length Cenp-A/Cid (Fig. 2A). When the N-terminal tail or the histone fold domain of Cenp-A/Cid was assayed separately, no interactions with the N-terminal Cal1 region could be detected (data not shown). Y2H experiments also revealed an interaction between Cal1 and Cenp-C. The C-terminal regions of Cal1 (residues 699–979) and Cenp-C (residues 1009–1411) were found to interact (Fig. 2B). The interacting region within Cenp-C could be narrowed down to a smaller C-terminal subfragment (residues 1201–1411), which no longer included the Cenp-C box, a motif that is characteristic of all Cenp-C homologs (Fig. 2B). The C-terminal Cenp-C domain, which is sufficient for the Y2H interaction with Cal1, is similar in fungal and animal Cenp-C homologs (Talbert et al., 2004). It adopts a cupin fold and can mediate homodimerization (Cohen et al., 2008).

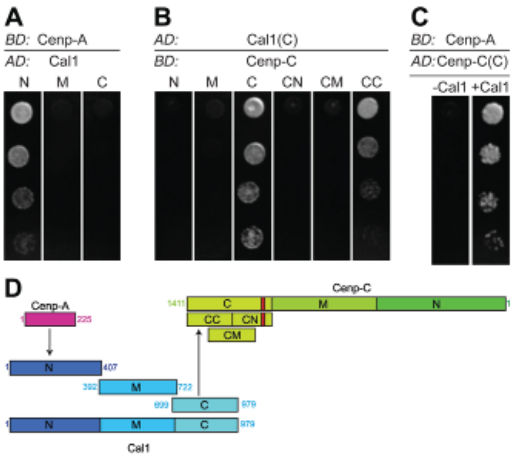

Fig. 2. Cal1 promotes interaction between Cenp-A/Cid and Cenp-C. (**A**) The N-terminal (N) but not the middle (M) or C-terminal (C) region of Cal1 interacts with Cenp-A/Cid. Full-length Cenp-A/Cid was fused to the DNA-binding domain (BD) and the Cal1 fragments to the transcriptional activation domain (AD) of Gal4 and interactions analyzed in Y2H experiments. (**B**) Y2H experiments reveal that the C-terminal domain of Cal1 [Cal1(C)] interacts specifically with C-terminal domains of Cenp-C [Cenp-C(C) and Cenp-C(CC)]. (**C**) Y3H experiments reveal that Cal1 expression results in an interaction between Cenp-A/Cid and Cenp-C(C). Cal1 expression is either repressed (–Cal1) or derepressed (+Cal1). (**D**) The observed protein interactions are indicated with arrows. Cal1 and Cenp-C were divided into N-terminal (N), middle (M) and C-terminal (C) domains. The C-terminal domain of Cenp-C was further split into three subregions (CN, CM, CC). The small red box indicates the position of the conserved Cenp-C box. Numbers indicate amino acid positions.

As Cenp-A/Cid and Cenp-C were observed to interact with distinct regions of Cal1, we evaluated whether Cal1 can bind to Cenp-A/Cid and Cenp-C simultaneously to form a trimeric complex (Fig. 2C). We generated a yeast strain constitutively expressing Cenp-A/Cid and Cenp-C(C) fused to the transcriptional activation and DNA-binding domain of Gal4, respectively. In addition, the strain allowed for regulated *cal1* expression. In the absence of *cal1* expression, we did not observe an interaction between Cenp-A/Cid and Cenp-C(C) (Fig. 2C). However, in the presence of *cal1* expression, we clearly observed a Cenp-A/Cid–Cenp-C(C) interaction (Fig. 2C). Control experiments demonstrated that the inducing growth conditions were unable to promote a Cenp-A/Cid–Cenp-C(C) interaction when the inducible *cal1* gene was absent (data not shown). The results of our yeast three-hybrid (Y3H) experiments therefore indicate that Cal1 can bridge Cenp-A/Cid and Cenp-C (Fig. 2D).

Centromere localization and function of Cal1 depends on both the Cenp-A/Cid- and Cenp-C-interacting regions

A perfect colocalization of Cenp-A/Cid, Cenp-C and Cal1 would be expected, if these proteins were present exclusively in a trimeric complex. Therefore, we carefully compared the localization of Cal1-EGFP with that of Cenp-A/Cid and Cenp-C in embryos and S2R+ cells expressing the *gcal1-EGFP* construct (supplementary material Fig. S3). Cal1-EGFP was observed at centromeres throughout the cell cycle. Importantly, during interphase, Cal1-EGFP signals, but not anti-Cenp-A/Cid and anti-Cenp-C signals, were also clearly enriched in and around the nucleolus. Our results therefore correspond to those described earlier (Erhardt et al., 2008) where antibodies against Cal1 were used. These results indicate that at least a fraction of Cal1 is not associated with Cenp-A/Cid and Cenp-C during interphase.

To evaluate which Cal1 domains contribute to localization, we generated constructs allowing expression of either the N-terminal, middle or C-terminal region fused to EGFP (Fig. 3A). The N- and C-terminal domains, which are sufficient for the interaction with either Cenp-A/Cid or Cenp-C, have been conserved more extensively during Drosophilid evolution than the middle region (Erhardt et al., 2008). None of the three Cal1 subregions was able to localize to the centromere in S2R+ cells (Fig. 3A). The middle, but not the terminal domains, became enriched in the nucleolus. To further define the requirements for Cal1 centromere localization, we generated constructs that allowed expression of different combinations of Cal1 domains (Fig. 3A). After expression of Cal1(N-M) or Cal1(M-C) we did not observe centromeric signals. However, these Cal1 fragments became enriched in the nucleolus (Fig. 3A), as expected because they contain the middle domain, which is sufficient for nucleolar localization. In agreement, Cal1(N-C), a Cal1 version lacking the middle domain, was not enriched in the nucleolus. Interestingly, however, this variant was found at the

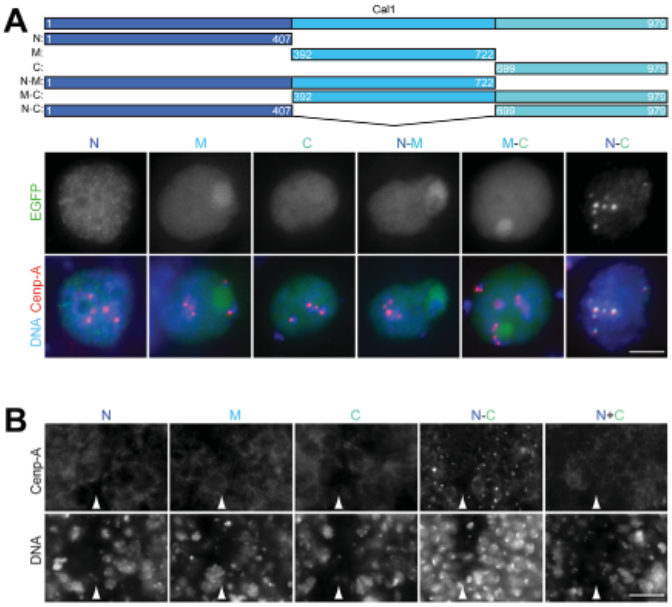

Fig. 3. Cal1 centromere localization and function require the linked Cenp-A/Cid and Cenp-C interacting regions. (**A**) Cal1 regions fused to EGFP were expressed in S2R+ cells after transient transfection with the illustrated constructs. Numbers indicate amino acid positions. Cells are labeled with an antibody against Cenp-A/Cid (Cenp-A) and a DNA stain (DNA). EGFP (EGFP) signals in representative nuclei are shown in the top row and merged images in the bottom row. Scale bar: 5 µm. (**B**) A covalent link between the N- and C-terminal domains of Cal1 is required to rescue the *cal1* mutant phenotype. *sca-GAL4* in combination with *UAS* transgenes was used for expression of different Cal1 regions in the central nervous system of *cal1* mutants. Embryos were fixed at stage 14 and labeled with a DNA stain (DNA), anti-Cenp-A/Cid (Cenp-A) and anti-β-galactosidase for genotype identification (not shown). Although the N-terminal (N), middle (M) and C-terminal (C) regions of Cal1 fail to restore centromeric Cenp-A/Cid localization and normal cell proliferation in *cal1* mutants, complete rescue is obtained with a Cal1 version with the N- and C-terminal regions directly linked (N-C). Simultaneous expression of the unlinked N- and C-terminal domains does not rescue the *cal1* mutant phenotype (N+C). Arrowheads indicate the midline of the CNS. Scale bar: 10 µm.

centromere throughout the cell cycle (Fig. 3A). Moreover, Y3H experiments indicated that Cal1(N-C) was still able to forge an interaction between Cenp-A/Cid and Cenp-C (data not shown). These findings suggest that Cal1 centromere localization depends on an interaction with Cenp-A/Cid and Cenp-C. Cal1 might be sequestered in the nucleolus when not in a complex with these centromeric proteins.

By expressing EGFP-tagged Cal1 variants in *cal1* mutant embryos, we evaluated to what extent the different Cal1 domains contribute to its function. Expression of the regions N, M or C (Fig. 3A) from *UAS* transgenes could be confirmed by the resulting EGFP signals (data not shown), but did not restore centromeric Cenp-A/Cid localization and normal cell proliferation in the CNS of *cal1* mutant embryos (Fig. 3B). However, expression of *UAS-cal1(N-C)-EGFP* prevented expression of the characteristic abnormalities in *cal1* mutant embryos (Fig. 3B). This rescue was just as effective as that with full-length Cal1 (*UAS-cal1-EGFP*, data not shown) and resulted in an apparently wild-type CNS. Moreover, ubiquitously expressed *UAS-cal1(N-C)-EGFP* allowed development of *cal1* mutants to the adult stage (data not shown). Importantly, simultaneous expression of *UAS-cal1(N)-EGFP* and *UAS-cal1(C)-EGFP* did not prevent the *cal1* mutant phenotype (Fig. 3B). In addition, EGFP signals were not centromeric, in contrast to those obtained with *UAS-cal1(N-C)-EGFP* (data not shown). Therefore, we conclude that centromere localization and function of Cal1 require the presence of its Cenp-A/Cid- and Cenp-C-interacting N- and C-terminal regions, which have to be linked, but not necessarily by its M region.

The amount of centromeric Cal1 is lower than that of Cenp-A/Cid and Cenp-C

The molecular interactions that are responsible for Cenp-C localization within the mitotic kinetochore are unknown. Human Cenp-C binds to DNA in vitro, although with very limited sequence preference (Yang et al., 1996; Sugimoto et al., 1997). Co-immunoprecipitation of human Cenp-C and Cenp-A has been reported (Erhardt et al., 2008; Trazzi et al., 2009), but others have failed to detect Cenp-C in Cenp-A nucleosomes (Hori et al., 2008). The co-immunoprecipitation data of Erhardt and colleagues (Erhardt et al., 2008) and our Y3H experiments are consistent with the notion that in *Drosophila*, Cal1 might function as a centromere component that stoichiometrically links Cenp-C to Cenp-A/Cid. To evaluate this possibility, we carefully quantified the centromeric amounts of these proteins. Wing imaginal discs of *Cenp-A/cid-*, *Cenp-C-* or *cal1*-null mutant larvae rescued by transgenes expressing functional EGFP fusions of these proteins were mounted next to *CSE4::EGFP* yeast cells (Fig. 4A). *CSE4* encodes the yeast Cenp-A homolog, which is thought to be present in two copies per centromere (Meluh et al., 1998; Collins et al., 2004). Accordingly, we used the clusters of the 16 centromeres in *CSE4::EGFP* anaphase or telophase cells (Fig. 4A; Joglekar et al., 2006) as an internal calibration standard for the quantification of Cenp-A/Cid-EGFP, Cenp-C-EGFP and Cal1-EGFP signal intensities in *Drosophila* centromeres. The measured Cse4-EGFP signal intensities were found to decrease with increasing distance of the centromere cluster from the coverslip (Fig. 4B), as described previously (Joglekar et al., 2006). In groups of cells with centromere clusters at similar focal positions, the s.d. values of the Cse4-EGFP signals were found to be lower than 36% of the average signal intensity. The EGFP signal intensities measured for the *Drosophila* centromere protein fusions that were expressed under the control of their own regulatory regions were also plotted against their average focal *z*-axis positions (Fig. 4C). The *y*-axis intercepts of linear regressions were used for comparison of the average amounts of different centromere proteins (Table 1). Moreover, the comparison of the EGFP signal intensities obtained in *Drosophila*

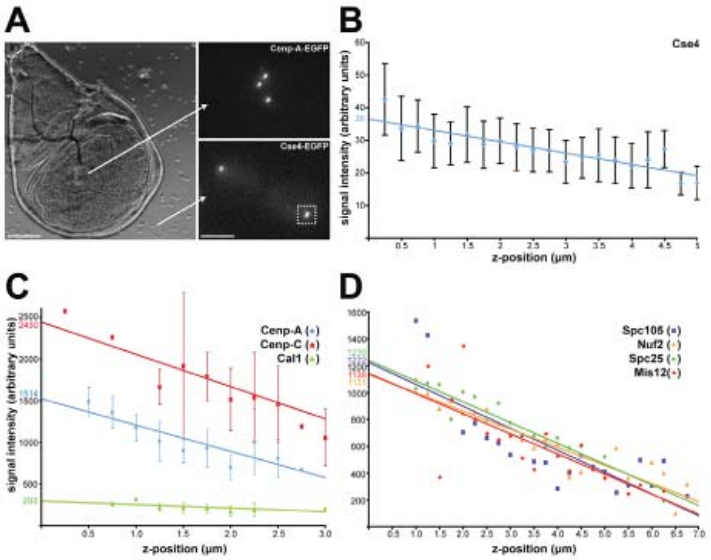

Fig. 4. Stoichiometry of *Drosophila* centromere and kinetochore proteins. (**A**) For EGFP signal quantification, *CSE4::EGFP* yeast cells were used as a reference (Joglekar et al., 2006) and mounted next to wing imaginal discs dissected from larvae homozygous for a null mutation and rescued by a transgene expressing an EGFP fusion of a particular *Drosophila* centromere or kinetochore protein. EGFP signals from *Drosophila* and yeast cells (e.g. Cenp-A/Cid-EGFP and Cse4-EGFP at late mitosis in the top and bottom panels on the right, respectively) were captured and quantified. Late mitotic yeast cells display two centromere clusters each containing 32 Cse4-EGFP protein copies (box). Scale bars: 100 µm (left), 3 µm (right). (**B**) As a reference, EGFP signal intensities of centromere clusters of late mitotic *CSE4::EGFP* cells were determined in all of the slides with different wing imaginal disc. Signal intensities show little variation between slides (data not shown), but they decrease with increasing focal depth of the centromere clusters (Joglekar et al., 2006). All the obtained values (664) are grouped into classes according to the focal depth of the centromere cluster. The mean signal intensities of the clusters in arbitrary units ± s.d. for each bin are plotted as a function of their *z* position. The *y*-axis intercept of a linear regression was used for comparison of Cse4-EGFP levels with those of *Drosophila* centromere and kinetochore proteins (Table 1). (**C**,**D**) The total centromeric signal intensity per cell quantified after expression of EGFP-fused centromere proteins (C: Cenp-A/Cid, Cenp-C or Cal1) or kinetochore proteins (D: Spc105, Mis12, Nuf2 or Spc25) in null mutant wing imaginal discs. Values are grouped according to the focal depth of the signals. The average signal intensity for each bin is plotted as a function of its *z* position. s.d. values are shown in C and omitted for clarity in D (but see supplementary material Fig. S4). *y*-axis intercepts of linear regressions were used for quantitative comparisons (see Table 1).

with those of Cse4-EGFP in yeast resulted in an estimate of the absolute protein copy numbers per centromere (Table 1). The accuracy of our quantifications was confirmed in competition experiments, where we observed the expected decrease in EGFP signal intensities when a given EGFP fusion protein was analyzed in a background that also expressed the untagged version of this protein from endogenous wild-type gene copies, rather than in a null-mutant background (supplementary material Fig. S4).

In case of Cal1-EGFP, specific signals were not only detected at the centromere as for Cenp-A/Cid-EGFP and Cenp-C-EGFP, but also in the nucleolus and weakly throughout the nucleus (supplementary material Fig. S4). Based on EGFP signal quantification, the centromeric, nucleolar and residual nuclear pools were estimated to comprise on average about 3.3%, 21% and 76%, respectively, of the total nuclear Cal1. Importantly, the amount of centromeric Cal1 was clearly far lower than that of Cenp-A/Cid and Cenp-C (Table 1). Our results therefore exclude models for centromeric Cenp-C localization where every Cenp-C monomer (or dimer) is stably linked via a single Cal1 protein to one or two copies of Cenp-A/Cid. The results of a comparison of the expression levels of the different EGFP fusion proteins (Cenp-A/Cid, Cenp-C, Cal1) by immunoblotting (supplementary material Fig. S5) was entirely consistent with this conclusion when taking into account the differential distribution of Cenp-A/Cid, Cenp-C and Cal1 into subnuclear regions (centromere, nucleolus, and elsewhere in the nucleus) as suggested by the quantitative in vivo imaging.

Quantitative imaging with imaginal discs was also used for a comparison of the amounts of the centromere proteins Cal1, Cenp-A/Cid and Cenp-C with those of the kinetochore proteins Spc105, Mis12, Spc25 and Nuf2 (Fig. 4D; Table 1). The levels of these kinetochore proteins were found to be all very similar and somewhat lower than the amounts of Cenp-A/Cid. The similar abundance measured for Spc25 and Nuf2 agrees with the established fact that they are stoichiometric components of the stable heterotetrameric Ndc80 complex (Santaguida and Musacchio, 2009). The comparison of the estimated numbers of protein copies per *Drosophila* kinetochore with those determined in yeast (Joglekar et al., 2006; Joglekar et al., 2008) indicated that the amounts of centromere and kinetochore proteins correlate rather with the number of kinetochore microtubules (1 in budding yeast, about 11 in *Drosophila*) (Winey et al., 1995; Maiato et al., 2006) than with the amount of centromeric DNA (125 bp in budding yeast, 420 kb in *Drosophila*) (Fitzgerald-Hayes et al., 1982; Sun et al., 1997).

Table 1. *Drosophila* centromere and kinetochore protein levels

Protein	Amount at centromere or kinetochore (arbitrary units)	Copy number per kinetochore[b]	Copy number per kMT[c]	Copy number of yeast homolog per kMT[d]
Cenp-A/Cid	1514[a]	84	7.6	2
Cenp-C	2430[a]	135	12.3	1–2
Cal1	293[e]/46[f]	2.5	0.23	Homolog?
Spc105	1222[g]	68	6.2	5
Mis12	1138[g]	63	5.7	5
Spc25	1239[g]	69	6.3	8
Nuf2	1131[g]	63	5.7	8

[a]Signals determined in interphase cells. In case of Cenp-C, signals were also quantified in prometaphase and metaphase cells where they were found to be comparable with the interphase value, as expected (Schuh et al., 2007).
[b]By comparison with the average Cse4-EGFP signal intensity, which was found to be 36 arbitrary units for a cluster of 16 kinetochores. Moreover, each kinetochore is assumed to contain two Cse4-EGFP molecules.
[c]Based on the assumption of 11 kMTs per *Drosophila* kinetochore (Maiato et al., 2006).
[d]Data from (Joglekar et al., 2006). Note that a budding yeast kinetochore binds a single kMT.
[e]Sum of centromeric and nucleolar Cal1-EGFP signals in interphase.
[f]Estimate for centromeric Cal1-EGFP signals in interphase.
[g]Signals determined in prometaphase and metaphase cells. In case of Mis12, signals were also quantified in interphase cells where they were found to be threefold lower than in mitosis. Centromeric signals cannot be detected during interphase in case of Spc105, Spc25 and Nuf2.

Interdependency between Cal1, Cenp-A/Cid and Cenp-C limit centromere expansion in combination with cell cycle control

Cenp-A/Cid deposition needs to be carefully controlled because the CenH3 variants of the CENP-A family have a crucial role in defining the epigenetic mark that specifies centromere identity in regional centromeres (Allshire and Karpen, 2008). In principle, the interdependence of centromeric Cenp-A/Cid, Cenp-C and the low levels of Cal1 might provide robust control of centromeric Cenp-A/Cid amounts and could effectively protect cells against the consequences of accidental unbalanced Cenp-A/Cid excess. However, previous studies have demonstrated that overexpression of Cenp-A/Cid is sufficient to cause ectopic incorporation all along the chromosome and consequential mitotic defects (Van Hooser et al., 2001; Heun et al., 2006; Moreno-Moreno et al., 2006). The massive overexpression applied in these studies (70-fold) (Heun et al., 2006), which is rather unlikely to occur in physiological conditions, even accidentally, might have over-run negative regulation. Therefore, we applied more limited overexpression in *Drosophila* embryos (up to fourfold; supplementary material Fig. S6), to evaluate the role of Cenp-A/Cid, Cenp-C and Cal1 interdependency in centromere confinement of these proteins.

Overexpression was achieved with the *prd-GAL4* driver, which directs *UAS* transgene expression in alternating segmental stripes within the embryonic epidermis (Fig. 5A). Overexpression starts during embryonic cell cycle 14. Embryos were fixed and analyzed 3 hours later, when the majority of the epidermal cells are in G2 of cycle 16. Intervening stripes that do not express *prd-GAL4* were used as internal controls.

Interestingly, when *UAS-Cenp-A/cid* was expressed, we could detect at most a marginal increase in the intensity of centromeric anti-Cenp-A/Cid signals in the *prd-GAL4* expressing stripes (Fig. 5B,C). However, when *UAS-Cenp-A/cid* and *UAS-cal1-EGFP* were simultaneously overexpressed, we observed a highly significant increase in centromeric Cenp-A/Cid (Fig. 5B,C; $P<0.001$, Student's *t*-test). *UAS-cal1-EGFP* without concomitant *UAS-Cenp-A/cid* expression did not result in increased centromeric anti-Cenp-A/Cid signals (Fig. 5B,C). Quantification of centromeric Cal1-EGFP fluorescence indicated that coexpression of *UAS-Cenp-A/cid* and *UAS-cal1-EGFP* resulted in slightly higher levels than when *UAS-cal1-EGFP* was expressed alone (Fig. 5B,C). We conclude that moderate overexpression of Cenp-A/Cid does not lead to increased centromeric Cenp-A/Cid levels because Cal1 levels are limiting. Similarly, Cenp-A levels limit centromeric Cal1 levels. These findings are consistent with the proposal that deposition of Cenp-A/Cid at the centromere requires complex formation with Cal1, probably by direct interaction as suggested by our Y2H experiments.

To analyze the interplay of Cenp-A/Cid and Cal1 with Cenp-C, we quantified centromeric anti-Cenp-C signals. As our Y3H experiments had indicated that Cal1 can form a bridge between Cenp-A and Cenp-C, these three proteins might be incorporated into the centromere as a stoichiometric stable complex. Accordingly, the increased Cenp-A/Cid and Cal1-EGFP incorporation observed after simultaneous overexpression is expected to be accompanied by a parallel increase in centromeric Cenp-C. However, we did not detect such an increase (Fig. 5C). This finding confirms that centromeres are not assembled by multimerization of stable persisting complexes of Cal1, Cenp-A/Cid and Cenp-C.

Expression of *UAS-Cenp-C* provided additional confirmation for the notion that centromeric accumulation of Cenp-A/Cid and Cenp-C are not necessarily coupled. Although *UAS-Cenp-C* expression clearly resulted in an increase of centromeric Cenp-C (Fig. 5C; $P<0.001$, Student's *t*-test), it was not paralleled with a comparable increase in centromeric Cenp-A (Fig. 5C). The increased centromeric anti-Cenp-C signals observed after *UAS-Cenp-C* expression suggest that the Cenp-C binding sites within the centromere are not saturated at the endogenous Cenp-C expression level. However, because *UAS-Cenp-C* expression caused increased anti-Cenp-C signals not only at the centromere, but also throughout the cell (data not shown), the centromeric Cenp-C binding sites appear to become limiting when Cenp-C is overexpressed.

Although our findings indicated that centromeric accumulation of Cenp-C is not necessarily coupled to that of Cal1-Cenp-A/Cid, simultaneous overexpression of all three centromere proteins clearly revealed synergism. In this case, maximal centromeric signals were obtained. Signals were significantly higher than after overexpression of *UAS-Cenp-A/cid*, *UAS-Cenp-C* and *UAS-cal1-EGFP* individually or in pairs (Fig. 5B; $P<0.01$ for all comparisons, Student's *t*-test). These findings are consistent with the suggestion that Cal1-mediated transient interactions between Cenp-A/Cid and Cenp-C support their centromeric deposition.

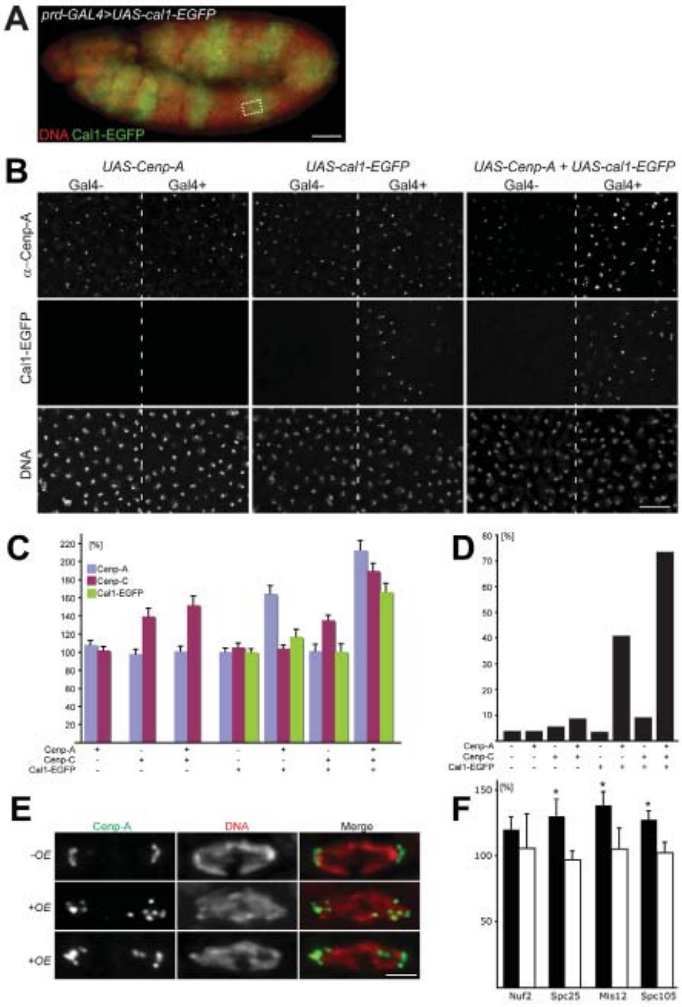

Fig. 5. Interdependence of Cenp-A/Cid, Cenp-C and Cal1 limits centromere expansion and genetic instability. (**A**) *prd-GAL4* was used to direct expression of *UAS-cal1-EGFP*, *UAS-Cenp-A/cid* and *UAS-Cenp-C* individually or in combination in alternating segmental stripes as illustrated by Cal1-EGFP signals (green) and DNA staining (red) in a stage 11 embryo expressing *UAS-cal1-EGFP*. The dashed rectangle indicates the position of the regions shown in B. Scale bar: 50 μm. (**B**) *prd-GAL4* was used for striped expression of *UAS-Cenp-A/cid* (left), *UAS-cal1-EGFP* (middle), or both these *UAS* transgenes (right). Epidermal regions are shown with dashed lines indicating the border between domains with ($Gal4^+$) and without ($Gal4^-$) expression of *UAS* transgenes. Top, anti-Cenp-A/Cid (α-*Cenp-A*); middle row, Cal1-EGFP signals; bottom, DNA. Increased centromeric Cenp-A/Cid and Cal1-EGFP signals result after co-overexpression, but not after individual overexpression of *UAS-cal1-EGFP* and *UAS-Cenp-A/cid* (see also C). Scale bar: 15 μm. (**C**) Centromeric signal intensities obtained after labeling with either anti-Cenp-A/Cid or anti-Cenp-C were quantified in embryos with *prd-GAL4*-driven overexpression of *UAS* transgenes in stripes (see A and B). Signal intensities observed in stripes without *UAS* transgene expression are set as 100%. Bars indicate relative centromeric signal intensities within the *UAS* transgene expressing stripes (average intensity with s.e.m., $n>5$ embryos). Cal1-EGFP signals were compared with those obtained within stripes expressing only *UAS-cal1-EGFP*, which were set as 100%. The type(s) of *UAS* transgenes expressed is indicated below the bars. (**D**) Percentage of abnormal late mitotic figures observed in the embryonic epidermis at the stage of mitosis 16 after α*4tub-GAL4-VP16*-driven expression of the different *UAS* transgenes. (**E**) Characteristic anaphase figures observed in the embryonic epidermis at the stage of mitosis 16 in either control embryos (–OE, top) or after α*4tub-GAL4-VP16*-driven expression of *UAS-Cenp-A/cid*, *UAS-Cenp-C* and *UAS-cal1-EGFP* (+OE, middle and bottom). Embryos were labeled with anti-Cenp-A/Cid (Cenp-A) and a DNA stain (DNA). Scale bar: 4 μm. (**F**) Various kinetochore proteins (Nuf2, Spc25, Mis12 and Spc105) were expressed as EGFP fusions from transgenes under control of the endogenous regulatory regions in embryos where *prd-GAL4* was also driving co-expressing *UAS-cal1*, *UAS-Cenp-A/cid* and *UAS-Cenp-C* (black bars) or only *UAS-cal1* and *UAS-Cenp-A/cid* (white bars). EGFP signals in kinetochores of prometaphase and metaphase cells were quantified. Those observed in stripes without *UAS* transgene expression were set as 100%. Bars indicate relative signal intensities within the stripes expressing the *UAS* transgene (average intensity with s.e.m., $n>5$ embryos). The increased signal intensities of Spc25, Mis12 and Spc105 in stripes expressing the *UAS* transgene are significant ($*P<0.05$, Student's *t*-test).

The observed increase in the centromeric levels of Cenp-A/Cid, Cenp-C and Cal1-EGFP after simultaneous *prd-GAL4*-driven overexpression did not appear to result in severe mitotic defects. Abnormal mitotic figures at the stage of mitosis 16 were rarely observed and chromosomal incorporation of Cenp-A/Cid, Cenp-C and Cal1-EGFP outside the centromere was not detected. However, clear mitotic defects resulted (Fig. 5D) when we used maternal *α4tub-GAL4-VP16*, which drives almost twofold higher expression than *prd-GAL4* (data not shown). The strongest defects were caused by simultaneous expression of all three centromere proteins. Milder defects were already apparent after combined expression of *UAS-Cenp-A/cid* and *UAS-cal1-EGFP* (Fig. 5D). By contrast, all other combinations or individual expression of the *UAS* transgenes did not result in a distinct enrichment of abnormal mitotic figures (Fig. 5D). Expression of *UAS* transgenes during eye and wing development further confirmed that the combined overexpression of the three centromere proteins is far more deleterious than individual overexpression (supplementary material Fig. S7).

To address how *α4tub-GAL4-VP16*-driven simultaneous expression of *UAS-Cenp-A/cid*, *UAS-Cenp-C* and *UAS-cal1-EGFP* affects progression through mitosis, we characterized the mitotic abnormalities in further detail. The most prominent defects observed in fixed embryos were abnormal anaphase and telophase figures with chromatin bridges containing lagging centromeres (Fig. 5E). Ectopic Cenp-A/Cid incorporation throughout the chromosome arm regions was rarely detectable in these abnormal mitotic figures. Focal ectopic Cenp-A/Cid incorporation within a chromosome arm might in principle lead to multicentric chromosomes and thereby explain the observed chromosome bridges with lagging centromeres after simultaneous overexpression of Cenp-A/Cid, Cenp-C and Cal1-EGFP. Therefore, we counted the number of kinetochores in mitotic cells. Even in wild-type controls, we were unable to detect all of the 16 centromeres as distinct Cenp-A/Cid or Cenp-C foci in every mitotic cell. Apart from the occasional immediate proximity of kinetochores, accessibility problems resulting in low anti-Cenp-A/Cid or anti-Cenp-C signals specifically during prometaphase and metaphase further impaired kinetochore identification. Therefore, we used EGFP-Nuf2-expressing embryos for kinetochore counting. Moreover, we determined kinetochore counts after expression of *prd-GAL4*-directed *UAS* transgenes in adjacent control and overexpressing regions to eliminate effects of fixation variability. Analyses after *prd-GAL4*-driven overexpression were possible because mitotic abnormalities were frequent at the stage of mitosis 16 when *UAS-cal1* was used instead of the *UAS-cal1-EGFP* transgene insertion selected for the initial experiments (Fig. 5A–C). The stronger effect of *UAS-cal1* presumably reflects transgene position effects on expression levels or absence of the EGFP tag which might be slightly deleterious. Despite the occurrence of late-mitotic figures with lagging centromeres within the overexpressing regions, the number of discrete kinetochore spots was not significantly increased within these regions (10.3±1.6 EGFP-Nuf2 spots compared with 10.7±1.6 spots in the intervening stripes; n>50 cells from more than 10 different embryos). These results suggest that ectopic kinetochores are not the primary cause for the mitotic abnormalities resulting from co-overexpression of Cal1, Cenp-A/Cid and Cenp-C.

As ectopic kinetochores could not be observed, we determined whether increased centromeric Cal1, Cenp-A/Cid and Cenp-C was accompanied with increased levels of kinetochore proteins. Transgenes expressing EGFP fusions of a given kinetochore protein (Nuf2, Spc25, Mis12 or Spc105) under the control of their normal cis-regulatory regions were used in combination with *prd-GAL4*-driven simultaneous overexpression of the three centromere proteins Cal1, Cenp-A/Cid and Cenp-C in stripes. The EGFP signals in the kinetochores of mitotic cells were found to be slightly but consistently enhanced within the overexpressing stripes (Fig. 5F). This enhancement was less extensive than that of Cal1, Cenp-A/Cid and Cenp-C (compare Fig. 5C and F). However, in these experiments the kinetochore proteins were not overexpressed from *UAS* transgenes in contrast to Cal1, Cenp-A/Cid and Cenp-C. The comparatively mild increase of kinetochore proteins observed after co-overexpression of Cal1, Cenp-A/Cid and Cenp-C might therefore reflect limiting kinetochore protein expression levels. Interestingly, when only Cal1 and Cenp-A/Cid but not Cenp-C was overexpressed, we were unable to detect a statistically significant increase in kinetochore protein levels (Fig. 5F), suggesting that the observed mitotic defects (Fig. 5D) do not depend on increased kinetochore protein levels.

To analyze the consequences of simultaneous overexpression of Cal1, Cenp-A/Cid and Cenp-C on the dynamics of progression through mitosis, we performed in vivo imaging with embryos expressing histone H2Av-mRFP and Cenp-A/Cid-EGFP in addition to *UAS-cal1*, *UAS-Cenp-A/cid* and *UAS-Cenp-C* (Fig. 6; supplementary material Movies 1 and 2). First abnormalities were already apparent during mitosis 15. Compared with controls, which did not overexpress the centromeric proteins, chromosome congression into a metaphase plate was always slower (2- to 8-fold; mean 3.7-fold; n=8 cells from two embryos) and metaphase prolonged (3- to 18-fold; mean 10-fold; n=10 cells from two embryos) except in one cell. Although chromosome segregation during anaphase appeared to be normal in about half of the cases (n=11 cells from two embryos), the other half displayed subtle to strong abnormalities. Characteristically, these abnormalities consisted in lagging centromeres (Fig. 6A, data not shown). During mitosis 16, these same mitotic defects were even more pronounced (Fig. 6A). The distances between sister kinetochores in metaphase plates were found to be scattered over a wider range after co-overexpression of Cal1, Cenp-A/Cid and Cenp-C (Fig. 6B). Collectively, our analyses of the observed mitotic abnormalities suggest that increased levels of centromeric Cal1, Cenp/Cid and Cenp-C compromise kinetochore function during mitosis.

Normally, centromere loading of Cenp-A/Cid and Cenp-C occurs during and depends on exit from mitosis (Jansen et al., 2007; Schuh et al., 2007). To evaluate whether the observed increase in centromere protein levels that results from simultaneous overexpression of Cal1, Cenp-A/Cid and Cenp-C also depends on progression through mitosis, we performed experiments in *string(stg)/cdc25* mutant embryos where cells remain arrested in G2 phase of cycle 14 (Edgar and O'Farrell, 1989). After overexpression of Cal1, Cenp-A/Cid and Cenp-C in these G2-arrested cells, we did not observe increased anti-Cenp-A/Cid and Cenp-C signals at centromeres (supplementary material Fig. S8). However, some ectopic accumulation throughout the cells was apparent. By contrast, an increased centromeric signal, at the expense of distributed signals was clearly obtained after progression through a successful mitosis, which was triggered with the help of a heat-inducible *hs-stg* transgene in *stg* mutant embryos overexpressing Cal1, Cenp-A/Cid and Cenp-C. We conclude that increased incorporation of Cal1, Cenp-A/Cid and Cenp-C into centromeres requires both overexpression and progression through

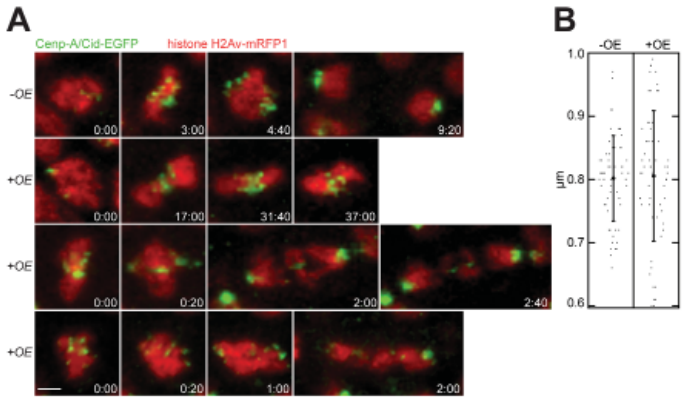

Fig. 6. Co-overexpression of Cenp-A/Cid, Cenp-C and Cal1 results in a metaphase delay. (**A**) Time-lapse in vivo imaging of the sixteenth round of mitosis in embryos expressing Cenp-A/Cid-EGFP and histone H2Av-mRFP1 with (+OE) or without (–OE) simultaneous α*4tub-GAL4-VP16*-driven overexpression of *UAS-cal1*, *UAS-Cenp-A/cid* and *UAS-Cenp-C*. The time (minutes:seconds) indicated in each frame is given relative to the start of prophase (first and second row) or the end of metaphase (third and fourth row), which was set to zero. Compared with controls (–OE; first row), embryos overexpressing Cal1, Cenp-A/Cid and Cenp-C (+OE; second row) show a delay in chromosome congression and during metaphase. Subsequent chromosome segregation is normal in only 50% of the observed anaphases (not shown). The other half display subtle or strong abnormalities, as illustrated in the third and fourth row. Scale bar: 3 µm. (**B**) The distances (in µm) between sister kinetochores in metaphase plates of embryos with (+OE) or without (–OE) α*4tub-GAL4-VP16*-driven overexpression of *UAS-cal1*, *UAS-Cenp-A/cid* and *UAS-Cenp-C* are illustrated in box plots. Each dot represents one sister kinetochore pair. Mean values (with s.d.) are indicated by the two larger dots. After co-overexpression of Cal1, Cenp-A/Cid and Cenp-C, the distances between sister kinetochores scatter over a wider range.

mitosis. Moreover, the excess levels of Cal1, Cenp-A/Cid and Cenp-C that were not yet incorporated into the centromere did not lead to mitotic defects during the *hs-stg*-induced mitosis.

Discussion

Drosophila Cal1 has been identified recently because its knockdown in cultured cells results in a loss of Cenp-A/Cid and Cenp-C from centromeres and a failure of chromosome alignment and segregation during mitosis (Goshima et al., 2007; Erhardt et al., 2008). Here, we demonstrate that Cal1 is a crucial component of the important regulatory mechanisms that prevent an excessive incorporation of Cenp-A/Cid and Cenp-C into centromeres and consequential chromosome mis-segregation.

cal1 is an essential gene that is expressed specifically in mitotically proliferating cells. To provide its function, the protein product needs its N-terminal domain, which interacts with Cenp-A/Cid, as well as its C-terminal domain, which interacts with Cenp-C. By contrast, the most rapidly diverging middle region of Cal1 seems to be of lesser importance because expression of the N-C version, which lacks the M domain, is sufficient to prevent the characteristic defects in *cal1* mutant embryos. The obvious functionality of the N-C version also emphasizes the importance of the centromeric localization of Cal1. The complete Cal1 protein is observed not only at the centromere, but also in the nucleolus. The M region is both sufficient and required for nucleolar localization. However, because this M domain is not required for *cal1* mutant rescue, the significance of the nucleolar Cal1 localization remains unclear.

Rescue of *cal1* mutants is not observed when the N- and C-terminal domains of Cal1 are expressed without a covalent linkage. The ability to recruit Cenp-A/Cid and Cenp-C into a complex, as clearly evidenced by our yeast three-hybrid experiments, is therefore likely to be crucial for Cal1 function. Co-immunoprecipitation of Cal1, Cenp-A/Cid and Cenp-C has previously indicated that these components can associate in vivo (Erhardt et al., 2008). However, our quantification of protein levels, which is largely dependent on the accuracy of our EGFP signal quantifications, demonstrates that Cenp-C is not exclusively anchored to centromeric chromatin via persistent and stoichiometric Cal1-mediated links to Cenp-A/Cid. Centromeric Cal1 levels are more than 40-times lower than those of Cenp-A/Cid and Cenp-C.

The centromeric amount of Cal1 is also far lower than that of the other kinetochore components that we have quantified (Spc105, Spc25, Nuf2). Interestingly, per kinetochore, the copy numbers of these components appear to be scaling well with the number of kinetochore microtubules (kMTs) when comparing our results from *Drosophila* with those described for budding and fission yeast (Joglekar et al., 2006; Joglekar et al., 2008). Spc25 and Nuf2 are constituents of the heterotetrameric Ndc80 complex, which binds directly to kMTs (Santaguida and Musacchio, 2009). Eight copies of the Ndc80 complex are thought to bind a single kMT to the budding yeast kinetochore (Joglekar et al., 2006). In *Drosophila*, where the number of kMTs per kinetochore appears to be around 11 (Maiato et al., 2006), about seven copies appear to be present per kMT according to our quantification. Our quantification of kinetochore proteins fits very well with the notion that the kinetochores of higher eukaryotes might be composed of several copies of a module that is present in one copy in budding yeast. By contrast, the centromere proteins Cenp-A and Cenp-C are scaling less well with the number of kMTs. The increased complexity of lateral co-ordination within animal kinetochores and of epigenetic specification of centromere identity might explain the higher relative amount of centromere proteins apparent in *Drosophila*. Despite this relative increase, centromeric Cenp-A/Cid allows packaging of only about 5% of the centromeric DNA in *Drosophila* under the assumption that Cenp-A/Cid nucleosomes

wrap about 200 bp of a 200 kb centromere (Sun et al., 1997; Allshire and Karpen, 2008).

Although our quantifications exclude the notion that Cal1 functions as a stable stoichiometric linker of Cenp-A/Cid and Cenp-C in mitotic kinetochores, our overexpression experiments provide further support for a role as a centromere protein-loading factor (Erhardt et al., 2008). Moreover, our experiments reveal additional layers of regulation that prevent excess incorporation of centromere proteins within the centromeric region. They also indicate that such excess incorporation is highly detrimental to kinetochore function. Previous work in *Drosophila* has demonstrated that strong overexpression of Cenp-A/Cid (about 70-fold) can lead to ectopic kinetochore formation (Heun et al., 2006). However, almost all Cenp-A/Cid that is incorporated ectopically within the chromosome arm regions is degraded rapidly (Moreno-Moreno et al., 2006), which is also observed in yeast (Collins et al., 2004). Here, we show that the limiting amounts of Cal1 provide additional, highly efficient protection against excessive chromosomal incorporation of Cenp-A/Cid. After bypassing this protection by Cal1 overexpression, even low levels of Cenp-A/Cid overexpression (about 2.5-fold) result in increased incorporation into centromeres (about 1.6-fold). When, in addition to Cal1 and Cenp-A/Cid, Cenp-C is also mildly co-overexpressed (about 3.5-fold), the levels of centromeric Cenp-A/Cid are further increased (about 2-fold) along with those of Cal1 and Cenp-C. Importantly, co-overexpression of these centromere proteins resulted not only in increased centromeric levels, but also in severe mitotic defects.

Although other interpretations are not excluded, our findings strongly suggest that the mitotic defects observed after overexpression of Cal1 and Cenp-A/Cid, and even more strongly when Cenp-C was also overexpressed, reflect the consequence of the increase in the centromeric levels of these proteins. The increase in centromeric levels of centromere proteins was accompanied by a significant increase in kinetochore proteins (Spc105 and the Mis12 and Ndc80 complex) but only to a very limited extent and only when all three centromere proteins were co-expressed. The increased amounts of centromeric Cenp-A/Cid observed after co-expression of Cal1 and Cenp-A/Cid, which were not accompanied by a statistically significant increase in kinetochore protein levels, might therefore be sufficient to disturb the spatial organization of the kinetochore, leading to inefficient chromosome congression, spindle checkpoint hyperactivation and chromosome segregation defects in anaphase.

Our experiments in *stg* mutant embryos, demonstrate that co-overexpression of centromeric proteins during interphase is not sufficient to cause excess centromeric incorporation, consistent with the previously demonstrated dependence of centromeric deposition of Cenp-A/Cid and Cenp-C on exit from mitosis (Schuh et al., 2007). Indeed, forcing progression through mitosis (by *hs-stg* induction) was observed to be sufficient to cause centromeric deposition of the overexpressed proteins. Moreover, the fact that the excess centromere proteins that were not yet incorporated into the centromere did not disturb the *hs-stg* induced mitosis, further supports our suggestion that the mitotic defects observed after co-expression of centromeric proteins depend on excessive incorporation into the centromere.

The severe mitotic defects observed after co-overexpression of Cal1, Cenp-A/Cid and Cenp-C emphasize the importance of careful control of centromere protein deposition. Several levels of control are effective. The interdependence of Cal1, Cenp-A/Cid and Cenp-C functions in conjunction with cell cycle control to prevent detrimental excessive centromeric incorporation. The cell cycle regulators cyclin A, Rca1/Emi1 and Fzr/Cdh1 have recently been implicated in the control of deposition of Cenp-A/Cid and Cenp-C at the centromere (Erhardt et al., 2008). How these and possibly additional cell cycle regulators control centromere protein deposition has yet to be clarified.

A possible scenario for centromere protein deposition in *Drosophila* might include a release of nucleolar Cal1 at the onset of mitosis, followed by conversion into a form that associates with non-centromeric soluble Cenp-A/Cid during exit from mitosis. After binding of soluble Cenp-A/Cid to the N-terminal domain of Cal1, its C-terminal domain might become exposed so that it can bind to centromeric Cenp-C and promote Cenp-A/Cid transfer onto the neighboring centromeric chromatin and thereby indirectly also additional Cenp-C deposition.

The mechanisms and the extent of control of centromeric Cenp-A deposition appear to have evolved. In fission yeast, overexpression of Cenp-A/Cid alone is sufficient to obtain excess centromeric Cenp-A/Cnp1, and this excess does not result in increased kinetochore protein levels (Joglekar et al., 2008). Spreading of Cenp-A within centromeric chromatin has also been clearly demonstrated in human cells after mild overexpression of Cenp-A (Lam et al., 2006). Mitotic defects were not detected in this case, perhaps because of the very limited increase in centromeric Cenp-A. Cal1 homologs from non-Drosophilid genomes have not yet been identified so far. Conversely, with the exception of Cenp-C, homologs of the 15 components of the vertebrate centromere chromatin-associated network (CCAN), which is related to the yeast Ctf19 and Sim4 complexes, have not been revealed in Drosophilid genomes, neither by thorough bioinformatic analyses (Meraldi et al., 2006) nor by genome-wide RNAi screens (Goshima et al., 2007; Erhardt et al., 2008). The CCAN seems also to be absent in *C. elegans* (Cheeseman et al., 2004; Sonnichsen et al., 2005; Gassmann et al., 2008). It is conceivable therefore that Cal1 is a functional analog of the CCAN, which has also been implicated in Cenp-A loading (Okada et al., 2006). However, because the evolutionary sequence conservation of centromere and kinetochore components is generally very low, it remains a possibility that Cal1 homologs also exist and function in centromere loading of human Cenp-A and Cenp-C.

Materials and Methods

Fly strains

cal1^{c03646} (Thibault et al., 2004), *cal1*^{MB04866} (Metaxakis et al., 2005) and *Df(3R)Exel6176* (Parks et al., 2004) were obtained from the Bloomington *Drosophila* Stock Center. *gEGFP-cal1* lines were generated using *ΦC31*-mediated germline transformation (Bischof et al., 2007) and *UAS-cal1*, *UAS-cal1-EGFP*, *UAS-cal1(N)-EGFP*, *UAS-cal1(M)-EGFP*, *UAS-cal1(C)-EGFP*, *UAS-cal1(N-C)-EGFP* and *gcal1-EGFP* with *pP{CaSpeR-4}* constructs (details provided upon request).

The wing imaginal discs analyzed for the quantification of centromere and kinetochore proteins fused to EGFP (Schuh et al., 2007; Schittenhelm et al., 2007; Schittenhelm et al., 2009) were from larvae with the following genotypes:
w; cid*$^{T12\text{-}1}$*/cid*$^{T22\text{-}4}$*; P{w*$^{+}$*, gcid-EGFP-cid} III.2*
w; P{w*$^{+}$*, giEGFP-Cenp-C} II.1; FRT82B Cenp-C*^{prl41}
w; P{w*$^{+}$*, gcal1-EGFP}II.2; cal1* ^{MB04866}
w; P{w*$^{+}$*, gSpc105-EGFP} II.1; Spc105*^{1}
w; gMis12-EGFP II.2; Mis12*^{f03756}*/Df(3L)BSC27*
w; P{w*$^{+}$*, gSpc25-EGFP} II.1; Spc25*^{c00064}
w; Nuf2*^{ex50}*; P{w*$^{+}$*, gEGFP-Nuf2} III.1.*

For the analyses in stg mutant embryos, we crossed *w*; P{w*$^{+}$*, UAS-cal1-EGFP} II.1/CyO, P{ry*$^{+}$*, ftz-lacZ}; P{w*$^{+}$*, UAS-Cenp-A/cid} III.5, P{w*$^{+}$*, UAS-Cenp-C} III.1, stg*^{7B}*/TM3, Sb, P{w*$^{+}$*, Ubx-lacZ}* males with either *w*; stg*^{7B}*, e, P{w*$^{+}$*, da-GAL4} G32/TM3, Sb, P{w*$^{+}$*, Ubx-lacZ}* or *w*; stg*^{7B}*, e, P{w*$^{+}$*, hs-stg} 3.1, P{w*$^{+}$*, da-GAL4} G32/TM3, Sb, P{w*$^{+}$*, Ubx-lacZ}* females.

Yeast two- and three-hybrid assays

Protein–protein interactions were analyzed essentially as described (Jäger et al., 2004). For Y3H analyses, the yeast strain MaV203 (Invitrogen) was cotransformed with a *pBridge-cal1* and a *pGADT7* construct and plated on *SD-Leu-Trp* selective drop-out medium. Colonies were transferred to appropriate selective drop-out medium plates (SD-Leu-Trp-Ura and SD-Leu-Trp-His) with or without methionine. *cal1* expression from the *pBridge* construct is controlled by the P_{Met25} promoter and occurs only in the absence of methionine.

Transfections, immunoblotting and immunolabeling

Transfection of S2R+ cells was conducted with the FuGeneHD Transfection Reagent (Roche) essentially as described (Schittenhelm et al., 2007). Immunofluorescence and DNA labeling of S2R+ cells and fixed embryos was also done essentially as described (Pandey et al., 2005; Schittenhelm et al., 2007). Rabbit antibodies against EGFP (1:3000), Cenp-A/Cid (Jäger et al., 2005), Cenp-C (Heeger et al., 2005) and Spc105 (Schittenhelm et al., 2009), as well as mouse anti-α-tubulin (DM1A, 1:50,000, Sigma) and anti-lamin Dm0 (ADL67.10, 1:200) were used for immunoblotting.

For quantification of centromeric anti-Cenp-A/Cid and anti-Cenp-C signal intensities (Fig. 5B,C), we crossed *prd-GAL4/TM3, Sb, P{w+, Ubx-lacZ}* females to males carrying various *UAS* transgenes individually or in combination (*UAS-Cenp-A/cid III.5, UAS-Cenp-C III.1* and *UAS-cal1-EGFP II.1*). Embryos were collected for 2 hours and aged for 5 hours at 25°C before fixation and immunolabeling with rabbit anti-Cenp-A/Cid or anti-Cenp-C, mouse anti-β-galactosidase (for genotype determination) and Hoechst 33258 (DNA stain).

For quantification of kinetochore protein levels (Fig. 5F), we crossed females carrying *prd-GAL4* recombined with a transgene driving expression of a kinetochore protein fused to EGFP under the control of the endogenous regulatory region (*gMis12-EGFP III.1, gSpc105-EGFP III.1, gEGFP-Nuf2 III.1* or *gSpc25-EGFP III.1*) over *TM3, Sb, P{w+, Ubx-lacZ}* to males carrying various *UAS*-transgenes individually or in combination (*UAS-Cenp-A/cid III.5, UAS-Cenp-C III.1* and *UAS-cal1 II.1*).

Quantification of signal intensities in embryos with *prd-GAL4* expressing and non-expressing regions was performed after acquisition of stacks with a 63×/1.4 oil-immersion objective and 250 nm spacing from the epidermal region of the second and third thoracic and the first abdominal segment. Within this imaged region, *prd-GAL4* drives expression in the outer but not in the middle segment. A Colibri light source (Zeiss) with a 470 nm light emitting diode was used for EGFP excitation with reproducible and temporally stable intensity. The stacks were deconvolved (Huygens Remote Manager v1.0 beta 2; Montpellier RIO Imaging) and subsequently converted into maximum projections using ImageJ.

For quantification of anti-Cenp-A/Cid and anti-Cenp-C signals, stacks with 12 sections were acquired from six different embryos for each genotype. A rectangle from the middle region that does not express *prd-GAL4* was first selected. Subsequently, the average intensity of the centromeric pixels within the selected rectangle was determined after applying a threshold to eliminate non-centromeric signals. Moreover, the average pixel intensity of non-centromeric pixels was determined and defined as background within the selected rectangle. Subtraction of this background from the intensity of centromeric pixels resulted in our measure of centromeric signal intensity within the middle internal control region that does not express *prd-GAL4*. Thereafter, rectangles from the flanking regions that express *prd-GAL4* were selected, followed again by thresholding to select centromeric pixels. To arrive at our measure of centromeric signal intensities within the *prd-GAL4*-expressing regions, we subtracted the background determined in the middle internal control region. By subtracting the background determined in the middle internal control region from the intensity of the non-centromeric pixels within the *prd-GAL4*-expressing regions, we arrived at a measure for the non-centromeric excess of the overexpressed centromere protein.

For Cal1-EGFP signal quantification, we were unable to use the intervening middle region as an internal control because *UAS-cal1-EGFP* was only expressed within the *prd-GAL4*-expressing regions, Therefore, we determined centromeric GFP signal intensities by applying a threshold to select the centromeric pixels within the *prd-GAL4*-expressing regions followed by subtraction of the background, which was obtained by averaging signal intensities of the non-centromeric pixels. The values obtained for all six embryos of a given genotype were averaged. The average obtained with embryos expressing only *UAS-cal1-EGFP* was set to 100% to arrive at the bars presented in Fig. 5C.

Quantification with or without prior deconvolution resulted in identical ratios of centromeric signal intensities between *prd-GAL4*-expressing and non-expressing regions in case of the anti-Cenp-A/Cid staining. In case of anti-Cenp-C and Cal1-EGFP, higher non-centromeric signals precluded a reliable, exclusive segmentation of centromeric signals without prior deconvolution. However, in these cases, quantification of individually selected centromeres using the two-square method with local background correction (see below) also resulted in very similar results, irrespective of prior deconvolution.

For quantification of EGFP-tagged kinetochore components, we acquired stacks with 12 sections from at least seven different embryos. Individual prometaphase or metaphase cells in the maximum projections were selected consecutively by two concentric squares (side length, 50 pixel and 55 pixels, respectively). The total pixel intensity of each square was determined and the average pixel intensity within the region encircled by the larger, but not by the smaller square was determined as local background. The average background pixel intensity integrated over the smaller square was subtracted from the total pixel intensity within the smaller square to yield the kinetochore signal intensity of a cell.

In vivo imaging

Embryos obtained from a cross of *α4tub-GAL4-VP16, gHis2AvD-mRFP II.2, gcid-EGFP-cid II.1 / CyO, P{ry+, ftz-lacZ}* females with *UAS-cal1 II.1; UAS-Cenp-A/cid III.5, UAS-Cenp-C III.1* males were analyzed by in vivo imaging essentially as described (Pandey et al., 2005) at the stage when epidermal cells progress through the fifteenth (4–5 hours) or sixteenth (6.5–7.5 hours) round of mitosis. Time-lapse imaging was performed with an Olympus FV1000 system. Stacks (four sections, 250 nm spacing) were acquired at intervals of 20 seconds using a 60× oil-immersion objective and converted to maximum projections. Embryos from *α4tub-GAL4-VP16, gHis2AvD-mRFP II.2, gcid-EGFP-cid II.1 / CyO, P{ry+, ftz-lacZ}* females crossed against w^1 males were analyzed for control.

For the comparison of the levels of *Drosophila* centromere and kinetochore proteins fused to EGFP with those of Cse4-EGFP in yeast, we dissected wing imaginal discs from third instar wandering stage larvae in Schneider's *Drosophila* medium (Invitrogen). The imaginal discs were mounted in phosphate-buffered saline (PBS) on a coverslip previously coated with yeast cells of strain KBY7006 (*S. cerevisiae* 473a CSE4-GFP:KAN; (Joglekar et al., 2006) kindly provided by Kerry Bloom (University of North Carolina, Chapel Hill, NC). Yeast cells from a fresh overnight culture grown in YPD at 25°C were resuspended in PBS after sedimentation and a wash in H_2O. The suspension was spread on a coverslip coated with concanavalin A for about 5 minutes. Immediately before mounting freshly dissected wing imaginal discs, a region in the center of the coverslip was wiped dry. Imaginal discs were mounted in this region with their peripodial membranes facing the cover slip. Stacks (20–27 sections, 250 nm spacing) were acquired using a 63×/1.4 oil immersion objective and a Zeiss Cell Observer HS. The stacks were converted into maximum projections using ImageJ. For Cse4-EGFP signal quantification, individual centromere clusters of anaphase or telophase cells were selected by two concentric squares (side length, 20 and 22 pixels, respectively) and centromeric signal intensity was determined after background subtraction as described above for kinetochore EGFP fusion proteins. For quantification of EGFP-tagged centromere and kinetochore components in imaginal wing discs, at least 40 individual cells from more than three wing discs per genotype were also selected by two concentric squares (side length, 50 and 55 pixels, respectively) followed by determination of centromeric signal intensity after background subtraction as described above.

We would like to thank Romanas Chaleckis for assistance during the Y2H experiments, Sebastian Heeger for initial characterization of Cenp-A/Cid and Cenp-C overexpression, Alf Herzig for the *stg*^{7B}, *hs-stg, da-GAL4* stock, Johannes Bischof and Konrad Basler for sharing the unpublished cloning vector *pattB*, as well as Brigitte Jaunich and Sina Niebur for technical help. This work was supported by grants of the Swiss National Science Foundation (SNF 3100A0-120276/1) and the Deutsche Forschungsgemeinschaft (DFG He 2354/2-4).

Supplementary material available online at
http://jcs.biologists.org/cgi/content/full/123/21/3768/DC1

References

Ahmad, K. and Henikoff, S. (2002). Histone H3 variants specify modes of chromatin assembly. *Proc. Natl. Acad. Sci. USA* **99**, 16477-16484.

Allshire, R. C. and Karpen, G. H. (2008). Epigenetic regulation of centromeric chromatin: old dogs, new tricks? *Nat. Rev. Genet.* **9**, 923-937.

Bischof, J., Maeda, R. K., Hediger, M., Karch, F. and Basler, K. (2007). An optimized transgenesis system for Drosophila using germ-line-specific phiC31 integrases. *Proc. Natl. Acad. Sci. USA* **104**, 3312-3317.

Blower, M. D., Sullivan, B. A. and Karpen, G. H. (2002). Conserved organization of centromeric chromatin in flies and humans. *Dev. Cell* **2**, 319-330.

Camahort, R., Shivaraju, M., Mattingly, M., Li, B., Nakanishi, S., Zhu, D., Shilatifard, A., Workman, J. L. and Gerton, J. L. (2009). Cse4 is part of an octameric nucleosome in budding yeast. *Mol. Cell* **35**, 794-805.

Cheeseman, I. M., Niessen, S., Anderson, S., Hyndman, F., Yates, J. R., 3rd, Oegema, K. and Desai, A. (2004). A conserved protein network controls assembly of the outer kinetochore and its ability to sustain tension. *Genes Dev.* **18**, 2255-2268.

Cohen, R. L., Espelin, C. W., De Wulf, P., Sorger, P. K., Harrison, S. C. and Simons, K. T. (2008). Structural and functional dissection of Mif2p, a conserved DNA-binding kinetochore protein. *Mol. Biol. Cell* **19**, 4480-4491.

Collins, K. A., Furuyama, S. and Biggins, S. (2004). Proteolysis contributes to the exclusive centromere localization of the yeast Cse4/CENP-A histone H3 variant. *Curr. Biol.* **14**, 1968-1972.

Dalal, Y., Wang, H., Lindsay, S. and Henikoff, S. (2007). Tetrameric structure of centromeric nucleosomes in interphase Drosophila cells. *PLoS Biol.* **5**, e218.

Dunleavy, E. M., Roche, D., Tagami, H., Lacoste, N., Ray-Gallet, D., Nakamura, Y., Daigo, Y., Nakatani, Y. and Almouzni-Pettinotti, G. (2009). HJURP is a cell-cycle-

dependent maintenance and deposition factor of CENP-A at centromeres. *Cell* **137**, 485-497.
Edgar, B. A. and O'Farrell, P. H. (1989). Genetic control of cell division patterns in the Drosophila embryo. *Cell* **57**, 177-183.
Erhardt, S., Mellone, B. G., Betts, C. M., Zhang, W., Karpen, G. H. and Straight, A. F. (2008). Genome-wide analysis reveals a cell cycle-dependent mechanism controlling centromere propagation. *J. Cell Biol.* **183**, 805-818.
Fitzgerald-Hayes, M., Buhler, J. M., Cooper, T. G. and Carbon, J. (1982). Isolation and subcloning analysis of functional centromere DNA (CEN11) from Saccharomyces cerevisiae chromosome XI. *Mol. Cell. Biol.* **2**, 82-87.
Foltz, D. R., Jansen, L. E., Bailey, A. O., Yates, J. R., 3rd, Bassett, E. A., Wood, S., Black, B. E. and Cleveland, D. W. (2009). Centromere-specific assembly of CENP-a nucleosomes is mediated by HJURP. *Cell* **137**, 472-484.
Fujita, Y., Hayashi, T., Kiyomitsu, T., Toyoda, Y., Kokubu, A., Obuse, C. and Yanagida, M. (2007). Priming of centromere for CENP-A recruitment by human hMis18alpha, hMis18beta, and M18BP1. *Dev. Cell* **12**, 17-30.
Furuyama, T. and Henikoff, S. (2009). Centromeric nucleosomes induce positive DNA supercoils. *Cell* **138**, 104-113.
Furuyama, T., Dalal, Y. and Henikoff, S. (2006). Chaperone-mediated assembly of centromeric chromatin in vitro. *Proc. Natl. Acad. Sci. USA* **103**, 6172-6177.
Gassmann, R., Essex, A., Hu, J. S., Maddox, P. S., Motegi, F., Sugimoto, A., O'Rourke, S. M., Bowerman, B., McLeod, I., Yates, J. R., 3rd et al. (2008). A new mechanism controlling kinetochore-microtubule interactions revealed by comparison of two dynein-targeting components: SPDL-1 and the Rod/Zwilch/Zw10 complex. *Genes Dev.* **22**, 2385-2399.
Goshima, G., Wollman, R., Goodwin, S. S., Zhang, N., Scholey, J. M., Vale, R. D. and Stuurman, N. (2007). Genes required for mitotic spindle assembly in Drosophila S2 cells. *Science* **316**, 417-421.
Hayashi, T., Fujita, Y., Iwasaki, O., Adachi, Y., Takahashi, K. and Yanagida, M. (2004). Mis16 and Mis18 are required for CENP-A loading and histone deacetylation at centromeres. *Cell* **118**, 715-729.
Heeger, S., Leismann, O., Schittenhelm, R., Schraidt, O., Heidmann, S. and Lehner, C. F. (2005). Genetic inteactions of Separase regulatory subunits reveal the diverged Drosophila Cenp-C homolog. *Genes Dev.* **19**, 2041-2053.
Heun, P., Erhardt, S., Blower, M. D., Weiss, S., Skora, A. D. and Karpen, G. H. (2006). Mislocalization of the Drosophila centromere-specific histone CID promotes formation of functional ectopic kinetochores. *Dev. Cell* **10**, 303-315.
Hori, T., Amano, M., Suzuki, A., Backer, C. B., Welburn, J. P., Dong, Y., McEwen, B. F., Shang, W. H., Suzuki, E., Okawa, K. et al. (2008). CCAN makes multiple contacts with centromeric DNA to provide distinct pathways to the outer kinetochore. *Cell* **135**, 1039-1052.
Jäger, H., Herzig, B., Herzig, A., Sticht, H., Lehner, C. F. and Heidmann, S. (2004). Structure predictions and interaction studies indicate homology of separase N-terminal regulatory domains and Drosophila THR. *Cell Cycle* **3**, 182-188.
Jäger, H., Rauch, M. and Heidmann, S. (2005). The Drosophila melanogaster condensin subunit Cap-G interacts with the centromere-specific histone H3 variant CID. *Chromosoma* **113**, 350-361.
Jansen, L. E., Black, B. E., Foltz, D. R. and Cleveland, D. W. (2007). Propagation of centromeric chromatin requires exit from mitosis. *J. Cell Biol.* **176**, 795-805.
Joglekar, A. P., Bouck, D. C., Molk, J. N., Bloom, K. S. and Salmon, E. D. (2006). Molecular architecture of a kinetochore-microtubule attachment site. *Nat. Cell Biol.* **8**, 581-585.
Joglekar, A. P., Bouck, D., Finley, K., Liu, X., Wan, Y., Berman, J., He, X., Salmon, E. D. and Bloom, K. S. (2008). Molecular architecture of the kinetochore-microtubule attachment site is conserved between point and regional centromeres. *J. Cell Biol.* **181**, 587-594.
Lam, A. L., Boivin, C. D., Bonney, C. F., Rudd, M. K. and Sullivan, B. A. (2006). Human centromeric chromatin is a dynamic chromosomal domain that can spread over noncentromeric DNA. *Proc. Natl. Acad. Sci. USA* **103**, 4186-4191.
Maddox, P. S., Hyndman, F., Monen, J., Oegema, K. and Desai, A. (2007). Functional genomics identifies a Myb domain-containing protein family required for assembly of CENP-A chromatin. *J. Cell Biol.* **176**, 757-763.
Maiato, H., Hergert, P. J., Moutinho-Pereira, S., Dong, Y., Vandenbeldt, K. J., Rieder, C. L. and McEwen, B. F. (2006). The ultrastructure of the kinetochore and kinetochore fiber in Drosophila somatic cells. *Chromosoma* **115**, 469-480.
Meluh, P. B., Yang, P., Glowczewski, L., Koshland, D. and Smith, M. M. (1998). Cse4p is a component of the core centromere of Saccharomyces cerevisiae. *Cell* **94**, 607-613.
Meraldi, P., McAinsh, A. D., Rheinbay, E. and Sorger, P. K. (2006). Phylogenetic and structural analysis of centromeric DNA and kinetochore proteins. *Genome Biol.* **7**, R23.
Metaxakis, A., Oehler, S., Klinakis, A. and Savakis, C. (2005). Minos as a genetic and genomic tool in Drosophila melanogaster. *Genetics* **171**, 571-581.
Mizuguchi, G., Xiao, H., Wisniewski, J., Smith, M. M. and Wu, C. (2007). Nonhistone Scm3 and histones CenH3-H4 assemble the core of centromere-specific nucleosomes. *Cell* **129**, 1153-1164.
Moreno-Moreno, O., Torras-Llort, M. and Azorin, F. (2006). Proteolysis restricts localization of CID, the centromere-specific histone H3 variant of Drosophila, to centromeres. *Nucleic Acids Res.* **34**, 6247-6255.
Okada, M., Cheeseman, I. M., Hori, T., Okawa, K., McLeod, I. X., Yates, J. R., 3rd, Desai, A. and Fukagawa, T. (2006). The CENP-H-I complex is required for the efficient incorporation of newly synthesized CENP-A into centromeres. *Nat. Cell Biol.* **8**, 446-457.
Pandey, R., Heidmann, S. and Lehner, C. F. (2005). Epithelial re-organization and dynamics of progression through mitosis in Drosophila separase complex mutants. *J. Cell Sci.* **118**, 733-742.
Parks, A. L., Cook, K. R., Belvin, M., Dompe, N. A., Fawcett, R., Huppert, K., Tan, L. R., Winter, C. G., Bogart, K. P., Deal, J. E. et al. (2004). Systematic generation of high-resolution deletion coverage of the Drosophila melanogaster genome. *Nat. Genet.* **36**, 288-292.
Perpelescu, M., Nozaki, N., Obuse, C., Yang, H. and Yoda, K. (2009). Active establishment of centromeric CENP-A chromatin by RSF complex. *J. Cell Biol.* **185**, 397-407.
Pidoux, A. L., Choi, E. S., Abbott, J. K., Liu, X., Kagansky, A., Castillo, A. G., Hamilton, G. L., Richardson, W., Rappsilber, J., He, X. et al. (2009). Fission yeast Scm3: A CENP-A receptor required for integrity of subkinetochore chromatin. *Mol. Cell* **33**, 299-311.
Przewloka, M. R., Zhang, W., Costa, P., Archambault, V., D'Avino, P. P., Lilley, K. S., Laue, E. D., McAinsh, A. D. and Glover, D. M. (2007). Molecular analysis of core kinetochore composition and assembly in Drosophila melanogaster. *PLoS ONE* **2**, e478.
Santaguida, S. and Musacchio, A. (2009). The life and miracles of kinetochores. *EMBO J.* **28**, 2511-2531.
Schittenhelm, R. B., Heeger, S., Althoff, F., Walter, A., Heidmann, S., Mechtler, K. and Lehner, C. F. (2007). Spatial organization of a ubiquitous eukaryotic kinetochore protein network in Drosophila chromosomes. *Chromosoma* **116**, 385-402.
Schittenhelm, R. B., Chaleckis, R. and Lehner, C. F. (2009). Essential functional domains and intrakinetochore localization of Drosophila Spc105. *EMBO J.* **28**, 2374-2386.
Schuh, M., Lehner, C. F. and Heidmann, S. (2007). Incorporation of Drosophila CID/CENP-A and CENP-C into centromeres during early embryonic anaphase. *Curr. Biol.* **17**, 237-243.
Sonnichsen, B., Koski, L. B., Walsh, A., Marschall, P., Neumann, B., Brehm, M., Alleaume, A. M., Artelt, J., Bettencourt, P., Cassin, E. et al. (2005). Full-genome RNAi profiling of early embryogenesis in Caenorhabditis elegans. *Nature* **434**, 462-469.
Sugimoto, K., Kuriyama, K., Shibata, A. and Himeno, M. (1997). Characterization of internal DNA-binding and C-terminal dimerization domains of human centromere/kinetochore autoantigen CENP-C in vitro: role of DNA-binding and self-associating activities in kinetochore organization. *Chromosome Res.* **5**, 132-141.
Sun, X., Wahlstrom, J. and Karpen, G. (1997). Molecular structure of a functional Drosophila centromere. *Cell* **91**, 1007-1019.
Takahashi, K., Chen, E. S. and Yanagida, M. (2000). Requirement of Mis6 centromere connector for localizing a CENP-A-like protein in fission yeast. *Science* **288**, 2215-2219.
Talbert, P. B., Bryson, T. D. and Henikoff, S. (2004). Adaptive evolution of centromere proteins in plants and animals. *J. Biol.* **3**, 18.
Thibault, S. T., Singer, M. A., Miyazaki, W. Y., Milash, B., Dompe, N. A., Singh, C. M., Buchholz, R., Demsky, M., Fawcett, R., Francis-Lang, H. L. et al. (2004). A complementary transposon tool kit for Drosophila melanogaster using P and piggyBac. *Nat. Genet.* **36**, 283-287.
Torras-Llort, M., Moreno-Moreno, O. and Azorin, F. (2009). Focus on the centre: the role of chromatin on the regulation of centromere identity and function. *EMBO J.* **28**, 2337-2348.
Trazzi, S., Perini, G., Bernardoni, R., Zoli, M., Reese, J. C., Musacchio, A. and Della Valle, G. (2009). The C-terminal domain of CENP-C displays multiple and critical functions for mammalian centromere formation. *PLoS ONE* **4**, e5832.
Vagnarelli, P., Ribeiro, S. A. and Earnshaw, W. C. (2008). Centromeres: old tales and new tools. *FEBS Lett.* **582**, 1950-1959.
Van Hooser, A. A., Ouspenski, II, Gregson, H. C., Starr, D. A., Yen, T. J., Goldberg, M. L., Yokomori, K., Earnshaw, W. C., Sullivan, K. F. and Brinkley, B. R. (2001). Specification of kinetochore-forming chromatin by the histone H3 variant CENP-A. *J. Cell Sci.* **114**, 3529-3542.
Williams, J. S., Hayashi, T., Yanagida, M. and Russell, P. (2009). Fission yeast Scm3 mediates stable assembly of Cnp1/CENP-A into centromeric chromatin. *Mol. Cell* **33**, 287-298.
Winey, M., Mamay, C. L., O'Toole, E. T., Mastronarde, D. N., Giddings, T. H., Jr, McDonald, K. L. and McIntosh, J. R. (1995). Three-dimensional ultrastructural analysis of the Saccharomyces cerevisiae mitotic spindle. *J. Cell Biol.* **129**, 1601-1615.
Yang, C. H., Tomkiel, J., Saitoh, H., Johnson, D. H. and Earnshaw, W. C. (1996). Identification of overlapping DNA-binding and centromere-targeting domains in the human kinetochore protein CENP-C. *Mol. Cell. Biol.* **16**, 3576-3586.

Journal of Cell Science

Figure S1

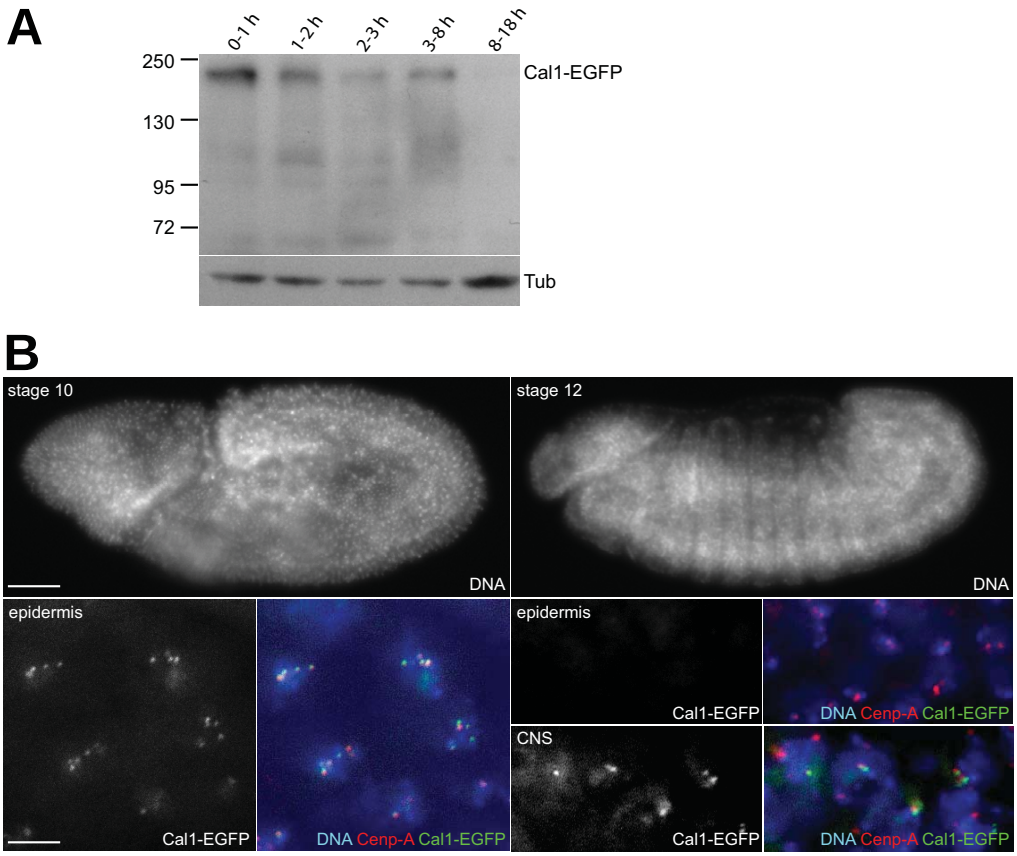

Figure S1. Cal1 expression during embryogenesis
(A) *gcal1-EGFP II.2* embryos were collected and aged as indicated above the lanes. Total embryo extracts were probed with anti-EGFP (Cal1-EGFP) and anti-α-tubulin (Tub), which served as a loading control. Migration of molecular weight markers (kDa) is indicated on the left side.
(B) *gcal1-EGFP II.2* embryos during stage 10 and 12 are shown in the left and right half, respectively, after double labeling with a DNA stain (DNA) and anti-Cenp-A/Cid (Cenp-A). High magnification views of regions from the epidermis or the central nervous system (CNS) are shown in the lower row, revealing Cal1-EGFP in mitotically proliferating cells but not in the post-mitotic epidermis at stage 12. Bars in the upper and lower row correspond to 60 and 5 µm, respectively.

Figure S2

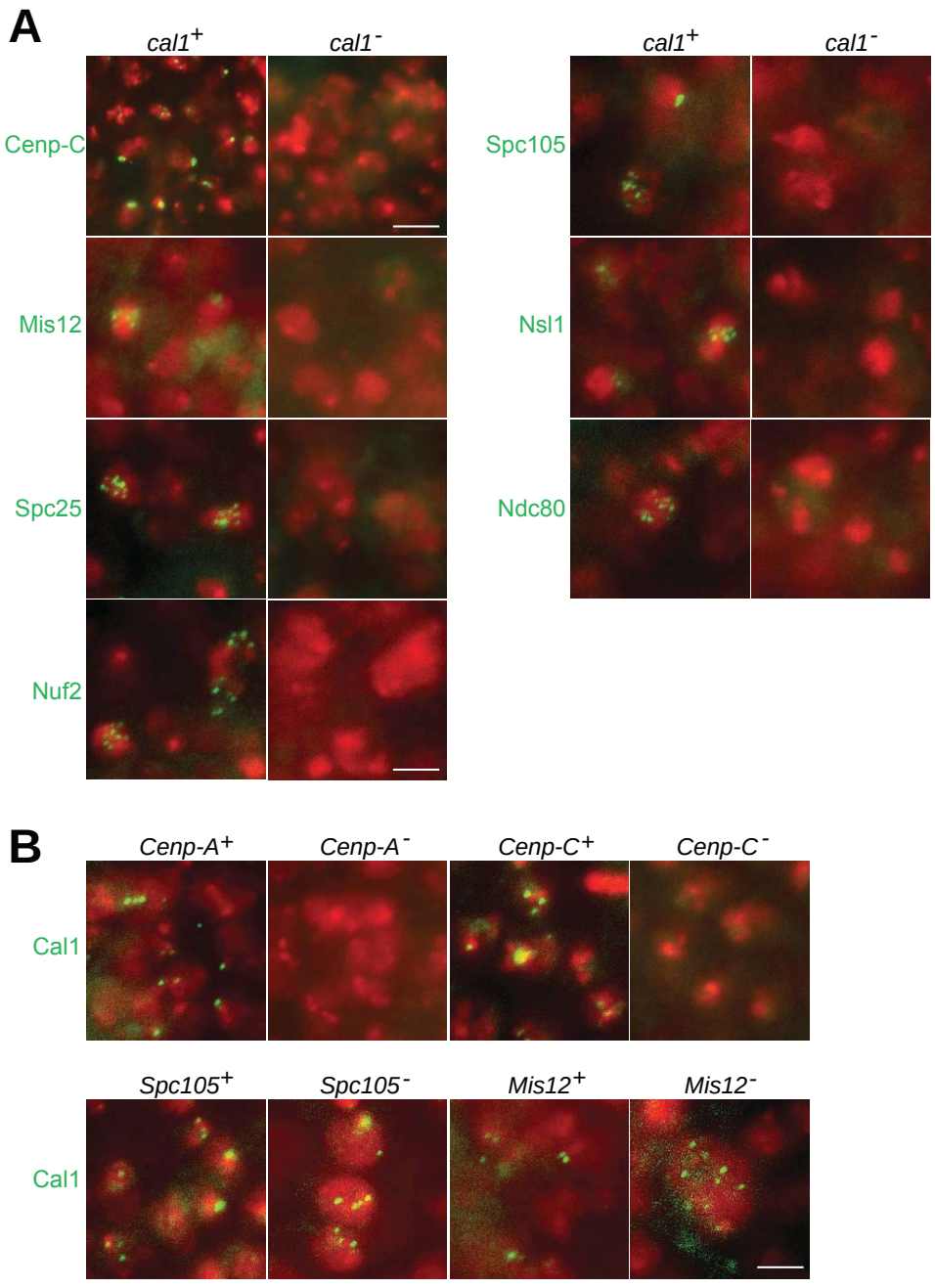
A
cal1+
cal1-
Cenp-C
Mis12
Spc25
Nuf2
cal1+
cal1-
Spc105
Nsl1
Ndc80
B
Cenp-A+
Cenp-A-
Cenp-C+
Cenp-C-
Cal1
Spc105+
Spc105-
Mis12+
Mis12-
Cal1

Figure S2. Cal1 acts at the top of the kinetochore assembly pathway.

(A) Localization of EGFP-fusions of Cenp-C, Spc105, Mis12, Nsl1, Spc25, Ndc80 and Nuf2 in homozygous *cal1*^{c03646} embryos (*cal1*$^{-}$) and in sibling control embryos (*cal1*$^{+}$) within the CNS after germband retraction. Representative mitotic figures are shown with the kinetochore proteins in *green* and DNA staining in *red*. Magnification in the first two Cenp-C panels is indicated by the upper bar = 6 μm; magnification in all other panels by the lower bar = 3 μm.

(B) Localization of Cal1-EGFP in *cid*$^{T12\text{-}1}$/*cid*$^{T22\text{-}4}$ (*Cenp-A*$^{-}$), *Cenp-C*^{prl41} (*Cenp-C*$^{-}$), *Spc105*^{1} (*Spc105*$^{-}$) and *Mis12*^{f03756} (*Mis12*$^{-}$) mutant embryos as well as in sibling control embryos (*Cenp-A*$^{+}$, *Cenp-C*$^{+}$, *Spc105*$^{+}$ and *Mis12*$^{+}$, respectively). Representative regions with Cal1-EGFP in *green* and DNA staining in *red* are shown at the stage where phenotypic abnormalities start in the mutant embryos, i.e. during mitosis 16 in *Cenp-C* and *Spc105* mutants and during the later mitotic divisions in the CNS in *Mis12* and *Cenp-A/cid* mutants. Bar = 3 μm.

Figure S3

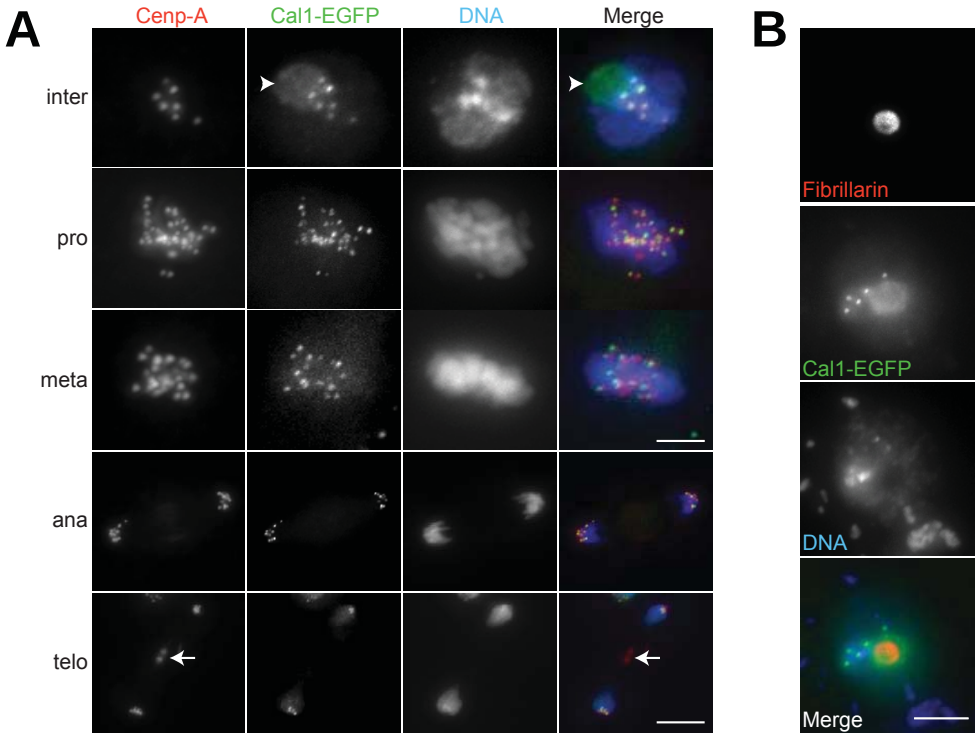

Figure S3. Intracellular localization of Cal1-EGFP
(A) Stably transfected S2R+ cells expressing Cal1-EGFP were double labeled with an antibody against Cenp-A/Cid (Cenp-A) and a DNA stain (DNA). Co-localization of Cal1-EGFP with Cenp-A/Cid at centromeres was observed throughout the cell cycle. In addition, Cal1-EGFP signals were also prominent in the nucleolus (arrowhead; see also B). The arrow indicates non-specific midbody staining by anti-Cenp-A/Cid. The bar in the third row illustrates magnification in the top three rows and corresponds to 5 μm; the bar in the bottom row illustrates magnification in the two bottom rows and corresponds to 7 μm.
(B) During interphase, Cal1-EGFP (Cal1-EGFP) is present in and around the nucleolus, as revealed by double labeling with an antibody against Fibrillarin (Fibrillarin) and DNA staining (DNA). Bar = 5 μm.

Figure S4

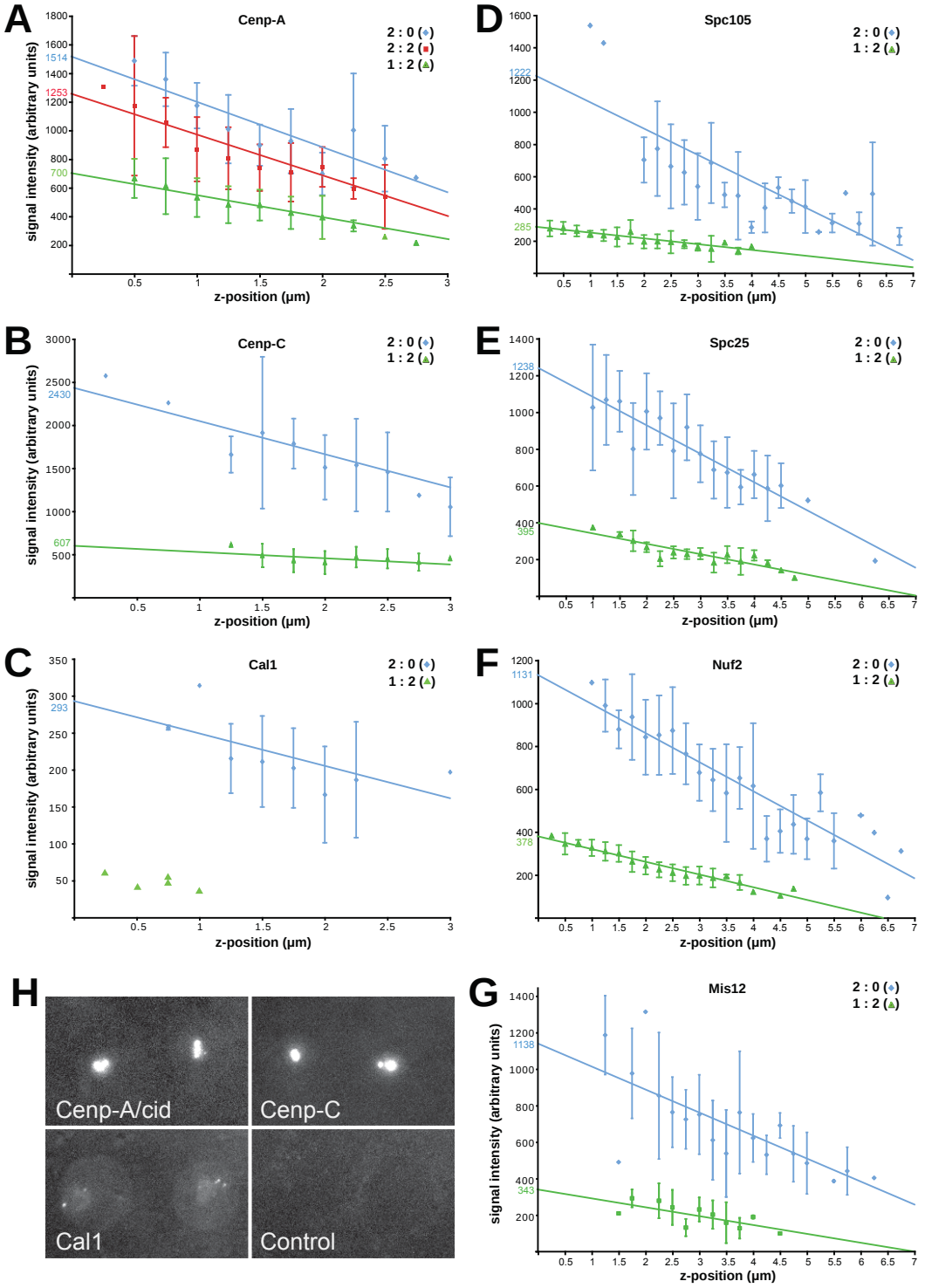
A
Cenp-A
2 : 0 (♦)
2 : 2 (■)
1 : 2 (▲)
signal intensity (arbitrary units)
z-position (µm)
B
Cenp-C
2 : 0 (♦)
1 : 2 (▲)
C
Cal1
D
Spc105
E
Spc25
F
Nuf2
G
Mis12
H
Cenp-A/cid
Cenp-C
Cal1
Control

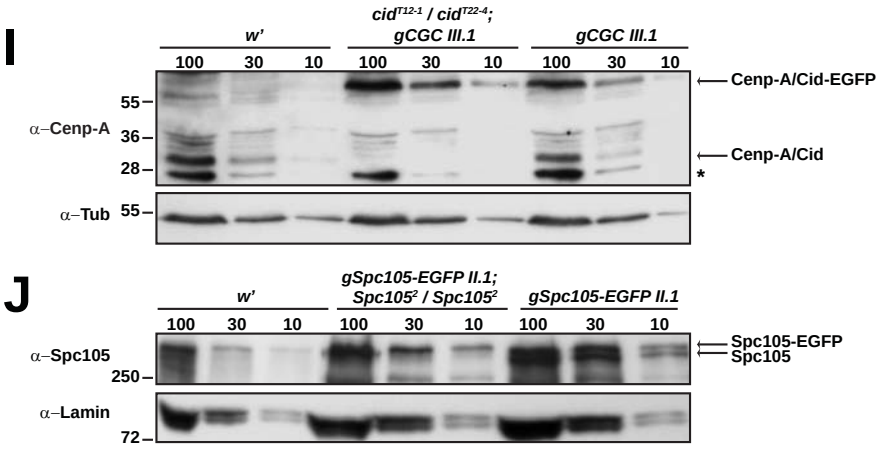

Figure S4. Stoichiometry of Drosophila centromere and kinetochore proteins.
(A-G) EGFP signal intensities observed in wing imaginal disc cells expressing EGFP fused to either the centromere proteins Cenp-A/Cid (A), Cenp-C (B) and Cal1 (C) or the kinetochore proteins Spc105 (D), Spc25 (E), Nuf2 (F) and Mis12 (G) were quantified and grouped according to their average focal depth. The average signal intensity (with s.d.) for each bin was plotted as a function of their z-position. Y intercepts of the linear regressions were used for comparisons of relative protein levels. To evaluate the accuracy of our quantifications, EGFP fusion proteins were expressed not only in a corresponding null mutant background but also in a background with functional endogenous genes. Untagged protein expressed from the endogenous genes is expected to compete with the EGFP-tagged protein and hence predicted to lower EGFP signal intensities at centromeres/kinetochores. Blue color represents data that was obtained with cells expressing two EGFP transgene copies and no functional endogenous copies (2:0), red color with cells expressing two EGFP transgene copies and two functional endogenous copies (2:2), and green color with cells expressing one EGFP transgene copy and two functional endogenous copies (1:2). In case of Cal1-EGFP, signals in the wild-type background were close to background and therefore difficult to detect, resulting in fewer data points which are shown individually as green triangles (C). Taking into account the observed relative expression levels of EGFP-tagged and untagged proteins (see also I and J) and assuming equal efficiency of incorporation into the centromere/kinetochore, the measured effects of competition deviate by less than 30% from the predicted competition effects.
(H) EGFP signals in live peripodial membrane cells of wing imaginal discs expressing either no EGFP (control) or EGFP fused to Cenp-A/Cid, Cenp-C or Cal1 in a corresponding null mutant background after identical acquisition and image processing (maximum projection). While Cal1-EGFP is detected not only at the centromere, but also in the nucleolus and weakly throughout the nucleus, strongly overexposed but exclusively centromeric signals are apparent in the case of Cenp-A/Cid-EGFP and Cenp-C-EGFP. Quantification of the Cal1-EGFP signals indicated that about 3.3% is centromeric, 21% nucleolar and 76% distributed throughout the nucleus (n = 5).
(I) Total extracts of 5-8 h old embryos (the exact genotypes are depicted above the lanes) were probed by immunoblotting with anti-Cenp-A/Cid (α-Cenp-A) and anti-α-Tubulin (α-Tub) to control for loading. The expression level of Cenp-A/Cid-EGFP was found to be approximately 3-fold higher than that of the endogenous Cenp-A/Cid, which explains the deviation between the expected and the observed centromeric incorporation of Cenp-A/Cid-EGFP in a null mutant compared to wild-type background (see also A). The numbers above the lanes indicate embryo equivalents loaded and the asterisk marks a prominent, unspecific band. The migration of the molecular weight marker (kDa) is indicated on the left side.
(J) Total extracts of 5-8 h old embryos (the exact genotypes are depicted above the lanes) were probed by immunoblotting with anti-Spc105 (α-Spc105) and anti-Lamin (α-Lamin), which served as a loading control. The expression levels of Spc105-EGFP and endogenous Spc105 were found to be similar, which is consistent with the observed decrease of centromeric incorporation of Spc105-EGFP in wild-type compared to null mutant background (see also D). The numbers indicate either embryo equivalents loaded (above the lanes) or the migration of the molecular weight marker (kDa; left side).

Figure S5

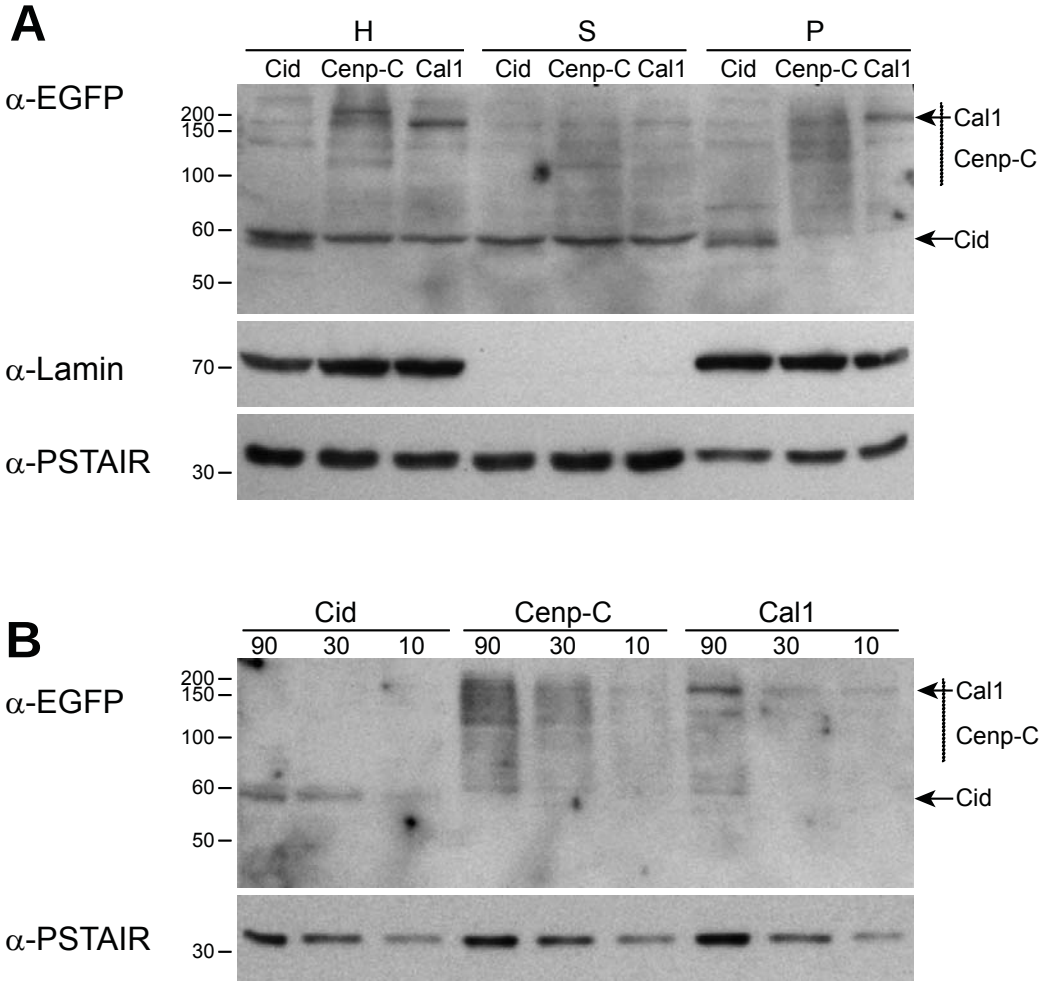

Figure S5. Expression levels EGFP fusion proteins of Cenp-A/Cid, Cenp-C and Cal1.
(A) Embryos were collected from strains with transgenes driving expression of EGFP fused to either Cenp-A/Cid, Cenp-C or Cal1 under control of the corresponding cis-regulatory regions in the corresponding null mutant backgrounds. 5-8 hour embryos were homogenized (H) followed by separation of a crude nuclear fraction (P) from the soluble material (S) by centrifugation. Immunoblotting with anti-EGFP (α-EGFP) was used to detect the different EGFP fusion proteins. Re-probing with anti-Lamin (α-Lamin) and anti-PSTAIR (α-PSTAIR) which reacts with Cdk1 was used to control the fractionation.
(B) For a comparison of expression levels, serial dilutions of crude nuclear fractions obtained from 90, 30, or 10 embryos, respectively, were immunoblotted with anti-EGFP (α-EGFP) and anti-PSTAIR (α-PSTAIR) as a loading control. Densitometric quantification indicated that the expression levels of Cenp-A/Cid-EGFP and Cal1-EGFP were 5.2 and 3.7 fold lower than that of Cenp-C-EGFP. Taking into account that only 3.3% of Cal1-EGFP is centromeric (Fig. S4H), this yields a stoichiometric ratio of centromeric Cenp-A/Cid, Cenp-C and Cal1 of about 20 : 100 : 0.9 compared to 60 : 100 : 1.9 obtained by purely microscopic EGFP signal detection and quantification (Table 1, Fig. 4C, Fig. S4A-C).

Figure S6

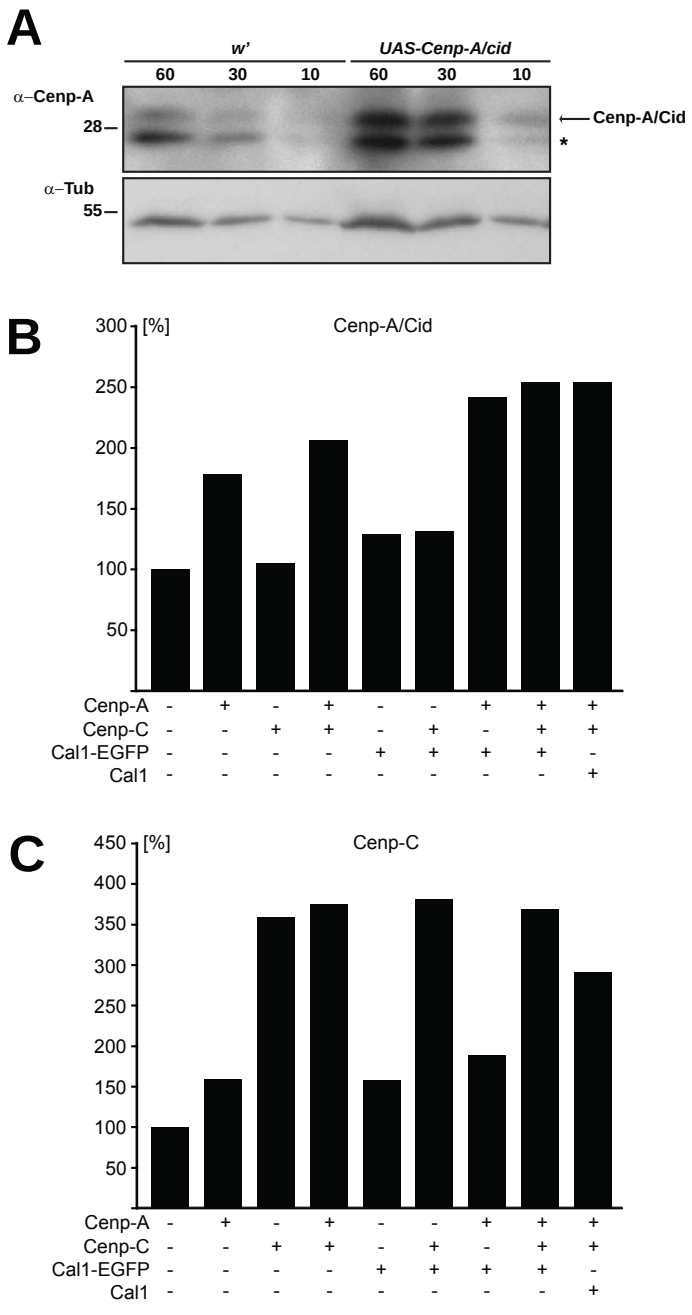
A
w'
UAS-Cenp-A/cid
60
30
10
60
30
10
α–Cenp-A
28
Cenp-A/Cid
*
α–Tub
55
B
[%]
Cenp-A/Cid
300
250
200
150
100
50
Cenp-A - + - + - - + + +
Cenp-C - - + + - + - + +
Cal1-EGFP - - - - + + + + -
Cal1 - - - - - - - - +
C
[%]
Cenp-C
450
400
350
300
250
200
150
100
50
Cenp-A - + - + - - + + +
Cenp-C - - + + - + - + +
Cal1-EGFP - - - - + + + + -
Cal1 - - - - - - - - +

Figure S6. Levels of overexpression of Cenp-A/Cid and Cenp-C in *Drosophila* embryos.

(A) Total extracts of 5-8 h old w^1 embryos and embryos overexpressing paternally derived *UAS-Cenp-A/cid* driven by maternal *α4tub-GAL4-VP16* were probed with anti-Cenp-A/Cid (α-Cenp-A) and anti-α-Tubulin (α-Tub), which served as loading control. The numbers indicate loading in embryo equivalents (above the lanes) or the position of molecular weight marker (kDa; left side). The asterisk marks a prominent, unspecific band.

(B and C) Paternally derived *UAS-Cenp-A/cid*, *UAS-Cenp-C* and *UAS-cal1-EGFP* or *UAS-cal1* were expressed individually or in combinations using maternal *α4tub-GAL4-VP16*. Total extracts were prepared and analyzed by immunoblotting as illustrated in panel A. The band intensities obtained with anti-Cenp-A/Cid (B) and anti-Cenp-C (C) were quantified (see Materials and Methods). The band intensity observed in the w^1 control embryos was set to 100%. The type(s) of *UAS* transgene expressed is indicated below the bars.

Figure S7

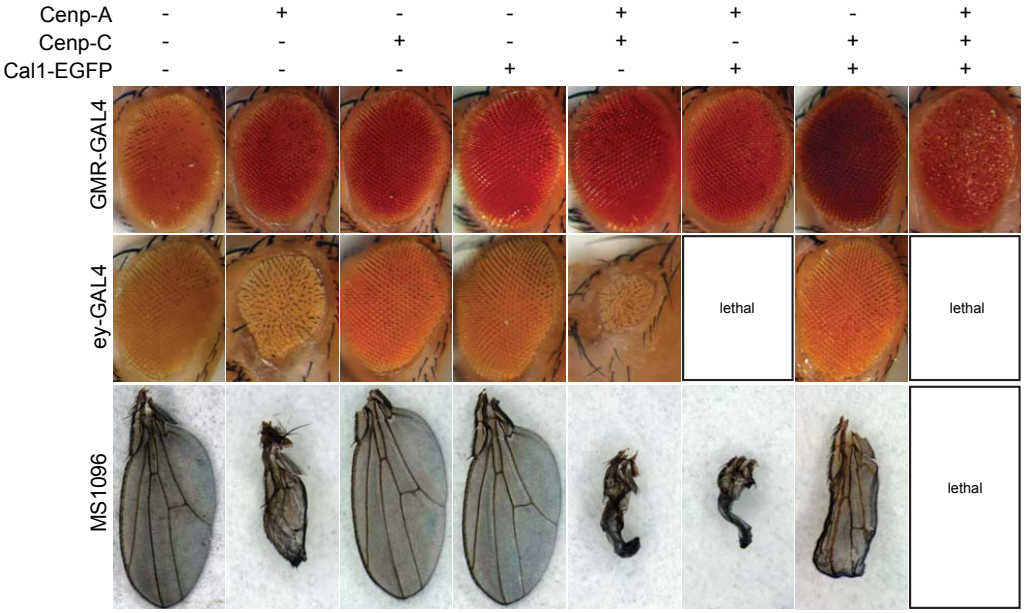

Figure S7. Synergistic effects of co-overexpression of Cenp-A/Cid, Cenp-C and Cal1 during eye and wing development.
The drivers *GMR-GAL4*, *ey-GAL4* or *MS1096* were used to express various *UAS* target transgenes (as indicated on top of the images) during eye and wing development. Wild-type eyes and wings were present in control flies with only one copy of one of these GAL4 driver transgenes and no *UAS* target transgenes. When *GMR-GAL4* as well as *UAS-Cenp-A/cid*, *UAS-Cenp-C* and *UAS-cal1-EGFP* were all present, an aberrant eye phenotype was observed. In contrast, the combination of *GMR-GAL4* with either double combinations or single *UAS* target transgenes did not result in aberrant phenotypes. In case of *ey-GAL4* and *MS1096*, expression of *UAS-Cenp-A/cid* alone already led to aberrant eye and wing phenotypes. In combination with *UAS-cal1-EGFP* or *UAS-Cenp-C*, these phenotypes became stronger, and overexpression of all three *UAS* target transgenes resulted in lethality.

Figure S8

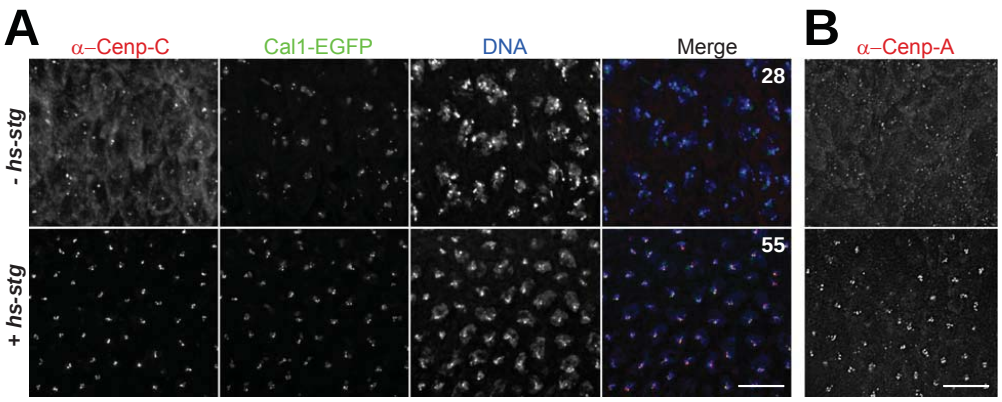

Figure S8. The increase in centromere protein levels after co-overexpression of Cenp-A/Cid, Cenp-C and Cal1 depends on progression through mitosis.
UAS-cal1-EGFP, *UAS-Cenp-A/cid* and *UAS-Cenp-C* were co-expressed ubiquitously in *string* (*stg*) mutant embryos in which a heat-inducible *stg* transgene was either absent (top row, -*hs-stg*) or present (bottom row, +*hs-stg*). 4-5 h old embryos were exposed to a heat shock (15 minutes at 37°C) followed by recovery (30 minutes at 25°C) and labeling with either anti-Cenp-C (A, α-Cenp-C) or with anti-Cenp-A/Cid (B, α-Cenp-A), as well as with a DNA stain (DNA) and anti-β-galactosidase for genotype determination (not shown). The number of nuclei present within the displayed regions is indicated in the merged panels. These numbers as well as the size of the nuclei demonstrate that *hs-stg* expression forces progression through a successful mitosis, while in the absence of *hs-stg* cells remain arrested in G2 (Edgar and O'Farrell, 1990). Increased levels of centromeric anti-Cenp-C and anti-Cenp-A/Cid labeling were only detected after progression through the *hs-stg*-induced mitosis. Bar = 10 μm.

Appendix 3:

Cell-Type-Specific TEV Protease Cleavage Reveals Cohesin Funtions in *Drosophila* Neurons

Pauli, A, Althoff, F, Oliveira, RA, Heidmann, S, Schuldiner, O, Lehner, CF, Dickson, BJ, Nasmyth, K

Dev Cell. 2008 Feb;14(2):239-51

Contribution to this part:

I generated flies for the observation of mitotic phenotypes after TEV induced Rad21 cleavage *in vivo* and in fixed samples and analyzed the efficiency of Rad21 cleavage (Figure S2 A). C.L. and me analyzed the mitotic phenotype after $Rad21^{TEV}$ cleavage *in vivo* and in fixed samples (Figure 4 and Figure S2) and contributed to the writing of the manuscript.

Developmental Cell
Article

Cell-Type-Specific TEV Protease Cleavage Reveals Cohesin Functions in *Drosophila* Neurons

Andrea Pauli,[1] Friederike Althoff,[2,6] Raquel A. Oliveira,[1,6] Stefan Heidmann,[3] Oren Schuldiner,[4] Christian F. Lehner,[2] Barry J. Dickson,[5] and Kim Nasmyth[1,*]
[1]Department of Biochemistry, University of Oxford, Oxford OX1 3QU, UK
[2]Institute of Zoology, University of Zurich, 8057 Zurich, Switzerland
[3]Department of Genetics, University of Bayreuth, 95440 Bayreuth, Germany
[4]Stanford University, Department of Biological Sciences, Stanford, CA 94305, USA
[5]Institute of Molecular Pathology, 1030 Vienna, Austria
[6]These authors contributed equally to this work.
*Correspondence: kim.nasmyth@bioch.ox.ac.uk
DOI 10.1016/j.devcel.2007.12.009

SUMMARY

Cohesin is a highly conserved multisubunit complex that holds sister chromatids together in mitotic cells. At the metaphase to anaphase transition, proteolytic cleavage of the α kleisin subunit (Rad21) by separase causes cohesin's dissociation from chromosomes and triggers sister-chromatid disjunction. To investigate cohesin's function in postmitotic cells, where it is widely expressed, we have created fruit flies whose Rad21 can be cleaved by TEV protease. Cleavage causes precocious separation of sister chromatids and massive chromosome missegregation in proliferating cells, but not disaggregation of polytene chromosomes in salivary glands. Crucially, cleavage in postmitotic neurons is lethal. In mushroom-body neurons, it causes defects in axon pruning, whereas in cholinergic neurons it causes highly abnormal larval locomotion. These data demonstrate essential roles for cohesin in nondividing cells and also introduce a powerful tool by which to investigate protein function in metazoa.

INTRODUCTION

The investigation of nonmitotic functions of proteins essential for cell proliferation poses a major technical challenge: namely, how to inactivate such proteins without compromising cell proliferation. A good example is the highly conserved multisubunit complex called cohesin (Guacci et al., 1997; Michaelis et al., 1997), which holds the products of DNA replication (sister chromatids) together and thereby ensures their segregation to opposite poles of the cells during mitosis and meiosis (reviewed in Nasmyth and Haering, 2005 and Hirano, 2006). Cohesin forms a large tripartite ring composed of a pair of Structural Maintenance of Chromosome (SMC) proteins, SMC1 and SMC3, and an α kleisin protein, Scc1/Rad21, whose cleavage by separase causes cohesin's dissociation from chromosomes and triggers sister-chromatid disjunction at the metaphase to anaphase transition. Sister-chromatid cohesion requires two other non-SMC subunits, namely, Pds5 and Scc3/SA, that bind to cohesin's α kleisin subunit. The establishment of cohesion depends on the cohesin loading complex Scc2/Scc4 and on the acetyltransferase Eco1/Ctf7.

The fact that cohesin forms a ring whose opening releases it from chromatin has led to the suggestion that it holds sister DNAs together by using a topological mechanism (Gruber et al., 2003). Importantly, this type of function could also be of value in regulating aspects of chromosome organization that are independent of sister-chromatid cohesion and are not directly required for chromosome segregation. It is notable in this regard that the majority of cohesin is removed from chromosome arms during prophase/prometaphase in most eukaryotic cells by a separase-independent mechanism (Gandhi et al., 2006; Kueng et al., 2006). Only cohesin that subsequently persists on chromosomes is cleaved by separase at the onset of anaphase (Waizenegger et al., 2000). As a consequence, there exists a large pool of cohesin ready to reassociate with chromosomes as soon as cells exit from mitosis during telophase. Cohesin is therefore tightly associated with chromosomes for much of the cell-division cycle and could have important functions on unreplicated genomes.

Much evidence has emerged recently that cohesin might have important roles in regulating gene expression (reviewed in Dorsett, 2007). Approximately half of the cases of a multisystem developmental disorder in humans called Cornelia de Lange syndrome (CdLS), which is characterized by mental retardation, upper limb abnormalities, growth delay, and facial dysmorphisms, are caused by mutations in genes encoding NIPBL/Delangin (the human Scc2 ortholog), SMC1A, or SMC3 (Deardorff et al., 2007; Krantz et al., 2004; Musio et al., 2006; Tonkin et al., 2004). Because even severe cases of CdLS appear not to be accompanied by defects in sister-chromatid cohesion, it has been suggested that CdLS is caused by misregulated gene expression during embryonic development. Consistent with this possibility, the *Drosophila* Scc2 ortholog, Nipped-B, facilitates long-range enhancer-promotor interactions, at least for certain genes whose regulatory sequences have been mutated (Dorsett et al., 2005; Rollins et al., 1999). Furthermore, mutations in *mau-2*, the *Caenorhabditis elegans Scc4* ortholog, cause defects in axon guidance (Bernard et al., 2006; Takagi et al., 1997). Recently, two cohesin subunits, Scc1/Rad21 and SMC3, have been implicated

Developmental Cell
TEV Cleavage Reveals Postmitotic Roles of Cohesin

in expression of the hematopoietic transcription factors *runx1* and *runx3* in zebrafish (Horsfield et al., 2007).

Despite these findings, it cannot be excluded that developmental "cohesinopathies" are in fact caused by "knock on" effects of compromising the establishment or maintenance of sister-chromatid cohesion. In the case of CdLS, for example, haploinsufficiency of NIPBL/Delangin might cause cell-type-specific sister-chromatid cohesion defects (Kaur et al., 2005) that would be overlooked by examining this process in only one type of cell. It is therefore vital to develop methods that permit observation of the effects on gene expression and development of eliminating cohesin's function completely without interfering with cell proliferation.

To analyze cohesin's function in a more sophisticated manner than hitherto possible, to our knowledge, in metazoa, we have used the tobacco etch mosaic virus (TEV) protease to cleave cohesin's α kleisin subunit in *Drosophila melanogaster* in a cell-type-specific and/or temporally controlled manner. This process opens the cohesin ring and presumably abolishes its topological embrace of chromatin fibers (Gruber et al., 2003). As expected, expression of TEV protease in proliferating cells of fly embryos whose sole form of Rad21 contains TEV-cleavage sites causes precocious separation of sister chromatids and has a devastating effect on chromosome segregation. More remarkably, TEV-induced Rad21 cleavage in postmitotic neurons is lethal. It causes defects in the developmental axon pruning of mushroom-body γ neurons within pupal brains and defects in cholinergic neurons that result in highly abnormal larval locomotion.

RESULTS

A System to Inactivate Pre-Existing Cohesin Complexes

To inactivate cohesin, we chose cleavage of its α kleisin subunit (Rad21). Although this does not directly affect any known functional domain of Rad21, it severs and thereby opens cohesin's tripartite ring (Figure 1A), leading to its rapid dissociation from chromosomes. To do this in *Drosophila*, it was necessary first to create a *Rad21* mutant strain, second to complement the *Rad21* mutation with a version of *Rad21* that contains cleavage sites for a site-specific protease, and lastly to express a version of the protease that can accumulate within nuclei in a tissue-specific and/or time-dependent manner. We used TEV protease because it has been used successfully for this purpose in the budding yeast *Saccharomyces cerevisiae* (Uhlmann et al., 2000).

Generation of a *Rad21* Mutant Fly

The *Rad21* gene (CG17436) is located within the centric heterochromatin of chromosome 3L (Markov et al., 2003), but no mutants were available. To create *Rad21* mutations, a P element inserted 4 kb upstream of the transcriptional start of *Rad21* was remobilized by P element Transposase. Among the homozygous lethal stocks, we identified four independent *Rad21* deletion alleles by using PCR ($Rad21^{ex3}$, $Rad21^{ex8}$, $Rad21^{ex15}$, $Rad21^{ex16}$) (Figure 1C). All four alleles lack exons 1 and 2, which encode the highly conserved N terminus of Rad21 that interacts with the ATPase head of SMC3 (Figure 1C; Figure S1, see the Supplemental Data available with this article online) (Haering et al., 2002).

Homozygous mutant *Rad21* embryos develop normally during early embryogenesis (data not shown). DNA staining suggests that mitoses are normal throughout the first 16 epidermal cell divisions. Late mitoses and cell divisions in embryonic neural precursors also appear to be unaffected (data not shown). The maternal gene product is presumably sufficient to execute the embryonic cell-division program. Despite this, most (95%) homozygous mutant embryos die before hatching. The rare mutant larvae that hatch possess almost no motor activity and fail to grow. It is therefore conceivable that embryonic death arises from a defective nervous system.

Flies Expressing TEV-Cleavable Rad21 Are Viable and Fertile

To rescue *Rad21* mutants, we generated transgenic flies that express C-terminally myc-epitope-tagged versions of Rad21 with TEV-cleavage sites. A tandem array of three TEV consensus recognition sequences was inserted into four poorly conserved and putatively unstructured regions within Rad21's central domain (Figure 1A; for details, see Figure S1). The cleavability of these proteins was initially tested by cotransfecting tissue-culture cells with vectors expressing TEV-cleavable Rad21 ($Rad21^{TEV}$) and TEV protease. This showed that all four versions of $Rad21^{TEV}$ were efficiently cleaved (data not shown). Equally important, $Rad21^{TEV}$ with three TEV sites at position 271 or 550 as well as a version lacking TEV insertions restored full viability and fertility of homozygous $Rad21^{ex}$ alleles when expressed from a tubulin promotor (Table S2). We were thus able to generate fly stocks that carry $Rad21^{TEV}$ as their sole source of Rad21.

Efficient TEV-Induced Rad21 Cleavage In Vivo

To test whether flies can tolerate TEV protease, we created transgenic flies that express v5-epitope-tagged TEV in an inducible manner, either directly from the heat-shock promotor (hs-TEV) or under the control of the Gal4/UAS system (Brand and Perrimon, 1993) (Figures 1Ba and 1Bb). TEV tagged with three nuclear localization sequences (NLS) accumulated within nuclei and did not cause any notable phenotypes when expressed ubiquitously or in a tissue-specific manner by using a variety of different Gal4 driver lines (data not shown). Western blot showed that TEV induction caused the appearance of cleavage fragments of the expected size from $Rad21^{TEV}$ proteins, but not from endogenous Rad21 or transgenic Rad21 proteins (Figure 1D and data not shown). Heat shock led to the accumulation of TEV and Rad21-cleavage fragments more rapidly when the protease was expressed from hs-TEV compared to hs-Gal4/UAS-TEV (data not shown). Importantly, TEV induction led to cleavage of most of the $Rad21^{TEV}$ pool within a few hours.

TEV-Induced Rad21 Cleavage Causes Chromosome Missegregation

To investigate the consequences of Rad21 cleavage in a single cell cycle, we made use of the fact that zygotic expression is specifically switched on during embryonic cycle 14. Maternal Gal4 (α4-tub-Gal4) was used to drive expression of paternally contributed UAS-TEV in embryos containing $Rad21^{TEV}$ as their sole source of Rad21. Western blot confirmed that the expression of TEV causes a reduction in the level of intact $Rad21^{TEV}$

Developmental Cell
TEV Cleavage Reveals Postmitotic Roles of Cohesin

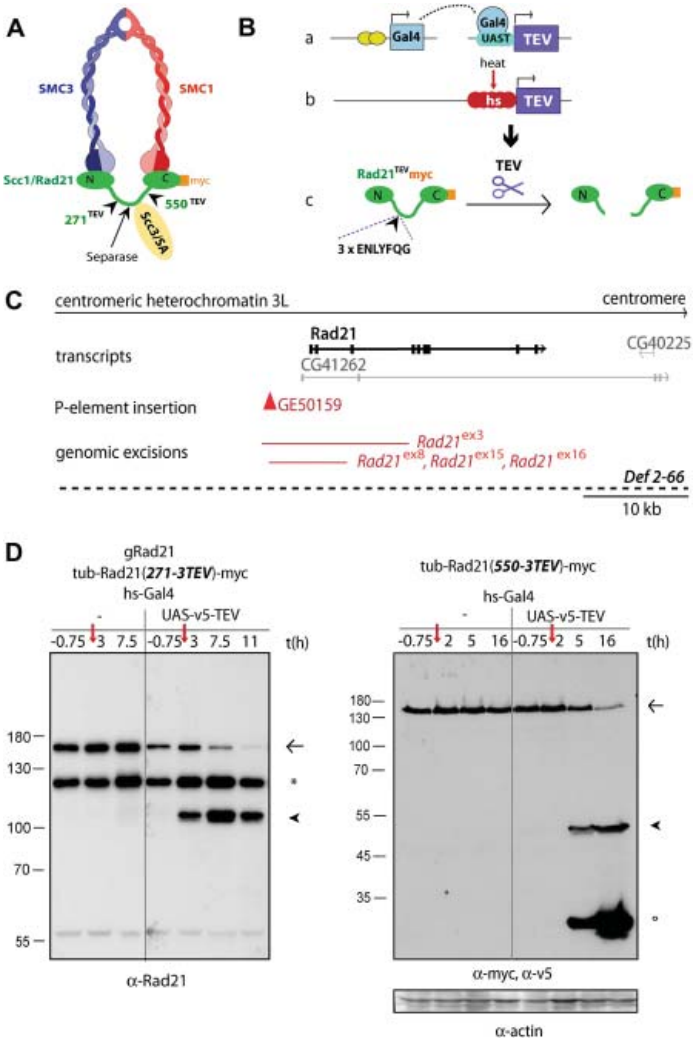

Figure 1. Outline of the TEV-Cleavage System

(A) Schematic of the cohesin complex containing TEV-cleavable Rad21 (green), SMC1 (red), SMC3 (blue), and Scc3/SA (yellow). Cleavage of Rad21 by separase occurs in the flexible linker region. Arrowheads indicate the sites of insertion of TEV-recognition sequences (numbers refer to amino acid positions).

(B) Outline of the TEV-cleavage system showing two alternative methods to express TEV in vivo in flies. (a) UAS-TEV is controlled by the UAS/GAL4 system, enabling TEV expression by specific Gal4 driver lines. (b) TEV directly fused to the heat-shock promotor allows for its ubiquitous induction in a time-specific manner. (c) Once expressed, catalytically active TEV protease cleaves Rad21^{TEV}.

(C) Representation of the genomic region of the *Rad21* locus. The *Rad21* gene (CG17436) resides in the centric heterochromatin of chromosome 3L. The exon-intron structure of the *Rad21* mRNA is shown in bold. EST-based transcript predictions of neighboring genes are depicted in lighter gray. The EP element GE50159 4 kb upstream of the transcriptional start of *Rad21* is represented by a red triangle. The four independently generated imprecise excision mutants of *Rad21* lack the chromosomal intervals indicated by solid, red lines. The *Rad21* locus is missing in the γ-ray-induced deficiency *Def 2-66* (dashed line). The scale bar is 10 kb.

(D) Pupal protein extracts were prepared before (t = −0.75 hr) and at different time points after a 45 min heat shock at 37°C (red arrow). Western blot analysis with antibodies against endogenous Rad21 (left panel) or myc (right panel) shows full-length Rad21^{TEV} (arrow) and the C-terminal TEV-cleavage product (arrowhead) as well as gRad21 (asterisk). V5-tagged TEV protease is detected by probing with v5 antibodies (open circle). Actin was used as a loading control. A molecular weight marker (in kDa) is shown on the left.

and the appearance of a ~90 kDa TEV-cleavage fragment before mitosis 14 (Figure S2A). The residual full-length protein presumably stems from embryos (50%) that did not inherit the TEV protease-containing chromosome. These results suggest that most, if not all, Rad21^{TEV} is cleaved during cycle 14.

Rad21^{TEV} cleavage had no effect on progression through the first 13 embryonic cell-division cycles, during which TEV is not expressed (data not shown). By contrast, as soon as zygotic expression is switched on, TEV had a devastating effect as cells embarked on mitosis 14. DNA staining and immunolabeling of embryos with anti-tubulin revealed the absence of any normal meta-, ana-, and telophase figures (Figure 2A). Despite the formation of bipolar spindles, condensed chromosomes failed to align on a metaphase plate and were found scattered throughout cells. Cells accumulated in this metaphase-like state, with high levels of Cyclin B and BubR1 concentrated at kinetochores.

These observations are consistent with the notion that Rad21 cleavage causes precocious loss of sister-chromatid cohesion. This would prevent the establishment of the tension at kinetochores needed to turn off the spindle-assembly checkpoint (SAC) and causes mitotic arrest (Logarinho et al., 2004; Tanaka, 2005). To test this, we used time-lapse microscopy to observe chromosomes marked with histone H2Av-mRFP1 and kinetochores marked with EGFP-Cid. This revealed that, upon Rad21 cleavage, chromosomes condense during prophase of cycle 14, usually with paired, presumably sister, kinetochores similar to those found in a wild-type strain (Figure 2B, t = 0–60 s, compare Movie S1 [WT] and Movie S2 [Rad21-depleted]). However, during prometaphase, soon after biorientation, sister chromatids disjoin prematurely and often segregate to opposite poles. This highly

Developmental Cell
TEV Cleavage Reveals Postmitotic Roles of Cohesin

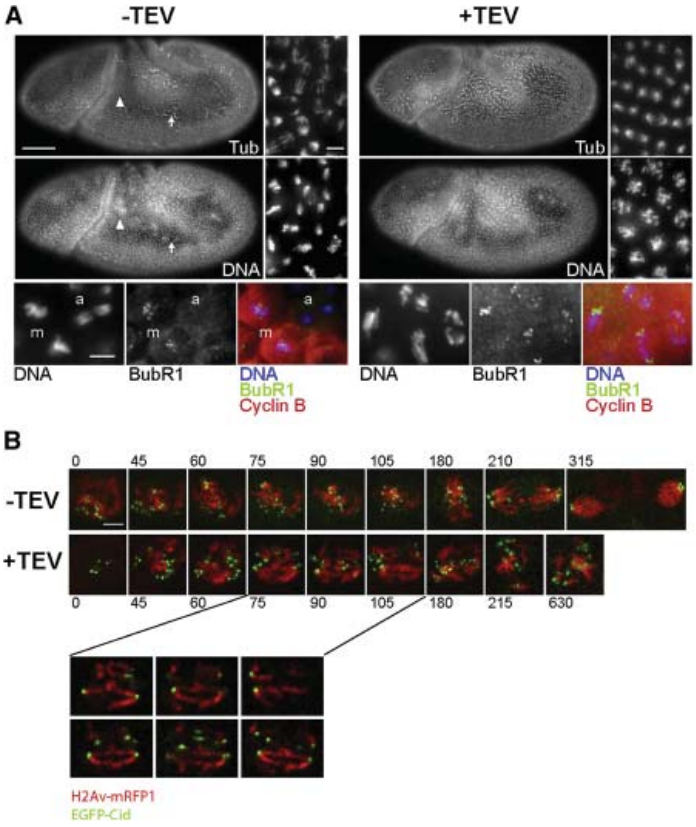

Figure 2. Cleavage of Rad21^{TEV} during Cycle 14 Causes Precocious Sister-Chromatid Separation and Transient Mitotic Arrest

(A) Cycle 14 embryos that survived on Rad21^{TEV} and expressed maternally contributed Gal4 were fixed and double labeled (top rows) with anti-α-tubulin (Tub) and a DNA stain (DNA) or were triple labeled (bottom row) with DNA stain (blue), anti-BubR1 (green), and anti-Cyclin B (red). +TEV indicates the additional presence of the UAS-TEV transgene. The scale bars are 50 μm in the top left panel, 10 μm in the top right panel, and 10 μm in the bottom panel. (Top) Most cells in −TEV embryos have already completed mitosis 14 (arrowhead in whole embryo views). Dividing cells (arrow) during various mitotic stages (pro-, meta-, ana-, telophase) are shown in the high-magnification view. In +TEV embryos, the entire dorsolateral epidermis is arrested in mitosis. (Bottom) In −TEV embryos, high levels of BubR1 and Cyclin B are only observed during metaphase (m), whereas anaphase (a) cells do not stain for BubR1 and Cyclin B. Arrested cells of +TEV embryos are Cyclin B positive and have high levels of BubR1 on separated sister kinetochores.

(B) Embryos surviving on Rad21^{TEV} and expressing either only maternal Gal4 (−TEV) or maternal Gal4-driven TEV protease (+TEV) were used for time-lapse imaging. DNA is marked with H2Av-mRFP1; kinetochores are marked with EGFP-Cid. The onset of chromosome condensation was set to zero. Time points are indicated in seconds. Whereas the top two rows represent Z projections, the bottom rows show single confocal sections. The scale bars are 2 μm. (−TEV) Chromosomes congress into a metaphase plate (t = 180), followed by anaphase (t = 210) and telophase (t = 315). (+TEV) Chromosomes fail to congress into a metaphase plate, and sister chromatids separate prematurely (t = 75–105). Note the substantial mitotic delay (t = 630).

abnormal process is asynchronous, with different chromosomes splitting at different times. As a result, chromosomes do not congress to a metaphase plate (Figure 2B; Movies S2 and S3). Exit from mitosis is delayed and cells arrest in a highly abnormal mitotic state, during which individual chromatids often lose their attachment to spindle poles, sometimes reorient, and move between poles (Figure S2B). After ~20 min, chromosome decondensation occurs abruptly and chromatids in the equatorial plane are cut by the cleavage furrow (Figure S2C; Movie S4). Although the mitotic arrest caused by Rad21 cleavage is only transient, mitosis nevertheless lasts approximately six times longer than in wild-type. These results are consistent with data from previous RNAi experiments in tissue-culture cells (Vass et al., 2003) and clearly show that Rad21 is essential for mitosis. We conclude that cohesin is necessary for sister-chromatid cohesion in the fly, as it is in yeast and vertebrate cells.

Cohesin Binds to Defined Regions on Polytene Chromosomes

We next used TEV cleavage to address whether cohesin has a role in holding together the multiple DNA molecules of polytene chromosomes in salivary glands. These chromosomes are generated by repeated rounds of DNA replication without intervening mitoses (endoreduplication) (reviewed in Zhimulev et al., 2004).

Immunostaining of wild-type polytene-chromosome squashes showed that Rad21, detected with a Rad21-specific antibody, localizes mainly to interband regions (Figure 3A), as has been suggested in previous reports (Dorsett et al., 2005; Gause et al., 2007; Markov et al., 2003). Several lines of evidence imply that these bands genuinely correspond to cohesin. First, coimmunostainings showed that myc-tagged Rad21^{TEV} is bound to the same chromosomal regions as endogenous Rad21 (Figure 3B). Second, cohesin's other three subunits (SMC1, SMC3, and SA/Scc3) colocalize with Rad21 on polytene-chromosome squashes (Figure S3A). Third, staining by myc-, Rad21-, and SMC1-specific antibodies is greatly reduced after TEV-induced cleavage of Rad21^{TEV} in flies in which this is the only form of Rad21 (Figure S3B). The fact that SMC proteins are also released implies that TEV cleavage of Rad21 releases the entire cohesin complex from chromosomes. Cohesin did not colocalize with known interband-specific proteins (Z4, BEAF32, Jil1, MSL2, CTCF), and its distribution differed

Developmental Cell
TEV Cleavage Reveals Postmitotic Roles of Cohesin

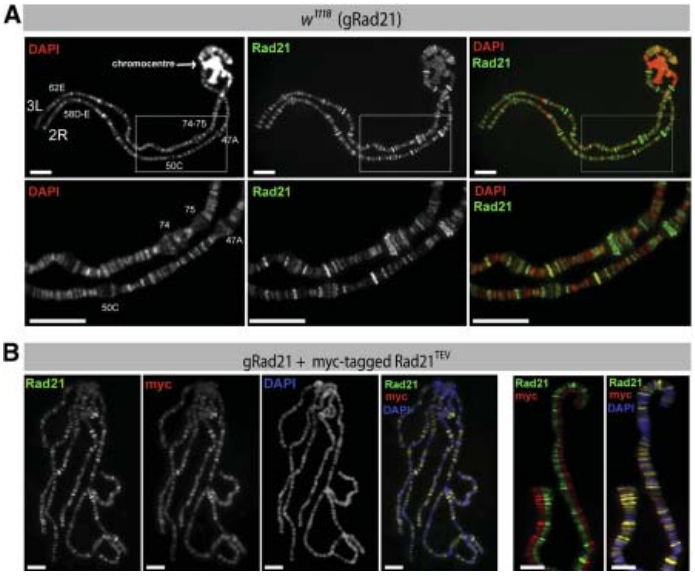

Figure 3. Cohesin Binds to Distinct Regions on Polytene Chromosomes

(A) Polytene chromosomes of wild-type flies (w^{1118}) were stained with Rad21 antibodies (green) and DAPI (DNA, red). The lower panel shows a higher-magnification view (2.5×). The strongly DAPI-stained heterochromatic chromocenter (arrow) is devoid of Rad21 staining. The scale bars are 20 μm.

(B) Polytene chromosomes from flies expressing myc-tagged Rad21^{TEV} in addition to endogenous Rad21 were coimmunostained with antibodies against Rad21 (green) and myc (red). DNA was visualized with DAPI (blue). In the right two frames, part of one chromosome arm is shown at higher magnification with split Rad21- and myc channels. The scale bars are 20 μm in the left four frames and 10 μm in the right two frames.

significantly from numerous other proteins whose localization on polytene chromosomes has been well documented (PolII, Rpb3, HSF, trx, Pc, Su[Hw], CP190, Mod[mdg4]) (Figures S4A and S4B and data not shown). The cohesin holocomplex appears to be bound to distinct but as yet undefined regions of polytene chromosomes.

Polytene Chromosomes Persist after Rad21 Cleavage

To address whether cohesin holds polytene chromosomes together, we induced TEV by heat shock (from hs-TEV) in late third-instar larvae surviving on transgenic Rad21 with or without TEV-cleavage sites and containing morphologically normal polytene chromosomes (Figure 4A). After heat shock, TEV caused rapid cleavage of Rad21^{TEV} and its disappearance from polytene chromosomes for at least 15 hr, but it had no effect on Rad21 without TEV sites or on the staining pattern of CTCF, a boundary-binding factor (Moon et al., 2005) (Figures 4B and 4C). Surprisingly, the morphology of polytene chromosomes was unaltered by cohesin's removal (see DAPI stainings in Figure 4C), even when hypotonic or noncrosslinking conditions were used during spreading, which should favor their disassembly (data not shown). It is conceivable that the chromosomes retain their integrity by virtue of the small amount of full-length Rad21^{TEV} (Figure 4B) that persists after TEV cleavage (either due to resistance to TEV or due to Rad21 resynthesis). However, the simplest explanation for our results is that cohesin is not required for maintaining the integrity of polytene chromosomes.

Interestingly, cohesin is required for the normal development of salivary glands. In contrast to hs-TEV, which does not cause significant TEV expression at 18°C, leaky expression of TEV under the control of hs-Gal4/UAS at 18°C led to smaller salivary glands (~1/2 the size) containing thinner polytene chromosomes in 100% of wandering late third-instar larvae that survived on Rad21^{TEV}, as compared to controls (Figure S5). Importantly, this decrease in organ size was due to smaller, not fewer, cells per gland. Similar results were obtained by expressing TEV by using a salivary-gland-specific driver (F4-Gal4) (data not shown). These results suggest that cohesin has an essential function in nonproliferating, endocycling salivary gland cells.

A Function for Cohesin in Neurons?

The finding that cohesin is required for normal salivary gland development suggests that cohesin does indeed have nonmitotic functions. Because cohesin is essential for cell proliferation, its putative additional functions would be best studied in postmitotic cells that do not require chromosome segregation. This raises two key questions. First, is cohesin widely present in postmitotic cells in the fly, and, second, is it possible to use TEV-mediated Rad21 cleavage to inactivate the complex in such cells? The answer to both questions is yes. Immunostaining showed that Rad21 is concentrated within the nuclei of most neurons in larval brains (Figure 5C and data not shown). Moreover, expression of TEV in neurons from Rad21^{TEV}-rescued flies during embryonic or larval development, by using the pan-neuronal drivers elav-Gal4 and nsyb-Gal4, causes developmental arrest and lethality (data not shown).

Cohesin Rings Are Essential for Axonal and Dendritic Pruning

To investigate in more detail cohesin's function in neurons, we concentrated on postmitotic γ neurons in the mushroom body of the fly brain. We focused on these particular cells because a recent mosaic screen for *piggyBac* insertions that cause abnormal pruning of γ-neuron axons has implicated two other subunits of the cohesin complex, namely, SMC1 and SA/Scc3 (Schuldiner et al., 2008, this issue of *Developmental Cell*). γ neurons are a specific subtype of postmitotic neurons in the mushroom body of the fly brain. During larval stages, the axons of γ neurons project into the dorsal and medial lobes of the mushroom body. During metamorphosis, at the time when α/β neurons

Developmental Cell
TEV Cleavage Reveals Postmitotic Roles of Cohesin

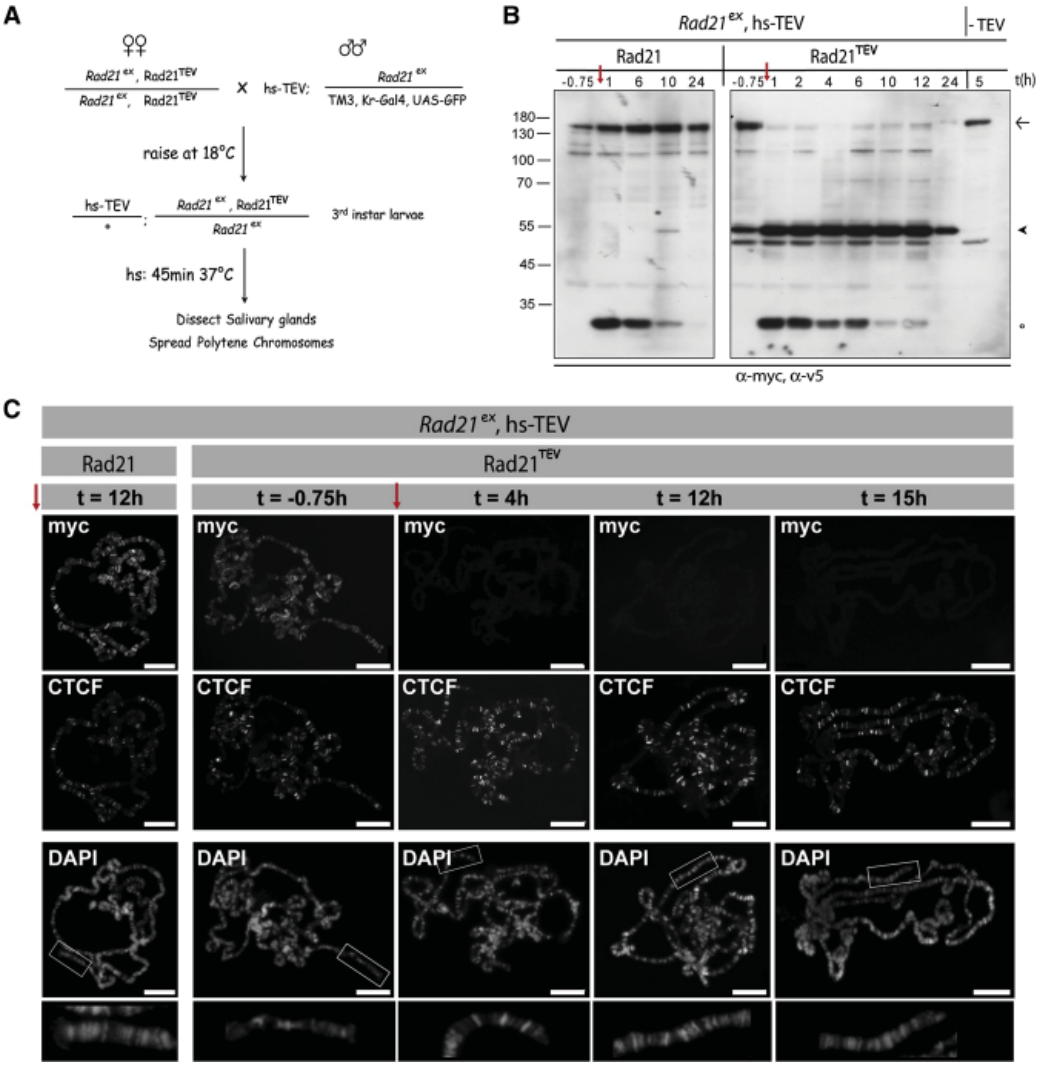

Figure 4. Cohesin Is Not Required for the Maintenance of Polytene-Chromosome Morphology

(A) Outline of the TEV-cleavage experiment in salivary glands.

(B) Western blot analysis of salivary gland extracts prepared either before (t = −0.75 hr) or at various time points after heat shock (red arrow) from GFP-negative larvae. The last lane shows a sample of salivary glands from Rad21^{TEV}-expressing flies that do not contain hs-TEV. Blots were probed with antibodies against myc (detecting full-length transgenic Rad21 [arrow] and the C-terminal TEV-cleavage fragment [arrowhead]) and v5 (detecting TEV protease [open circle]).

(C) Representative polytene-chromosome spreads of third-instar larvae that carry hs-TEV and express either transgenic Rad21 (left panel) or Rad21^{TEV} as their only source of Rad21 were prepared before (t = −0.75 hr) and at various time points after heat shock (red arrow). Polytene chromosomes were coimmunostained with antibodies against myc (recognizing Rad21) and CTCF. The morphology of the polytene chromosomes was visualized by DAPI staining (bottom row, higher magnification [2.5×]). All pictures were acquired by using the same acquisition settings. The scale bar is 20 μm.

are born, larval γ-neuron projections are selectively eliminated in a process called "axonal pruning" (Figure 5A) (Lee et al., 1999; Watts et al., 2003).

We first addressed whether Rad21 is normally expressed in γ neurons. Immunostaining with Rad21-specific antibodies detected endogenous Rad21 within the nuclei of γ neurons

Developmental Cell
TEV Cleavage Reveals Postmitotic Roles of Cohesin

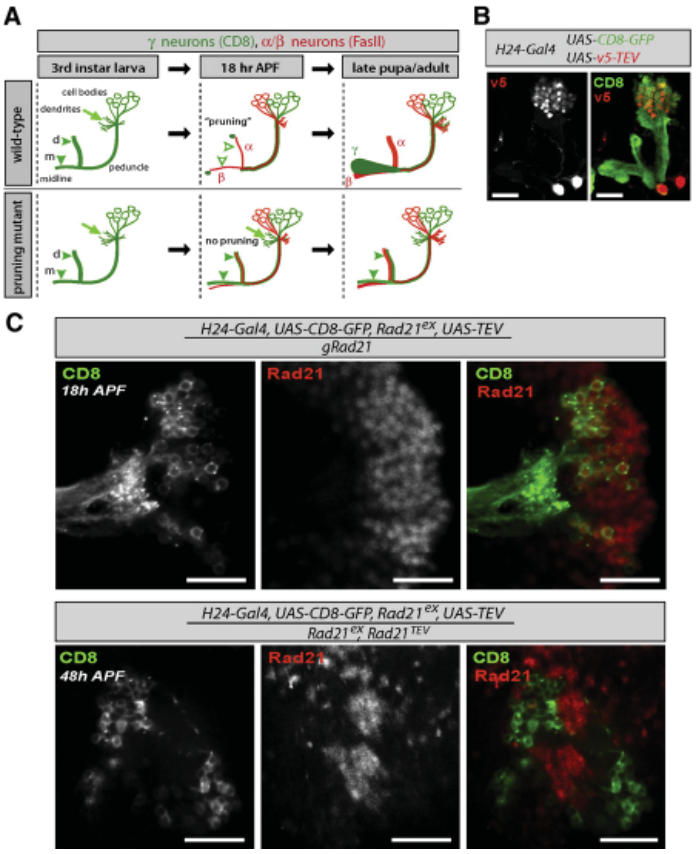

Figure 5. Cohesin Is Expressed in γ Neurons and Can Be Selectively Destroyed by TEV Cleavage

(A) Schematic representation of axonal projections of γ (green) and α/β (red) neurons of wild-type and pruning-defective mutants at three characteristic time points during development. Only the right hemisphere is shown. α′/β′ neurons are omitted from the scheme. In third-instar larva, γ-neuron axons are bundled in the peduncle before they bifurcate to project into the dorsal (d) and medial lobes (m) (filled, green arrowheads). At 18 hr after puparium formation (APF), the dorsal and medial projections from wild-type γ neurons are selectively eliminated ("pruned," open, green arrowheads). In a pruning mutant, γ-neuron axon projections and dendrites persist (filled, green arrowheads). α/β neurons project into the dorsal and medial lobes. In late pupae/adults, axons of wild-type γ neurons grow out again toward the midline. In a pruning mutant, larval axon projections of γ neurons persist in the dorsal and medial lobes.

(B) H24-Gal4 was used to drive expression of v5-tagged nuclear TEV protease and mCD8 in γ neurons of the mushroom body. Third-instar larval brains were immunostained with antibodies against mCD8 (green) and the v5 epitope (red). Images show Z projections of single confocal sections of the right brain hemisphere. The scale bar is 20 μm.

(C) H24-Gal4 was used to drive expression of TEV and mCD8 in γ neurons of the mushroom body from flies that expressed endogenous Rad21 (gRad21, top) or Rad21^{TEV} as their sole source of Rad21 (bottom). Brains were stained with antibodies against mCD8 (green) and Rad21 (red). Images show a single confocal section in the plane of γ-neuron cell bodies. Note that there is no overlap between the mCD8 and Rad21 stainings after TEV cleavage in γ neurons from Rad21^{TEV} flies. The scale bars are 20 μm.

and those of their neuronal neighbors (Figure 5C). TEV protease can be expressed in γ neurons via specific Gal4 driver lines (e.g., H24-Gal4) (Zars et al., 2000) and localizes to their nuclei (Figure 5B). Crucially, TEV expression in Rad21^{TEV}-rescued flies largely eliminated Rad21^{TEV} from γ neurons, but not from interspersed neighboring neurons (Figure 5C). In contrast, it had no effect on endogenous Rad21, which is not susceptible to TEV-induced cleavage.

We next analyzed the consequences of cohesin cleavage. The driver line 201Y-Gal4 is expressed in mushroom-body γ neurons and has therefore been widely used in previous studies of the pruning process (Lee et al., 1999). In strains surviving on Rad21 without TEV sites and expressing 201Y-Gal4-driven TEV, the dendrites and axons of CD8-positive γ neurons and of FasII-positive α/β neurons were indistinguishable from wild-type. The axons of γ neurons initially projected into both dorsal and medial lobes (not shown) but were pruned by 18 hr after puparium formation (APF) (Figure 6A, pruned axons are indicated with open arrowheads). In Rad21^{TEV} larvae, γ neurons also projected their axons into dorsal and medial lobes (Figure S6A), but they failed to prune these projections during pupariation (Figure 6A, middle row). However, the absence of axons of later-born α/β neurons (with high levels of FasII) in the center of the dorsal and medial lobes at 18 hr APF (compare upper right panel to middle right panel in Figure 6A) suggests that pupae arrest early after pupariation, before α/β neurons are born. This raises the possibility that the pruning defect is in fact caused by arrest at a developmental stage that preceeds γ-neuron pruning.

Although specific for γ neurons within the central nervous system, the 201Y-Gal4 driver is also expressed in muscles (O.S. and L. Luo, unpublished data). The developmental arrest might therefore be caused by inactivation of cohesin in muscles. To test this, we expressed Gal80 under control of the muscle-specific myosin heavy-chain (mhc) promoter (C. Winter and L. Luo, personal communication) to prevent TEV expression and hence cohesin cleavage in muscles. Remarkably, this enabled pupae to develop well beyond the stage when pruning normally occurs. FasII-positive α/β neurons were now readily detected from 18 hr APF (Figure 6A, bottom panels). Because α/β neurons are descended from neuroblasts that proliferate after giving rise to γ neurons (Lee et al., 1999), the mere presence of α/β neurons

Developmental Cell
TEV Cleavage Reveals Postmitotic Roles of Cohesin

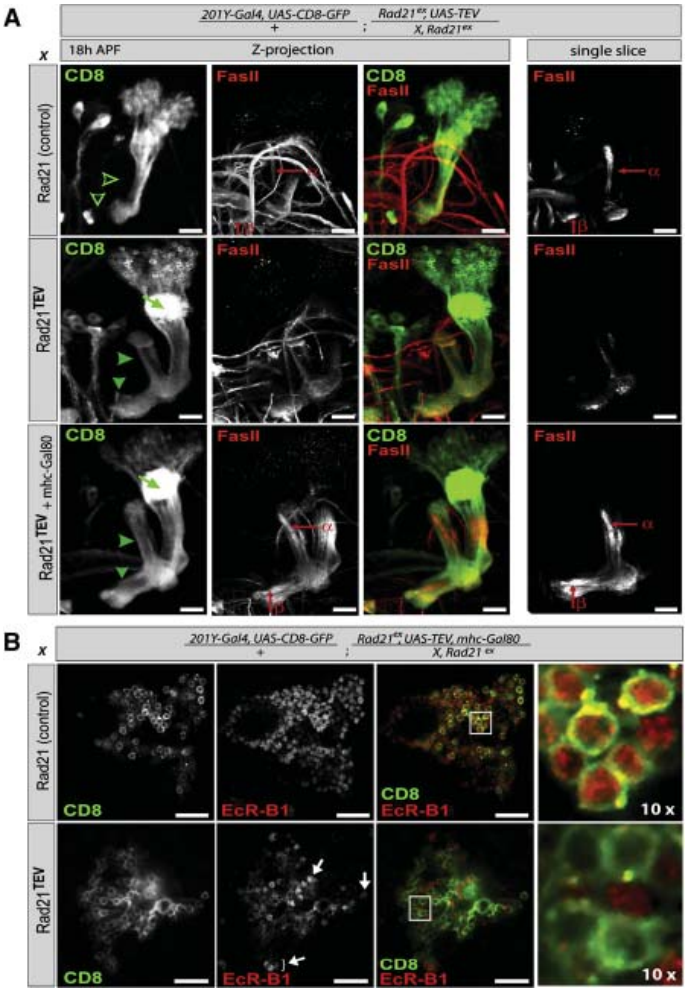

Figure 6. TEV Cleavage of Rad21 in γ Neurons Causes a Defect in Pruning

(A and B) 201Y-Gal4 was used to drive expression of TEV and mCD8 in γ neurons of the mushroom body from flies that survived on transgenic Rad21 with or without TEV-cleavage sites. The scale bars are 20 μm. (A) Brains were dissected at 18 hr APF and were stained with antibodies against mCD8 (green) and FasII (red). Z projections of single confocal sections of the right brain hemisphere (left three panels). A single FasII-stained slice in the plane of α/β neurons (right panel). Absence/presence of γ-neuron projections (open/filled, green arrowheads), dendrites (green arrow), and α/β neurons (red arrows). In the bottom row, expression of Gal4 was suppressed in muscles by mhc-Gal80 in Rad21^{TEV} flies. (B) Brains of Rad21^{TEV} flies, in which Gal4 expression in muscles was suppressed by mhc-Gal80, were dissected at 18 hr APF and were stained with antibodies against mCD8 (green) and EcR-B1 (red). Images show single confocal sections in the plane of γ-neuron cell bodies. A higher-magnification view (10×) of the white-boxed area is shown on the right.

implies that neuroblast proliferation is not blocked by the cleavage of Rad21 orchestrated by 201Y-Gal4. Importantly, the pruning defect in γ neurons caused by Rad21 cleavage was still observed (Figure 6A, bottom panels).

If the pruning defect of postmitotic γ neurons is caused by inactivation of cohesin in γ neurons themselves and is not an indirect consequence of its inactivation in some other cell type, then expression of TEV protease under control of a different γ-neuron-specific Gal4 driver should cause a similar phenotype. TEV expression via the H24-Gal4 driver confirmed that Rad21 cleavage in γ neurons causes axonal pruning defects (Figure S6B). Furthermore, comparison of γ-neuron projections between strains with and without cohesin in H24-Gal4-positive cells revealed that γ neurons also failed to prune their dendrites upon Rad21 cleavage (Figure S6B). Although we did not observe axon-targeting defects during larval and early pupal stages, the axonal projections of brains from late pupae (>4 days APF), which contain fully differentiated adult structures, were very often disorganized and mistargeted (Figure S6C). Our finding that a similar pruning defect accompanies Rad21 cleavage induced by two different Gal4 drivers, whose only common (known) feature is expression in γ neurons, implies that cohesin is needed for pruning of γ-neuron axons and dendrites.

How might cohesin regulate pruning? Previous work has implicated the ecdysone receptor EcR-B1 as a key regulator of γ-neuron pruning (Lee et al., 2000). Indeed, pruning defects caused by *SMC1* mutations are suppressed by overexpression of EcR-B1 (Schuldiner et al., 2008). The TEV-cleavage system should be ideal for testing whether cohesin is needed for EcR-B1 expression in all γ neurons. We found that Rad21 cleavage caused a major drop (at 18 hr APF) in the concentration of EcR-B1 within nuclei from most γ neurons, but not from nuclei of other interspersed neurons (Figure 6B). Only a minority of γ neurons still contained detectable levels of EcR-B1 upon Rad21 cleavage (indicated by white arrows). These data suggest that cohesin is required for cell-type-specific EcR-B1 expression.

Cohesin Is Required in Cholinergic Neurons for Larval Locomotion

One of the advantages of the TEV system is that it enables protein inactivation in all neurons of a given type and thereby has the potential to cause changes in animal behavior. To

Developmental Cell
TEV Cleavage Reveals Postmitotic Roles of Cohesin

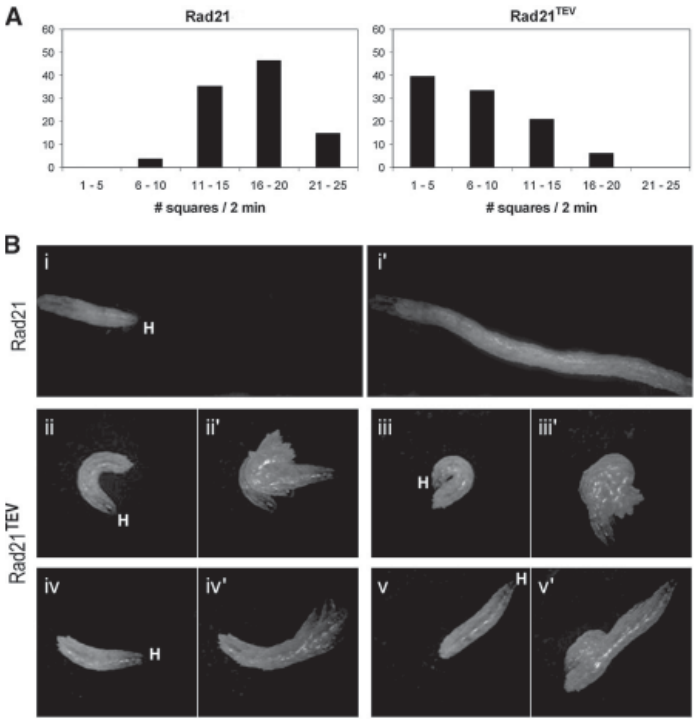

Figure 7. TEV Cleavage of Rad21 in Cholinergic Neurons Induces Severe Locomotion Defects in Third-Instar Larvae

(A) Wandering third-instar larvae expressing TEV under the control of Cha-Gal4 and surviving on transgenic Rad21 with and without TEV sites were tested for motility (Rad21: *Cha-Gal4/+; Rad21^{ex3}, Rad21-myc/Rad21^{ex3}, UAS-TEV*; Rad21^{TEV}: *Cha-Gal4/+; Rad21^{ex15}, Rad21^{TEV}/Rad21^{ex3}, UAS-TEV*). Larval movements were tracked and superimposed to a grid. Locomotion was measured by the number of grid squares each larva traveled through. The number of larvae that traveled through the indicated number of squares (1–5, 6–10, etc.) is shown as a percentage of the total number of larvae tested (54 and 48 for strains containing Rad21 and Rad21^{TEV}, respectively).

(B) Representative images and temporal projections of movements from larvae that express TEV in cholinergic neurons and survive on either transgenic Rad21 (i and i′) or Rad21^{TEV} (ii–v′) (same genotypes as in [A]). (i)–(v) show the initial position of the larvae. H indicates the position of the head. (i′)–(v′) show the temporal projections of the images taken over a 20 s interval (images taken every 2 s). Note that controls move mostly straight, whereas larvae in which Rad21^{TEV} has been cleaved in cholinergic neurons show frequent episodes of turns, head movement, and backward motion.

investigate this, we expressed TEV under control of Cha-Gal4, which expresses Gal4 specifically in cholinergic neurons (Salvaterra and Kitamoto, 2001). We noticed that this reduced the ability of Rad21^{TEV}, but not Rad21, third-instar larvae to crawl up the sides of the vials. The larvae nevertheless pupariate, albeit within their food, and die as late pupae, with fully developed adult organs (data not shown). We used video imaging to compare locomotion of Rad21^{TEV} and transgenic Rad21 third-instar larvae after placing them in the center of a Petri dish containing nonnutritive agar. This revealed that larvae with TEV sites in Rad21 moved less far than those without (Figure 7A). More detailed analysis showed that larvae without TEV sites in Rad21 moved mostly in straight lines, whereas Rad21^{TEV} larvae curved repetitively (Figure 7Bii and 7Biii), frequently turned their heads (Figure 7Biv), and even moved backward (Figure 7Bv; see also Movies S5 and S6).

Three lines of evidence suggest that these dramatic changes are not caused by mitotic defects. First, chromosomes from brain cells expressing CD8-GFP driven by Cha-Gal4 were never positive for the mitosis-specific phosphohistone H3 marker (Figure S7A), implying that Cha-Gal4 does not drive expression in dividing cells. Second, brains from larvae surviving on Rad21^{TEV} and expressing TEV protease in cholinergic neurons do not have any detectable mitotic defects (<1%). Cohesion defects during mitosis would greatly delay passage through mitosis and therefore cause an increase in the percentage of phosphohistone H3-positive cells. No such effect was seen (Figure S7). Third, we were unable to detect any gross morphological defects in the pattern of cholinergic neurons marked by CD8-GFP driven by Cha-Gal4 or any reduction in their numbers, either in the central nervous system (Figure S7B) or in peripheral sensory organs (data not shown). We conclude that correct larval locomotion requires cohesin in cholinergic neurons.

DISCUSSION

A Tool by Which to Study Protein Function in Metazoa

Although it was known that TEV protease can inactivate protein function in budding yeast (Uhlmann et al., 2000), it was unclear whether TEV could be used in a complex metazoan organism. Our work shows that TEV can be expressed in a wide variety of *Drosophila* tissues without causing overt toxicity. More important, we show that TEV expression induces quantitative cleavage of TEV-site-containing, but not wild-type, Rad21 protein, and that this is accompanied by penetrant phenotypes both in proliferating tissues and, more unexpectedly, in cells not engaged in mitosis, such as neurons and salivary gland cells.

The system we have developed has many attractive features that should make it a powerful and versatile tool for studying protein function in vivo. First, the method causes protein inactivation within a few hours and does not rely on a gradual depletion of the protein, as occurs in methods that interfere with the protein's synthetic capacity, such as recombinase-mediated gene deletion or RNA interference. Second, the system is reversible.

Developmental Cell
TEV Cleavage Reveals Postmitotic Roles of Cohesin

By using Gal80ts, TEV protease can be turned both on and off. Third, it is possible to be certain that phenotypes are caused by cleavage of the target protein by comparing the effect of TEV expression in animals whose target protein either does or does not contain TEV sites. Fourth, by targeting the protease to particular locations inside or even (by using a secreted protease) outside cells, it should be possible to direct inactivation of the target protein to specific intra- or extracellular compartments. The restriction of protein inactivation to specific cellular compartments may be easier to devise by using TEV than degron systems relying on the much more complex process of ubiquitin-mediated proteolysis (Dohmen et al., 1994). Unlike the MARCM system, which uses FLP/FRT-induced mitotic recombination to generate homozygous mutant clones in proliferating tissues, TEV cleavage can be triggered in all cells of a given tissue and at any stage of development, features that will greatly facilitate phenotypic and biochemical analyses. Because many eukaryotic proteins contain multiple functional domains connected by unstructured polypeptide chains, protein inactivation through TEV cleavage should be applicable to a large variety of proteins. It could also be used to clip off protein domains and thereby alter protein activity.

The Integrity of the Cohesin Ring Is Essential for Sister-Chromatid Cohesion in Mitosis

Our first priority upon developing a system to cleave Rad21 was to use it to investigate the role of cohesin during mitosis. In yeast, cohesin has a vital role in holding sister chromatids together until all chromosomes have bioriented during mitosis, whereupon cleavage of Scc1/Rad21 by separase triggers sister-chromatid disjunction (reviewed in Nasmyth and Haering, 2005). The consequences of depleting Scc1/Rad21 from tissue-culture cells by using RNA interference are, on the whole, consistent with the above-mentioned notion (Coelho et al., 2003; Vass et al., 2003). However, results from depletion experiments have not been able to directly explain the effects of inactivating cohesin within a single cell cycle.

We engineered a situation in which efficient cleavage of Rad21 occurred precisely as embryonic cells embarked on cycle 14, causing a devastating effect on mitosis. Chromosomes enter mitosis with paired sister kinetochores; however, instead of stably biorienting on a metaphase plate, they disjoin precociously, usually segregating to opposite poles. Importantly, these highly abnormal movements all take place prior to the APC/C-dependent activation of separase. These observations imply that cohesin is essential for the sister-chromatid cohesion necessary to resist mitotic-spindle forces in metazoan organisms as well as in yeast.

Our finding that most sister chromatids (in cells with cleaved Rad21) disjoin to opposite spindle poles, albeit precociously, suggests that their chromosomes possess sufficient cohesion to establish a transient form of biorientation, though possibly with low accuracy. We cannot at this stage determine whether this cohesion is mediated by cohesin complexes that have survived Rad21 TEV cleavage or by an independent cohesive mechanism such as residual sister DNA catenation. We can nevertheless conclude that the latter, if it exists, is incapable of resisting spindle forces and cannot therefore maintain sister-chromatid cohesion during a period in which the SAC has been activated and errors in chromosome biorientation are corrected. Thus, what really distinguishes cohesion mediated by cohesin from DNA catenation is its ability to be regulated by the SAC, and this may be the reason why eukaryotic cells appear to use cohesin for mitosis.

The Cohesin Ring Has Key Functions in Nonmitotic Cells

Mutations in Scc2's human ortholog as well as in SMC1 and SMC3 cause the developmental defects associated with CdLS (reviewed in Dorsett, 2007). It is unclear whether these defects are caused by mitotic errors during development or by defects in nonmitotic cohesin functions. The first clue that cohesin might indeed play key roles during development other than holding sister chromatids together was the finding that mutations in *D. melanogaster Nipped-B*, the ortholog of *Scc2*, alters the expression of genes whose regulatory sequences have been mutated (Rollins et al., 1999).

If cohesin has nonmitotic functions during development, then these could occur in proliferating and nonproliferating (postmitotic) cells. To analyze cycling cells, it would be necessary to restrict analysis either to a short, specific cell-cycle stage (e.g., the G1 period) or to develop a means of differentially inactivating cohesin complexes engaged in nonmitotic functions, leaving intact those engaged in chromosome segregation. Analysis of postmitotic cells is easier. It is merely necessary to devise a protocol for inactivating cohesin only after cell proliferation has ceased.

Cleavage of Rad21 induced by postmitotic pan-neuronal drivers caused lethality, suggesting that cohesin has key functions in neurons. To investigate these in greater detail, we analyzed the effects of Rad21 cleavage in specific neuronal subtypes. The finding that the proliferative defects caused by a *SMC1* mutation in clones of mushroom-body neuroblasts are accompanied by defective pruning of axons (Schuldiner et al., 2008) led us to investigate the effects of Rad21 cleavage in γ neurons. Our results show that Rad21 cleavage abolished the developmentally controlled pruning of both axons and dendrites in γ neurons. These defects cannot have been caused by failures in cell division because cleavage had no effect on the birth of γ neurons or on their initial axonal projections.

Previous work on *mau-2* (the *C. elegans* Scc4 ortholog) has already provided a link between cohesin and axon development (Benard et al., 2004). Whereas Mau-2 was reported to act as a guidance factor required for correct axon and cell migration, investigation of γ neurons in *Drosophila* suggests that cohesin mediates the elimination of axon projections and dendrites. However, our results do not rule out a function for cohesin in regulating axon guidance because Rad21 cleavage might not be complete when γ-neuron axons start growing out in the first place. Indeed, we observed axon-projection defects in developmentally arrested late pupae.

It has not thus far been possible to show that γ-neuron pruning defects cause changes in animal behavior. Cleavage of cohesin in the entire population of cholinergic neurons, in contrast, has a dramatic effect, causing larvae to turn frequently, move their heads back and forth, and even crawl backward. Importantly, the neurons clearly survive without functional cohesin and must be at least partially active, because larvae are not paralyzed by cohesin cleavage, a phenotype seen when cholinergic

Developmental Cell
TEV Cleavage Reveals Postmitotic Roles of Cohesin

transmission is switched off (Kitamoto, 2001). The locomotion defects are not dissimilar to those caused by mutations in *scribbler* (*sbb*) (Yang et al., 2000). *sbb*, also known as *brakeless* (*bks*) and *master of thickveins* (*mtv*), codes for a ubiquitously expressed corepressor of transcription (Haecker et al., 2007 and references therein). Expression of a *sbb* transcript exclusively in cholinergic neurons is sufficient to rescue locomotion defects of *sbb* mutants (Suster et al., 2004). It therefore appears that the lack of *sbb* and cohesin in cholinergic neurons causes similar locomotion defects. Future work will have to show whether there is a link between *sbb* and cohesin. Our finding that cohesin has roles in neurons that are essential for normal behavior is consistent with the notion that the mental retardation invariably found in patients with CdLS is also due to defective neuronal function, as opposed to defective cell proliferation during development.

We have shown that suppression of 201Y-Gal4-induced TEV expression, specifically in muscles, bypasses the early pupal arrest in Rad21^{TEV}-rescued flies and indicates that cohesin is essential in muscles as well as in neurons. In addition, although cohesin does not seem to be required for the maintenance of polytene-chromosome morphology, it is essential for normal progression through the endocycle in salivary glands. It is therefore conceivable that cohesin has key functions in most postmitotic cell types. What might these functions be? Cohesin is known to be required for efficient double-strand break repair as well as sister-chromatid cohesion (reviewed in Nasmyth and Haering, 2005), and it promotes repair by facilitating homologous recombination between sister chromatids. Its action in postmitotic neurons, however, must be on unreplicated chromatids. We suggest therefore that cohesin's function in neurons and other postmitotic G0 cells is more likely to be in regulating gene expression. The finding that cohesin cleavage reduces the accumulation of EcR-B1 within γ neurons is consistent with this notion. Interestingly, recent data have shown that cohesin binds to the EcR gene in several fly cell lines (Misulovin et al., 2007). Future experiments should address whether cohesin acts as a general regulator of gene expression.

In summary, we provide definitive evidence that the cohesin ring has essential functions in cells with unreplicated chromosomes. It will be important in the future to establish whether cohesin functions by trapping chromatin fibers, as it appears to do in cells that have replicated their genomes.

EXPERIMENTAL PROCEDURES

Fly Strains

TEV-cleavage experiments were performed in a *Rad21* null background. Four independent *Rad21^{ex}* alleles were generated by imprecise excision of the P element *GE50159* (see the Supplemental Data for details). For the generation of transgenic flies expressing TEV-cleavable versions of Rad21 under control of the tubulin-promotor (Rad21^{TEV}), three TEV-recognition sites were introduced into a previously generated *pCaSpeR-Rad21-myc$_{10}$* vector. To generate a nuclear v5-tagged TEV protease expression construct, three NLS- and one v5-epitope tag were added to the coding region of TEV. For cloning details, see the Supplemental Data. Transgenic lines were produced by standard P-element-mediated germline transformation.

The fly stock *Rad21^{ex15}, Rad21(550-3TEV)-myc* was used as a source of TEV-cleavable Rad21 (Rad21^{TEV}). The only exceptions are the western blot experiment in Figure 1D and the characterization of the zygotic Rad21 mutant phenotype (Figure 2, Figure S2, Movies S1–S4), for which *Rad21^{ex8}, Rad21(271-3TEV)-myc* and *2x Rad21(271-3TEV)-myc; Rad21^{ex3}*, respectively, were used as sources of Rad21^{TEV}.The fly stock *Rad21^{ex3}, Rad21-myc* served as a control (transgenic Rad21 without TEV sites).

Further details on stocks can be found in the Supplemental Data. A complete stocklist with all genotypes and abbreviations used in the text can be found in Table S1.

Immunofluorescence of Embryos after TEV Cleavage of Rad21

For analysis of mitosis after TEV-induced cleavage of Rad21^{TEV} in fixed samples, 3–6 hr embryos were collected from a cross between *α4-tub-Gal4/2x Rad21(271-3TEV); Rad21^{ex3}* females and *UAS-TEV, hs-Gal4, Rad21^{ex3}/TM3, Kr-Gal4, UAS-GFP* males. Immunofluorescence labeling of embryos was performed according to standard procedures (Knoblich and Lehner, 1993) after a preincubation in 0.7 μM taxol before fixation. Pictures were acquired with a Zeiss Axioplan 2 imaging system by using the Zeiss AxioVision software. The following initial experiment allowed us to distinguish between +TEV and −TEV embryos: *α4-tub-Gal4/2x Rad21(271-3TEV); Rad21^{ex3}* females were crossed to either *UAS-TEV, hs-Gal4, Rad21^{ex3}/TM3, Kr > GFP* (+TEV) or *hs-Gal4, Rad21^{ex3}/TM3, Kr > GFP* (−TEV) males. Embryos were fixed during mitosis 14 and were stained with anti-tubulin and a DNA stain. 50% of the embryos from the first cross displayed a drastic mitotic delay, whereas the other 50% were phenotypically wild-type. In contrast, all embryos from the second cross were phenotypically wild-type. These observations indicate that +TEV embryos can be identified readily based on their severe mitotic abnormalities.

In Vivo Imaging of Embryos after TEV Cleavage of Rad21

For in vivo imaging of mitosis after TEV-induced cleavage of Rad21, Rad21^{TEV}-rescued flies that contained fluorescent markers for DNA (His2Av-mRFP1) and kinetochores (EGFP-Cid) as well as the maternal Gal4 driver α4-tub-Gal4 on their second chromosome were generated. *α4-tub-Gal4, His2Av-mRFP1, EGFP-Cid/2x Rad21(271-3TEV)-myc; Rad21^{ex3}* females were crossed with *UAS-TEV, hs-Gal4, Rad21^{ex3}/TM3, Kr-Gal4, UAS-GFP* males. Embryos of this cross either displayed the characteristic severe mitotic abnormalities and were thus considered to be TEV expressing (+TEV) or they were entirely normal and thus considered to lack the UAS-TEV transgene (−TEV). In vivo imaging was performed essentially as described (Schuh et al., 2007). Time-lapse confocal laser scanning microscopy was performed with an inverted Leica TCS SP1 system equipped with a 40×/1.25 oil immersion objective at 22°C–24°C. One stack of five frames was acquired every 15 s. The Leica confocal software was used for maximum projection, Gaussian filtering, and contrast adjustment.

Immunoblotting

Pupae or dissected salivary glands were homogenized in SDS-sample loading buffer and boiled for 5 min. Western blot was performed according to standard procedures.

Immunostaining of Polytene-Chromosome Squashes

Polytene-chromosome spreads were prepared according to standard procedures as outlined in the Supplemental Data. Fluorescent images were acquired with an AXIO Imager.Z1 microscope (Zeiss) and a CoolSNAP HQ CCD camera (Photometrics) by using MetaMorph software (Universal Imaging).

Immunostaining of Brains

Immunostaining of whole-mount brains was performed as described previously (Lee and Luo, 1999). Confocal pictures were obtained by using a Zeiss LSM 510 Axiovert 200M. Maximal projections of Z stacks were generated by using Zeiss software.

Antibodies

The following primary antibodies were used (WB, western blot; IF, immunofluorescence): guinea-pig α-Rad21 (WB, 1:3000, IF, 1:600) (Heidmann et al., 2004), mouse α-myc 9E10 (WB, 1:200; Sigma-Aldrich), mouse α-myc 4A6 (IF, 1:500; Upstate), mouse α-v5 (WB, 1:5000, IF, 1:500; Invitrogen), mouse α-Cyclin B (F2) (1:3) (Knoblich and Lehner, 1993), mouse α-tubulin (DM1A) (1:8000; Sigma-Aldrich), rabbit α-BubR1 (1:2000) (Logarinho et al., 2004), rabbit α-CTCF (1:200) (Moon et al., 2005), rat α-mCD8 α subunit (1:100; Abcam), mouse α-FasII (1D4) (1:50; Developmental Studies Hybridoma Bank

Developmental Cell
TEV Cleavage Reveals Postmitotic Roles of Cohesin

[DSHB]), mouse α-EcR-B1 (AD4.4) (1: 25; DSHB), rabbit α-phosphohistone H3 (1:500; Upstate), and rabbit α-actin (1:1000; Abcam). For WB, HRP-linked secondary antibodies (Amersham) were detected by Enhanced Chemi-Luminescence (ECL) (Amersham). For IF, Alexa-conjugated secondary antibodies (Molecular Probes) were used as 1:500 dilutions.

Larval Behavior

Larval locomotion was tested essentially as previously described (Yang et al., 2000), with minor modifications. Late third-instar larvae of control strains were selected based on their characteristic wandering stage. Since Rad21-depleted larvae do not crawl up the walls of food vials, $Rad21^{TEV}$ larvae were considered as "wandering" based on their size and the fact that they stopped foraging within the food. "Wandering" third-instar larvae were placed in the center of 90 mm diameter Petri dishes coated with nonnutritive 2% agar. After 1 min of adaptation, the movement was recorded over a period of 2 min by taking images every 5 s with a Canon Power Shot S70 digital camera. Movies were assembled, and larval movement was manually tracked by using ImageJ 1.38× software. Total locomotion was measured by superimposing trails onto a 6 mm grid and counting the number of squares through which larvae moved. For detailed analysis of locomotion behavior, higher magnification movies were taken on a dissection scope coupled to a Canon Power Shot S70 digital camera. For temporal projection of larval movement, single images were extracted from the recorded movies with a time lapse of 2 s. Projections of 10 images (corresponding to 20 s periods) were obtained by using ImageJ software.

Supplemental Data

Supplemental Data include Supplemental Experimental Procedures, two tables, seven figures, six movies, and Supplemental References and are available at http://www.developmentalcell.com/cgi/content/full/14/2/239/DC1/.

ACKNOWLEDGMENTS

We thank L. Luo, G. Miesenboeck, J. Simpson, F. Schnorrer, D. Dorsett, C. Sunkel, R. Paro, J. Lis, P. Harte, J. Zhou, H. Saumweber, U. Laemmli, G. Struhl, K. Keleman, S. Gruber, Gene Exel Korea, and the Bloomington Stock Center for reagents. We are especially grateful to Liqun Luo for sharing unpublished data and for comments and discussion on the manuscript. We also thank H. White-Cooper for providing fly facilities in Oxford and for discussions and comments; A. Graf, K. Jaeger, and R. Fuchs for help with the generation of transgenic flies; and G. Miesenboeck, I. Davis, A. Brand, and all members of the K.N. lab for helpful discussions and comments. Work in the laboratory of K.N. and B.J.D. was supported by funds from Boehringer Ingelheim GmbH (IMP) and grants from the Medical Research Council (MRC) and Wellcome Trust. Work in the laboratories of C.F.L. and S.H. was supported by grants from the Deutsche Forschungsgemeinschaft (DFG Le987/3-4 and He 2354/2-3).

Received: November 5, 2007
Revised: December 7, 2007
Accepted: December 12, 2007
Published: February 11, 2008

REFERENCES

Benard, C.Y., Kebir, H., Takagi, S., and Hekimi, S. (2004). mau-2 acts cell-autonomously to guide axonal migrations in *Caenorhabditis elegans*. Development *131*, 5947–5958.

Bernard, P., Drogat, J., Maure, J.F., Dheur, S., Vaur, S., Genier, S., and Javerzat, J.P. (2006). A screen for cohesion mutants uncovers Ssl3, the fission yeast counterpart of the cohesin loading factor Scc4. Curr. Biol. *16*, 875–881.

Brand, A.H., and Perrimon, N. (1993). Targeted gene expression as a means of altering cell fates and generating dominant phenotypes. Development *118*, 401–415.

Coelho, P.A., Queiroz-Machado, J., and Sunkel, C.E. (2003). Condensin-dependent localisation of topoisomerase II to an axial chromosomal structure is required for sister chromatid resolution during mitosis. J. Cell Sci. *116*, 4763–4776.

Deardorff, M.A., Kaur, M., Yaeger, D., Rampuria, A., Korolev, S., Pie, J., Gil-Rodriguez, C., Arnedo, M., Loeys, B., Kline, A.D., et al. (2007). Mutations in cohesin complex members SMC3 and SMC1A cause a mild variant of cornelia de Lange syndrome with predominant mental retardation. Am. J. Hum. Genet. *80*, 485–494.

Dohmen, R.J., Wu, P., and Varshavsky, A. (1994). Heat-inducible degron: a method for constructing temperature-sensitive mutants. Science *263*, 1273–1276.

Dorsett, D. (2007). Roles of the sister chromatid cohesion apparatus in gene expression, development, and human syndromes. Chromosoma *116*, 1–13.

Dorsett, D., Eissenberg, J.C., Misulovin, Z., Martens, A., Redding, B., and McKim, K. (2005). Effects of sister chromatid cohesion proteins on cut gene expression during wing development in *Drosophila*. Development *132*, 4743–4753.

Gandhi, R., Gillespie, P.J., and Hirano, T. (2006). Human Wapl is a cohesin-binding protein that promotes sister-chromatid resolution in mitotic prophase. Curr. Biol. *16*, 2406–2417.

Gause, M., Webber, H.A., Misulovin, Z., Haller, G., Rollins, R.A., Eissenberg, J.C., Bickel, S.E., and Dorsett, D. (2007). Functional links between *Drosophila* Nipped-B and cohesin in somatic and meiotic cells. Chromosoma in press. Published online October 2, 2007. 10.1007/s00412.007.0125.5.

Gruber, S., Haering, C.H., and Nasmyth, K. (2003). Chromosomal cohesin forms a ring. Cell *112*, 765–777.

Guacci, V., Koshland, D., and Strunnikov, A. (1997). A direct link between sister chromatid cohesion and chromosome condensation revealed through analysis of MCD1 in *S. cerevisiae*. Cell *91*, 47–57.

Haecker, A., Qi, D., Lilja, T., Moussian, B., Andrioli, L.P., Luschnig, S., and Mannervik, M. (2007). *Drosophila* brakeless interacts with atrophin and is required for tailless-mediated transcriptional repression in early embryos. PLoS Biol. *5*, e145.

Haering, C.H., Lowe, J., Hochwagen, A., and Nasmyth, K. (2002). Molecular architecture of SMC proteins and the yeast cohesin complex. Mol. Cell *9*, 773–788.

Heidmann, D., Horn, S., Heidmann, S., Schleiffer, A., Nasmyth, K., and Lehner, C.F. (2004). The *Drosophila* meiotic kleisin C(2)M functions before the meiotic divisions. Chromosoma *113*, 177–187.

Hirano, T. (2006). At the heart of the chromosome: SMC proteins in action. Nat. Rev. Mol. Cell Biol. *7*, 311–322.

Horsfield, J.A., Anagnostou, S.H., Hu, J.K., Cho, K.H., Geisler, R., Lieschke, G., Crosier, K.E., and Crosier, P.S. (2007). Cohesin-dependent regulation of Runx genes. Development *134*, 2639–2649.

Kaur, M., DeScipio, C., McCallum, J., Yaeger, D., Devoto, M., Jackson, L.G., Spinner, N.B., and Krantz, I.D. (2005). Precocious sister chromatid separation (PSCS) in Cornelia de Lange syndrome. Am. J. Med. Genet. A *138*, 27–31.

Kitamoto, T. (2001). Conditional modification of behavior in *Drosophila* by targeted expression of a temperature-sensitive shibire allele in defined neurons. J. Neurobiol. *47*, 81–92.

Knoblich, J.A., and Lehner, C.F. (1993). Synergistic action of *Drosophila* cyclins A and B during the G2-M transition. EMBO J. *12*, 65–74.

Krantz, I.D., McCallum, J., DeScipio, C., Kaur, M., Gillis, L.A., Yaeger, D., Jukofsky, L., Wasserman, N., Bottani, A., Morris, C.A., et al. (2004). Cornelia de Lange syndrome is caused by mutations in NIPBL, the human homolog of *Drosophila melanogaster* Nipped-B. Nat. Genet. *36*, 631–635.

Kueng, S., Hegemann, B., Peters, B.H., Lipp, J.J., Schleiffer, A., Mechtler, K., and Peters, J.M. (2006). Wapl controls the dynamic association of cohesin with chromatin. Cell *127*, 955–967.

Lee, T., and Luo, L. (1999). Mosaic analysis with a repressible cell marker for studies of gene function in neuronal morphogenesis. Neuron *22*, 451–461.

Lee, T., Lee, A., and Luo, L. (1999). Development of the *Drosophila* mushroom bodies: sequential generation of three distinct types of neurons from a neuroblast. Development *126*, 4065–4076.

Developmental Cell
TEV Cleavage Reveals Postmitotic Roles of Cohesin

Lee, T., Marticke, S., Sung, C., Robinow, S., and Luo, L. (2000). Cell-autonomous requirement of the USP/EcR-B ecdysone receptor for mushroom body neuronal remodeling in *Drosophila*. Neuron *28*, 807–818.

Logarinho, E., Bousbaa, H., Dias, J.M., Lopes, C., Amorim, I., Antunes-Martins, A., and Sunkel, C.E. (2004). Different spindle checkpoint proteins monitor microtubule attachment and tension at kinetochores in *Drosophila* cells. J. Cell Sci. *117*, 1757–1771.

Markov, A.V., Zakharov, A.A., Galkin, A.P., Strunnikov, A.V., and Smirnov, A.F. (2003). Localization of cohesin complexes of polytene chromosomes of Drosophila melanogaster located on interbands. Genetika *39*, 1203–1211.

Michaelis, C., Ciosk, R., and Nasmyth, K. (1997). Cohesins: chromosomal proteins that prevent premature separation of sister chromatids. Cell *91*, 35–45.

Misulovin, Z., Schwartz, Y.B., Li, X.Y., Kahn, T.G., Gause, M., Macarthur, S., Fay, J.C., Eisen, M.B., Pirrotta, V., Biggin, M.D., et al. (2007). Association of cohesin and Nipped-B with transcriptionally active regions of the *Drosophila melanogaster* genome. Chromosoma, in press. Published online October 27, 2007. 10.1007/s00412.007.0129.1.

Moon, H., Filippova, G., Loukinov, D., Pugacheva, E., Chen, Q., Smith, S.T., Munhall, A., Grewe, B., Bartkuhn, M., Arnold, R., et al. (2005). CTCF is conserved from *Drosophila* to humans and confers enhancer blocking of the Fab-8 insulator. EMBO Rep. *6*, 165–170.

Musio, A., Selicorni, A., Focarelli, M.L., Gervasini, C., Milani, D., Russo, S., Vezzoni, P., and Larizza, L. (2006). X-linked Cornelia de Lange syndrome owing to SMC1L1 mutations. Nat. Genet. *38*, 528–530.

Nasmyth, K., and Haering, C.H. (2005). The structure and function of SMC and kleisin complexes. Annu. Rev. Biochem. *74*, 595–648.

Rollins, R.A., Morcillo, P., and Dorsett, D. (1999). Nipped-B, a *Drosophila* homologue of chromosomal adherins, participates in activation by remote enhancers in the cut and Ultrabithorax genes. Genetics *152*, 577–593.

Salvaterra, P.M., and Kitamoto, T. (2001). *Drosophila* cholinergic neurons and processes visualized with Gal4/UAS-GFP. Brain Res. Gene Expr. Patterns *1*, 73–82.

Schuh, M., Lehner, C.F., and Heidmann, S. (2007). Incorporation of *Drosophila* CID/CENP-A and CENP-C into centromeres during early embryonic anaphase. Curr. Biol. *17*, 237–243.

Schuldiner, O., Berdnik, D., Ma Levy, J., Wu, J.S.-Y., Luginbuhl, D., Gontang, A.C., and Luo, L. (2008). *piggyBac*-based mosaic screen identifies a postmitotic function for cohesin in regulating developmental axon pruning. Dev. Cell *14*, this issue, 227–238.

Suster, M.L., Karunanithi, S., Atwood, H.L., and Sokolowski, M.B. (2004). Turning behavior in *Drosophila* larvae: a role for the small scribbler transcript. Genes Brain Behav. *3*, 273–286.

Takagi, S., Benard, C., Pak, J., Livingstone, D., and Hekimi, S. (1997). Cellular and axonal migrations are misguided along both body axes in the maternal-effect *mau-2* mutants of *Caenorhabditis elegans*. Development *124*, 5115–5126.

Tanaka, T.U. (2005). Chromosome bi-orientation on the mitotic spindle. Philos. Trans. R. Soc. Lond. B Biol. Sci. *360*, 581–589.

Tonkin, E.T., Wang, T.J., Lisgo, S., Bamshad, M.J., and Strachan, T. (2004). NIPBL, encoding a homolog of fungal Scc2-type sister chromatid cohesion proteins and fly Nipped-B, is mutated in Cornelia de Lange syndrome. Nat. Genet. *36*, 636–641.

Uhlmann, F., Wernic, D., Poupart, M.A., Koonin, E., and Nasmyth, K. (2000). Cleavage of cohesin by the CD clan protease separin triggers anaphase in yeast. Cell *103*, 375–386.

Vass, S., Cotterill, S., Valdeolmillos, A.M., Barbero, J.L., Lin, E., Warren, W.D., and Heck, M.M. (2003). Depletion of Drad21/Scc1 in *Drosophila* cells leads to instability of the cohesin complex and disruption of mitotic progression. Curr. Biol. *13*, 208–218.

Waizenegger, I.C., Hauf, S., Meinke, A., and Peters, J.M. (2000). Two distinct pathways remove mammalian cohesin from chromosome arms in prophase and from centromeres in anaphase. Cell *103*, 399–410.

Watts, R.J., Hoopfer, E.D., and Luo, L. (2003). Axon pruning during *Drosophila* metamorphosis: evidence for local degeneration and requirement of the ubiquitin-proteasome system. Neuron *38*, 871–885.

Yang, P., Shaver, S.A., Hilliker, A.J., and Sokolowski, M.B. (2000). Abnormal turning behavior in *Drosophila* larvae. Identification and molecular analysis of scribbler (sbb). Genetics *155*, 1161–1174.

Zars, T., Fischer, M., Schulz, R., and Heisenberg, M. (2000). Localization of a short-term memory in *Drosophila*. Science *288*, 672–675.

Zhimulev, I.F., Belyaeva, E.S., Semeshin, V.F., Koryakov, D.E., Demakov, S.A., Demakova, O.V., Pokholkova, G.V., and Andreyeva, E.N. (2004). Polytene chromosomes: 70 years of genetic research. Int. Rev. Cytol. *241*, 203–275.

Developmental Cell, volume 14
Supplemental Data

Cell-Type-Specific TEV Protease Cleavage Reveals Cohesin Functions in *Drosophila* Neurons

Andrea Pauli, Friederike Althoff, Raquel A. Oliveira, Stefan Heidmann, Oren Schuldiner, Christian F. Lehner, Barry J. Dickson, and Kim Nasmyth

Supplemental Experimental Procedures

Fly stocks

The line *P{w$^+$, EP}GE50159* was obtained from GenExel, Korea. Deficiencies in heterochromatin 3 and the *α4-tub-Gal4* driver line are available from the Bloomington stock center. Transgenic lines with *His2Av-mRFP1, EGFP-Cid* (Schuh et al., 2007), *gSMC3-HA* (Heidmann et al., 2004), *201Y-Gal4* (Yang et al., 1995), *H24-Gal4* (Zars et al., 2000) and *Cha-Gal4* (Salvaterra and Kitamoto, 2001) have been described previously. A *mhc-Gal80* fly stock (C. Winter and L. Luo, unpublished) was kindly provided by Liqun Luo. A complete stocklist with all genotypes and abbreviations used in this paper can be found in Supplemental Table S1.

Generation of *Rad21* alleles

The insertion site of the homozygous viable *P{w$^+$, EP}GE50159* line 4 kb upstream of the transcription start site of *Rad21* was confirmed by inverse PCR according to a standard protocol. Imprecise excisions were generated by crossing the GE50159 line to flies expressing a stable source of the P-element transposase. Out of 500 excision events, 23 homozygous lethal lines were isolated. 4 independently generated deletions affecting *Rad21* were subsequently identified by PCR (*Rad21^{ex3}*, *Rad21^{ex8}*, *Rad21^{ex15}*, *Rad21^{ex16}*) and confirmed by sequencing DNA fragments spanning the breakpoints.

Generation of transgenic flies expressing TEV protease

To generate a NLS- and v5-epitope-tagged TEV protease expression construct (nuclear TEV protease), one N-terminal consensus sequence of the SV40 nuclear localization signal (NLS) followed by one v5-epitope tag were introduced by PCR at the 5'end of the coding sequence of TEV-NLS_2, using the yeast vector YIplac204 (Uhlmann et al., 2000) as template. Primer sequences are listed below. The PCR product *NLS-v5-TEV-NLS_2* was cloned as EcoRI/NotI fragment into the pUAST (Brand and Perrimon, 1993) or pCaSpeR-hs (Thummel, 1992) transformation vectors to obtain *UAS-NLS-v5-TEV-NLS_2* or *hs-NLS-v5-TEV-NLS_2*, respectively.

Transgenic lines were produced by standard P-element-mediated germline transformation (Rubin and Spradling, 1983) and either recombined to the *$Rad21^{ex3}$* allele (*$Rad21^{ex3}$, UAS-TEV/TM3, Sb, Kr-Gal4, UAS-GFP*) or crossed into the *$Rad21^{ex3}$* background (*hs-TEV; $Rad21^{ex3}$/TM6B, Tb*).

Generation of flies surviving on transgenic $Rad21^{TEV}$

C-terminally 10xmyc-tagged Rad21 was created based on the EST clone LD14219 obtained from the Berkeley Drosophila Genome Project (BDGP). The coding sequence of the 10xmyc-tag was amplified by PCR from the plasmid *gthr-myc* (Leismann et al., 2000) and cloned as Bst-BI fragment into the unique Bst-BI site in LD14219, located 12 nucleotides upstream of the Rad21 translational stop codon. The sequence encompassing *Rad21-myc_{10}* was excised as a 2790 bp Eco-RI//Kpn-I fragment and cloned into pUAST (Brand and Perrimon, 1993) to obtain *pUAS-Rad21-myc_{10}*.

To generate TEV-cleavable versions of Rad21 (Rad21^{TEV}), SpeI-restriction sites were introduced into the coding region of *Rad21* after amino acids 175, 197, 271 or 550 by site-directed PCR-mutagenesis, using *pUAS-Rad21-myc$_{10}$* as template (primer sequences see below). An AvrII/NheI restriction fragment encoding 3 tandem arrays of the TEV-recognition sequence ENLYFQG (kindly provided by Stephan Gruber, for details on the sequence see below) was inserted into the newly generated SpeI-site. The *Rad21(3TEV)-myc$_{10}$* fragment (EcoRI/KpnI-blunt) was introduced into the multiple cloning site (MCS) of a modified EcoRI/blunt cut pBS vector containing a MCS and 3'UTR flanked by FRT-sites (<). Next, the sequence comprising <*Rad21(3TEV)-myc$_{10}$-3'UTR*< was excised with KpnI and inserted into a KpnI-cut modified pCaSpeR transformation vector (derived from 10xUAS, G. Dietzl), in which the 10xUAS-sequence had been replaced with the sequence of the tubulin-promotor (derived from plasmid M>P^2, Casali and Struhl, 2004) (final vectors: *tubpr<Rad21(3TEV)-myc$_{10}$-3'UTR<SV40)*.

To generate vectors expressing myc-tagged Rad21 without TEV-cleavage sites, the open reading frame of *Rad21-myc$_{10}$* was PCR-amplified from *pUAS-Rad21-myc$_{10}$* and introduced into the same modified vector (final vector: *tubpr-Rad21-myc$_{10}$-SV40).*

Transgenic lines were produced by standard P-element-mediated germline transformation (Rubin and Spradling, 1983). Transgenes were tested for their ability to rescue the lethality of *Rad21* null mutations. Transgenes with TEV-cleavage sites at positions 271 or 550 and a transgene without TEV-sites were functional.

Immunoblotting

For the preparation of embryonic extracts, dechorionated embryos were homogenized in SDS-sample loading buffer 3-6 hours after egg deposition. Proteins were resolved by SDS-polyacrylamide gel electrophoresis and transferred to a PVDF membrane. The blot was probed with mouse anti-myc 9E10 (1:15, Sigma-Aldrich) and mouse anti-α-tubulin (DM1A) (1:20000, Sigma-Aldrich) using ECL detection (Amersham). Protein extracts from pupae, 3rd instar larval salivary glands and 3rd instar larvae without salivary glands were prepared after dissection in PBS essentially as described in Experimental Procedures.

Immunostaining of polytene chromosome squashes

Salivary glands from wandering 3rd instar larvae were dissected in PBS, permeabilized in PBX* (PBS, 0.1% Triton X-100, 3.7% formaldehyde) for 30 seconds, fixed in 45% acetic acid/3.7% formaldehyde for 5-7 minutes and squashed according to standard procedures. Slides were blocked for 1 hour at room temperature in PBST + 5% BSA (PBS, 0.01% Tween20, 5% BSA) and incubated with primary antibodies (diluted in blocking solution) overnight at 4°C. After washing in PBST (3x10 minutes), slides were incubated with Alexa-conjugated secondary antibodies at room temperature for 1.5 hours, washed as before and mounted using VECTASHIELD mounting medium containing DAPI (Vector Laboratories).
The following (additional) primary antibodies were used: guinea-pig anti-SA (1:100, Dorsett et al., 2005), rabbit anti-SMC1 (1:100, Dorsett et al., 2005), rat anti-SMC1 (1:500, Malmanche et al., 2007), mouse anti-HA 16B12 (1:250, Covance), mouse anti-polymerase II 8WG16 (1:20, Covance), rabbit anti-trx (1:50, Chinwalla et al., 1995), rabbit anti-Pc (1:200, Zink and Paro, 1989), rabbit anti-HSF (1:80, Andrulis et al., 2000), rabbit anti-BEAF32 (SCBP) (1:50, Zhao et al., 1995) and mouse anti-Z4

(1:1, Saumweber et al., 1980).

Primer and DNA sequences

Restriction enzyme sites are shown in lower case, the start codon **ATG** in bold, the *v5*-epitope sequence in *italics*, the NLS sequence underlined.

NLS-v5-TEV-NLS$_2$

AP2f 5'-AAAgaattcAAA**ATG***CCTAAGAAAAAGAGGAAGGTT*GCATCCG GTAAGCCTATCCCTAACCCTCTCCTCGGTCTCGATTCTACGG GAGAAAGCTTGTTTAAGGGACCACG-3'

AP4r 5'-AAAAACCCTCGAGCCgcggccgcAG-3'

pUAS-Rad21-myc$_{10}$

SH28 5'-CGATTATTCGAAAACCCAAAAATTGTTCGCCATGGTATG G-3'

SH29 5'-CGATTA TTCGAA TGCCCCATGTTCGCCCAAG-3'

tubpr-Rad21-myc$_{10}$* and *tubpr<Rad21(3TEV)-myc$_{10}$-3'UTR<

AP28-EcoRIRad21f 5'-AAAgaattcAAA**ATG**TTCTATGAGCACATTATTTTG-3'

AP29-Rad21NotIr 5'-AAAgcggccgcATTAAAACAGATTTACATTCAAC-3'

AP20-TEV175SpeIf 5'-CCTCTATTTTCAAGGCactagtATACCTTCAAATATTA ATGATAAA-3'

AP21-175NheISpeIr 5'-actagtGCCTTGAAAATAGAGGTTCTCGCTAGCTTCAA AGCCTATATCACCAAA-3'

AP22-197SpeIf 5'-TTTTGGAAAATATTGAGactagtTCTCTGGATCCACAT TCATTGG-3'

AP23-197SpeIr 5'-actagtCTCAATATTTTCCAAAACGTC-3'

AP24-271SpeIf 5'-CATAATGTCCCTTCGCCTactagtGCAACCTCGCTCGTT AATTCGATTG-3'

AP25-271SpeIr 5'-actagtAGGCGAAGGGACATTATGAATATT-3'

AP26-550SpeIf 5'-TCAAGGAGACTCAACGactagtCCAGCTGGGTTGGATC ATGGTC-3'

AP27-550SpeIr 5'-actagtCGTTGAGTCTCCTTGATTAAAA-3'

3 TEV recognition sites (3TEV)

c/ctagGGCTAGAGAGAATTTGTATTTTCAGGGTGCTTCTGAAAACCTTTACT

TCCAAGGAGAGCTCGAAAATCTTTATTTCCAGGGAg/ctagc

protein sequence: "-RAR**ENLYFQG**AS**ENLYFQG**EL**ENLYFQG**AS-"

Supplemental References

Andrulis, E.D., Guzman, E., Doring, P., Werner, J., and Lis, J.T. (2000). High-resolution localization of Drosophila Spt5 and Spt6 at heat shock genes in vivo: roles in promoter proximal pausing and transcription elongation. Genes Dev *14*, 2635-2649.

Brand, A.H., and Perrimon, N. (1993). Targeted gene expression as a means of altering cell fates and generating dominant phenotypes. Development (Cambridge, England) *118*, 401-415.

Casali, A., and Struhl, G. (2004). Reading the Hedgehog morphogen gradient by measuring the ratio of bound to unbound Patched protein. Nature *431*, 76-80.

Chinwalla, V., Jane, E.P., and Harte, P.J. (1995). The Drosophila trithorax protein binds to specific chromosomal sites and is co-localized with Polycomb at many sites. Embo J *14*, 2056-2065.

Dorsett, D., Eissenberg, J.C., Misulovin, Z., Martens, A., Redding, B., and McKim, K. (2005). Effects of sister chromatid cohesion proteins on cut gene expression during wing development in Drosophila. Development (Cambridge, England) *132*, 4743-4753.

Heidmann, D., Horn, S., Heidmann, S., Schleiffer, A., Nasmyth, K., and Lehner, C.F. (2004). The Drosophila meiotic kleisin C(2)M functions before the meiotic divisions. Chromosoma *113*, 177-187.

Leismann, O., Herzig, A., Heidmann, S., and Lehner, C.F. (2000). Degradation of Drosophila PIM regulates sister chromatid separation during mitosis. Genes Dev *14*, 2192-2205.

Malmanche, N., Owen, S., Gegick, S., Steffensen, S., Tomkiel, J.E., and Sunkel, C.E. (2007). Drosophila BubR1 is essential for meiotic sister-chromatid cohesion and maintenance of synaptonemal complex. Curr Biol *17*, 1489-1497.

Rubin, G.M., and Spradling, A.C. (1983). Vectors for P element-mediated gene transfer in Drosophila. Nucleic acids research *11*, 6341-6351.

Salvaterra, P.M., and Kitamoto, T. (2001). Drosophila cholinergic neurons and processes visualized with Gal4/UAS-GFP. Brain research *1*, 73-82.

Saumweber, H., Symmons, P., Kabisch, R., Will, H., and Bonhoeffer, F. (1980). Monoclonal antibodies against chromosomal proteins of Drosophila melanogaster: establishment of antibody producing cell lines and partial characterization of corresponding antigens. Chromosoma *80*, 253-275.

Schuh, M., Lehner, C.F., and Heidmann, S. (2007). Incorporation of Drosophila CID/CENP-A and CENP-C into centromeres during early embryonic anaphase. Curr Biol *17*, 237-243.

Thummel, C.S. (1992). Mechanisms of transcriptional timing in Drosophila. Science *255*, 39-40.

Uhlmann, F., Wernic, D., Poupart, M.A., Koonin, E., and Nasmyth, K. (2000). Cleavage of cohesin by the CD clan protease separin triggers anaphase in yeast. Cell *103*, 375-386.

Weiss, A., Herzig, A., Jacobs, H., and Lehner, C.F. (1998). Continuous Cyclin E expression inhibits progression through endoreduplication cycles in Drosophila. Curr Biol *8*, 239-242.

Yang, M.Y., Armstrong, J.D., Vilinsky, I., Strausfeld, N.J., and Kaiser, K. (1995). Subdivision of the Drosophila mushroom bodies by enhancer-trap expression patterns. Neuron *15*, 45-54.

Zars, T., Fischer, M., Schulz, R., and Heisenberg, M. (2000). Localization of a short-term memory in Drosophila. Science *288*, 672-675.

Zhao, K., Hart, C.M., and Laemmli, U.K. (1995). Visualization of chromosomal domains with boundary element-associated factor BEAF-32. Cell *81*, 879-889.

Zink, B., and Paro, R. (1989). In vivo binding pattern of a trans-regulator of homoeotic genes in Drosophila melanogaster. Nature *337*, 468-471.

Supplemental Tables

Table S1: Strains used in this study

Genotype	Abbreviation	Source
w^{1118}	*w*	Bloomington stock centre
w; lethal/CyO; TM2, {Δ2-3}/Sb, {Δ2-3}	P-element transposase	kindly provided by Frank Schnorrer
w; P{w+, EP}GE50159 (III)	*GE50159*	GenExel, Korea
Gal4 driver		
w; act-Gal4/CyO	*act-Gal4*	Barry Dickson lab stocks
w; hs-Gal4 (III)	*hs-Gal4*	Barry Dickson lab stocks
w; P{w+, mata4-tub-Gal4-VP16}	*a4-tub-Gal4*	Bloomington stock centre
w; P{w+, GawB}F4 (II)*	*F4-Gal4*	Weiss et al., 1998
w; elav-Gal4 (3AF) (III)	*elav-Gal4*	Barry Dickson lab stocks
w; nsyb-Gal4/CyO	*nsyb-Gal4*	kindly provided by Julie Simpson
y, w; 201Y-Gal4, UAS-mCD8-GFP/CyO; MKRS, Sb/TM6B, Tb	*201Y-Gal4, UAS-mCD8-GFP*	Liqun Luo lab stocks
w; Pin/CyO; H24-Gal4, UAS-mCD8-GFP	*H24-Gal4, UAS-mCD8-GFP*	Liqun Luo lab stocks
w; Cha-Gal4 (II)	*Cha-Gal4*	Salvaterra and Kitamoto, 2001
Transgenes and Mutants		
w; P{w+, His2Av-mRFP1} (II.2)*	*His2Av-mRFP1*	Schuh et al., 2007
w; P{w+, EGFP-Cid} (II.1)*	*EGFP-Cid*	Schuh et al., 2007
w; P{w+, gSMC3-HA12} (III.2)*	*gSMC3-HA*	Heidmann et al., 2004
y, w; P{w+, mhc-Gal80} (III)	*mhc-Gal80*	C. Winter and L. Luo, unpublished
Df(3L)2-66, kni[ri-1] p[p]/TM3, Sb, Ser	*Df(3L)2-66*	Bloomington stock centre
Rad21-excisions		
w; Rad21^{ex3}*/TM3, Sb, Kr-Gal4, UAS-GFP*	*Rad21*^{ex3}	present study
w; Rad21^{ex8}*/TM3, Sb, Kr-Gal4, UAS-GFP*	*Rad21*^{ex8}	present study
y, w; Rad21^{ex15}*/TM3, Sb, Kr-Gal4, UAS-GFP*	*Rad21*^{ex15}	present study
w; Rad21^{ex16}*/TM3, Sb, Kr-Gal4, UAS-GFP*	*Rad21*^{ex16}	present study

TEV protease transgenes		
w; P{w+, UAS-NLS-v5-TEV-NLS2} (III)	*UAS-TEV*	present study
w; P{w+, hs-NLS-v5-TEV-NLS2} (II)	*hs-TEV*	present study
Rad21-excision + TEV-protease		
w; Rad21^{ex3}, P{w+, UAS-NLS-v5-TEV-NLS2}/TM3, Sb, Kr-Gal4, UAS-GFP	*Rad21^{ex3}, UAS-TEV/TM3, Sb, Kr>GFP*	
w; Rad21^{ex3}, P{w+, UAS-NLS-v5-TEV-NLS2}, hs-Gal4/TM3, Sb, Kr-Gal4, UAS-GFP	*Rad21^{ex3}, UAS-TEV, hs-Gal4/TM3, Sb, Kr>GFP*	present study
w; P{w+, hs-NLS-v5-TEV-NLS2 }; Rad21^{ex3}/TM6B, Tb, ubiquitin-GFP	*hs-TEV ; Rad21^{ex3}/TM6B, Tb*	present study
transgenic Rad21 (+/- TEV-sites)		
w; P{w$^+$, tubpr<Rad21(550-3TEV)-myc$_{10}$<SV40} (III)	*Rad21(550-3TEV)-myc (Rad21^{TEV})*	present study
w; P{w$^+$, tubpr<Rad21(271-3TEV)-myc$_{10}$<SV40} (III)	*Rad21(271-3TEV)-myc (Rad21^{TEV})*	present study
w; P{w$^+$, tubpr-Rad21-myc$_{10}$-SV40} (III)	*Rad21-myc (Rad21)*	present study
w; P{w$^+$, tubpr<Rad21(271-3TEV)-myc$_{10}$<SV40} (II.3)	*Rad21(271-3TEV)-myc (Rad21^{TEV})*	present study
w; P{w$^+$, tubpr<Rad21(271-3TEV)-myc$_{10}$<SV40} (II.7)	*Rad21(271-3TEV)-myc (Rad21^{TEV})*	present study
w; P{w$^+$, tubpr<Rad21(271-3TEV)-myc$_{10}$<SV40}* (II.3), *P{w$^+$, tubpr<Rad21(271-3TEV)-myc$_{10}$<SV40}* (II.7)	*2x Rad21(271-3TEV)-myc (2x Rad21^{TEV})*	present study
Rad21-excision + transgenic Rad21 (+/- TEV-sites)		
w; Rad21^{ex15}, P{w$^+$, tubpr<Rad21(550-3TEV)-myc$_{10}$<SV40} (III)	*Rad21^{ex15}, Rad21^{TEV}*	present study
w; Rad21^{ex8}, P{w$^+$, tubpr<Rad21(271-3TEV)-myc$_{10}$<SV40}* (III)	*Rad21^{ex8}, Rad21^{TEV}*	present study
w; P{w$^+$, tubpr<Rad21(271-3TEV)-myc$_{10}$<SV40} (II.3), *P{w$^+$, tubpr<Rad21(271-3TEV)-myc$_{10}$<SV40}* (II.7); *Rad21^{ex3}*	*2x Rad21^{TEV}; Rad21^{ex3}*	present study
w; Rad21^{ex3}, P{w$^+$, tubpr-Rad21-myc$_{10}$-SV40} (III)	*Rad21^{ex3}, Rad21*	present study
w; Rad21^{ex15}, P{w$^+$, tubpr<Rad21(550-3TEV)-myc$_{10}$<SV40}, P{w$^+$, mhc-Gal80} (III)	*Rad21^{ex15}, Rad21^{TEV}, mhc-Gal80*	present study
Rad21-excision + Gal4 (+ TEV-protease or transgenic Rad21^{TEV})		
w; Rad21^{ex3}, hs-Gal4/TM3, Sb, Kr-Gal4, UAS-GFP	*Rad21^{ex3}, hs-Gal4/TM3, Kr-Gal4, UAS-GFP*	present study
w; P{w$^+$, α4-tub-Gal4-VP16}/CyO, wg-lacZ; Rad21^{ex3}/TM3, Sb, ubx-lacZ*	*α4-tub-Gal4/CyO, wg-lacZ; Rad21^{ex3}/TM3, ubx-lacZ*	present study
w; P{w$^+$, α4-tub-Gal4-VP16}, P{w$^+$, His2Av-mRFP1}* (II.2), *P{w$^+$, EGFP-Cid}* (II.1)*/CyO, wg-lacZ; Rad21^{ex3}/TM3, Sb, ubx-lacZ*	*α4-tub-Gal4, His2Av-mRFP1, EGFP-Cid/CyO; Rad21^{ex3}/TM3, ubx-lacZ*	present study

w; P{w+, GawB}F4/CyO, Kr-Gal4, UAS-GFP; Rad21^{ex15}, P{w$^+$, tubpr<Rad21(550-3TEV)-myc$_{10}$<SV40}*	*F4-Gal4/CyO, Kr-Gal4, UAS-GFP; Rad21^{ex15}, Rad21(550-3TEV)-myc*	present study
w; Rad21^{ex3}, P{w$^+$, UAS-NLS-v5-TEV-NLS$_2$ }, elav-Gal4/TM3, Sb, Kr-Gal4, UAS-GFP	*Rad21^{ex3}, UAS-TEV, elav-Gal/TM3, Kr-Gal4, UAS-GFP*	present study
w; nsyb-Gal4/CyO; Rad21^{ex3}, P{w$^+$, UAS-NLS-v5-TEV-NLS$_2$}/TM3, Sb, Kr-Gal4, UAS-GFP	*nsyb-Gal4/CyO; Rad21^{ex3}, UAS-TEV/TM3, Kr-Gal4, UAS-GFP*	present study
w; Rad21^{ex3}, P{w$^+$, UAS-NLS-v5-TEV-NLS$_2$}, H24-Gal4, UAS-mCD8-GFP/TM6B, Tb	*Rad21^{ex3}, UAS-TEV, H24-Gal4, UAS-mCD8-GFP/TM6B, Tb*	present study
w; 201Y-Gal4, UAS-mCD8-GFP/(CyO); Rad21^{ex15}, P{w$^+$, tubpr<Rad21(550-3TEV)-myc$_{10}$<SV40}	*201Y-Gal4, UAS-mCD8-GFP; Rad21^{ex15}, Rad21^{TEV}*	present study
w; 201Y-Gal4, UAS-mCD8-GFP/(CyO); Rad21^{ex3}, P{w$^+$, tubpr-Rad21-myc$_{10}$-SV40}	*201Y-Gal4, UAS-mCD8-GFP; Rad21^{ex3}, Rad21*	present study
w; 201Y-Gal4, UAS-mCD8-GFP/CyO; Rad21^{ex3}, P{w$^+$, mhc-Gal80}, P{w$^+$, UAS-NLS-v5-TEV-NLS$_2$}/TM6B, Tb	*201Y-Gal4, UAS-mCD8-GFP/CyO; Rad21^{ex3}, mhc-Gal80, UAS-TEV/TM6B, Tb*	present study
w; Cha-Gal4; Rad21^{ex3}, P{w$^+$, UAS-NLS-v5-TEV-NLS$_2$}/TM6B, Tb	*Cha-Gal4; Rad21^{ex3}, UAS-TEV/TM6B, Tb*	present study
w, UAS-CD8-GFP; If/CyO; Rad21^{ex15}, P{w$^+$, tubpr<Rad21(550-3TEV)-myc$_{10}$<SV40}	*UAS-CD8-GFP; If/CyO; Rad21^{ex15}, Rad21^{TEV}*	present study
w; Rad21^{ex3}, P{w$^+$, tubpr-Rad21-myc$_{10}$-SV40}, P{w$^+$, UAS-NLS-v5-TEV-NLS$_2$}/TM6B, Tb*	*Rad21^{ex3}, Rad21, UAS-TEV/TM6B, Tb*	present study

Table S2: Rescue of *Rad21* excision alleles by ectopic expression of either Rad21-myc or Rad21^{TEV}-myc

	Relative Viability *			
	♂ ***Rad21^{ex16}/TM3 Sb, Kr>GFP***		♂ ***Rad21^{ex3}/TM3 Sb, Kr>GFP***	
	Pupae$^{\#}$	**Adults$^{\#\#}$**	**Pupae$^{\#}$**	**Adults$^{\#\#}$**
♀ ***Rad21^{ex16}/TM3 Sb, Kr>GFP***	0	0	0	0
♀ ***Rad21^{ex3}/TM3 Sb, Kr>GFP***	0	0	0	0
♀ ***Rad21^{ex3}, Rad21-myc***	95.1	101	105	93.9
♀ ***Rad21^{ex15}, Rad21(550-3TEV)-myc***	111	81.4	107	78.4
♀ ***Rad21^{ex8}, Rad21(271-3TEV)-myc***	87.5	96.6	90.6	96.4

* Relative Viability: percentage of rescued pupae/adults, normalized to the values obtained when *Rad21^{ex}/TM3 **Sb, Kr>GFP*** males were crossed to *w^{1118}* females.

Rescued pupae were identified by the absence of GFP-expression (n ≥ 400).

Rescued adults were identified by the absence of *Sb* (n ≥250).

Supplemental Figures

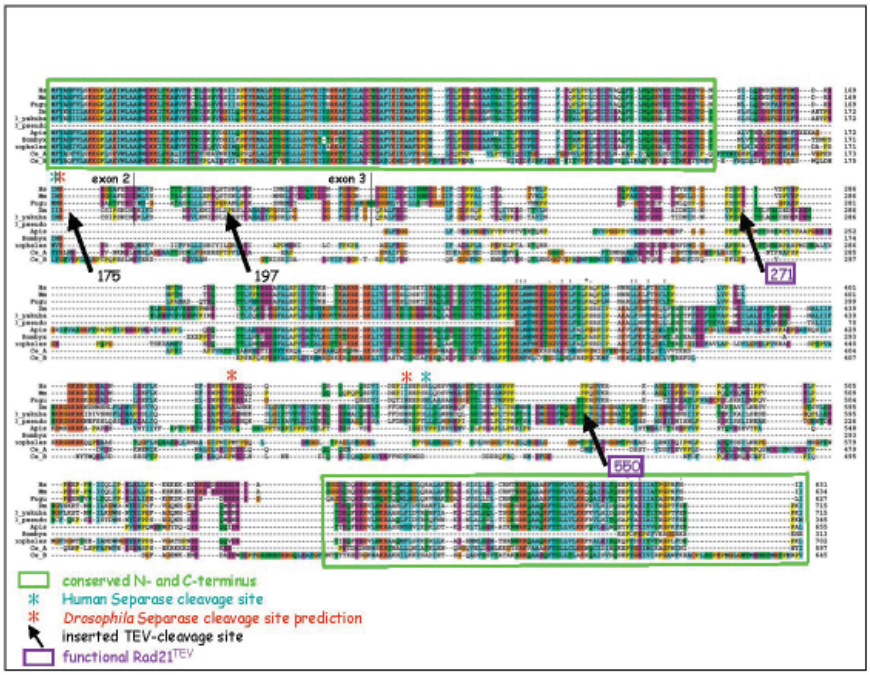

Figure S1. Multiple sequence alignment of protein-sequences of metazoan Rad21-homologs.

Annotated Rad21-protein sequences or sequence fragments were aligned to each other using ClustalW (Alexander Schleiffer, unpublished data). The conserved N-and C-terminal domains (green frames), human and (predicted) *D. melanogaster* separase cleavage sites (blue and red asterisks, respectively) and the boundaries of exons 2-3 and 3-4 are indicated. Four poorly conserved regions were chosen to introduce 3 tandem arrays of TEV recognition sequences (black arrows). The amino acid position after which the TEV sites had been introduced is indicated. TEV sites that rendered a functional Rad21^{TEV} protein (271 and 550) are highlighted in purple boxes.

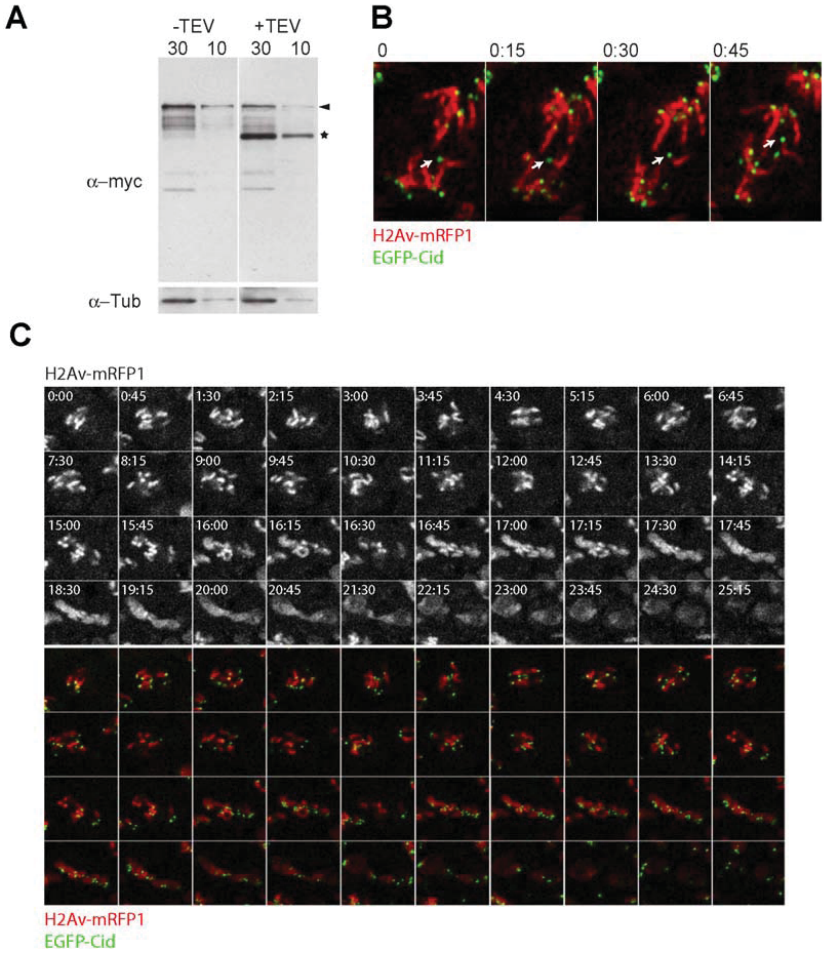

Figure S2. Rad21^{TEV} is cleaved by zygotically expressed TEV before mitosis 14.

(A) Total extracts corresponding to 30 or 10 embryos were analyzed by immunoblotting with antibodies against myc and α-tubulin 3-6 hours after egg deposition. (-TEV) Embryos surviving on myc-tagged Rad21^{TEV} express maternal Gal4, but do not contain the UAS-TEV transgene. (+TEV) Embryos surviving on myc-tagged Rad21^{TEV} express maternal Gal4, which drives zygotic TEV

expression. The arrowhead indicates the position of full-length myc-tagged $Rad21^{TEV}$, the asterisk that of the C-terminal TEV-cleavage product. Note that only 50% of the embryos used for the +TEV extracts contain the UAS-TEV construct (for details on genetic crosses see Supplemental Experimental Procedures). Therefore, the data is fully consistent with complete or almost complete cleavage of $Rad21^{TEV}$.

(B) Unstable kinetochore attachment after TEV expression. Frames shown were taken at 15 second intervals from a cell during the mitotic arrest resulting from zygotic TEV expression in embryos surviving on $Rad21^{TEV}$. DNA is marked with His2Av-mRFP1 (red), kinetochores with EGFP-Cid (green). The arrow follows the movement of a single kinetochore.

(C) Frames were taken at times indicated (min:sec) from a cell in a TEV-expressing embryo surviving on $Rad21^{TEV}$. DNA is marked with His2Av-mRFP1 (red), kinetochores with EGFP-Cid (green). After an initial mitotic arrest, chromosome decondensation starts abruptly (16:00) and unattached chromatids in the central region are cut by the cleavage furrow.

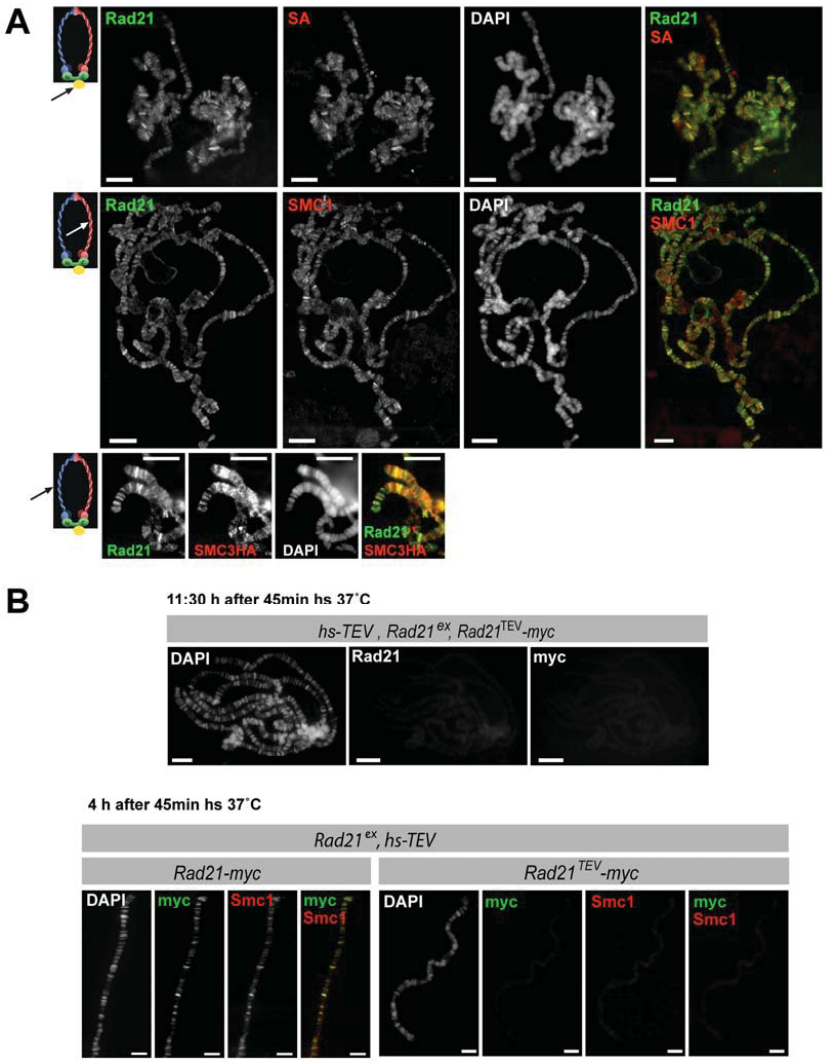

Figure S3. The cohesin complex binds to polytene chromosomes.

(A) Polytene chromosomes from wild-type flies (top two rows) or flies transgenic for HA-tagged SMC3 (bottom row) were coimmunostained with antibodies against endogenous Rad21 (green) and either endogenous SA (top row), endogenous SMC1 (middle row) or the HA-epitope (bottom row) (red). A schematic of the cohesin complex is shown at the left of each row (arrow points to the subunit costained with

Rad21). DNA was visualized with DAPI. Scale bars, 15µm.

(B) Polytene chromosome spreads from 3rd instar larvae, which express heat-inducible TEV (hs-TEV) and myc-tagged Rad21^{TEV} as their only source of Rad21, were prepared after a 45 min heat shock. Spreads were coimmunostained with antibodies against endogenous Rad21 and myc (top) or myc (green) and SMC1 (red) (bottom). Note the absence of Rad21-, myc- and SMC1-staining after TEV cleavage of Rad21^{TEV}. DNA was visualized with DAPI. Scale bar, 15µm (top), 10µm (bottom).

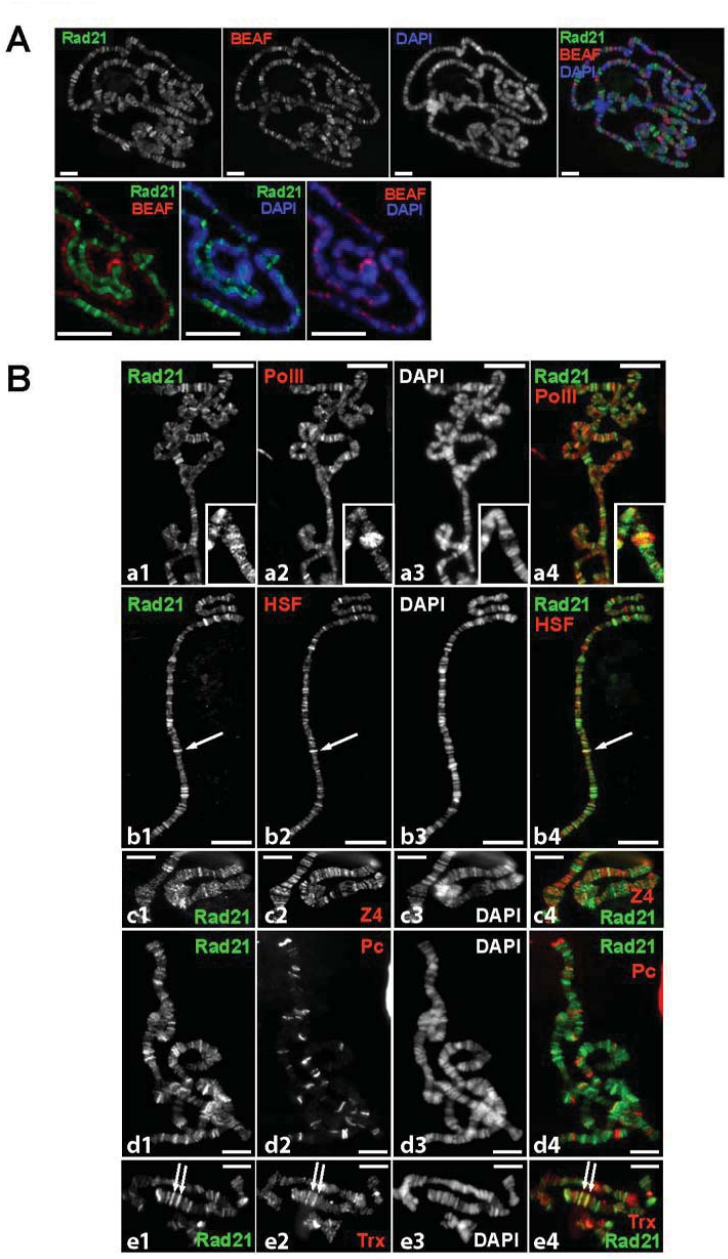

Figure S4. Rad21 binds to distinct regions on polytene chromosomes.

(A) Polytene chromosomes from wild-type flies (w^{1118}) were coimmunostained with

antibodies against Rad21 (green) and BEAF (red), a well-characterized boundary-associated factor. DNA is shown in blue in merged images. Two different magnifications are shown (top row: 40x objective; bottom row: 100x objective, split channels). BEAF and Rad21 localize to distinct interband regions. Scale bar, 20µm. (B) Polytene chromosomes from wild-type flies (w^{1118}) were coimmunostained with antibodies against Rad21 and (a) PolII (RNA Polymerase II), (b) HSF (Heat-Shock Factor), (c) Z4 (interband-specific Zinc-finger protein), (d) Pc (Polycomb) and (e) trx (Trithorax). DNA was visualized with DAPI. As seen in the merged images (Rad21 in green, other proteins in red), the distribution of cohesin and of the other tested factors differs significantly. White arrows point to the few regions, in which an overlap between Rad21 and the other factor tested could be detected. The insets in a1-a4 show a higher magnification (3x) of a PolII-stained chromosomal puff, which is flanked by Rad21-bound regions. Scale bars, 20µm (a and b), 10µm (c-e).

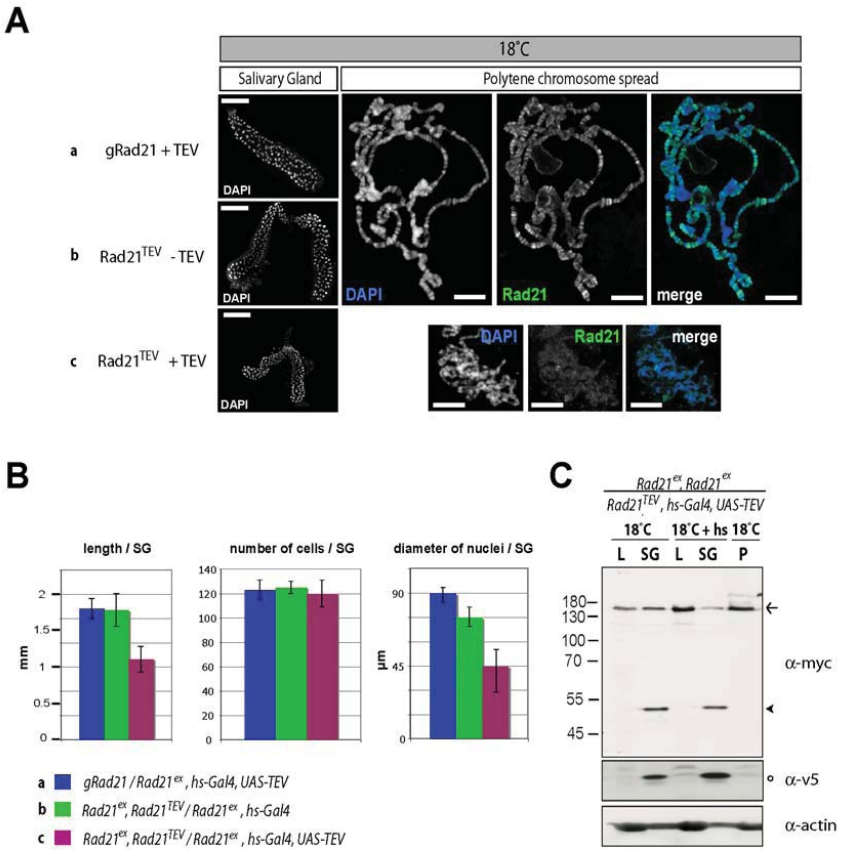

Figure S5. Cohesin is required for salivary gland development.

(A) Salivary glands were dissected from 3rd instar larvae that had been raised at 18˚C throughout development. (Left) In the whole-mount preparations, DNA was stained with DAPI. (Right) Polytene chromosome spreads were immunostained with antibodies against Rad21 (green). DNA was visualized with DAPI (blue). Three different genotypes were compared: a) *gRad21/Rad21^{ex3}, hs-Gal4, UAS-TEV*; b) *Rad21^{ex15}, Rad21^{TEV}/Rad21^{ex3}, hs-Gal4*; c) *Rad21^{ex15}, Rad21^{TEV}/Rad21^{ex3}, hs-Gal4, UAS-TEV*. Since polytene chromosome spreads from genotypes (a) and (b) are similar, only a representative spread from (a) is shown. Note that salivary glands with reduced amounts of Rad21 have smaller but not fewer cells. Scale bar, 500µm (whole

mount salivary glands), 20µm (polytene chromosome spreads).

(B) Quantitative analysis of salivary glands average length (in mm), total number of cells per salivary gland and the average diameter per nucleus (in µm) was performed from salivary glands from 3rd instar larvae of the indicated genotypes (>10 per genotype). Larvae in which $Rad21^{TEV}$ has been cleaved show smaller salivary glands with smaller nuclei. The number of cells per salivary glands remains unaltered.

(C) Protein extracts from a strain carrying hs-Gal4, UAS-TEV and surviving on myc-tagged $Rad21^{TEV}$ were analyzed by Western Blotting. Extracts of larvae lacking salivary glands (L), dissected salivary glands (SG) or pupae (P) were prepared from crosses raised at 18°C. Samples from lanes 3 and 4 were prepared 1 hour after heat shock treatment (45 min 37°C). Western Blot analysis was performed with antibodies against myc (detecting full-length $Rad21^{TEV}$-myc (arrow) and the C-terminal TEV-cleavage fragment (arrowhead)), v5 (detecting TEV-protease) and actin (loading control). Before heat shock induction of TEV, significant levels of the protease could be detected in salivary glands (open circle). The TEV cleavage fragment of Rad21 is also observed. Neither TEV protease nor $Rad21^{TEV}$ cleavage fragments were detected in larvae without salivary glands or pupae before TEV induction. A Molecular Weight Marker (in kDa) is shown on the left.

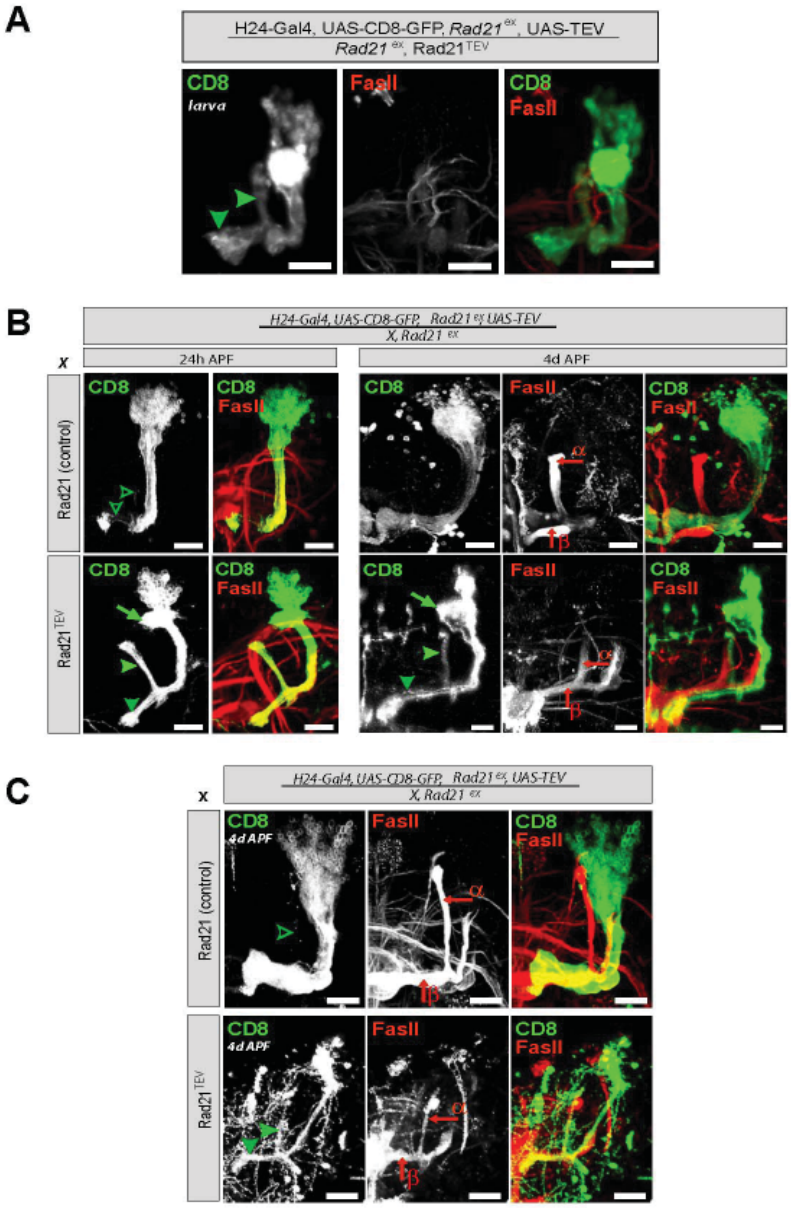

Figure S6. Analysis of pruning in γ neurons with H24-Gal4-induced TEV cleavage of Rad21.

H24-Gal4 was used to drive expression of TEV and mCD8 in γ neurons of the

mushroom body from flies that survived on transgenic Rad21 with ($Rad21^{TEV}$) or without (Rad21) TEV cleavage sites. Shown are maximal Z projections of single confocal sections of a right brain hemisphere, stained with antibodies against mCD8 (green) and FasII (red). Scale bars, 20μm.

(A) Larval γ neurons from a $Rad21^{TEV}$ brain project into the dorsal and medial lobes (filled green arrowheads).

(B) (24h APF, left) In the presence of Rad21 (control), γ neurons have pruned their medial and dorsal axon projections (open arrowheads) as well as their dendrites. In γ neurons of $Rad21^{TEV}$ pupae, larval axon-projections persist in the medial and dorsal lobes (filled green arrowheads). Note also the presence of unpruned dendrites (green arrow). (4d APF, right) In the presence of Rad21 (control), γ neurons have re-extended their axons medially towards the midline. Axons of α/β neurons in the dorsal and medial lobes are labeled with FasII (red arrows). In γ neurons of $Rad21^{TEV}$ pupae, larval axon-projections as well as dendrites (filled green arrowheads and green arrow, respectively) persist in the dorsal and medial lobe. Projections of α/β neurons are normal (red arrows).

(C) In the presence of Rad21 (top), γ neurons are tightly bundled and project exclusively towards the midline at 4d APF. No γ neurons are found in the FasII-positive dorsal lobe (open green arrowhead). In the absence of Rad21 (bottom), γ neuronal projections persist in the dorsal and medial lobes (filled green arrowheads), but are often disorganized and mistargeted. Although the FasII staining for α/β neurons appears weaker than in the control, the projection pattern is normal.

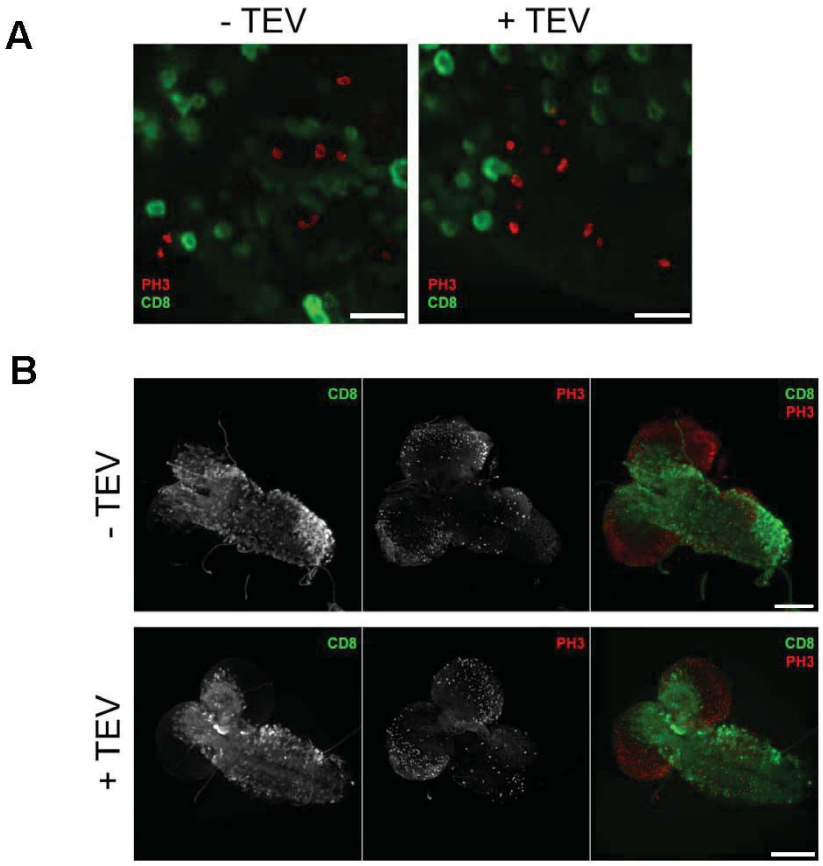

Figure S7. TEV cleavage of Rad21 in cholinergic-neurons does not cause mitotic defects.

Brains from control (-TEV: *UAS-CD8-GFP; Cha-Gal4/CyO; Rad21^{ex15}*, *Rad21^{TEV}/TM6B*) and TEV-cleaved brains (+TEV: *UAS-CD8-GFP; Cha-Gal4/CyO; Rad21^{ex15}*, *Rad21^{TEV}/Rad21^{ex3}*, *UAS-TEV*) were immunostained for CD8 (green) and the mitotic marker phospho-histone H3 (PH3, red).

A) High magnification images show that there is no co-localization between the CD8 positive cells and the mitotic marker. Additionally, mitotic figures in TEV-cleaved brains look similar to the controls. Scale bars, 20μm.

B) Confocal images of brains and ventral nerve cords from both control and TEV-cleaved brains. PH3 staining reveals that there is no detectable accumulation of mitotic figures after TEV cleavage, and that there are no obvious morphological defects in the CD8 positive cholinergic neurons. Scale bars, 100μm.

Lebenslauf

Zuname:	ALTHOFF
Vornamen:	Friederike Erika Andrea
Geburtsdatum:	30.08.1982
Nationalität:	Deutsch

Ausbildung:

1992 - 2001 Heinrich-von-Gagern Gymnasium, Frankfurt/Main, Deutschland
Abschluss: Abitur

2001 - 2006 Universität Bayreuth, Deutschland, Diplomstudiengang Biochemie
Abschluss: Diplom
Diplomarbeitsfach: Genetik

Titel der Diplomarbeit:
Untersuchungen zu Funktion und Lokalisierung von *Drosophila* Mps1

2006 - 2007 Universität Bayreuth, Lehrstuhl für Genetik, Deutschland, Promotionsstudium

seit 2007 Universität Zürich, Zoologisches Institut / IMLS, Schweiz, Promotionsstudium

Als Doktorandin an der Universität Zürich angestellt seit 2007.

Publikationen:

Althoff, F., Viktorinová, I., Kastl, J., Lehner, C. F., 2009. *Drosophila* Cyclin J is a mitotically stable Cdk1 partner without essential functions. Dev Biol. 333**,** 263-72.

Pauli, A., **Althoff, F.**, Oliveira, R. A., Heidmann, S., Schuldiner, O., Lehner, C. F., Dickson, B. J., Nasmyth, K., 2008. Cell-type-specific TEV protease cleavage reveals cohesin functions in *Drosophila* neurons. Dev Cell. 14**,** 239-51.

Schittenhelm, R. B., Heeger, S., **Althoff, F.**, Walter, A., Heidmann, S., Mechtler, K., Lehner, C. F., 2007. Spatial organization of a ubiquitous eukaryotic kinetochore protein network in *Drosophila* chromosomes. Chromosoma. 116**,** 385-402.

Schittenhelm, R. B., **Althoff, F.**, Heidmann, S., Lehner, C. F., 2010. Detrimental incorporation of excess Cenp-A/Cid and Cenp-C into *Drosophila* centromeres is prevented by limiting amounts of the bridging factor Cal1. J Cell Sci. 123**,** 3768-79.